PROCESSING COMPONENTS IN Π-CONJUGATED POLYMERS: CONTROLLING SOLUBILITY, MORPHOLOGY, AND FUNCTIONALITY THROUGH STRUCTURAL DESIGN

A Dissertation
Presented to
The Academic Faculty

by

Brian Joseph Schmatz

In Partial Fulfillment
of the Requirements for the Degree
Doctor of Philosophy in the
School of Chemistry and Biochemistry

Georgia Institute of Technology
August 2018

PROCESSING COMPONENTS IN Π-CONJUGATED POLYMERS: CONTROLLING SOLUBILITY, MORPHOLOGY, AND FUNCTIONALITY THROUGH STRUCTURAL DESIGN

Approved by:

Dr. John R. Reynolds, Advisor
School of Chemistry and Biochemistry
Georgia Institute of Technology

Dr. Elsa Reichmanis
School of Chemical and Biomolecular Engineering
Georgia Institute of Technology

Dr. David M. Collard
School of Chemistry and Biochemistry
Georgia Institute of Technology

Dr. Zhiqun Lin
School of Materials Science and Engineering
Georgia Institute of Technology

Dr. Will R. Gutekunst
School of Chemistry and Biochemistry
Georgia Institute of Technology

Date Approved: June 18th, 2018

“The future cannot be predicted, but futures can be invented.”
- Dennis Gabor

“The impossible often has a kind of integrity which the merely improbably lacks”
- Douglas Adams

To Liz and my parents

For providing a constant source of love and encouragement

ACKNOWLEDGEMENTS

Choosing to pursue a Ph.D. in chemistry at Georgia Tech was one of the most difficult decisions in my life, and was one that took a fair amount of encouragement and convincing. I was hesitant to leave the life, friends, and city I had grown to love for a place I knew nothing about and a path that I was uncertain was right for me. After 5 years in Atlanta at Georgia Tech, I can safely say I made the right decision. Although challenging, and at times stressful, this journey has led me to new friends, mentors, and experiences that have shaped me into a mature person and an ambitious scientist. I would like to thank the people who encouraged me to take this step and supported me along the way.

I would first and foremost like to thank Liz for taking this journey with me. Thank you for always being by my side to cheer me on, for listening and taking an interest in my ideas even if you didn't fully understand my chemistry jargon, and for calming me down when I came home stressed about synthesis woes. When I first came to Atlanta I couldn't wait to graduate and move on to the next chapter, but with you this past 5 years became an adventure with memories I will always cherish. I love you, and I'm excited to continue our journey together knowing you will always be there to support me.

I would also like to thank my Mom, Dad, and my brothers Jim and Dan for their love and support. To my Mom, for always being there with positive words of encouragement throughout my life. Thank you for teaching me by example what it means to be a good person, how to treat others, and how to have fun and enjoy life to the fullest. The optimistic, caring, and well-mannered person I am today is because of you. To my

Dad, for always serving as my personal and professional role model. You always prioritized the happiness of your sons, and never once pressured me to follow in your footsteps. Instead, you showed me where a Ph.D. could take you in life, how you can create a positive impact on the world and help others while pursuing an intellectually stimulating career. You inspired me to become the scientist I am today, and I'm proud to follow in your footsteps. I love you both, and thank you for raising me to be the person I am today.

I would like to thank my graduate advisor, Dr. Reynolds. Thank you for serving as a supportive and inspiring Ph.D. mentor to me and the rest of your students. You always said you were in the business of developing Ph.D. students, and you have stayed true to that message. Thank you for prioritizing our scientific growth over your own research career interests. Thank you for nurturing the creative side within me. I remember a stressful point in my Ph.D. after my first project when I felt as if my creative ideas were not panning out, and I should just do something straightforward that would yield results. You believed in me, and told me to do something I found truly interesting, leading me to the multistage side chain project that became the crux of my thesis work. Through this and countless other instances you have shown me how to be an excellent leader and nurture the strengths within your peers. I would also like to thank my undergraduate research advisors, Dr. Adam Braunschweig and Dr. Luis Campos, for providing me with the opportunity to work in your labs and begin my training as a synthetic organic chemist. It was through these experiences that my interest in graduate research became cemented.

To the members of the Reynolds group, thank you for creating one the most fun and intellectually stimulating workplaces I have ever been a part of. Whether it was in the

lab discussing research or on the field playing kickball, the group has always been encouraging and collaborative, and I can only hope to find coworkers and friends like this in my future. Special thanks to Rylan Wolfe, Kin Lo, and James Ponder, who served as synthetic mentors to me, and Dr. Anna Österholm and Dr. Eric Shen, who served as mentors for my work in electrochemistry, devices, and academic writing. Thank you for all of your help in the lab, and your patience during the countless occasions I asked you for advice.

I would also like to thank my collaborators and coauthors, Gus Lang, Zhibo Yuan, Ian Pelse, James Ponder, Jeff Hernandez, and Abigail Advincula. I had some wild ideas, some that worked and some that didn't, but you always approached our collaborations with optimism and enthusiasm, and it was a pleasure to have the opportunity to work alongside you.

I would like the thank the on-campus organizations and programs of which I was involved, including the Ti:GER program, the Student Polymer Network, the Sustainability Committee. Thank you to the Ti:GER administration and faculty team for funding and the opportunity to take part in this unparalleled professional experience, and to my Ti:GER team, Rajat Khanna, Jamie Foss, Caleb Small, and Alexandra Rajic for exploring the market potential and IP landscape of my research with me. Thank you to Alyssa Blake, Paul Balding, Sandy Pittelli, and Zhibo Yuan, who helped create and maintain the Student Polymer Network, and to Dr. Reynolds, Dr. Reichmanis, Dr. Russo, Dr. Gutekunst, and Dr. Brettmann, who served as excellent advisors and champions of this organization. Thank you to the undergraduate members of the Sustainability

Committee, and to Anne Rogers, Ryan Lisk, Meagan Fitzpatrick, Kevin Brantley, and Jason Robinson, who helped me initiate several on-campus Green Labs programs.

Finally, I would like to thank all my friends who have been there for me along the way. Thank you to my friends from back in New York: Sam, Hannah, and Ross. I remember when I was deciding whether or not to make the move to Georgia Tech, and I was ready to abandon the Ph.D. pursuit to stay in New York where I had grown comfortable. Thank you for telling me that this is what I was meant to do and encouraging me along the way. Thank you to the friends I've made in Atlanta: Hilary, Rob, Dakota, Kyle, Danny, Alex, and AJ. Thank you for making my time in Atlanta fun and full of memories. You have been a positive and encouraging family to me throughout this time.

TABLE OF CONTENTS

LIST OF TABLES

LIST OF FIGURES

LIST OF SYMBOLS AND ABBREVIATIONS

AcDOT	3,4-diethylhexyoxythiophene
ACN	Acetonitrile
AFM	Atomic force microscopy
BDT	Benzodithiophene
BHJ	Bulk heterojunction
BLA	Bond-Length Alternation
CB	Chlorobenzene
CP	Continuous Processing
CPE	Conjugated Polyelectrolyte
CV	Cyclic Voltammetry
D-A	Donor-Acceptor
DCM	Dichloromethane
DIO	1,8-diiodooctane
Đ	Dispersity
DHAP	Direct Hetero-Arylation Polymerization
DMF	*N,N*-dimethylformamide
DPP	Diketopyrrolepyrrole
DPV	Differential Pulse Voltammetry
DSC	Differential Scanning Calorimetry
EC	Electrochromic
EDOT	3,4-ethylenedioxythiophene

E_g	Energy Gap
EGOT	Electrolyte-Gated Organic Transistor
Fc/Fc+	Ferrocene/Ferrocenium
FF	Fill Factor
GIWAXS	Grazing Incidence Wide Angle X-Ray Scattering
GPC	Gel Permeation Chromatography
HOMO	Highest Occupied Molecular Orbital
iI	Isoindigo
IPA	Isopropyl Alcohol
ITO	Indium Tin Oxide
J_{SC}	Short Circuit Current
k_B	Boltzmann's Constant
LUMO	Lowest Unoccupied Molecular Orbital
M_n	Number Average Molecular Weight
MW	Molecular Weight
μ_h	Hole Mobility
NBS	N-Bromosuccinimide
NMR	Nuclear Magnetic Resonance
OECT	Organic Electrochemical Transistor
OFET	Organic Field-Effect Transistor
OLED	Organic Light-Emitting Diode
OPV	Organic Photovoltaic
P3HT	Poly(3-hexyl)thiophene

$PC_{71}BM$	[6,6]-Phenyl-C71-butyric acid methyl ester fullerene
PCE	Power Conversion Efficiency
$Pd(PPh_3)_4$	Tetrakis(triphenylphosphine)palladium(0)
$Pd_2(dba)_3$	Tris(dibenzylideneacetone)dipalladium(0)
PEDOT:PSS	Poly(3,4-ethylenedioxythiophene):poly(styrenesulfonate)
PLED	Polymer Light-Emitting Diode
ProDOT	3,4-propylenedioxythiphene
R2R	Roll-to-Roll
SCLC	Space-Charge Limited Current
$TBAPF_6$	Tetrabutylammonium hexafluorophosphate
THF	Tetrahydrofuran
TPA	Triphenylamine
TPD	Thienopyrrolodione
V_{OC}	Open Circuit Voltage
XPS	X-Ray Photoelectron Spectroscopy
ε_r	Dielectric Constant

SUMMARY

Over the past 30 years conjugated polymers have demonstrated performance strides in solution-printed photovoltaics, transistors, displays, and sensors. With fundamental structure-property relationships in place, the next step is to prepare these materials for use in large-scale, high-throughput printing facilities where reproducibility, tolerance to the environment, safety, and sustainability will all play a pivotal role in the ultimate success of conjugated polymer based electronics. This dissertation explores how to achieve that next step through the use of *processing components,* or structural moieties that embed a desired processing property.

Chapter 1 will provide an introduction to the design, fundamental properties, and methods of processing soluble conjugated polymers, placing specific emphasis on the interplay between molecular structure, processability, and ultimately performance. Polymer synthesis, characterization, and processing methodology unique to this dissertation will be presented in detail in Chapter 2. Chapter 3 describes the use of triphenylamine as a *processing comonomer* in dioxythiophene polymers. The triphenylamine comonomer templates an amorphous thin-film morphology by embedding backbone torsion and conjugation breaks, providing reproducible films that are tolerant to fluctuations in processing conditions. Chapter 4 explores the use of polymer side chains with multiple functionalities, or *multistage side chains*, to control solubility for aqueous printable conjugated polymers. Finally, Chapter 5 delves into the intricate morphological effects of polymer side chain placement in organic photovoltaic donor-acceptor blends. Specifically, the study utilizes a novel family of donor-acceptor polymers with methylated acceptor monomers to observe how side chain steric interactions affect

morphology and optoelectronic properties in blends of polymeric donors and molecular acceptors.

CHAPTER 1

INTRODUCTION

1.1 Background of Conjugated Polymer Electronics

The term Organic Electronics describes the general field of synthetically derived π-conjugated materials that exhibit the electronic attributes of conductors or semiconductors. These unique materials bring promise for a new generation of cost-effective, lightweight, flexible, and functional electronics. While there are a variety of new application spaces for these materials that continue to emerge, the core applications include organic light-emitting diodes (OLEDs)[1-3], organic field-effect transistors (OFETs)[4-5], organic photovoltaics (OPVs)[6-8], electrochromic devices (ECDs)[9] and photodetectors[10-11]. These organic electronic devices typically trail behind their inorganic counterparts in terms of performance, but instead offer numerous advantages including mechanical flexibility[12], adaptability to low-cost processing techniques[13], synthetic tunability[14], and biocompatibility[15], providing a competitive edge in both commodity and niche markets.

On the commodity side, the ability to formulate liquid inks out of organic electronic materials opens up manufacturing possibilities through low-cost printing techniques such as screen-printing, blade coating, inkjet printing, rotogravure printing, aerosol spray coating, and slot-die coating. Many of these techniques are amenable to roll-to-roll (R2R) processing, in which reels of substrate are continuously moved through coating, drying, laminating, and cutting processes similar to what is done in the graphic

printing industry. The high throughput nature of R2R processing reduces the costs associated with manufacturing, allowing for simple electronic devices including sensors, logic circuits, photovoltaics, etc. to be produced more rapidly and at lower costs than electronic components composed of inorganic materials such as doped silicon. On the niche side, the ability to print onto a variety of substrates opens up opportunities for the integration of electronics into plastic and paper based products. Additionally, the ability to create flexible electronics can reduce the design limitations caused by rigid electronic components. Synthetic tunability of organic electronic materials allows for components to be made transparent or in a variety of colors. Finally, designing for biocompatibility can lead to new ways for electronics to interface with living systems. For these reasons, research in organic electronics is not solely focused on increasing performance metrics to compete with traditional electronics, but is also focused on exploring the properties and processing methods that cannot be achieved through inorganic materials.

1.1.1 Fundamental Concepts of Organic Semiconductors

Organic electronic materials, whether molecular or polymeric, all rely on the ability to move electrons through π-conjugated structures, which consist of alternating single bonds and double bonds that create a plane of sp^2 hybridized orbitals with $2p_z$ orbitals left perpendicular to that plane. These $2p_z$ orbitals overlap to form a network of π bonds that can move electrons across the plane of conjugation. The impact of increasing the extent of conjugation can be best understood by the progression from ethylene to butadiene and further to varying lengths polyenes. With increasing number overlapping $2p_z$ orbitals comes a decrease in the energetic bandgap (E_g) between the highest-occupied molecular orbital (HOMO) and lowest-unoccupied molecular orbital (LUMO) of the

system, transitioning these materials from insulators to materials that have similar bandgaps between HOMO and LUMO as the bandgaps seen between valence bands (VB) and conduction bands (CB) in inorganic semiconductors, exemplified in Figure 1-1. If this trend were to continue, it could be assumed that eventually an extent of conjugation would lead to a negligible bandgap between the HOMO and LUMO, as is seen between the VB and CB in metal conductors. However, the instability of a quasi one-dimensional structure of sp^2 hybridized carbon-carbon bonds leads to a distortion of the chain in order to provide stabilization through a lower energy arrangement.[16-17]

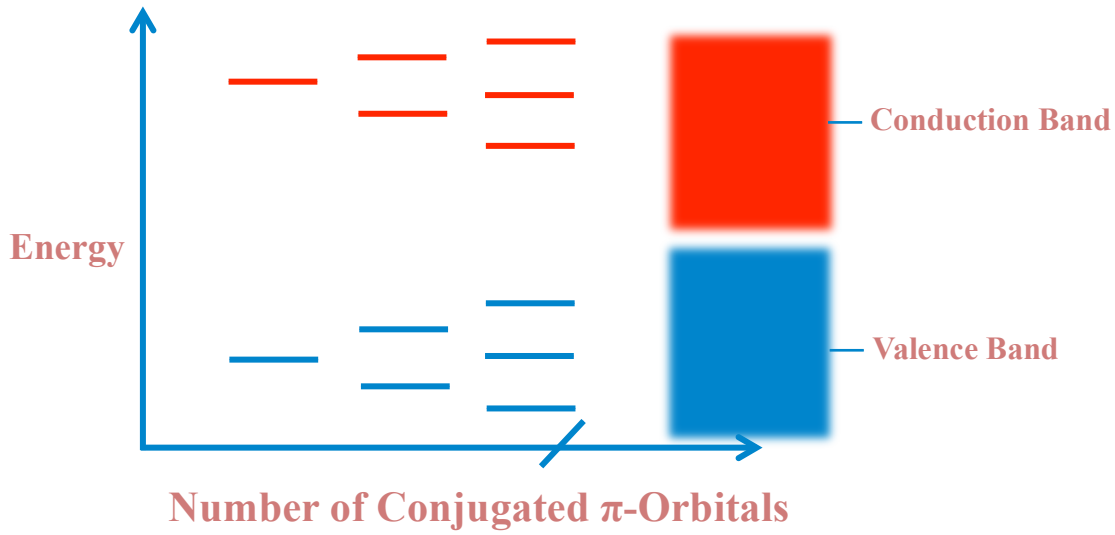

Figure 1-1. Diagram displaying the effect of decreasing bandgap between the highest-occupied molecular orbital (HOMO) and lowest occupied molecular orbital (LUMO) as conjugation length increases, ultimately resembling the band-like structure seen within inorganic semiconductors.

Known as Peierl's distortion, the physical effect of this stabilization is seen through bond-length alternation (BLA) of shorter bonds and longer bonds. This stabilization lowers the HOMO and raises the LUMO, preventing conjugated materials from achieving the zero-energy bandgap seen in conducting metals. However,

conductivity can be achieved in conjugated materials through doping mechanisms, as is the case in PEDOT:PSS[18], but for the most part conjugated organic materials are used as semiconducting materials because of this limitation.

One of the key drawbacks of organic materials is relatively low charge carrier mobility compared to inorganics. Charge carrier mobility (μ) is a defined as the ratio between charge drift velocity, v, and the amplitude of the applied electric field, E:

$$\mu = v/E \tag{1-1}$$

and is typically reported in $cm^2V^{-1}s^{-1}$. Mobility is effectively a measure of a material's ability to transport charge, and therefore plays an important role in semiconductors. For crystalline inorganic materials, a highly ordered covalent network of atoms allows charges to delocalize into valence and conduction bands. Charges can be easily moved within these bands, giving inorganic semiconductors mobility values in the range of 10^2 – 10^3 $cm^2V^{-1}s^{-1}$.[19] Since organic materials are held together by weak intermolecular interactions (Van der Waals forces, dipole-dipole), charges are localized to single molecules and are transported through a slower 'hopping' mechanism. In this mechanism, each molecule contributes discrete molecular orbitals, and charges can move between the frontier molecular orbitals of each individual molecule. In this sense, the array of HOMO and LUMO energy levels contributed from each molecule serve as an analogue to the valence and conduction bands seen for inorganic materials. Charge transport is therefore governed by a diffusion-related 'hopping' between charged and neutral molecules, giving organic materials lower mobility values in the range of 10^{-5} – 10 $cm^2V^{-1}s^{-1}$. This broad mobility range can be attributed to the vast differences in

molecular structure, intermolecular interactions, and morphology amongst organic materials. For instance, highly pure rubrene single crystals have shown hole mobility values as high as 40 $cm^2V^{-1}s^{-1}$ due to their high degree of crystallinity and lack of grain boundaries.[20] On the other hand, semicrystalline polymers such as P3HT show hole mobility values on the order of 10^{-3}-10^{-2} $cm^2V^{-1}s^{-1}$.

In semiconductor applications, the speed at which a material sweeps charges in, out, or across a device is often highly correlated with its performance.[21] For this reason, high mobility materials are typically sought after for charge transport layers between device active layers and electrodes.[22] These materials can either transport holes (p-type), electrons (n-type), or both (ambipolar). In organic semiconductors, this distinction is usually made in relation to the energetic overlap with another material, and does not imply a difference in intrinsic ability to transport holes or electrons.[23] Consider the diagram in Figure 1-2 of a conventional solar cell. After the generation and separation of an exciton in the donor-acceptor (D-A) blend active layer, the hole-transport material (HTM) is able to donate an electron from its HOMO to the donor (receive a hole), while the electron-transport material (ETM) is able to receive an electron into its LUMO.

In this architecture, the HTM is p-type and the ETM is n-type because of their energetic relationship to adjacent transport materials, but it is possible that they have similar values for hole (μ_h) and electron (μ_e) mobility. Therefore, while choosing materials with favorable energetic overlap can optimize organic electronic devices, performance will still be limited by the intrinsically low mobility of those materials.

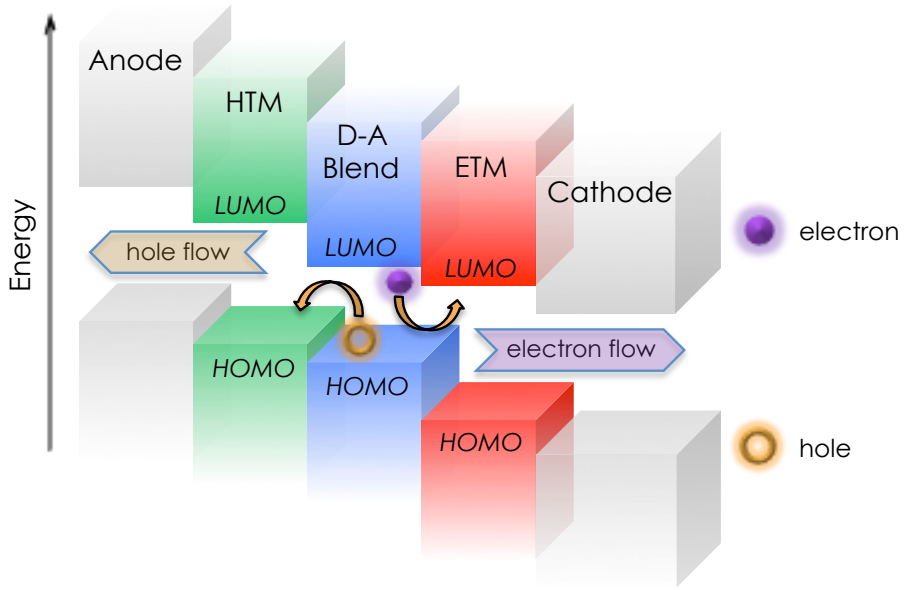

Figure 1-2. Simplified energy level diagram of an organic solar cell. Electrons flow through the LUMO of the ETM to the cathode, while holes flow through the HOMO of the HTM to the anode.

To understand how to raise mobility in organic materials we can approach charge 'hopping' as a diffusion process described by the Einstein-Smoluchowski equation:

$$\mu = \frac{eD}{k_B T} \tag{1-2}$$

where e is the electronic charge, D is the diffusion coefficient, and k_B is the Boltzmann constant[24]. If considering charge transport between two identical molecules, the diffusion coefficient is proportional to the charge transfer rate k, which can be predicted using Marcus theory[19]:

$$D \propto k = \frac{V^2}{\hbar}\sqrt{\frac{\pi}{\lambda k_B T}}\exp\left(-\frac{\lambda}{4k_B T}\right) \tag{1-3}$$

where V is the transfer integral between initial and final states, and λ is the reorganization energy corresponding to geometric relaxation during charge transfer. From equation 3 it

can be seen that increasing V or decreasing λ will lead to higher diffusion coefficients, and therefore higher charge mobility values. The transfer integral V is strongly correlated with intermolecular interactions, meaning crystallographic information is required for the calculations. While this is possible for highly crystalline systems, many organic small molecules and polymers form disordered solids and a crystal structure cannot be easily elucidated. On the other hand, reorganization energy can be readily predicted through energetic calculations. Pictured in Figure 1-3 is a potential energy diagram for a molecule transitioning between its neutral and charged (oxidized or reduced) state.

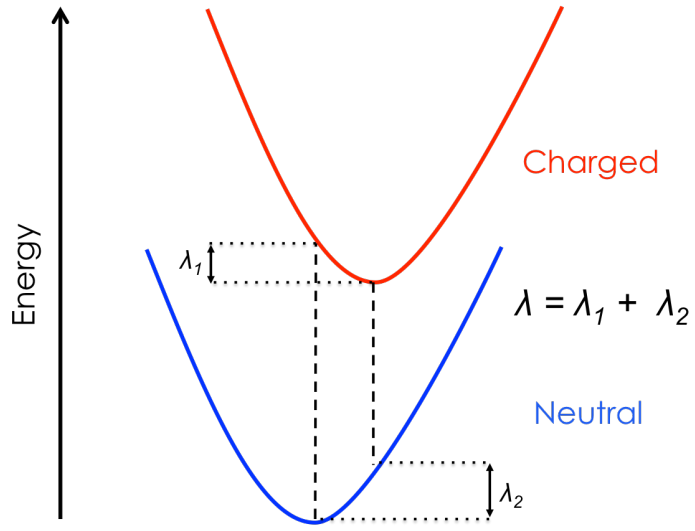

Figure 1-3. State diagram depicting the relative energy levels of a molecule in its neutral and charged (oxidized or reduced) states. The reorganization energy (λ) is made up of two parts: the energy consumed in geometric relaxation upon charging (λ_1), and upon returning to the neutral state (λ_2).

Outlined by the Frank-Condon principle, an electronic transition is often accompanied by a change in vibrational energy level due to significant wave-function overlap. This is followed by molecular relaxation to an optimal geometry. The sum of the energy associated with this relaxation in both the neutral→charged transition (λ_1) and

charged→neutral transition (λ_2) is defined as the reorganization energy (λ).[23] Density functional theory (DFT) calculations of the neutral and charged states of a molecule can be used to determine λ along with the optimal geometries taken in each state.

Since geometric fluctuations upon charging are related to intramolecular degrees of freedom, rigid molecules are traditionally pursued for high charge mobility systems. Fused aromatic systems like polyacenes have low degrees of rotational freedom and therefore have small reorganization energies associated with their transitions. As an example, by restricting torsional rotation, the reorganization energy for naphthalene is about 100 meV less than biphenyl.[25-26] Rigid molecules that are also highly planar benefit from both small reorganization energy and the ability to closely pack in the solid phase. Efficient packing increases the charge transfer integral and allows for the formation of an ordered network analogous to the covalent lattice seen within inorganic systems. Using this design approach, organic molecules with hole mobility values on the order of 10 $cm^2V^{-1}s^{-1}$ have been successfully created.[20] While the design of flat, rigid molecules has become the paradigm for high mobility materials in the organic electronics community, there are significant drawbacks to this method in terms of processability. Rigid and flat organic materials that have the ability to tightly pack in the solid state tend to suffer from insolubility, removing one of the main advantages of organic electronics. For this reason there is a delicate balance to be reached between solubility and the ability to pack efficiently in the solid state.

1.1.2 Fundamental Concepts of Organic Semiconductors

Both molecular and polymeric conjugated materials have seen continuing use within organic electronics research, and each have their own advantages and disadvantages. Discrete molecular materials are monodisperse and can be purified *via* workups traditional to organic chemistry, for example column chromatography, distillation, and sublimation. While batch-to-batch variations in yield may exist, discrete molecules can always be purified to the extent that the final materials will always be identical, facilitating their scale-up and industrial use. Polymeric materials by nature will always have a degree of polydispersity. Purification is not as straightforward as options are limited to fractionation of disperse materials through precipitation, Soxhlet extraction, size exclusion chromatography, and continuous spin fractionation. Because of this limitation there can be significant difficulty arising from batch-to-batch variations caused by changes in molecular weight and dispersity. Moreover, variations in molecular weight and dispersity are not trivial and can have impacts on both optoelectronic and mechanical properties.

The dispersity, chain entanglements, chain-ends, and existence of both amorphous and crystalline solid-state domains in polymeric systems inherently lead to a certain degree of disorder, which can be viewed as both an advantage and a flaw. Disorder can contribute to the solubility of polymeric materials, leading to favorable processing attributes, and can also contribute to a degree of mechanical malleability in thin films sought after for many flexible electronics applications. On the other hand, disorder can disturb intermolecular interactions between conjugated backbones and create charge traps, leading to decreased charge mobility. Discrete molecules have a greater tendency

towards order in the solid state; creating efficiently packed, crystalline morphologies that contribute to higher values of charge mobility. But this degree of order can cause discrete molecules to aggregate in solution, causing difficulties in solubility and therefore processability. For this reason many high performance molecular systems are processed through vacuum deposition, a high energy process that is not amenable to R2R type manufacturing. Increased crystallinity in the solid-state morphology can also make these materials brittle, inhibiting their use in flexible electronics applications, and can also lead to grain boundaries that act as charge traps.

All that being said, many of these differences between molecular and polymeric materials are continuously becoming blurred. Discrete molecules are being made larger and appended with long, aliphatic solubilizing chains that contribute to increased solubility and mechanical flexibility, while conjugated polymeric systems with rigid backbones are achieving high degrees of order and charge mobility values that rival crystalline discrete molecules. Advancements in living polymerization of conjugated polymers through chain transfer coupling techniques are also leading to polymeric materials with low dispersities, removing the difficulties arising from bath-to-batch variations. While discrete molecular systems have obvious merit in the field of organic electronics, the focus on processing of this dissertation lends itself to polymeric systems, which will be further discussed in this introduction.

1.1.3 Brief History of Conjugated Polymers

Some of the earliest research into conjugated polymers dates back to the 1960s, with Donald Weiss and coworkers observing electronic properties in doped polypyrrole[27-

[29], and the work of René Buvet and Marcel Jozefowicz on doped polyaniline[30-31]. Perhaps the most notable work came from the combined work of Alan MacDiarmid, Hideki Shirakawa, and Alan Heeger on metallic-like conductivity in iodine-doped polyacetylene.[32-34] Synthesized through Ziegler-Natta polymerization of acetylene, Shirakawa and coworkers observed the formation of a silvery film from the resulting polyacetylene. Though the neutral polymer displayed low conductivities, vapor-doping the films with iodine resulted in an increase in conductivity to ~10^2 S/cm. This seminal work kicked off the field of conjugated polymers, and earned the three principal scientists the Nobel Prize in chemistry in 2000. In the following decades, research focused on extending the oxidative polymerization of other aromatic units to create conjugated heterocyclic polymers including polythiophenes and polydioxythiophenes.

1.1.4 Creating Soluble Conjugated Polymers

Much of the early work in conjugated polyheterocycle synthesis surrounded oxidative polymerization techniques, and often involved electropolymerization of monomers onto an electrode. While useful for obtaining conjugated polymers whose electronic properties could be studied, the ability to effectively characterize the resulting materials, expand the scope of monomers beyond electron-rich aromatics, and process them in a high throughput fashion was lacking. The resulting polymers were typically insoluble in their neutral forms, and so understanding molecular weights and dispersity was not a trivial exercise. Other conjugated polymers including polyphenylenes and poly(phenylenevinylenes) were synthesized through polycondensation reactions, for instance Wittig and Knoevenagel reactions, but also produced insoluble materials. For these reasons, the field has largely moved towards soluble conjugated polymers.

Much of this progression in the 2000s focused on the attachment of side chains, typically aliphatic in structure, onto the conjugated backbone. This modification not only afforded a final polymer that dissolved in organic solvents, but provided a synthetic handle over molecular weight and dispersity. Side chains expanded the toolbox for conjugated polymer chemists and led to new families of soluble polymers based on thiophenes, dioxythiophenes, p-(phenylenevinylenes), pyrroles, fluorenes, and new aromatic monomers that were previously inaccessible. A representative set of these polymers is shown in Figure 1-4. These new families were enabled by new solution based polymerization methods, notably Grignard metathesis (GRIM) and palladium-catalyzed cross coupling polymerizations. The McCullough group's development of GRIM polymerization for polythiophenes in 1999 marked a pivotal point for the area of soluble conjugated polymers.[35] This work enabled the room temperature synthesis of poly(3-hexylthiophene) (P3HT) with controlled degrees of polymerization and regioregularity, providing researchers with a controlled conjugated polymer "fruitfly" that has served as the basis for understanding structure-property relationships across the field. In terms of monomer scope, GRIM polymerization was also limited primarily to electron-rich aromatic monomers. Advancements in palladium-catalyzed cross coupling reactions, notably Suzuki and Migita-Stille-Kosugi methods, and their application to polymerizations has largely expanded the scope of monomer breadth to include electron-deficient monomers, and has also enabled a host of new conjugated homopolymers, copolymers, random copolymers, and block copolymers. These cross-coupling polymerizations have revolutionized the area of soluble conjugating polymers, providing

the tools for an organic chemist to design new monomers and polymers with nearly endless possibilities.

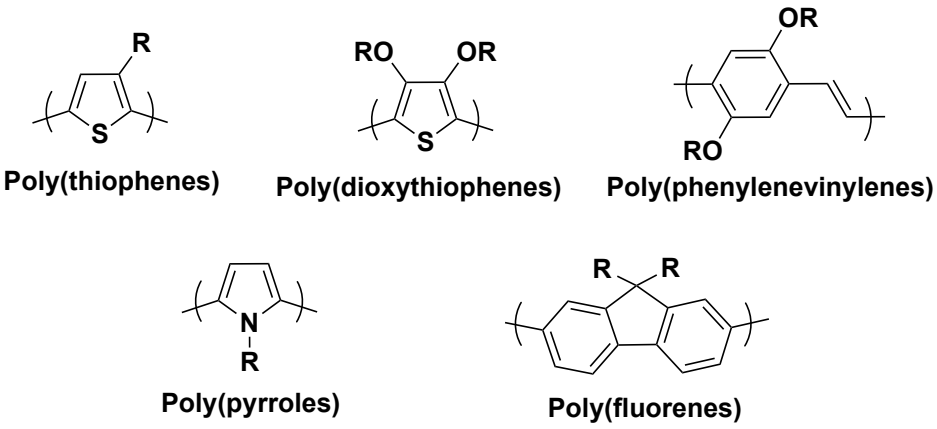

Figure 1-4. Examples of conjugated polymer backbones that were commonly transitioned into soluble polymers via attachment of side chains. The R group typically consisted of saturated alkyl chains of varying length.

Aside from these synthetic drivers for creating soluble conjugated polymers, solubility provides the ability to purify and characterize these materials using standard solution-based techniques. Final polymers can be purified of catalysts and salts used in the polymerization through precipitation, filtration, and chromatography, and can also be fractionated *via* Soxhlet extraction to reduce dispersity and obtain samples of varying molecular weight. These polymers can then be characterized in solution using common techniques like NMR, GPC, UV-vis, *etc*., providing structural information that could not be obtained through solid-state analytical techniques. Another key driver for solubility is enabling solution-based processing methods, bringing conjugated polymers into the realm of printed electronics.

1.2 Design Principles Conjugated Polymers

1.2.1 Polymer Backbone

Most optoelectronic properties of conjugated polymers stem from the attributes of the conjugated backbone, making the polymer backbone design one of the most important aspects to consider when creating new materials tailored to a specific organic electronic application. The primary handles a synthetic chemist can control in conjugated polymer backbones include conjugation length, inter-ring torsion or dihedral angles, electron density of the monomers, and the interplay between electron-rich and electron-poor comonomers in donor-acceptor architectures. Many of these handles exhibit synergistic effects, however, and so understanding structure-property relationships related to the backbone must often be thought of as a combination of these elements.

1.2.1.1 Conjugation Length

Chapter 1.1.1 introduced the concept that increasing the number of overlapping $2p_z$ orbitals leads to a decrease in E_g until the effects of BLA limit any further reduction. However, for many conjugated polymer systems the bandgap and other electronic properties can be limited by the *effective conjugation length* of the backbone. The effective conjugation length can be thought of as the minimum number of monomer units necessary to saturate the optoelectronic properties of a conjugated polymer. Bredas, Silbey, Boudreaux, and Chance found a linear relationship for E_g and ionization potential to $1/n$, with n corresponding to the number of aromatic rings in a chain.[36] This means that increasing chain length will decrease the bandgap and increase λ_{max} of the polymer absorption, but that the changes with diminish as the chain size increases, effectively

reaching a plateau. As an example, Miller and coworkers experimentally observed this trend using discrete oligomers of 9,9-di-n-hexylfluorenes from 3 to 10 units.[37] The absorption profile, shown in Figure 1-5, continuously red-shifted with increasing chain length, but by 10 units the λ_{max} already began to saturate around the level of poly(9,9-di-n-hexylfluorene) with an average length of 54 fluorene units. Using the linear extrapolation of $1/n$ to λ_{max}, the authors determined the effective conjugation length of the polymer to be ~12 fluorene units, or 24 aromatic rings. This type of analysis has also been used to estimate effective conjugation length of polyacetylene to ~30 double bonds[38], ~20 rings for polythiophene[39], and ~14 rings for P3HT[40]. One of the main explanations for differences in effective conjugation length in polymers is the presence of inter-ring torsion, of dihedral angles between aromatic monomer units, that hinder the ability for a conjugated polymer to achieve periodicity in its conjugation.

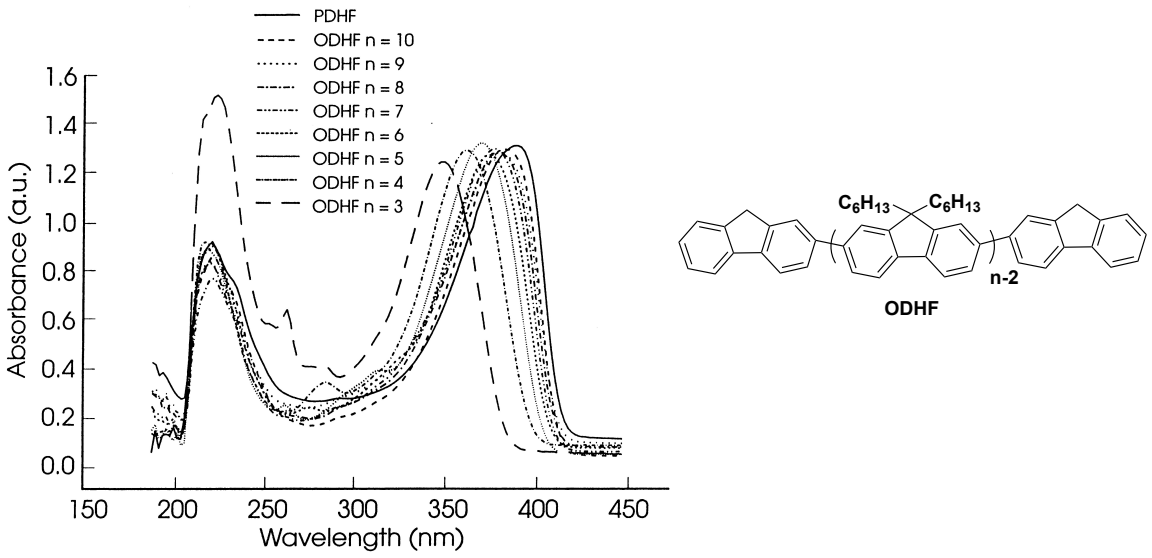

Figure 1-5. Absorption spectra of oligomers of dihexylfluorene (ODHF) of increasing length compared to poly(dihexylfluorene) (PDHF) showing the red-shifting effect of increasing conjugation length. Reproduced from reference [37].

1.2.1.2 Torsion

Torsion between aromatic rings in conjugated polymers is one of the most approachable handles a synthetic chemist can use to alter optoelectronic properties. Torsion can be manipulated most commonly through steric interactions, which can exist between aromatic units or through the substitution of aromatics with alkyl side chains. Modeling dimers of pyrrole, thiophene, and benzene show that increasing the dihedral angle between the rings leads to an increase in E_g.[41] One manifestation of this effect is seen through control over regioregularity in P3HT, where higher regioregularity lowers the E_g because of a smaller number of head-to-head couplings.[42] The steric hindrance brought on by the hexyl chains in head-to-head coupling, shown in Figure 1-6a, serves to increase the dihedral angle between thiophene rings, lowering the effective conjugation length and therefore increasing E_g. In copolymers, choice of steric interactions between comonomers can be used to tune the bandgap as well. The Reynolds group has used a series of dioxythiophene monomers to fine tune backbone planarity and achieve color control in electrochromic copolymers.[43] Moving from the small dioxy ring in 3,4-ethylenedioxythiophene (EDOT) to a larger ring of 3,4-propylenedioxythiophene (ProDOT) increases torsional strain along the backbone and leads to a decrease in planarity and extent of conjugation, leading to higher gap systems.[44] Even more backbone strain can be introduced upon moving to the acyclic monomer, 3,4-diethylhexyloxythiophene (AcDOT), demonstrated in Figure 1-6b.

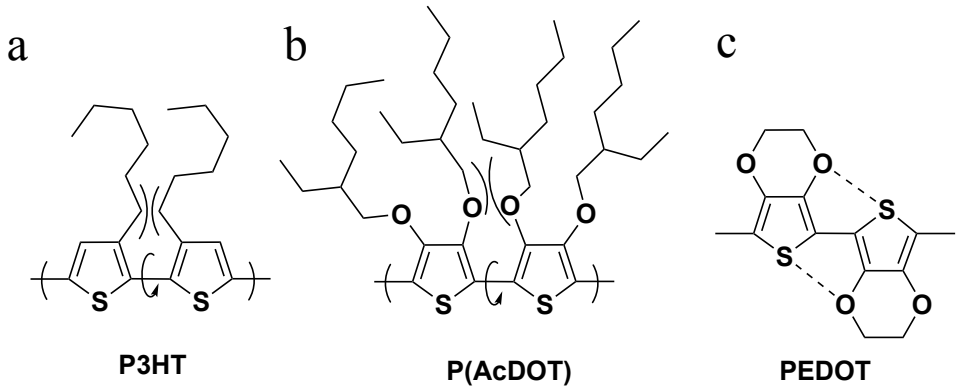

Figure 1-6. Examples of structural moieties that can affect polymer backbone torsion. Head-to-head coupling in P3HT (a) and steric bulk from branched side chains in P(ADOT) (b) can lead to significant torsion, while heteroatom interactions help to decrease torsion in PEDOT (c).

Aside from sterics caused by alkyl chains, torsion can be modified through electronic effects through heteroatom interactions. The greater degree of planarity found in PEDOT can be attributed to interactions between the sulfur atoms in the thiophene backbone and the oxygen atoms of the dioxyethylene bridge, shown in Figure 1-6c, effectively locking the backbone into coplanarity.[45] Fluorine substitution on the polymer backbone has also been shown to drive rings into coplanarity when adjacent to thiophene units.[46] Aside from working to extend the effective conjugation length and lowering E_g, decreasing inter-ring torsion to achieve a higher degree of planarity along the backbone can facilitate π-π interactions, enable a higher degree of electron donation into the backbone from donating substituents, and increase the delocalization of charge across donor-acceptor copolymers.

1.2.1.3 Electron Density

The extent to which monomers in the polymer backbone are electron-rich or electron-poor plays a pivotal role in the electronics of conjugated polymer systems.

Electron-rich monomers are more easily oxidized, contributing to a lower oxidation potential of the resulting polymer. Lowering the oxidation potential can also be thought of as raising the HOMO level of the polymer, and therefore incorporation of electron-poor monomers serves to deepen the HOMO level. Since energy levels play an important role within organic electronic applications, allowing the polymer to inject or receive electrons from adjacent materials, the electron density of the monomers that makeup a conjugated polymer is another approachable handle for organic chemists when designing new materials tailored for a specific application. Aside from the aromatic unit that builds the conjugated backbone, side chain substituents can also be chosen for their ability to donate or withdraw electrons from the backbone as a handle over energy levels.

1.2.1.4 Donor-Acceptor Copolymers

Another significant approach to tuning E_g within conjugated polymers is the use of a donor-acceptor, or push-pull, architecture along with backbone. Proposed by Havinga *et al.* and visualized in Figure 1-7, the donor-acceptor approach makes use of the orbital mixing between covalently connected electron-rich (donor) and electron-poor (acceptor) monomers to lower E_g in the resulting conjugated copolymers and push absorption out to the near-IR.[47] The built-in dipole created from the donor to the acceptor aids in the delocalization of electron density in the backbone, which has made these systems popular for BHJ OPV active layers in which the polymer is excited by ambient light and the resulting electron can be shuttled from the donor moiety to the acceptor moiety, and finally transferred to the LUMO of the acceptor (e.g. fullerene) in the blend.

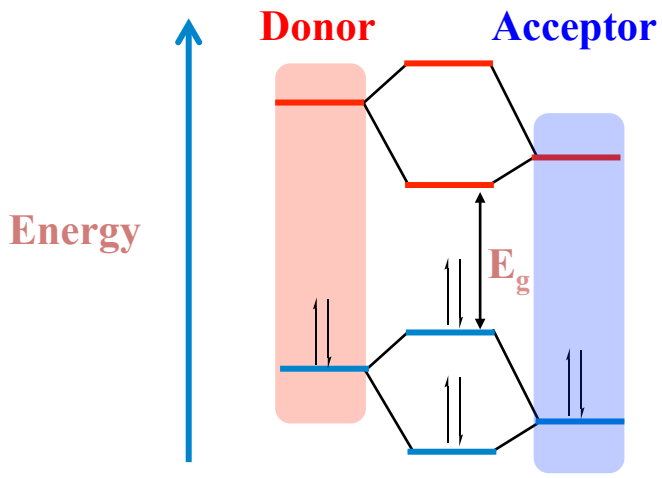

Figure 1-7. Orbital mixing diagram showing the effect of reduced bandgap (E_g) achieved when bonding an electron-rich moiety (donor) with an electron-poor moiety (acceptor). Adapted from reference [47].

1.2.2 Polymer Side Chains

As introduced in Chapter 1.1.4, the incorporation of side chains onto conjugated polymers backbones has vastly expanded the field by allowing for new structures to be synthesized through solution-based polymerizations, characterized through standardized methods, and processed *via* solution-based methods. However, solubility is just one of the many properties that can be obtained through the use of side chains. In the following section we will explore how side chains can be used to modify solubility, solid-state morphology and microstructure, materials functionality, and the interplay that exists between these properties.

1.2.2.1 Solubility

Obtaining solubility is one of the more straightforward properties achieved through side chains. Using aliphatic side chains is the most common approach used for solubility, affording materials that dissolve into organic solvents such as toluene and

chloroform. In terms of n-alkyl side chains, longer chains typically result in greater solubility as more rotational degrees of freedom are added to the structure. Branched alkyl chains can be used to enhance solubility in organic solvents without the need to increase the chain length, as the branching disrupts side chain interdigitation and also creates a chiral center, both leading to a more disordered, and more soluble, structure. Oligoether side chains can be used to impart solubility in polar solvents, and have recently proved to be promising candidates for organic electrochemical transistors (OECTs) where ionic interactions play a major role.[48] Side chains terminated with ionic groups have also been used to achieve solubility in polar solvents, notably water. These conjugated polyelectrolytes (CPEs) have seen usage across both biological applications and as interlayers and work-function modifiers in organic electronics devices.[49] Sulfonates and carboxylates are common for anionic CPEs, and pyridinium and quaternary amines are common for cationic CPEs, though many other ionic systems are also prevalent. These commonly used side chain motifs are shown below in Figure 1-8. In all of these examples, it must be noted that side chains are not simply supplemental pieces of the conjugated polymer that can be used purely for solubility purposes, but will have an impact on the polymer's structure and materials properties.

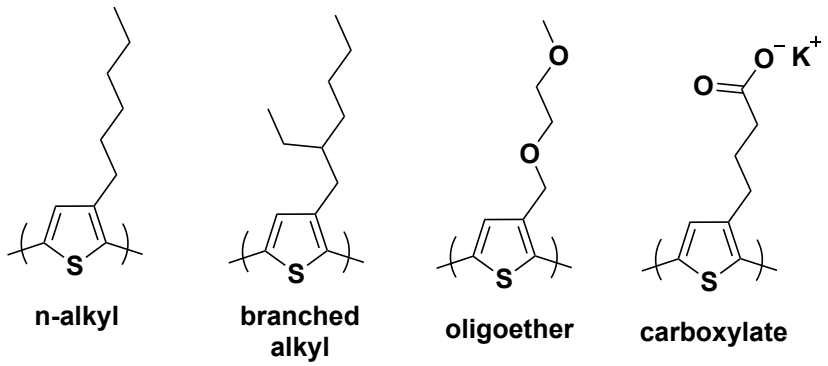

Figure 1-8. Examples of common side chain motifs found in conjugated polymer systems.

1.2.2.2 Impact on Morphology, Structure, and Optoelectronics

Side chains have been known to affect solid-state structure for some time, with evidence of interdigitation of long, aliphatic side chains on polythiophenes promoting increased crystallinity in thin films.[50] However as the field moved towards branched aliphatic side chains in efforts to further increase solubility, it became apparent that there was a complex relationship between solubility and solid-state structure. Replacing linear side chains with branched alternatives disrupts the ability to interdigitate, and while this greatly increases the solubility of the polymer, it also prevents the formation of ordered domains in the solid-state. A recent example in the Reynolds group shows an isoindigo-terthiophene polymer that achieves ~5.1% in OPV devices when using linear hexyl chains, but drops to ~0.3% when using 2-ethylhexyl branched chains due to the total disruption of solid-state order.[51] Despite the tendency to disrupt order, branched side chains are still ubiquitous in modern conjugated polymer design due to their ability to solubilize flat, conjugated molecular units, and work from the OFET community has revealed that their effect on solid-state packing can be minimized by pushing the branching point further away from the conjugated backbone.[52]

The difficulty with side chains is that their effects, beyond solubility, can be difficult to predict and are often dependent on both repeat unit structure and intended application. Copolymers containing three or four side chain sites per repeat unit are now commonplace, and each site adds another variable to contribute to the overall complexity. A notable example of the complex nature of side chain effects is the hypothesis put forward by Graham *et al.* that in donor-acceptor copolymers for use in PCBM blend OPVs, having bulky side chains on the donor moiety and linear chains on the acceptor moiety yields the optimum device metrics.[53] The idea is that the bulky side chains direct PCBM molecules towards the less sterically hindered acceptor moiety, thereby improving electronic interactions and facilitating charge transfer. While this hypothesis holds true for a handful of systems, there are certainly outliers, and it is likely there will be no universal theory for predicting how side chains will impact a conjugated polymer backbone in the solid-state. Therefore, it is important for polymer chemists to perform side chain optimization studies on new conjugated backbones and observe the effects on solid-state structure through X-ray scattering techniques like GIWAXS, GISAXS and RSOXS. While many structure-property relationships can be hypothesized, new materials will emerge in direct conflict of those relations, and ultimately much of the field is still in a state of trial and error when it comes to side chains.

Aside from morphology, side chains can also affect the optoelectronic properties by donating or withdrawing electron density and altering inter-ring torsion angles. An interesting example from Guo *et al.* shows large changes in a series of naphthalene diimide (NDI) bithiophene copolymers by varying the side chains on the bithiophene.[54] Because the side chains are arranged in a head-to-head position, bulky branched chains

create significant torsion between the thiophene units and render the polymer amorphous in the solid-state. When moving to linear chains, the torsion is decreased, leading to an increase in effective conjugation length observed by a red-shift (~38 nm) of the thin film's maximum absorption. Finally, using linear alkoxy chains leads to interactions between the oxygen on the side chain and sulfur on the thiophene backbone, causing an increase in planarity and also an increase in electron density due to the alkoxy donation. The combined effects red-shift thin film absorption max by ~278 nm relative to the branched side chain derivative. In this manner, side chains have been widely used to modify planarity and electron density to control both the absorption profile and electronic bandgap.

1.2.2.3 Functional and Reactive Side Chains

Side chains containing reactive and functional components have been used to append additional functionality into conjugated polymer designs. Common types of functionality include crosslinkability, solubility modifiers, and side chain cleavage. For crosslinking and substrate binding, azide-terminated side chains can be incorporated to react *via* click chemistry[55-56], vinylenes can be thermally initiated to crosslink[57], bromides[58], oxetanes[59], and acrylates[60-61] can offer UV crosslinking properties, and Diels-Alder units can participate in reversible crosslinking mechanisms.[62] Crosslinking conjugated polymers has been useful for achieving robust, solvent resistant films, allowing for facile orthogonal processing steps, binding the substrates and analytes, and can even be leveraged to control morphology.

Ester side chains are in interesting example of solubility modifiers. As precursors to carboxylate CPEs, they can be polymerized *via* traditional solution methods using long aliphatic chains connected to the ester, and then hydrolyzed to afford the water-soluble conjugated polycarboxylate.[63-64] After coating thin films, the polycarboxylate can subsequently be introduced to an acidic environment to create an insoluble conjugated polycarboxylic acid. Alternatively, the Frechet group has shown multiple examples of solid-state thermal cleavage of ester side chains.[65-66] These polymers could be coated from solution and heated to 200° C to cleave the esters resulting in solvent resistant conjugated polymers with pendant carboxylic acids that exhibited up to a 0.5 eV decrease in bandgap compared to their noncleaved counterparts.

Ester side chains can also be oriented in such a way that hydrolysis leads to cleavage of the carboxylate, leaving behind an insoluble, alcohol functionalized conjugated polymer backbone. Using this design, polymers have been designed that can be coated from organic solution and subsequently dipped into a basic solution to remove the ester side chains.[67] Side chain cleavage provides the ability to make use of side chains for the solubilizing properties, but then remove them in the solid-state to increase the density of conjugated backbone within thin films. Alternative approaches use silyl side chains that can be cleaved with strong acids, and *o*-nitrobenzyl units that can be cleaved *via* UV light and offer the ability to photopattern conjugated polymers.[68-70] These examples clearly demonstrate the potential for side chains to impact more than just solubility, and over the last decade researchers are just beginning to scratch the surface of the possibilities that exist within functional side chains.

1.2.3 Polymer Synthesis

The shift towards solution-based polymerizations to synthesize soluble conjugated polymers has increased the number of viable options for polymerization. As mentioned in section 1.1.4, while GRIM polymerization led the way in the early development of soluble conjugated polymers, advancements in palladium cross-coupling reactions and their use in polymerizations has vastly expanded the scope of monomers that can be incorporated into conjugated polymer architectures. While there exists a variety of cross-coupling methods, this dissertation will solely focus on Migita-Stille-Kosugi polymerization and Direct Hetero-Arylation Polymerization (DHAP) since these are the primary methods used to develop the materials presented in this work.

1.2.3.1 Migita-Stille-Kosugi Polymerization

Migita-Stille-Kosugi polycondensation is one of the most versatile polymerization methods for synthesizing high molecular weight conjugated polymers. Migita-Stille-Kosugi coupling describes the reaction between an organotin and an organic electrophile in the presence of a palladium catalyst to generate a carbon-carbon bond. Kosugi and Migita first explored the reaction in the 1970s as a means to couple organotins to acyl chlorides and aryl halides.[71] John K. Stille followed and extensively studied the reaction mechanism and substrate scope beginning in 1978.[72] Alongside the Suzuki coupling reaction, Migita-Stille-Kosugi coupling has become one of the most efficient and versatile routes to forming sp^2 carbon-carbon bonds in organic chemistry, in part because of its tolerance to a wide-array of substrates and functional groups as well as its mild reaction conditions.[73]

By the late 1980s and early 1990s, chemists began to explore the use of the Migita-Stille-Kosugi coupling reaction of distannane and dihalides to synthesize polymers.[74-76] Much of the work exploring monomer scope and optimization of reaction conditions is attributed to Luping Yu and coworkers, who synthesized a series of conjugated copolymers through Migita-Stille-Kosugi coupling.[77-78] Their work highlighted many important factors needed to obtain high molecular weight polymers, such as using a solvent that could both stabilize the palladium catalyst and solubilize the growing polymer chain, functionalizing an electron-rich monomer as the distannane and the electron-poor monomer as the dihalide, and the necessity of ligands when using Pd(II) catalysts. To this day Migita-Stille-Kosugi coupling is still a widely used method for polymerization of conjugated polymers. Reactions tend to have high yields and result in high molecular weight polymers, distannane and dihalide monomers are stable and are relatively simple to prepare, the conditions works well for polymerizing both electron-rich and electron-poor monomers, and the reaction conditions generally do not affect any additional functionality on the polymer side chains.

The general reaction mechanism of Migita-Stille-Kosugi coupling is shown in Figure 1.9. The reaction begins with the oxidative addition of the organohalide to the Pd(0) catalyst, forming the Pd(II) complex. The transmetallation step exchanges the halide of the Pd(II) complex with the R group on the organotin compounds. The final step is a reductive elimination to form the carbon-carbon bond, regenerating the palladium catalyst to Pd(0), which can enter the catalytic cycle to continue the coupling process. It should be noted that Pd(II) catalysts can be used in the process due to a reduction to

Pd(0) *via* the organotin. A thorough exploration and mechanistic study of Migita-Stille-Kosugi coupling can be found in an extensive review by Espinet *et al*.[79]

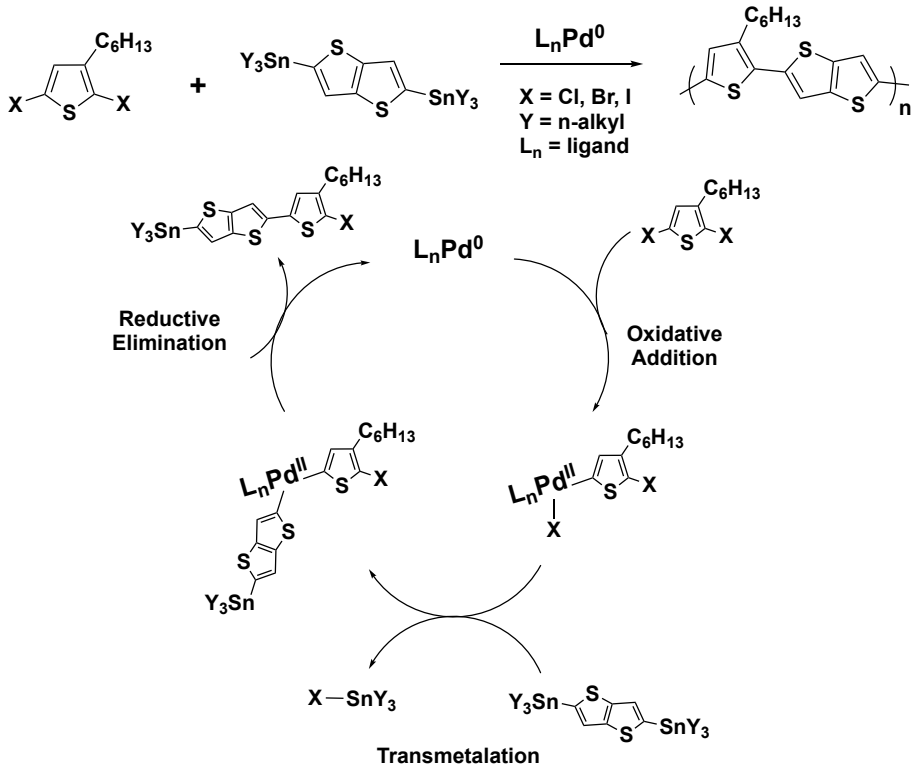

Figure 1-9. Migita-Stille-Kosugi polymerization mechanism outlining palladium cycle of oxidative addition, transmetalation, and reductive elimination. Adapted from reference [79].

1.2.3.2 Direct Hetero-Arylation Polymerization

A more recent polymerization method that has generated excitement in the field of conjugated polymers is Direct Hetero-Arylation Polymerization (DHAP). Using transition-metal catalyzed C-H activation, DHAP avoids the transmetallation step seen in most cross coupling catalytic cycles, and therefore does not require a transmetallating reagent to be attached to the monomer (e.g. stannanes and boronic esters used for Migita-Stille-Kosugi and Suzuki, respectively). Coupling through DHAP typically proceeds through a hydro group and a halide group, but can also take place between two hydro

groups through oxidative C-H activation methods.[80] Bypassing the requirement of adhering transmetallating functionality onto monomers reduces the number of synthetic steps needed, and can also reduce the environmental and safety hazards associated with transmetallating reagents like organotins. Additional benefits include shorter reaction times needed to reach high molecular weight polymers, and in some instances improved electronic performance due to minimal organometallic impurities.[81] However, DHAP can be highly sensitive to monomer choice and reaction conditions. While traditional Migita-Stille-Kosugi polymerization conditions are tolerant to variations in temperature, concentration, and catalyst loadings, DHAP can require careful optimization to successfully obtain high molecular weight polymers, and many times it will not work at all with certain monomers.

The general DHAP methods have been used since the 1970s to form carbon-carbon bonds in molecular systems, but it was not until the past decade that the methods became popular for synthesis of conjugated polymers.[82-84] In 2010 the Ozawa group reported the use of DHAP on a 2-bromo-3-hexyl thiophene monomer with a palladium catalyst to produce high molecular weight, regioregular P3HT.[85] In the following years, the groups of Leclerc, Thompson, Kanbara, and Sommer have pioneered these techniques, explored the monomer scope, and optimized reaction conditions to synthesize a wide array of conjugated polymer systems through DHAP.[86] The proposed catalytic cycle for DHAP is shown in Figure 1-10. The cycle is similar to what is accepted for Migita-Stille-Kosugi coupling, with oxidative additions and reductive elimination steps remaining the same. The key difference between the two is the C-H activation step in place of a transmetallating step. The generally accepted mechanism of this C-H activation

is referred to as a concerted metalation deprotonation, where the Pd complex can coordinate with a π system to form a six membered intermediate, which then simultaneously transfers a proton from the dihydro monomer ring to the carboxylate and the electrons from the C-H bond move to form a bond between the carbon and Pd atoms.[87]

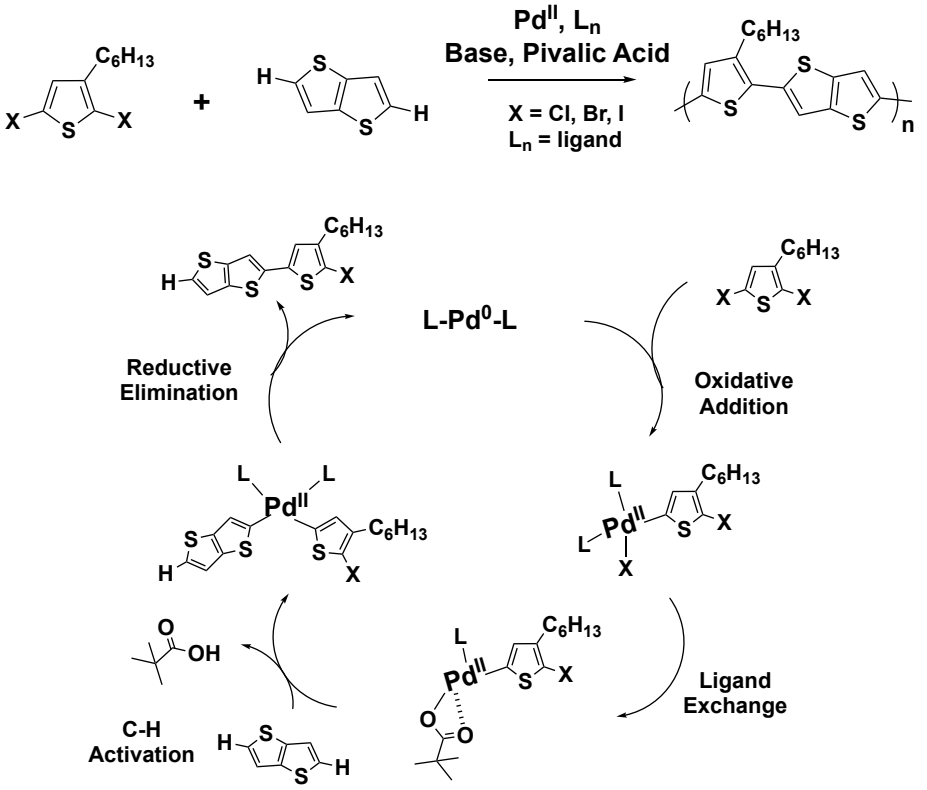

Figure 1-10. Direct Hetero-Arylation polymerization mechanism outlining palladium cycle of oxidative addition, ligand exchange, C-H activation, and reductive elimination. Adapted from reference [87].

Conditions for DHAP polymerization follow two different trends, one using a Pd(II) catalyst with the addition of a phosphine ligand in solvents with low dielectric constants (THF, toluene, dioxane), and the other using Pd(II) catalysts without a phosphine ligand in solvents with higher dielectric constants (DMAc, NMP, HMPA). The

former proceeds at a slower rate, potentially due to the lower solubility of the catalysts and the lower stability of C-H activation transition states in less polar solvents. The phosphine ligands in this method presumably facilitate the solubility of the catalyst system and aid in the stabilization of transition states. The latter proceeds at a much faster rate due to the increased solubility of the catalyst and stabilization of C-H activation in more polar solvents. However, this acceleration of the catalytic cycle can lead to C-H activation on non-desirable sites, leading to defects, branching, and crosslinking in some cases.[88] For this reason, the polar solvent reaction conditions are typically preferred for monomers without additional reactive C-H sites, notably sites at the β position to the desired activation site. Owing to its relatively short lifespan as a polymerization technique, DHAP is still being actively studied for new conditions and monomer scope, as its benefits over Migita-Stille-Kosugi and Suzuki polymerization make this method an exciting new opportunity in the conjugated polymer community.

1.2.3.3 Impact of Molecular Weight and Dispersity

Lack of control in terms of molecular weight and dispersity made the early development of structure-property relationships in conjugated polymers challenging, with the same polymer showing orders of magnitude differences in performance in organic electronic device testing. The synthetic developments that provided increased control over molecular weight and dispersity in conjugated polymers, namely McCullough's synthethis of regioregular P3HT, has since enabled researchers to study the effects of these variables on physical, morphological and optoelectronic properties. The most noticeable physical properties affected by MW are solubility and aggregation. High MW polymers tend to aggregate, which can lead to lower solubility in organic solvents.

Increased aggregation can also be noted in the UV-vis spectra of conjugated polymers, in which higher MW polymers are often red-shifted to lower bandgaps than their lower MW counterparts due to increased aggregation. While the extent of aggregation may increase with molecular weight, the absorption profile of conjugated polymers generally remains unchanged. Slight red-shifting can be observed, but typically the changes saturate at the effective conjugation length, which happens for many conjugated polymers at around ~10-20 kDa. For redox applications like electrochromism and charge storage, electronic properties also saturate around this MW.

The most pronounced effects of MW in conjugated polymers are observed for morphology and charge mobility. An early example from the Frechet group found that mobility values in P3HT based OFETs increased from 1.7×10^{-6} to 9.4×10^{-3} $cm^2V^{-1}s^{-1}$ as the MW is increased from 3.2 to 36.5 kDa.[89] The authors hypothesized that higher crystallinity would boost charge transport, but found that the higher crystallinity, low MW polymers exhibited lower mobility than the more amorphous high MW polymers. The low MW polymers formed well-defined crystallites in thin films, but the crystalline domains followed no preferred orientation, leading to a large amount of grain boundaries that could serve as charge traps. Brinkmann *et al.* subsequently determined that low MW P3HT essentially exists in a "fully extended" rigid rod state, while high MW P3HT contains both "fully extended" domains and amorphous domains that contain chain folds, chain ends, and tie-molecules.[90] The general hypothesis was that longer polymer chains could carry a charge further through a film before necessitating a hopping event to another chain, and that limiting the occurrence of hopping events increased charge mobility. This hypothesis has been reaffirmed as newer conjugated polymers, notably

more disordered polymers, have emerged and followed the same trend of increased mobility with increased molecular weight. In a comprehensive study by Noreiga *et al.,* the authors put forward the hypothesis that high mobility in conjugated polymers is obtained when a series of crystalline, aggregate domains are interconnected *via* long tie-molecules, as portrayed in Figure 1-11.[91] By this logic, high MW is essential to achieve this optimal morphology, and therefore to achieve high charge mobility.

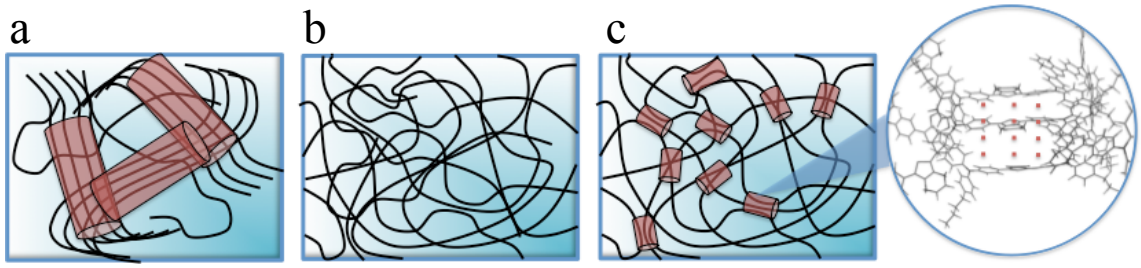

Figure 1-11. Schematic representation of polymer microstructure in highly ordered films (a), amorphous films (b), and disordered films with tie-chains connecting local aggregates (c).

Building off of this hypothesis, the Salleo group sought to understand whether this optimal morphology could be obtained by mixing crystalline low MW P3HT with a small amount of high MW P3HT to serve as tie-molecules.[92] Using a combination of computational modeling, XRD data, and OFET device statistics, the authors instead found that the presence of any amount of low MW P3HT (~8 kDa) blended with high MW P3HT (~61 kDa) was detrimental to the charge mobility. However, a medium MW P3HT (~29 kDa) could be blended with the high MW polymer in any ratio without affecting the charge mobility values. The authors hypothesize that polymers below their *disorder threshold*, the MW in which changes in crystallinity and charge mobility with respect to MW begin to plateau, can act as low mobility charge traps even when

connected by longer tie-molecules. This work emphasizes the importance of not only having high MW, but also having a narrow dispersity in which the low MW fractions are still about the *disorder threshold*.

Molecular weight effects are also seen in OPV devices of conjugated polymer and fullerene blends.[93-96] While many of the effects are caused by the aforementioned impact to morphology and charge mobility, the relationships become significantly more complex as variables like domain size, purity, and orientation are affected by changes in MW. Unlike neat polymers for OFETs, donor polymers for OPV applications show peak performance at an optimal MW, typically between 30-60 kDa, before encountering device problems at very high MW.

1.3 Solution Processability

The ability to process conjugated polymers from solution is one of the dominant differentiators from inorganic electronic materials, so it is meaningful to address the needs of various solution-based processing techniques when designing new conjugated polymer systems. The following sections will explore the different methods of solution processing and delve into their unique requirements, and will also detail how conjugated polymer inks are formulated and characterized for their use in thin-film, printed electronics.

1.3.1 Printed Electronics

Printing is a general term that covers a variety of solution-based processing methods that use inks to deposit material onto a substrate. The scope of printing is broad

and diverse, covering small format applications (e.g. desktop inkjet printers) up to large format applications (e.g. newspaper printing press). While printing is most commonly used for graphics applications, the advent of solution processable organic, metal nanoparticles (Cu, Ag, Au), and metal-oxide electronic materials has developed a nascent industry of printed electronics. The ability to print electronic components has captured the imagination of many researchers and innovators due to several core advantages over traditional inorganic electronics. Possibly the most alluring prospect is the ability to print onto nearly any substrate, ranging from rigid glass surfaces to flexible plastics even paper based substrates. This development would bring electronic functionality to places and products that are currently not viable, and would also change the nature of product design, where engineers currently must accommodate for rigid, sometimes bulky electronic components.

The other revolutionary prospect of printed electronics is the decrease in cost, time, and waste associated with the manufacturing of electronics. Manufacturing of traditional semiconductors typically involves very high temperatures ($> 600^{o}C$) for long periods of time, a large number of sequential steps performed in a cleanroom, etching with hazardous acids, energy intensive vacuum steps, and often make use of rare-earth metals that are becoming increasing sparse and expensive. Rare-earth metals also typically involve their own energy intensive processes involved in their mining and purification. On the other hand, organic semiconductors are versatile and synthetically tunable. While some may involve a number of energy intensive and atom inefficient synthetic steps to produce, there is a push within the field to move towards simpler architectures with inexpensive and widely available starting materials.[97] Printing from

solution is also a much faster and lower energy method of processing in comparison to inorganic semiconductor production and doping.[98] Printing can often take place at room temperature, produces small amounts of hazardous waste, and can be performed rapidly using R2R techniques.

1.3.1.1 Motivation for Roll-to-Roll Processing

Roll-to-roll (R2R) processing describes a host of processing techniques that can be applied to a reel of substrate in a continuous fashion, providing high throughput results similar to an assembly line. Often seen in the graphics printing and coating industry, the term derives from the use of rollers to wind and unwind reels of substrate through various processes such as coating, curing, drying, laminating, and cutting.[13] It should be noted that R2R describes specific techniques of the substrate being unwound from a roll at the beginning of the process and rewound to a roll at the end, but similar continuous processing methods can also be achieved via sheet-to-sheet, sheets-on-shuttle, and roll-to-sheet methods depending on the specific application.[99] While these methods vary in terms of speed, accuracy of printing, versatility, complexity, and machine costs, they essentially describe the idea of continuous processing of inks onto mobile substrates, and for the purpose of this dissertation will be consolidated into the term continuous printing (CP).

The primary motivation for achieving CP processability in organic electronics is low costs compared to traditional inorganic semiconductors. One driver of cost reduction is the speed and high throughput nature of CP. Manufacturing of integrated circuits using inorganic semiconductors like doped silicon can take multiple days to multiple weeks, and the throughput of the process is limited to batches of wafers that are standardly 300

mm. In contrast to this process, CP manufacturing can be performed using substrates that are hundreds of meters long, moving at speeds of 1 – 60 m/s through sequential processes, allowing for many more devices to be produced in a much shorter period of time.

Another driver of cost reduction comes from lower energy inputs to the overall manufacturing process. High temperature inputs would likely be limited to drying and annealing, both of which could take place below 200^{o} C. Processes under vacuum would also be limited and often eliminated, decreasing the energetic costs associated with maintaining low pressure. The goal of CP manufacturing of organic electronics is to perform these processes in an ambient environment, which would not necessitate the use of inert gas enclosures that add a significant amount of energy to maintain. Finally, since the process is performed rapidly, manufacturing equipment would not need to be run for as long to attain a large amount of product, further decreasing energetic costs per unit.

The last driver of cost reduction comes from the decreased capital investment needed to develop a CP line. As previously mentioned, investment in a cleanroom would not be necessary and most of the process can be performed in ambient environments. Since CP techniques are ubiquitous in the graphics printing industry, there is also the possibility of converting existing graphics printing lines into organic electronics printing lines. For most flexible substrates, purchasing rolls of material is typically cheaper than pre-cut substrates, and aside from the inks that are being deposited, there would be a minimal amount of supplementary chemicals needed to run the process. All in all, while setting up a CP manufacturing line for organic electronics would by no means be inexpensive, the amount of specialized, dedicated, and high-energy equipment that would

need to be purchased is less than what is commonly found in semiconductor manufacturing facilities.

It should also be noted that CP manufacturing would excel at producing inexpensive electronic materials that do not necessarily require high performance. Printed integrated circuits are far behind in terms of the complexity and number of transistors compared to the wafers produced through traditional semiconductor fabrication, and so printed electronics will not likely fully displace the need for traditional semiconductor manufacturing. Rather, these low cost printed electronic components could find their own market in niche and commodity sensors, integrated circuits, displays, photovoltaics, and photodetectors.

1.3.1.2 Motivation for Continuous Processing

Spin-coating and drop casting techniques, while common deposition methods for research labs working with small area devices, are not amenable with CP methods. It is therefore important to address the needs of CP compatible methods and simulate those methods on research lab scales in order to effectively design organic electronic devices that have the capacity to be scaled up outside of a lab. The most common CP compatible deposition methods include blade-coating, slot-die coating, screen-printing, gravure printing, flexographic printing, inkjet printing, and aerosol spray coating, all of which are briefly discussed below.

Blade Coating: Also referred to as knife coating, this coating technique is one of the most widely used CP methods in the organic electronics literature due to its ease of simulating on a research lab scale. Shown schematically in Figure 1-11a, blade coating is contact-

free method where the ink is supplied to one side of the blade and fills the narrow gap between the blade edge and the moving substrate. As the substrate moves it is continuously coated by the ink that exists within the blade gap, and film thickness can be modulated through adjustments to the blade gap and the speed of the substrate. This technique is commonly simulated in research lab environments by affixing the blade to a motor and passing the blade across a fixed substrate. Blade coating has been optimized in several research labs for the active layers in OPVs, OFETs, and ECs, and has achieved comparable properties to what is found for spin-coated devices.[100-102]

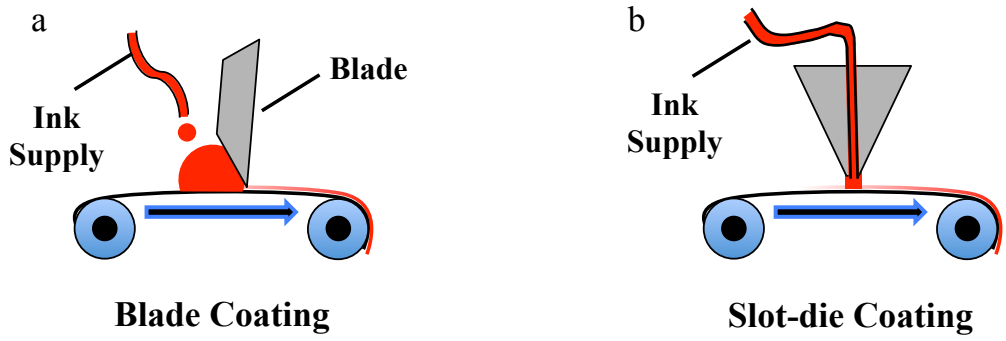

Figure 1-12. Schematic of CP methods for blade coating (a) and slot-die coating (b).

Slot-Die Coating: Similar to blade coating, this technique is a contact-free printing method where a meniscus of ink is applied to a mobile substrate. However, instead of using a blade with a small gap to form the ink meniscus, a coating head continuously pumps ink to fill the meniscus and coat a thin film, as shown in Figure 1-12b. Slot-die coating can be advantageous over blade coating due to its ability to pattern well defined strips of material while creating very little ink waste.[103] While this deposition methods is not as easily accessible for research lab prototypes, several groups have created pilot lines using slot-die coaters to fabricate large area OPV devices, light-emitting electrochemical cells (LECs), and OFETs.[104-107]

Screen-Printing: This technique makes use of a patterned mesh screen laid over the substrate, with inks being squeegeed over the screen to force the ink into the open spaces of the mesh, creating thin films with defined 2D patterning as shown in Figure 1-13a. An advantage of screen-printing is the ability to print patterned films, which is especially useful for printing electrodes in organic electronic devices. For this technique to be successful, high viscosity inks with shear thinning properties are necessary. Screen-printing is not common for research labs developing new materials, but the method has been demonstrated as a means to print OPV electrodes, active layers, and interlayers, electrodes of OFETs, OLED active layers, and electrodes and electrolyte layers in ECs.[108-112]

Gravure and Flexographic Printing: Both of these techniques share similarities in that a patterned roller is used to deposit inks onto a substrate. Gravure printing uses a hard metallic roller engraved with a pattern of cavities that pick up ink and utilize surface tension to transfer it to a substrate, shown in Figure 1-13b. Flexographic printing uses a soft polymeric roller where the desired pattern stands out as a relief, much like a traditional rubber stamp, as seen in Figure 1-13c. This roller picks up inks and subsequently stamps it onto a substrate through direct contact. Both techniques are fairly common in graphics printing, making organic electronics adaptation of these techniques highly desirable. Gravure printing has been used for the electrodes, dielectric, and polymer semiconductor in OFETs, OPV active layers, and PLED emitting layers.[113-115] Flexographic printing is less commonly seen in the literature, but has been used for OPV active layers and electrodes, along with dielectrics and electrodes for OFETs.[116-118]

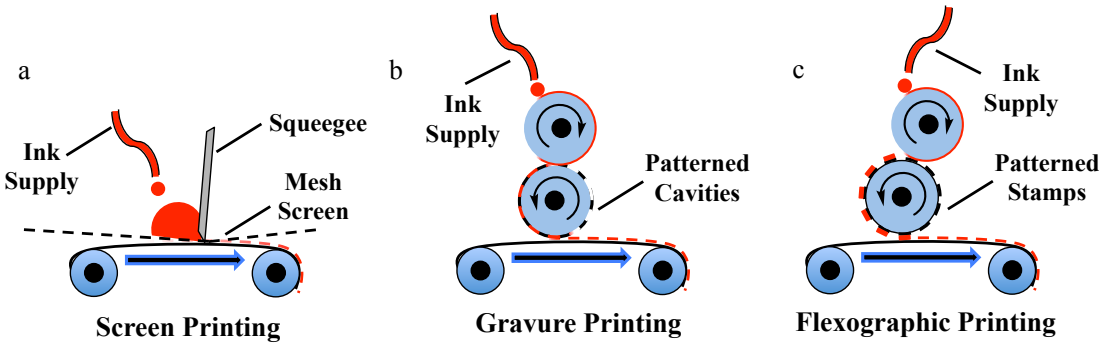

Figure 1-13. Schematic of CP methods for screen printing (a), gravure printing (b), and flexographic printing (c).

Inkjet Printing: Unlike the previously mentioned techniques, inkjet printing is a fully digitalized form of non-contact printing with the ability to generate custom patterns on demand. These printers commonly used drop-on-demand methods, where a piezoelectric material is used to dispense ink droplets from a nozzle in areas of the substrate dictated by the inputted digital file, shown in Figure 1-14a. Inkjet printers are commonly found in small-scale digital printers, including some desktop printers, and are just beginning to be seen for large area, high throughput printing as many graphics industries are transitioning towards digital. The main advantage of inkjet printing is that deposition patterns can be easily switched between runs, and unlike other 2D patterning methods like screen, gravure, and flexographic printing, inkjet does not require dedicated screen, plates, or rollers for each individual pattern. However, applying inkjet printing to CP manufacturing is relatively new, and therefore has some limitations in processing speed. Ink formulation also presents difficulties for organic electronic inks, as achieving the correct viscosity without clogging the nozzle can be challenging. That being said, inkjet printing has been demonstrated for printing entire OPV devices including silver nanowire electrodes, EC active layer inks, and entire OFET devices.[119-121]

Aerosol Spray Coating: This method involves atomization of inks through pneumatic-spray nozzles, where pressurized gas dispenses the ink solution as droplet particles as seen in Figure 1-14b. Spray processing can be heavily influenced by the ink properties, pressure of the gas, distance from the substrate, coating speed, and number of additive layers. Spray coating can be highly amenable to CP methods, but is not ideal for patterning, as a shadow mask is necessary. This method is ideal for covering entire substrates, and for applications where electronic performance is not highly dependent on drying and film formation kinetics, like OPV blends and OFETs. Spray processing is most often seen in EC applications, where the Reynolds group has made extensive use of the method.[122] The method has also been found within to OPV literature to coat active layer blends.[123]

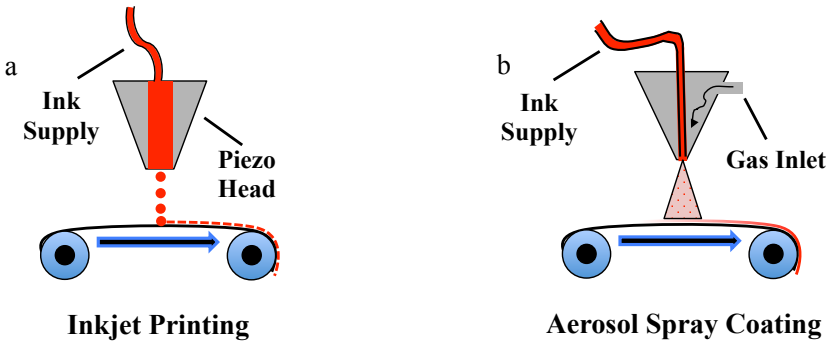

Figure 1-14. Schematic of CP methods for inkjet printing (a), and aerosol spray coating (b).

1.3.1.3 Defining Material Processability Metrics

When designing new organic electronic inks, it is important to think beyond performance and to consider the material's processability. As a hypothetical example, if an OPV active layer ink produces record high efficiencies, but requires drop casting from dichlorobenzene at 200^{o} C within an inert environment to achieve those efficiencies, it is

not the optimal material to consider for scaling up production. Unless the material were to rival efficiencies found in silicon based solar cells, it should not be forgotten that the real value of organic electronics does not come from high performance, but rather from their advantages in processability. Discussed below is a selection of important processability metrics to consider when designing and processing new organic electronic materials.

Solubility: Perhaps one of the most well-understood processability metrics in way of material design is solubility. Solubility is central to the field of printed electronics as it allows for inks to be formulated and printed in the myriad of deposition methods mentioned in the previous section. Typically higher degrees of solubility are sought after, allowing for inks of higher concentration and viscosity to be formulated. Many deposition techniques require high viscosity, and so the ability to make concentrated solutions of highly soluble materials facilitates their versatility in various printing methods.

Environmental Health & Safety: Aside from the general solubility of the material, it is also important to consider the safety of the type of solvents needed to achieve solubility. Many research labs make use of chlorinated solvents such as chloroform, chlorobenzene, and dichlorobenzene as the carrier solvent in their organic electronic inks. When considering industrial scale-up, these solvents raise many concerns in terms of their toxicity, environmental hazards, and in some cases flammability. These risks would require many checks to be put in place to contain their dangers to employees and the environment, and in many cases would be a hindrance to their adoption by the graphics printing industry. For this reason it is essential for materials designers to move towards

solvents that are less dangerous and more common in the printing industry, such as xylenes and THF derivatives or polar solvents such as alcohols, esters, and even water.

Reproducibility: Designing materials and ink formulations that produce the same thin film morphology and achieve the same optoelectronic properties over a wide area and across various processing variables is a difficult but important task. Reproducibility is vital to the success of the industrial scale-up of printed electronics since the resulting devices will be marketed and sold. Achieving reproducible thin films can be especially challenging with organic electronic materials, as it is often the case that a property is directly linked to a specific morphology and microstructure, which can be highly dependent on processing variables like ink concentration and viscosity, temperature, coating speed, drying rates of carrier solvents, deposition method, and the presence of additives. It is therefore important in this field to report averages of device performance with a standard deviation value that represents a large data set to accurately portray the reproducibility of the materials under investigation.

1.3.2 Processing Conjugated Polymer Inks

Conjugated polymer inks can be characterized in solution and thin film solid state to gain an understanding of the relationship between ink formulation, processing conditions, and the resulting thin film morphology. These studies can be useful to determine the optimal carrier solvent, processing temperature, and other processing conditions needed to achieve high performance thin films.

1.3.2.1 Characterization of Polymer Solutions

While basic chemical structure characterization can be determined through NMR and GPC experiments, UV-vis characterization of conjugated polymer solutions can be a powerful tool for understanding a material's processability. Mainly, UV-vis absorption spectra can be useful for understanding the extent to which a polymer tends to aggregate in a particular solvent system. It has been observed within OPV active layer blends that polymer aggregation in solution can play an important role in the resulting thin film morphology formed after deposition.[124] While aggregation can lead to decreased solubility and difficulty in room temperature processing, it can also template thin film morphology to enhance order across polymer chains.

Polymer aggregation can commonly be observed in solution UV-vis as a red-shifted absorption spectrum that contains multiple features. These features can represent multiple polymer aggregates that have unique optical bandgaps caused by differences in their polymer-polymer interactions, with highly ordered aggregates achieving lower bandgaps. These features can be confirmed as aggregates through variable temperature UV-vis experiments, in which absorption spectra are recorded at multiple temperatures. Shown in Figure 1-15 is variable temperature UV-vis data collected by the Yan group on their high performing PCE-11 polymer.[125] While the lower temperature solution spectra resemble the solid-state film spectrum, increasing the solution temperature leads to a blue shifting of the absorption and a loss of noticeable peak features. To obtain the solubility needed to spin coat this polymer, the solution had to be heated to 85^{o}C prior to deposition, accessing the less aggregated state. However, the authors found that the optimal substrate temperature was 70^{o}C, allowing for aggregates to form while the film

dried, while higher substrate temperatures of 110°C led to a decrease in PCE from 10.2% to 3.6%. In this instance any many others, observation of polymer aggregation behavior in UV-vis absorption profiles allowed for an understanding of optimal processing conditions.

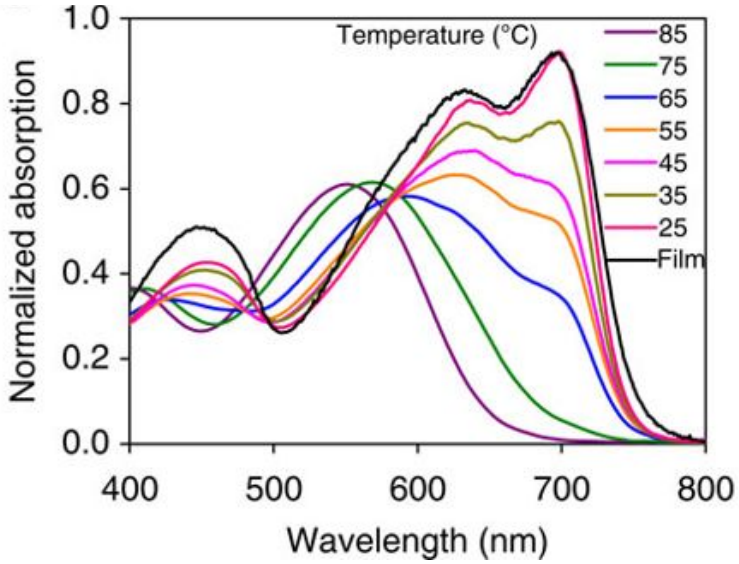

Figure 1-15. Solution thermochromism of PCE-11 in *o*-dichlorobenzene showing aggregation peaks diminishing with higher temperatures. Reproduced from [125].

1.3.2.2 Characterization of Polymer Thin Films

Characterizing the solid-state morphology and microstructure of conjugated polymer thin films is the most informative method for developing relationships between polymer structure, processing, and material properties. Figure 1-16 summarizes some of the relevant morphological features in the systems and the length scales in which they can be observed. Some of the smallest features, polymer-polymer lamellar and π-stacking, are arguably the most important to conjugated polymer properties due to their relevance across many applications. Some of the larger length-scale features are important for characterizing the formation of long-range order through fibular networks of polymer

chains and for observing the presence of crystalline and amorphous domains, but are typically much more relevant when looking at phase separation and domain sizes of polymer blends or polymer/molecular blends. These length scales can be probed through X-ray measurements, particularly Grazing Incidence Wide Angle X-ray Scattering (GIWAXS) and Grazing Incidence Small Angle X-ray Scattering (GISAXS).

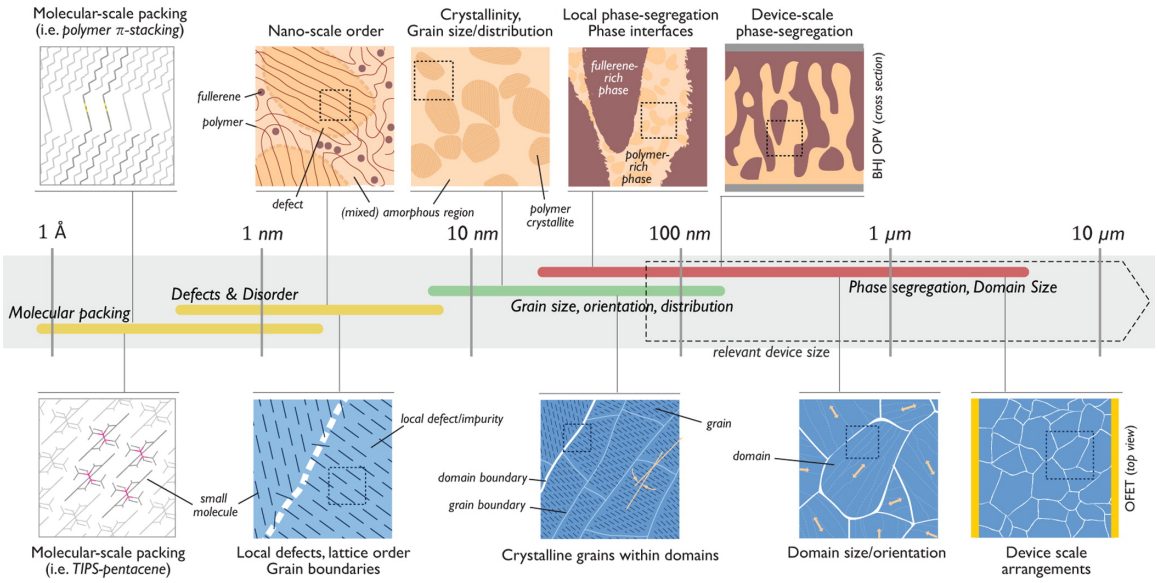

Figure 1-16. Size scale of morphological features relevant to organic electronic films. Reproduced from [126].

Molecular scale features of polymer repeat units such as inter-ring torsion and steric bulk dictate polymer-polymer, polymer-molecule, and polymer-substrate interactions in the solid-state, which in turn have large effects on electronic properties like charge transport, charge delocalization, and optical absorption.[127-128] GIWAXS measurements can be used to observe these interactions, and is therefore a powerful tool for developing structure-property relationships in conjugated polymers. An example of the diffraction patterns and their interpretation is shown in Figure 1-16 for the highly ordered polymer PBTTT. The peaks seen closer to the origin (lower q, larger length

scales) are attributed to lamellar stacking across polymer backbones, and are often strongly affected by the presence of side chains. The peaks seen further out (higher q, smaller length scales) are attributed to π-π stacking of aromatic units in the backbone, and are strongly influenced by backbone planarity. The placement of these peaks can be used to determine the spacing between polymer backbones and π systems. Whether these peaks lie on the q_z or q_{xy} axis denotes the directionality of these interactions with respect to the substrate. Figure 1-17a shows powder-pressed PBTTT, which adopts a randomly oriented arrangement, causing the lamellar peaks and π-π stacking peaks to appear as isotropic arcs.

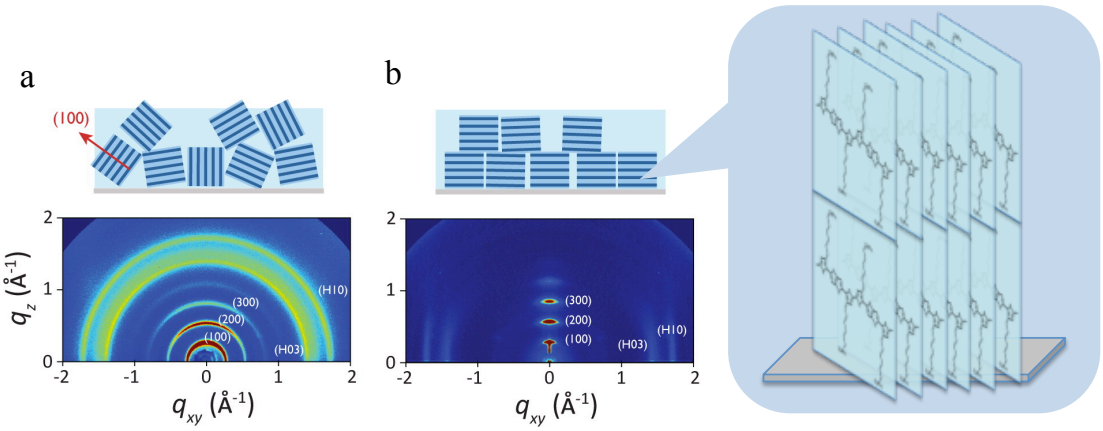

Figure 1-17. GIWAXS diffraction pattern analysis example using PBTTT pressed from powder (a) and spun coat from solution (b). Inset shows the edge-on packing arrangement of PBTTT that leads to the highly anisotropic scattering seen in b. Adapted from [126].

Figure 1-17b shows a thin film of PBTTT from spin coating, which adopts an edge on confirmation, meaning the π-π stacking plane is parallel to the substrate. The opposite configuration (lamellar peaks on q_{xy} and π-π peaks on q_z) would denote a face-on orientation, where the π-π stacking plane is perpendicular to the substrate. Directionality can play an important role in the nature of charge transport within a

conjugated polymer film, with edge-on often facilitating transport across a substrate (relevant for OFETs) and face-on facilitating transport through a film (relevant for OPVs).

When dealing with blends of polymers or polymers and discrete molecules, GISAXS can be a useful method for obtaining details about domain sizes and purity. In these blends, phase separation of the materials leads to separate domains of the pure materials as well as domains where the materials are intermixed. GISAXS can be used to approximate the sizes of those domains and the degree to which they are pure or mixed. This is especially relevant in OPVs, where the specific morphology between a conjugated polymer and a fullerene molecule has a large impact on device performance.[129-130] Other common methods for probing longer length scales include Atomic Force Microscopy (AFM), which can be used to analyze surface morphology features on the lengths of hundreds of nanometers to microns, and optical microscopy, which can be used to view surfaces on the lengths of microns to hundreds of microns. While these are surface measurements, they can often be used in conjunction with GIWAXS or GISAXS to corroborate morphological features.[51]

1.3.2.3 Influence of Processing Parameters

Although structural design of polymer repeat units can play a primary role in solid-state morphology and microstructure, the methods in which thin films of these polymers are processed can also play a major role. Processing variables that can affect morphology and performance include: carrier solvent, solvent additives, solvent concentration, temperature of ink when processed, temperature of substrate when

processed, temperature after processing (annealing), and deposition method. The difficulty with these variables is that they are numerous and often do not have a universal relationship linked to morphology, meaning they need to be optimized for every new material. For instance, Neher *et al.* observed mobility differences between annealed and as-cast films of P3HT, while Sirringhaus *et al*. also observed differences in P3HT mobility due to solvent choice.[131-132] In both cases the differences were as large as an order of magnitude. Even spin-coating speed has been shown to noticeably affect polymer mobility.[133] Using additives such as diiodooctane, diphenylether, and chloronaphthalene have been used to alter crystallization kinetics to obtain a favorable morphology in both OPV and OTFT applications, but this addition can also be material dependent and often serves to add a new variable to the equation.[134-135] There are numerous examples of the large effects that changes in processing conditions can affect throughout the literature, most of which can be found in supporting information or simply not published because the conditions led to poor results. The strong dependence on specific processing variables is one of the greatest challenges in the commercialization of new organic electronic materials, and is a challenge that may prove difficult to overcome.

1.4 Thesis of Dissertation

The significance of processing and its effects on the performance of organic electronic devices cannot be overlooked. Since the inherent value of organic electronics lies within their ability to be scaled up at lower costs than inorganic semiconductors, the performance gap between small area, research lab scale devices and large-area R2R manufactured devices must be addressed. With many fundamental structure-property relationships in place, the next step in this field is to prepare new materials for use in

large-scale, high-throughput printing facilities where reproducibility, tolerance to the environment, safety, and sustainability will all play a pivotal role in the ultimate success of conjugated polymer based electronics. This dissertation explores how to achieve that next step through the use of *processing components,* or structural moieties that embed a desired processing property. While this gap between small scale and large scale processing will undoubtedly require the attention of device engineers who can optimize processing variables, organic chemists can alleviate their challenges by designing materials with processability in mind. *Processing components* can take on several forms, ranging from modifications to the polymer backbone to the polymer side chains. These components can be utilized to enhance solubility, reproducibility, and the safety of formulated inks. Through conjugated polymer modification with *processing components*, this dissertation seeks to answer the question, "Can processability be designed into conjugated polymers without negatively impacting performance?"

Chapter 2 will describe the molecular and polymer syntheses that have enabled the work discussed within this dissertation. Materials characterizations involving chemical structure, solid-state structure and morphology, optical, electronic, and thermal properties will be reported. Device design, fabrication, and testing methods will be outlined for OFETs, OPVs, PLEDs, SCLC, and electrochromics. Specific detail will be given to the methodology surrounding the production and processing of polymers with *multistage side chains*.

Chapter 3 describes the use of triphenylamine as a *processing comonomer* in a family of four triphenylamine copolymers. The triphenylamine comonomer templates an amorphous thin-film morphology by embedding backbone torsion and conjugation

breaks, providing reproducible films that are tolerant to fluctuations in processing conditions. This chapter will provide background on disordered conjugated polymers, the motivation for creating amorphous conjugated polymers, as well as the challenges and pitfalls of this approach.

In Chapter 4, an argument will be given for using environmentally benign solvents in conjugated polymer processing, and will detail the background of strategies for both aqueous and nonhalogenated solvent processing. A novel approach through the use of *multistage side chains* will be presented as a means to enable aqueous processing of conjugated polymers. A proof-of-concept polythiophene multistage polymer will be used to teach the concept and methodology surrounding the use of *multistage side chains*, and then p-type DPP multistage polymer will be discussed in terms of exploring the universal nature of this approach and it's use in high performance systems.

Finally, Chapter 5 delves into the intricate morphological effects of polymer side chain placement in organic photovoltaic donor-acceptor blends. Specifically, the study utilizes a novel family of three donor-acceptor polymers with methylated acceptor monomers to observe how side chain steric interactions affect morphology and optoelectronic properties in blends of polymeric donors and molecular acceptors. The three *methyl acceptor* polymers will be compared to PCE-11 in PCBM and ITIC blends to probe the impact of removing bulky side chains from common acceptor moieties.

CHAPTER 2

EXPERIMENTAL METHODS

2.1 Synthesis of Conjugated Polymers

As discussed in detail in Chapter 1.2.3, the primary methods used to polymerize the conjugated polymers presented in this dissertation include Migita-Kosugi-Stille polymerization and direct hetero-arylation polymerization. The monomers used for polymerization were either purchased from various commercial sources or synthesized as outlined in their respective chapters. Since the fundamentals of these polymerization techniques have been discussed in Chapter 1, the following sections will provide general methodology and considerations when running these reactions.

2.1.1 Migita-Stille-Kosugi Polymerization

Migita-Stille-Kosugi polymerization is a robust and versatile technique for synthesizing conjugated polymers from a dibromo monomer and a distannyl monomer. The background and mechanism of this reaction are presented in Chapter 1.2.3.1.

To an oven-dried 3-neck flask 1 mmol of an aryl dibromide, 1 mmol of an aryl distannane, 0.03 mmol $Pd_2(dba)_3$ chloroform adduct, 0.12 mmol P(*o*-tolyl)$_3$, and 20 mL of dry toluene (0.05M to the aryl dibromide) were added in an argon glovebox. The reaction was sealed with a rubber septa in the glovebox, then removed and brought to a hot plate within a lab hood. The reaction was kept under an argon atmosphere *via* a needle connected to an argon outlet from a Schlenk line. The reaction was stirred at 100^{o}C for 24-48 hours. For end capped polymers, a monostannylated monomer, for example 2-

(tributylstannyl)thiophene, was added at this point and allowed to stir for 6 hours. Afterwards, a monobrominated monomer, for example 2-bromothiophene, was added and allowed to stir for another 6 hours. For all polymerizations, end capped or not, the reaction was cooled to ~60^{o} C and a spatula tip of palladium scavenger, diethylammonium diethyldithiocarbamate, was added and allowed to stir for 1 hour. The reaction was then cooled to room temperature, and the solution was precipitated into methanol. After precipitating the toluene solution, the flask was rinsed with chloroform or chlorobenzene to dissolve remaining material, and again precipitated into the methanol solution. The precipitate was allowed to stir in methanol for 1 hour, after which the solution was filtered over a 0.45 μm nylon filter. The precipitate was collected and prepared for fractionation and isolation *via* Soxhlet purification.

This methodology was used for all polymers in this study synthesized *via* Migita-Stille-Kosugi polymerization, but there are modifications that can be made. Other Pd^{0} catalysts such as $Pd(PPh_3)_4$ can be used, and catalyst loading ratio can be altered typically between 1% - 5%. For conjugated polymers that precipitate into toluene before reaching high molecular weight, chlorobenzene can be substituted as the solvent system. While a concentration of 0.05M to the aryl dibromide was the standard for the polymerizations in this work, occasionally additional solvent is required to induce stirring if the solution begins to gel.

Another factor to consider when setting up Migita-Stille-Kosugi polymerizations is the physical states of the monomers used. Long, branched aliphatic side chains often produce oily or waxy monomers, which can be difficult to weigh into a flask using a spatula or pipette. To facilitate transfer of these monomers, a solvent can be used to

dissolve the material and transfer it into a tared reaction flask. The solvent can then be removed using a rotary evaporator before recording the weight of the monomer. The flask can then be transferred to a glovebox where the other monomer, catalysts, and solvent can be added in an inert atmosphere.

When designing synthetic pathways for alternating conjugated polymers, these types of waxy monomers should always be the dibromide for ease of purification. Distannyl monomers cannot be commonly purified through column chromatography without inducing degradation, and therefore usually require recrstallization to achieve purity, which cannot be efficiently performed with waxy materials.

2.1.2 Direct Hetero-Arylation Polymerization

Direct hetero-arylation polymerization (DHAP) is a relatively new polymerization method that can be used to couple a dihydro monomer and a dibromo monomer, bypassing the need for toxic stannane monomers. The background and mechanism of this reaction are presented in Chapter 1.2.3.2.

1 mmol of an aryl dibromide, 1 mmol of an aryl distannane, 0.02 mmol of $Pd(OAc)_2$, 0.33 mmol of pivalic acid (0.33 mmol), and 3 mmol potassium carbonate were added to an oven-dried roundbottom flask. The flask was vacuum pumped and refilled with argon 3 times before adding 10mL of DMAc (0.1M to the aryl dibromide) to the reactants under argon. The flask was equipped with an oven-dried condenser, and the solution was stirred at 140°C for a material dependent amount of time, ranging from minutes to days. After completion, the solution was cooled to ~60^o C and a spatula tip of palladium scavenger, diethylammonium diethyldithiocarbamate, and a spatula tip of

potassium scavenger, 18-crown-6, were added and allowed to stir for 1 hour. The reaction was then cooled to room temperature and precipitated into methanol. Chloroform was used to dissolve any material remaining in flask, and was also precipitated into methanol. After 1 hour of stirring in methanol, the solution was filtered over a 0.45μm nylon filter. The filtered precipitate was collected and prepared for fractionation and isolation *via* Soxhlet purification.

Unlike Migita-Stille-Kosugi polymerization, the reaction times for DHAP were material dependent, with some completing in 15 minutes and others reacting overnight. Molecular weight can be modulated through reaction time, with molecular weight increasing until the polymer becomes insoluble in the reaction solvent.[136] Often a series of small-scale polymerizations were necessary to determine the optimal reaction time necessary to achieve high weight polymers that were still soluble in common organic solvents. To prevent defects caused by dihydro monomers with reactive hydrogen in the β position, the catalyst system can be exchanged for a palladium catalyst system and solvent that would react slower. For these reactions, P(o-anisyl)3 (10 mol%) was used as a ligand, cesium carbonate was used in place of potassium carbonate, and toluene was used instead of DMAc and the reaction was allowed to proceed overnight.

2.1.3 Purification and Fractionation

Conjugated polymers synthesized by Migita-Stille-Kosugi or DHAP were purified and fractionated through successive Soxhlet extractions in methanol (removes catalyst, salts, monomers, scavengers), acetone, hexanes (removes oligomers and low molecular weight polymers), dichloromethane, chloroform, and chlorobenzene (collects high

molecular weight fractions). Soxhlet extractions were typically performed for 24 hours each, or until coloration from the conjugated polymer could no longer be observed in the draining solution. Higher molecular weight fractions were condensed on a rotary evaporator to <10 mL and precipitated into methanol and allowed to stir for ~30 minutes, after which the solution was filtered over a 0.45 μm nylon filter. The precipitate was then collected and dried under vacuum before using for characterization or device experiments.

2.2 Polymer Characterization

2.2.1 Structural Characterization

^{1}H NMR spectra of conjugated polymers were collected using a Bruker Corporation DRX 500 MHz spectrometer and a Bruker Corporation DRX 700 MHz spectrometer. The chemical shifts for chloroform-d as the internal standard were referenced to the residual solvent peak, ^{1}H: δ = 7.26 ppm. The chemical shifts for 1,1,2,2-tetrachloroethane-d_2 as the internal standard were referenced to the residual solvent peak, ^{1}H: d= 6.00 ppm. The chemical shifts for DMSO-d_6 were referenced to the residual solvent peak ^{1}H: d= 2.50 ppm. For conjugated polymers, relaxation delay time was set to 5 seconds. Elemental compositions were analyzed for the carbon, hydrogen, nitrogen, and sulfur contents at Atlantic Microlab, Inc. Number average molecular weight (M_n) and dispersity (Đ) estimations of polymeric materials were obtained using gel permeation chromatography (GPC) performed using a THF GPC at 35° C, a $CHCl_3$ GPC at 40^o C, or a 1,2,4-trichlorobenzene GPC at 140^o C, all reference vs. polystyrene standards.

2.2.2 Optical Characterization

Characterization of optical absorption is fundamental for understanding a polymer's color for electrochromic applications, its light absorption in respect to the solar spectrum for OPV applications, as well as its optical bandgap, determined by the low energy onset of an absorption peak. Absorption measurements were taken in solution and film using a Varian Cary 5000 Scan UV-Vis-NIR spectrophotometer. After recording a baseline from the pure solvent, 5 μL at a time of a stock solution of 5 mg/mL polymer in toluene, chloroform, or chlorobenzene were mixed into the pure solvent until an absorption max around 1 a.u. was reached. The stock solution would then be used to spin or blade coat the polymer onto a 1" x 1" microscope slide to obtain a thin film absorption spectrum.

2.2.3 Electrochemical Characterization

Cyclic Voltammetry (CV) and Differential Pulse Voltammetry (DPV) were used to determine the polymer's ionization and electron affinities. For the electrochemical measurements the polymers were drop cast onto glassy carbon electrodes with a fixed volume of 2 μL from a 5 mg/mL solution. Electrochemical measurements were performed in a three-electrode cell with a Pt flag as the counter electrode, a Ag/Ag^{+} (10 mM $AgNO_3$ in 0.5 M $TBAPF_6$−ACN, $E^{1/2}$ for ferrocene: 68 mV) as the reference electrode, and a polymer-coated glassy carbon button electrode as the working electrode. Propylene carbonate (PC) was used as the electrolyte solvent and $TBAPF_6$ was used as the supporting electrolyte for the electrochemical and spectroelectrochemical measurements. The voltage and current were controlled and monitored with an EG&G

PAR 273A potentiostat/galvanostatic under CorrWare control. All films were characterized via cyclic voltammetry between −0.8 and 0.8 V at 50 mV/s for 25 cycles; the onset of oxidation was determined by differential pulse voltammetry.

Using the onset of oxidation from DPV experiments, polymer HOMO values could be estimated. Based on measurements of the formal potential of Fc+/Fc vs. saturated calomel electrode (SCE) as 0.4V, SCE vs. normal hydrogen electrode (NHE) as 0.2V, and 0.0V being equivalent to -4.5eV, the potential of Fc+/Fc vs. vacuum is taken to be -5.1 eV.[137] Using this value for vacuum, onset of oxidation for the polymer was used to calculate HOMO energy levels from the following equation:

$$E_{HOMO} = -(E_{onset,ox\ vs.\ Fc+Fc} + 5.1) \quad (2\text{-}1)$$

This calculation takes many assumptions into account, and therefore energy level values should primarily be taken as relative and not absolute.

2.2.4 Thermal Characterization

Thermogravimetric analysis (TGA) and differential scanning calorimetry (DSC) were utilized to observe the polymers' thermal properties, including degradation behavior, glass transition temperature (T_g), and evidence of melting or crystallization behavior. TGA was carried out on a PerkinElmer Pyrus 1 TGA. 5-10 mg of material was placed into a platinum pan and heated from 50 ˚C to 500 ˚C with a heating rate of 10˚ C/min under a continuous flow of nitrogen (20 mL/min). Differential scanning calorimetry (DSC) was performed using a TA Instruments Q200 DSC with a heating and cooling rate of 10˚ C/min. The typical temperature range was from -50 ˚C to 300 ˚C, but

would be adjusted depending on the thermal stability recorded from TGA data. Typically three heating and cooling cycles were performed to assess reproducibility of any T_g, T_m, and T_c features observed.

2.3 Multistage Side Chain Methodology

Chapter 4 introduces the concept of conjugated polymers with multistage side chains that undergo two orthogonal post-polymerization cleavage mechanisms that provide desired solubility changes. The first transition is a hydrolysis of ethyl esters to carboxylates, shifting the organic solvent soluble polymer to an aqueous solution soluble polymer. At this point, the conjugated polymer can be processed into thin films from an aqueous solution. The second transition is a UV cleavage of a photolabile *o*-nitrobenzyl moiety in the side chain, rendering the final polymer film insoluble. The methods for processing these novel multistage side chain polymers are presented in this section.

2.3.1 Side Chain Ester Hydrolysis

Hydrolysis of side chain esters to carboxylates takes place in solution after the polymerization and purification of a multistage side chain polymer. To an oven dried roundbottom flask, 100 mg of the organic soluble multistage polymer and 100 mL of a 1M solution of KOH in methanol were added. The solution was refluxed at 70^{o} C overnight. The solid polymer never fully dissolves into the methanol, stirring as a suspension throughout the reaction. The solution was cooled and filtered over a 0.45 μm nylon filter and the resulting solid was washed with methanol and chloroform. The solid was collected and dried under vacuum to afford the polyelectrolyte version of the multistage polymer. An example of this reaction is shown is Scheme 2-3. Successful

hydrolysis was determined by the shift in solubility form organic to aqueous using a biphasic solution of water and chloroform as shown in Figure 2-1. The ^{1}H NMR of polyelectrolyte can also be measured in DMSO-d_6 to observe the loss of peaks associated with the ester chains.

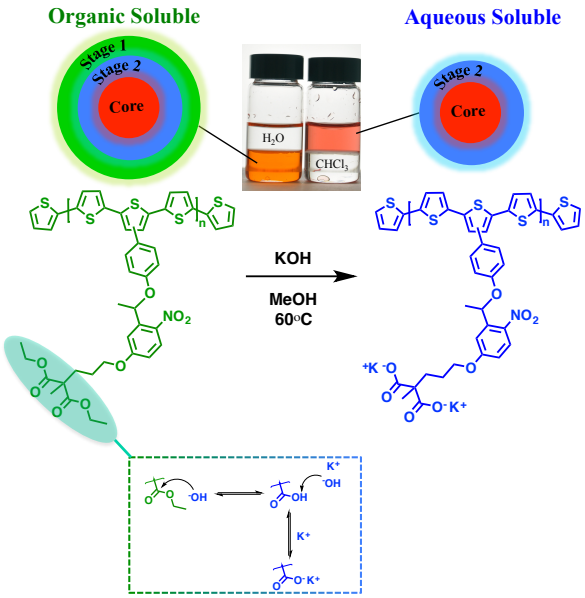

Figure 2-1. Example and mechanism of multistage side chain hydrolysis of **P(T3-MS)-O** to form the polyelectrolyte **P(T3-MS)-PE**. Biphasic solutions of chloroform (bottom) and water (top) show the shift in solubility after hydrolysis.

2.3.2 Blade Coating of Aqueous Solutions

Blade coating conjugated polymers from aqueous solutions is advantageous due to the safety of aqueous solutions in comparison to organic solvents such as chloroform and chlorobenzene, but producing high quality thin films water-borne coatings can be challenging due to the high surface tension of water. Water beads up on glass substrates, and obtaining uniform films is difficult even after UV-ozone treatment of glass to reduce the hydrophobicity of the surface. For this reason, solutions of water and isopropanol

were used to reduce their surface tension and enhance wettability for uniform thin films. Addition of isopropanol to water reduces the surface tension, with a 1:1 mix lowering the surface tension of water from 72 mN/m to 25 mN/m, which is similar to chloroform's value of 26 mN/m.[138] Using a 1:1 water:IPA mixture, a 5-10 mg/mL solution of multistage polyelectrolyte was stirred at 40^{o} C overnight, and then filtered through a 1 μm. The solution was then blade coated onto glass substrates at 40^{o} C to produce uniform thin films for optical measurements, EC films, and OFET devices.

2.3.3 UV Photocleavage of *o*-nitrobenzyl Moiety

UV cleavage of the *o*-nitrobenzyl moiety on the multistage side chain was performed on thin films of both the organic soluble and aqueous soluble version of the multistage polymers. After blade coating films onto glass substrates, the films were loaded into a UV chamber for irradiation under 5 mW/cm intensity light. 365 nm UVA light was used and required irradiation times up to 150 minutes, while 302 nm UVB light was able to cleave side chains with irradiation times of 10 minutes. An example and mechanism of this UV cleavage is shown in Figure 2-2. Since the photolabile the *o*-nitrobenzyl moiety absorbs in the range of 305 nm – 325 nm, UVB light sources are optimal for inducing cleavage without affecting the lower energy absorption of the conjugated polymer main chain. Using a high intensity 365 nm UVA light source (80 mW/cm) allowed for cleavage in 10 seconds of irradiation, providing evidence that with the proper light source (UVB) and high intensity > 100 mW/cm it may be possible to cleave the side chains in under 1 second, which would be relevant for industrial scale printing.

After UV irradiation, the side chain is removed but still remains within the polymer film. Rinsing in methanol is required for removal of the cleaved side chain, leaving behind the conjugated polymer main chain as a solvent resistant film. Although the cleaved polymer becomes solvent resistant after irradiation, delamination often occurs if rinsed right away into water. By rinsing in methanol first, delamination is prevented in any further rinses with water or other aqueous and organic solvents. It is also possible to combine the irradiation and rinsing steps by irradiating within a bath of methanol.

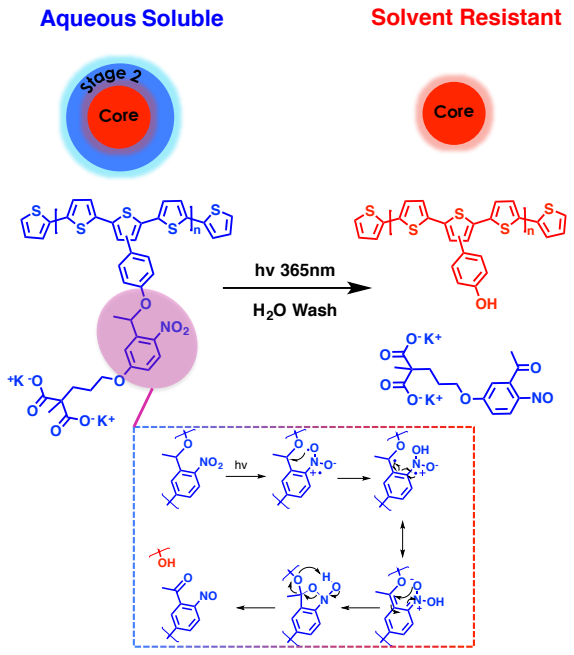

Figure 2-2. Example and mechanism of multistage side chain photocleavage of **P(T3-MS)-PE** to form the solvent resistant **P(T3-MS)-I** using UV light irradiation.

Side chain cleavage of the photolabile *o*-nitrobenzyl moiety can be monitored using UV-vis absorption, where a red-shifting of the peak corresponding to the *o*-nitrobenzyl unit (~310 nm) signifies cleavage and formation of the molecular nitroso product that is cleaved off the polymer chain. Films can be irradiated in small time increments until changes in the absorption spectra can no longer be observed. After

irradiation is complete, rinsing films in methanol will cause the red shifted peak to significantly diminish, signaling the removal of the cleaved side chain product. Details of these spectral changes are discussed in detail within Chapter 4. Cleavage can also be monitored by changes in the elemental composition measured by X-ray Photoelectron Spectroscopy (XPS) experiments, changes in the scattering pattern found through Grazing Incidence Wide-Angle X-ray Scattering (GIWAXS) measurements, and changes in water droplet contact angle on films, all of which are further detailed in Chapter 4.

2.4 Device Fabrication and Testing

The novel conjugated polymers presented throughout this dissertation have been applied to a variety of organic electronics applications including OPVs, OFETs, and PLEDs. This section will provide a brief description of the fabrication and testing of these devices.

2.4.1 Organic Photovoltaic Devices

OPV devices were fabricated onto pre-patterned ITO substrates supplied by Tinwell Technology (tinwell@incnets.com, project TI1678D). Substrates were cleaned *via* successive sonication in 0.1% sodium dodecyl sulfate solution, ultrapure water (Millipore system, resistivity 18.2 MΩ·cm), and isopropyl alcohol for 15 minutes each. Substrates were dried with pressurized N_2 gas before undergoing 15 minutes of UV-ozone treatment.

Conventional architecture devices were fabricated with the layered structure of ITO/PEDOT:PSS/Polymer-Fullerene Blend/Ca/Al. PEDOT:PSS (Clevios™ P VP AI

4083, purchased from Heraeus Deutschland GmbH & Co. KG) was passed through a 0.45 μm filter and was spin coated in air onto the ITO substrate at 5,000 RPM for one minute (45 nm), followed by annealing at 120° C for 10 minutes. A polymer-fullerene blend solution was then either spin coated within a glovebox under an argon atmosphere or blade coated in air onto the substrate. Top contacts of Ca (10 nm) and Al (100 nm) were evaporated onto the active layer at 10^{-6} torr through a metal mask to produce 0.07 cm^2 active pixels.

Inverted architecture devices were fabricated with the layered structure of ITO/ZnO/Polymer-Fullerene blend/MoO_3/Ag. ZnO sol-gel was made from 0.32 g of Zn acetate dihydrate (Sigma Aldrich) in 1920 μL of 2-methoxyethanol (Sigma Aldrich) and 80 μL of ethanolamine (Sigma Aldrich). The ZnO sol-gel was spin coated in air onto precleaned ITO substrates at 800 rpm for 50 sec, and was then annealed in air at 400º C for 5 minutes on a hotplate. A polymer-fullerene blend solution was then either spin coated within a glovebox under an argon atmosphere or blade coated in air onto the substrate. Top contacts of MoO_3 (10 nm) and Ag (160 nm) were evaporated onto the active layer at 10^{-6} torr through a metal mask to produce 0.07 cm^2 active pixels.

OPV devices were tested within an argon atmosphere glovebox using AM 1.5 illumination at 100 mW/cm^2 generated using a Newport Oriel 69907 power supply connected to a 150 W xenon arc lamp (Newport 6255) with collimating lenses in a Newport Oriel 94021A simulator lamp housing. J-V characteristics were recorded with 2410 Keithley SourceMeter® SMU Instruments. Current was measured while a voltage sweep from -1 V to + 1 V was applied to the device under illumination. The resulting current-voltage curve is converted to current density using the known active layer area.

From the current density and voltage curve plot the Jsc, Voc, FF and PCE% was calculated. Multiple devices were tested in order to gain an average and standard deviation of solar cell performance.

2.4.2 Organic Field-Effect Transistors

Bottom-Gate Bottom-Contact (BG/BC) OFETs were fabricated on a heavily n doped silicon wafer <100> as the gate electrode with a 300 nm thick layer of thermally grown SiO_2 as the gate dielectric. The capacitances of the dielectric layers were measured using an Agilent 4284A Precision LCR Meter. The SiO_2 dielectric has a capacitance of ca. 1.08×10^{-4} F/m^2. Au source and drain contacts (50 nm of Au contacts with 3 nm of Cr as the adhesion layer) with fixed channel dimensions (50 μm in length and 2 mm in width) were deposited via E-beam using a photolithography lift-off process. Prior to deposition of polymer semiconductors, the devices were cleaned in acetone for 30 min and subsequently rinsed sequentially with acetone, methanol and isopropanol. The SiO_2 surface was pretreated by UV/ozone for 30 min for cleaning purposes. The devices were then cleaned under a flow of nitrogen. Polymer solutions were then blade-coated onto substrates in ambient atmosphere, and then dried by vacuum oven at 100° C for 24 hours before tested.

All OFET characterizations were performed using a probe station inside a nitrogen atmosphere glovebox using an Agilent 4155C semiconductor parameter analyzer. The FET mobilities were calculated from the saturation regime in the transfer plots of V_G versus I_{SD} by extracting the slope of the linear range of V_G vs. $I_{SD}^{1/2}$ plot and using the following equation:

$$\frac{\partial I_{SD}^{1/2}}{\partial V_G} = (\mu_e C_{ox} \frac{W}{2L})^{1/2} \quad (2\text{-}2)$$

where I_{SD} and V_{SD} are the source-drain current (A) and source-drain voltage (V), respectively; V_G is the gate voltage (V) scanning from 40 to -80 V (for BG/BC OFETs) in the transfer plot; C_{ox} is the capacitance per unit area of the gate dielectric layer. W and L refer to the channel length and width; μ_e represents the electron field-effect mobility in the saturation regime ($cm^2V^{-1}s^{-1}$). Threshold voltage, V_{th}, was calculated by extrapolating $V_T = V_G$ at $I_{SD} = 0$ in the V_G vs. $I_{SD}^{1/2}$ curve. Current on/off ratio, $I_{ON/OFF}$, was determined through dividing maximum I_{SD} (I_{ON}) by the minimum I_{SD} at about V_G in the range of -80 to 40 V (I_{OFF}).

2.4.3 Polymer Light-Emitting Diodes

PLED devices were fabricated according the methods for conventional OPV devices outlined in chapter 2.4.3 with the architecture ITO/PEDOT:PSS/EL Polymer/Ca/Al. The only difference was the use of an electroluminescent (EL) polymer in place of the polymer-fullerene blend. Each film was comprised of 4 devices with an area of 0.25 cm^2 each, with active layer thicknesses of 110 nm±10 nm. PLED devices were tested in an argon atmosphere glovebox. A Keithley 2410 1100V Sourcemeter was used to control the voltage sweep from 0 V to 8 V and measure current. PLED luminance was measured in the dark with calibrated photodiode (FDS 100 from Thorlabs, Inc.) fixed at the surface normal of the PLED under measurement during the voltage sweep.

2.4.4 Electrochromic Films

While full EC devices were not fabricated for this dissertation work, polymer films on ITO/glass were used to assess EC capabilities through spectroelectrochemistry. Polymer solutions were blade coated in air onto ITO/glass (25 x 75 x 0.7 mm^3, sheet resistance: 8-12 ohm/sq, Delta Technologies, pre-cleaned with toluene and isopropanol). The films were placed in a cuvette and a three-electrode cell was setup with the ITO serving as the working electrode, a platinum flag as the counter electrode, a reference electrode (Ag/Ag^+, 10 mM $AgNO_3$ in 0.5 M $TBAPF_6$/ACN, $E_{1/2}$ for ferrocene: 68 mV), and 0.5 M $TBAPF_6$/PC as the supporting electrolyte. Spectra of the pristine films were taken followed by an electrochemical break-in by redox switching (by CV) the polymers over their stable potential windows for 10 cycles. The films were then set at constant potentials within the electrochemical window and absorbance spectra were obtained. Photographs of the polymer films where then taken in the extreme redox states.

Transmittance at the polymer's λ_{max} was measured as a function of switching time to assess the switching speed. Switching speed was calculated as the time taken to reach 95% of the peak contrast at $\lambda_{max.}$ Colorimetric values (L^*,a^*,b^*) were calculated from recorded spectra using the standard observer functions with a D50 illuminant. The color was quantified using CIE Lab color coordinates where three coordinates: L^*, a^*, and b^* are defined to quantify the lightness (L^*) and the color of an object from green to red (a^*) and from blue to yellow (b^*).

2.4.5 Fully Printed Electrolyte-Gated Organic Transistors

EGOT devices were fabricated using all solution processed methods onto glass substrates that had been cleaned *via* 15 minutes of sonication in acetone, methanol, and isopropanol, followed by 20 minutes of UV/ozone treatment. PEDOT:PSS ink was prepared by adding 5 wt% ethylene glycol (Millipore Sigma 99.8%) and 0.1 wt% of Triton-X100 to Clevios PH1000 (Haraeus). The ink was then diluted to 0.65 wt% solids with Millipore ultrapure water. Inkjet printing of the PEDOT:PSS ink was performed using MicroFab Jetlab II inkjet printer equipped with a 50 μm diameter piezoelectric nozzle and a temperature controlled stage. To achieve stable jetting, a 600 Hz bipolar square wave pulse was used to dispense the ink and jetting parameters were adjusted to obtain droplets of ca. 70 μm (~150 pL) with 3 m/sec jetting speed as measured by a horizontal camera. The substrate was kept at 60˚ C during printing. The printed source/drain electrodes were defined using a bitmap image file to give transistor channel width and length of 200 μm and 2.0 mm, respectively. Two layers of PEDOT:PSS ink were printed to give ca. 300 nm thick electrodes (400 S/cm). After printing, the PEDOT:PSS electrodes were dried in a vacuum oven at 50˚C overnight. Polymer films were then blade coated over the source/drain electrodes using the previously detailed film preparation conditions. Cleaved films of P(DPP-DTT-MS)-PE were irradiated for 10 minutes within a methanol bath. All coatings were dried by vacuum oven at 75° C for at least 3 hours, followed by drop-casting of 2 μL of a solution of the ion gel dielectric P(VDF-HFP) + [EMI][TFSI] in acetone on top of the source/drain channel. [EMI][TFSI] was synthesized as previously reported[139] according to a literature procedure.[140] The iongel electrolyte was prepared according to a literature method where (PVDF-HFP,

Sigma Aldrich, M_n = 130 kDa, $Đ$ = 3.08) was co-dissolved with [EMI][TFSI] in acetone in a 1:4:7 ratio.[141] Ion gels were dried by vacuum oven at 75° C for at least 3 hours. Top-gate devices were prepared by printing 5 layers of PEDOT:PSS onto the ion gel electrolyte over the channel.

All EGOT characterizations were performed using a probe station inside a nitrogen atmosphere glovebox using an Agilent 4155C semiconductor parameter analyzer. A source-drain bias (V_D) of 0.5 V was held while gate voltage (V_G) was swept from +1 V to -1.5 V at a rate of 50 mV/sec while drain current (I_D) was recorded. Transconductance was calculated as the absolute value of $\Delta I_D/\Delta V_G$ from device transfer curves.

2.4.6 Space-Charge Limited Current Mobility Measurements

Space-charge limited current (SCLC) was used throughout this dissertation to determine polymer hole mobility (μ_h) through the bulk of the material. SCLC is a useful measurement to understand the role of charge transport in the operation of OPVs and PLED because these devices rely on charges moving vertically through the bulk of the polymer film. OFET mobility measurements typically produce higher mobility values, but do not accurately represent the operation of charge transport in OPV and PLED devices since the charge transport takes place at an interface instead of through the bulk of the polymer film.

In diode-like devices for SCLC modeling of hole transport, hole mobility can be isolated and probed by selecting the appropriate work function of the charge injecting (which needs to be an Ohmic contact, i.e. not injection-limited) and collecting electrodes.

At low voltage bias, the number of charge carriers in the devices does not impact the internal field, and the current follows Ohm's law. As the voltage bias is increased, the density of charge carriers in the device increases, leading to the formation of a space-charge region, which impacts the internal electric fields and limits the current out of the device (SCLC regime).[142]

The current density *J* in the trap-free space-charge limited-current region can be described by Child's law:

$$J = \frac{9}{8}\varepsilon_r\varepsilon_0\mu\frac{V^2}{L^3} \tag{2-3}$$

where ε_r is the dielectric constant of the material, ε_0 is the permittivity of free space, μ is the charge carrier mobility, V is the effective voltage (applied voltage minus the built-in voltage) and L is the semiconductor layer thickness. Transport in disordered materials is often limited by the presence of shallow traps whose heights are field dependent. As described by the Poole-Frenkel effect, trap barrier height decreases in the presence of stronger electric fields.[143] Taking this dependence into account, the mobility can calculated as:

$$\mu = \mu_0 \exp\left(0.891\Upsilon\sqrt{E}\right) \tag{2-4}$$

where μ_0 is the zero-field mobility, γ is the field dependence parameter and E is the electric field through the semiconductor. Substituting equation 2-4 into equation 2-3 allows for the determination of mobility from the measured J-V curve of the device through equation 2-5.

$$J = \frac{9}{8}\varepsilon_r\varepsilon_0\mu_0 \exp\left(0.891\Upsilon\sqrt{E}\right)\frac{V^2}{L^3} \quad (2\text{-}5)$$

It is important to note in equation 2-5 that $J \sim 1/L^3$, meaning current density will decrease with thicker polymer films. When measuring SCLC mobility, multiple thicknesses of material should be tested to quantify that this relationship holds true in order to determine the accuracy of the measured mobility. Typically, films thinner than 100 nm will not display an SCLC regime, so thicker films ranging from 100 nm to 1 μm should be used for thickness studies. For these experiments, at least three films of varying thickness, typically greater than 100 nm difference in thickness between them, were used to calculate SCLC mobility.

SCLC hole mobility was measured from hole only devices with the architecture ITO/MoO_3/Polymer/MoO_3/Ag. Pre-patterned ITO substrates supplied by Tinwell Technology (tinwell@incnets.com, project TI1678D) were cleaned *via* successive sonication in 0.1% sodium dodecyl sulfate solution, ultrapure water (Millipore system, resistivity 18.2 MΩ·cm), and isopropyl alcohol for 15 minutes each. Substrates were dried with pressurized N_2 gas before undergoing 15 minutes of UV-ozone treatment. 10 nm of MoO_3 was evaporated onto cleaned ITO glass slides at 10^{-6} torr. Polymers to be tested were then spin coated in an argon atmosphere glovebox onto the ITO/MoO_3 substrates to three different thicknesses to confirm thickness dependence of $J \sim 1/L^3$. To vary thickness, a concentrated solution (30-50 mg/mL) was first used for one device and was subsequently diluted for the following devices to progressively achieve thinner films. Afterwards, 10 nm MoO_3 followed by 100 nm Ag was evaporated onto the films at 10^{-6} torr through a metal mask to produce 0.07 cm^2 active pixels.

J-V characteristics of the SCLC devices were recorded with 2410 Keithley SourceMeter® SMU Instruments. Current was measured while a voltage sweep from 0.01 V to 1 V, 5 V, or 10 V was applied to the device. The resulting current-voltage curve is converted to current density using the known active layer area. Since conjugated polymers can display an SCLC regime at a variety of voltages, and importantly can also break down at varying voltages, it is important to begin testing to lower voltages (1 V) and continue testing to higher voltages until an SCLC regime is seen. J-V curves should be plotted on a log-log scale to view the onset of a SCLC regime. Since $J \sim V^2$ in the SCLC regime as shown in equation 2-5, a slope of 2 will be seen in the log-log plot of the J-V curve within the SCLC regime. An exemplary curve is shown in Figure 2-3. At lower voltages the charge transport follows Ohm's law and a slope on 1 on the J-V log-log plot will be seen. Therefore an SCLC curve should follow the progression of a shift in slope from 1 to 2.

Once an SCLC curve is obtained and the voltage region where the slope is equal to 2 on a log-log plot is identified, the SCLC regime is fit across that voltage range using equation 2-5 to determine the mobility. ε_r was assumed to be 4 based on values found commonly in other conjugated polymers.[144-145] The electric field E was assumed to be the voltage of the sweep V over the film thickness L. Since MoO_3 was used as both interlayers, the built-in voltage across the device V_{bi} was determined to be zero. The field dependence variable Υ is left as an open variable in the fit, and typically has values around 10^{-4} for highly field dependent polymers and approaches zero for polymers that have less traps and are more field independent. Mobility data was averaged across 8 pixels per device, and then averaged between the three thicknesses. To assess the validity

of the measurements the three or more devices of varied thickness were tested for the relationship of $J \sim 1/L^3$. A voltage within the SCLC regime of the polymer was chosen, and the value for J at that voltage was plotted as a function of thickness on a log-log plot, as shown in Figure 2-4. The slope should be ~ -3 in order to fit the SCLC model and verify the measurements.

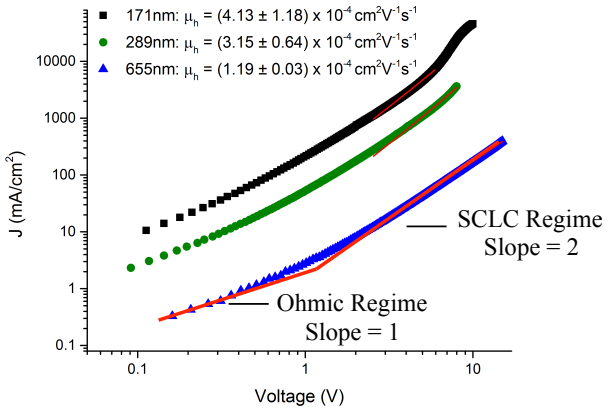

Figure 2-3. J-V curves of conjugated polymer **P(T4-iI-M)** at three different thicknesses showing the progression from the Ohmic regime (slope = 1) to the SCLC regime (slope = 2).

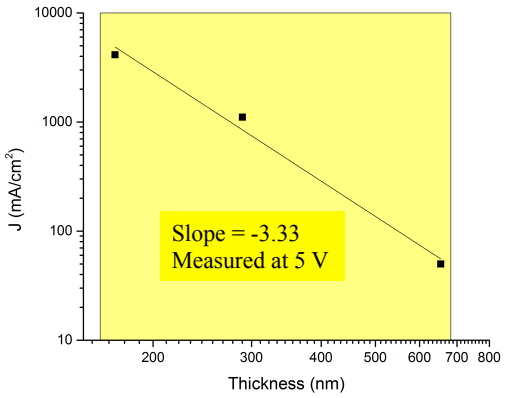

Figure 2-4. J-L curves of conjugated polymer **P(T4-iI-M)** at three different thicknesses to assess the relationship $J \sim 1/L^3$ from the SCLC model. Values for J were taken at 5 V, which was within the SCLC regime. The slope close to -3 verifies that the measurements taken for mobility accurately fit with equation 2-5.

CHAPTER 3

TWISTED TRIPHENYLAMINE AS A PROCESSING COMONOMER TO ENABLE MULTIFUNCTIONAL AND AMORPHOUS CONJUGATED POLYMERS

3.1 Background and Motivation

Most organic electronic materials are tailor-made for specific applications and are rarely designed or tested for multi-functionality. While the active materials in different organic electronic devices share many similar attributes, such as the reliance on conjugated molecular structures, each application has its own set of unique material requirements, leading to a divergence in design principles. The ability of a material to operate in multiple device architectures is beneficial for the development of multifunctional devices, which include dual EC/EL displays and organic light-emitting transistors (OLETs).[146,147] These devices integrate two separate electronic functions through the use of one common active layer. The challenge in creating materials for multifunctional devices comes from the careful balance of different, and sometimes contradictory, requirements. For example, close intermolecular packing may be beneficial for charge mobility, broad visible light absorption, and charge separation, but may be a hindrance to the recombination necessary for electroluminescent (EL) capabilities. EL materials generally do not pack in an ordered manner, creating an amorphous solid-state morphology favorable to recombination and light emission. However, the redox switching capabilities of electrochromic (EC) polymers are not significantly sensitive to

disorder in the solid-state, so EC functionality is often compatible with amorphous EL polymers.

In this chapter, a new design for obtaining multifunctional materials will be described through the use of amorphous conjugated polymers. In this work, triphenylamine (TPA) is used as a *processing comonomer* in a family of four triphenylamine copolymers. The TPA comonomer provides disorder along the polymer backbone, which leads to enhanced solubility, and templates an amorphous thin-film morphology, which produces smooth films that are tolerant to fluctuations in processing conditions. This chapter will highlight the advantages of utilizing amorphous conjugated polymers for multifunctional materials, describe the synthesis of TPA copolymers through Direct Arylation polymerization, and will detail the results of using these polymers for hole transport, electrochromism, electroluminescence, and as donor polymers in OPV active layers.

3.1.1 Properties of Amorphous Polymers

Amorphous polymers are a class of polymeric materials that do not exhibit any crystalline features and therefore form a uniform, isotropic solid-state morphology. Many polymeric systems, both classical and conjugated, show some degree of amorphous and crystalline domains, but evidence of fully amorphous polymers can be seen through isotropic scattering in X-ray experiments and the lack of crystallization or melting peaks in differential scanning calorimetry (DSC). Because of their isotropic and low degree of light scattering, classical amorphous polymers have been widely used for their optical

transparency. This property can also be useful in conjugated polymer applications where optical clarity and low degree of haze is important, such as EC applications.

In conjugated polymers, an amorphous morphology has not generally been viewed as advantageous for optoelectronic properties. Typically, in efforts to mimic crystalline inorganic semiconductors and single crystals of conjugated molecules, many studies focus on developing semicrystalline polymers with planar backbones and an affinity for intermolecular π-π packing, features that are lacking in amorphous polymers. However, highly disordered and amorphous conjugated polymers have gained renewed interest as some systems have shown high charge mobility despite their lack or crystalline order.[148-150] Noriega *et al.* have put forward an explanation for how these materials transport charge through a film despite any evidence of long-range order.[91] In their study, which spanned numerous reported charge transport polymers, the authors found that the primary requirement for high mobility in these systems was not long range order, but rather an interconnection of aggregate domains. In classical semicrystalline polymers, P3HT for example, charge transport is governed by the ordered regions and is limited by the presence of amorphous domains.[151] The energy barrier to hop across grain boundaries turns these disordered domains into charge traps. On the other hand, completely amorphous polymers have weak intermolecular interactions that lead to low mobility through a macromolecular film. The middle ground constitutes a class of highly disordered polymers that are able to transport charge through small intermolecular aggregates while maintaining the desirable properties of amorphous films. In this model, intramolecular charge transport across polymer chains is dominant, while small aggregates create junctions for intermolecular transport, as portrayed in Figure 3-1.

Therefore, the key to designing high mobility materials is to increase the efficiency of short-range charge transport within these localized aggregates.

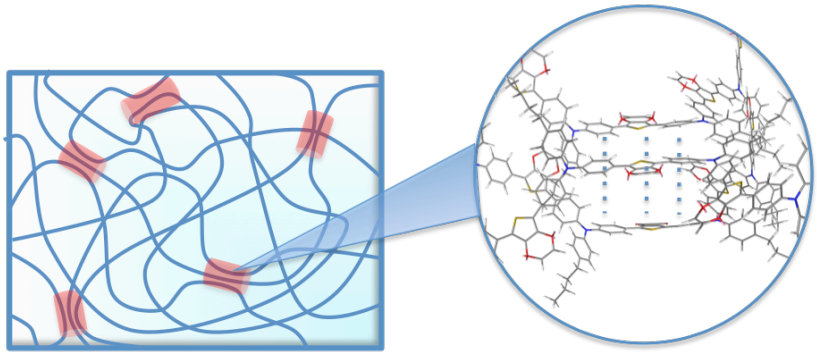

Figure 3-1. Charge transport in highly disordered polymer films. Small aggregates act as junctions for intermolecular charge transport.

Several groups have also suggested that amorphous conjugated polymers can be useful for their reproducibility over semi-crystalline systems.[152-154] This reproducibility can be attributed to the uniformity of amorphous polymer films, in which optoelectronic properties are not dependent on particular crystallization kinetics or orientations. As mentioned in Chapter 1.3.2.3, the properties of many semicrystalline polymers can be highly dependent on a multitude of processing variables.[131-135] Many of these variables affect performance by altering crystallization kinetics, leading to changes in crystal orientation, size, and purity. By circumventing the dependence on precise formation of crystalline domains, amorphous polymers can offer a high level of reproducibility across the spectrum of processing conditions; a feature that is advantageous for large scale, industrial printing where reproducibility over large areas is a necessity. By drying as a homogeneous film, amorphous materials also allow for uniform contact with electrodes or adjacent organic materials.[22]

3.1.2 Triphenylamine Polymers

Triphenylamine (TPA) is a common aromatic building block utilized in amorphous, conjugated molecules and polymers. The phenyl groups are oriented in a propeller-like structure around the central nitrogen, contributing to its inability to pack efficiently and form an amorphous solid-state morphology. Additional benefits of incorporating TPA compounds in conjugated materials include low ionization potential, thermal stability, and ambient stability.[155] For many of these reasons, TPA derivatives are commonly used throughout the OLED, dye sensitized solar cell (DSSC), and perovskite solar cell (PSC) communities as hole transport layers, with poly-TPD and spiro-OMeTAD as prominant examples.[156-159] Computations by Bredas *et al.* determined relatively low reorganization energy (λ=120 meV) for the TPA unit, but when moving to the dimer, triphenyldiamine, reorganization energy greatly increases (λ=290 meV) and begins to approach that of biphenyl (λ=360 meV).[25] The increase is centered about the large difference in phenyl-phenyl torsional angle between the neutral (34°) and oxidized (23°) states, as shown in Figure 3-2, demonstrating that additional torsion and disorder is present when functionalizing TPA or using it as a comonomer with other aromatics. The ability for TPA based materials to transport charge is highly dependent on this degree of torsion and its impact on reorganization energy.

While many TPA materials exhibit modest hole mobility values on the order of 10^{-4} $cm^2V^{-1}s^{-1}$, there are several examples of extending conjugation through the phenyl rings to achieve higher mobility values despite remaining amorphous. Shirota *et al.* reported triphenylamine (TPA) based small molecules that achieved hole mobility values on the order of 10^{-2} $cm^2V^{-1}s^{-1}$ by extending conjugation off all three phenyl rings with

thiophenes and selenophenes.[160] McCulloch *et al.* showed that incorporation of TPA units as comonomers into fluorene polymers resulted in air-stable materials with hole mobility values on the order of 10^{-2} $cm^2V^{-1}s^{-1}$ as cast.[161] These polymers showed no drop in mobility after months of air-storage and were unaffected by thermal annealing steps. A noteworthy feature in TPA based conjugated polymers is a conjugation break arising from the sp^3 nitrogen atom. Because these breaks prevent long-range intrachain charge transport, the increase in mobility from poly-TPA to TPA-fluorene copolymers was attributed to increased conjugation length caused by the fluorene unit. These studies exemplify how modification of the TPA unit, either through functionalization of molecules or copolymerization with aromatic units, can serve as an effective strategy for enhancing electronic properties without sacrificing a favorable amorphous morphology.

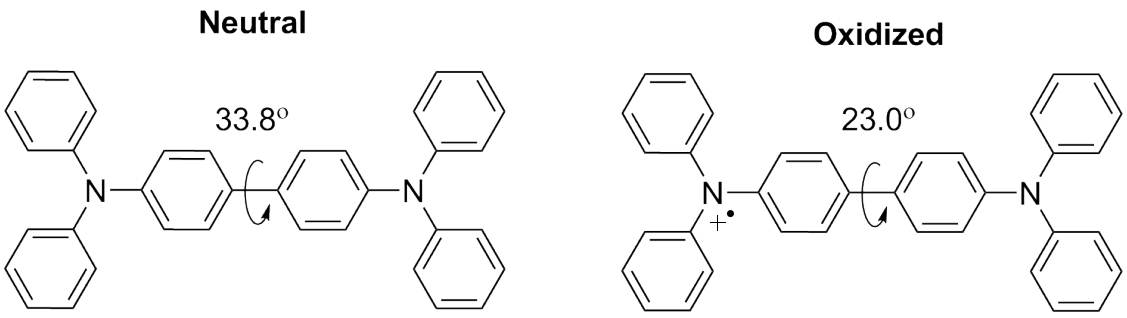

Figure 3-2. Changes in phenyl-phenyl dihedral angle between neutral and oxidized states that lead to an overall increase in reorganization energy of a triphenyldiamine molecule.

3.1.3 Triphenylamine as a Processing Comonomer

The aforementioned TPA-fluorene copolymers achieve higher charge mobility by modifying the TPA backbone with planar, conjugated units, but still retain the amorphous properties found in TPA homopolymers. In a similar method, Yasuda *et al.* use benzothiadiazole (BTD) as a comonomer with TPA to achieve broadened light absorption

for OPV active layers while retaining amorphous polymer properties.[154] These materials exemplify how in copolymers, TPA can be leveraged for its amorphous film forming properties, while the other aromatic comonomer can be leveraged for additional optoelectronic properties. In this sense, TPA can be thought of as a *processing comonomer*, bringing favorable processing properties such as high solubility and the ability to form uniform thin films. By extending the conjugation between TPA units with various conjugated comonomers, amorphous materials can be designed for a host of properties including charge mobility, electrochromism, electroluminescence, and light absorption.

This work explores this idea of TPA as a *processing comonomer* to achieve multifunctional materials that can serve as hole transport layers, electrochromic active layers, electroluminescent active layers in PLEDs, and as donor polymers in OPV active layers while retaining the advantageous processing properties of amorphous conjugated polymers. The copolymers used in this study are shown as **P2-P5** in Figure 3-3, and are compared to the TPA homopolymer **P1**. With electron rich dioxythiophene monomers (**P2-P4**), TPA polymers exhibit yellow to transmissive electrochromism with up to 45% contrast at 415-430 nm, yellow-green electroluminescence up to 450 cd/m^2 in conventional PLEDs, and SCLC hole mobilities on the order of 10^{-5} cm^{2}V^{-1}s^{-1}. With an electron deficient donor-acceptor-donor (D-A-D) monomer, bis-thienyl diketopyrrolopyrrole (DPP-2T), the TPA polymer **P5** has a hole mobility of 10^{-4} cm^{2}V^{-1}s^{-1} and can be blended with $PC_{71}BM$ in conventional OPV devices to obtain ~2.3% PCE.

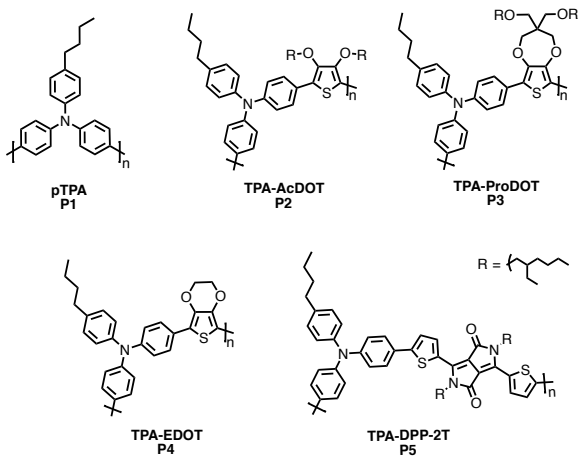

Figure 3-3. Repeat unit structures of TPA polymers designed for redox switching, visible light absorption and charge transport.

3.2 Synthesis of Triphenylamine Polymers *via* Direct Hetero-Arylation Polymerization

The polymers in this study were synthesized via Direct (Hetero) Arylation Polymerization (DHAP) from dibromo-TPA (**1**) and the corresponding dioxythiophene or DPP-2T monomer as shown in Figure 3-4. While DHAP has been used to synthesize TPA based small molecules, to our knowledge this is the first use of DHAP to synthesize TPA polymers. DHAP is a fast, atom-efficient, low-impurity route to making conjugated polymers.[84, 162] The ability to couple dihydro monomers to dibromo monomers eliminates the need for stannanes or boronic esters, and has been shown to improve electronic performance compared to polymers prepared *via* Stille or Suzuki polymerization due to minimal residual impurities.[81, 163] For **P5**, DHAP conditions outlined by Leclerc and coworkers were used to avoid reaction of the 3-position on the thiophenes of the DPP-2T monomer (**5**).[164] Molecular weight data is summarized in Figure 3-4, and reveals that DHAP is an efficient method for preparing high molecular weight (M_n>20 kDa) TPA

polymers. All polymers in this study were highly soluble in chloroform and toluene, with 40 mg/mL solutions easily accessible for both solvents. The polymer **P4** has been previously synthesized via Suzuki polymerization in the Leclerc group, achieving an M_n of 9 kDa, showing that DHAP is an effective alternative to synthesizing TPA polymers with high molecular weight.[165]

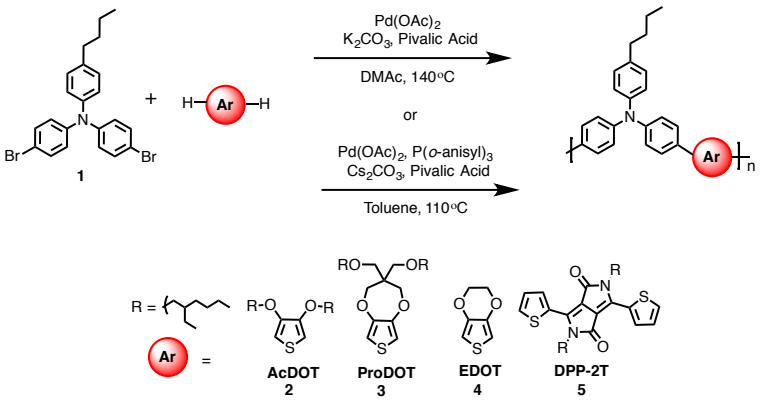

Compound	M_n (kDa)	$Đ$
[P1]	28	1.5
[P2]	33	2.7
[P3]	60	2.0
[P4]	29	2.2
[P5]	20	3.0

Figure 3-4. DHAP polymerization conditions for the synthesis of TPA polymers and table of molecular weight and dispersity values obtained *via* GPC.

3.3 Characterization of Triphenylamine Polymers

3.3.1 Absorption and Emission Properties

The absorption and emission spectra of **P2-P5** films and solutions are shown in Figure 3-5. Compared to the thin-film absorption profile of the colorless pTPA parent polymer, TPA-XDOT polymers are red-shifted to varied shades of yellow and show yellow-green fluorescence under UV light. This red shifting, noted by the arrow in Figure 3-5a, could be the result of several factors including increased degree of aggregation, increased conjugation length, decreased bond-length alternation (BLA) or electronic

effects from substituents on the backbone.[166] The progression from the sterically bulky AcDOT unit to the less bulky EDOT unit likely alters a combination of these effects. **P2-P4** differ slightly in bandgap, but overall they share similar optical properties. When TPA is coupled with a D-A-D unit (DPP-2T), the resulting purple polymer **P5** shows a characteristic donor-acceptor absorption profile, with a strong low-energy peak and a weaker high-energy peak as shown in Figure 3-5b. Aside from a slight peak broadening, films of **P2-P5** closely resemble the solution absorbance and emission spectra shown in Figure 3-5c-f, which can also signify a lack of increased order in the solid-state.

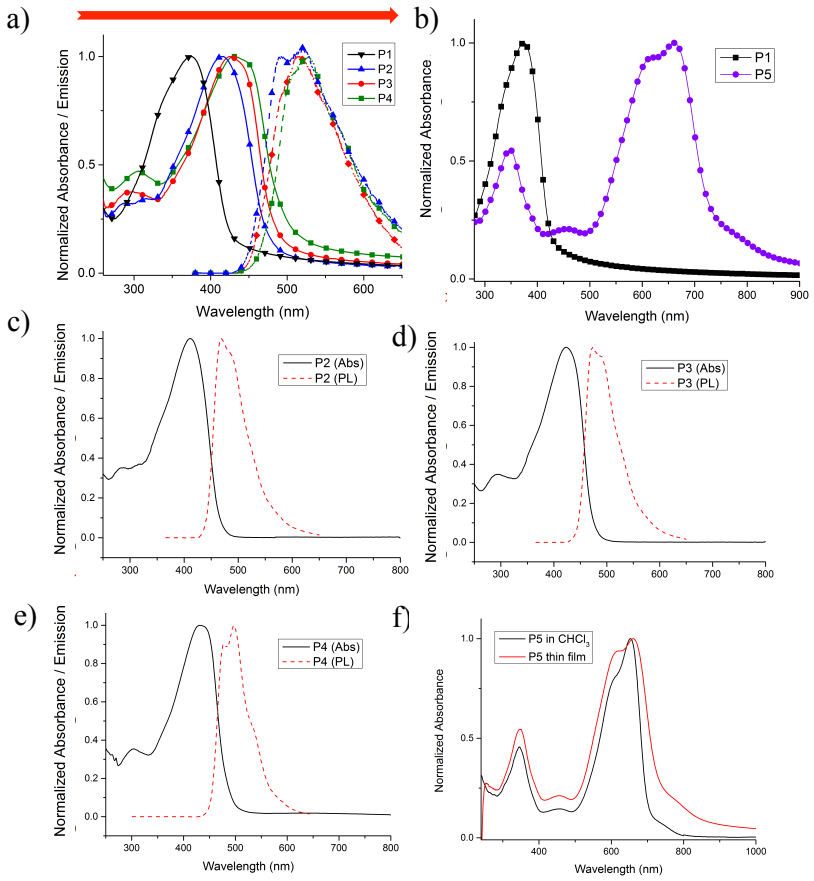

Figure 3-5. UV-vis absorption and fluorescence spectra of TPA-XDOT polymer thin films (a) showing slight red shifting moving from **P1** to **P4**, comparison of the thin film UV-vis absorption of **P5** to the parent polymer pTPA (b), dilute solution absorption and emission spectra in chloroform of **P2-P4** (c-e) and solution absorption spectra of **P5** (f).

3.3.2 Electrochemical Properties

While the absorption profiles of **P2-P4** are very similar, their electrochemical properties are much more varied. Cyclic Voltammetry (CV) and Differential Pulse Voltammetry (DPV) data of **P1-P5** is summarized in Figure 3-6. By decreasing the steric bulk between XDOTs and TPA, the XDOT becomes more capable of donating electron density to the TPA and the backbone becomes more planar, which in turn lowers the onset of oxidation for the polymer. This is believed to be the reason **P4** has an onset of oxidation about 400 mV lower than **P2**. However, this electron richness and lack of an electron accepting moiety prevents the TPA-XDOT copolymers from undergoing electrochemical reduction. In contrast, **P5**'s donor-acceptor structure provides a bandgap almost 1 eV lower than the TPA-XDOT materials and is stable to both oxidation and reduction.

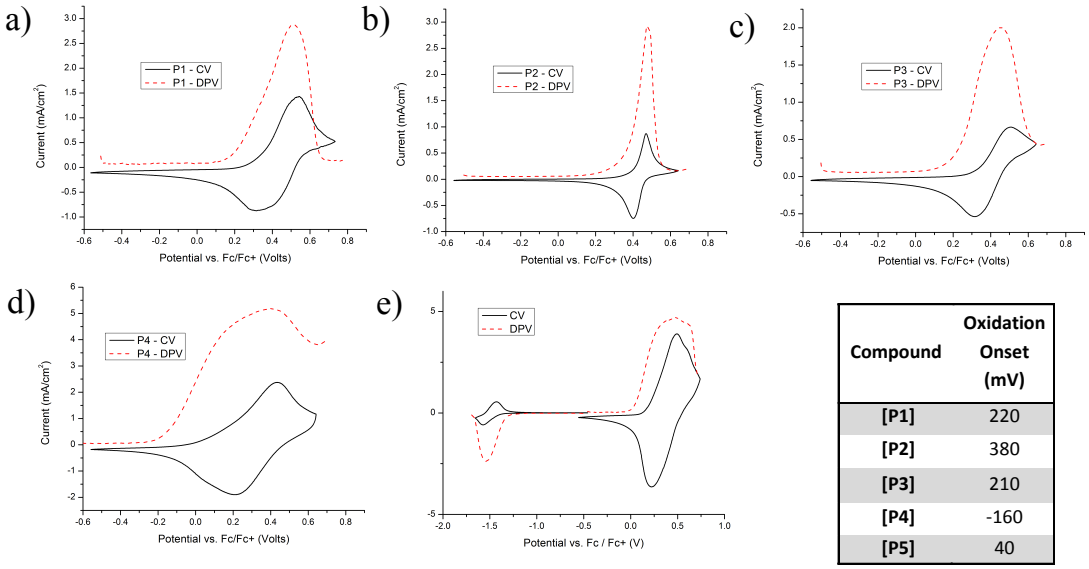

Compound	Oxidation Onset (mV)
[P1]	220
[P2]	380
[P3]	210
[P4]	-160
[P5]	40

Figure 3-6. CV and DPV oxidation data for **P1-P4** (a-d) and oxidation and reduction data for **P5** (e) with a table summarizing onsets of oxidation. Onset of oxidation measured from DPV scans vs. Fc/Fc+ reference.

3.3.3 Space-Charge Limited Current Hole Transport

The bulk hole mobilities of TPA thin films were measured using Space-Charge Limited Current (SCLC) methods on hole only devices with the architecture ITO/MoO_3/Polymer/MoO_3/Ag. While SCLC measurements typically yield lower mobility values in comparison to OFET device testing, this method was chosen due to its analysis of bulk mobility, which is more relevant for OPVs and PLEDs. The methods for fabricating devices and fitting the J-V curves for mobility are detailed in Chapter 2.4.6. Hole only device J-V curves, SCLC regime fits, mobility values, and thickness dependence tests of **P2-P5** are shown in Figure 3-7. Compared to the parent pTPA, whose mobility could not be determined due to too low of a J-V response, polymers **P2-P4** have comparable mobilities on the order of 10^{-5} $cm^2V^{-1}s^{-1}$. The incorporation of the XDOT units serves to increase the bulk mobility of the film, but the subtle differences between the three TPA-XDOT polymers yield no significant effect. These polymers are strongly field dependent, evidenced in Figure 3-7a-c, where the slope begins to increase above the expected value of 2 in the SCLC regime, indicating the presence of traps and hopping transport.

When polymerized with a D-A-D unit as in **P5**, the mobility increases by an order of magnitude to 10^{-4} $cm^2V^{-1}s^{-1}$. This increase is likely due to the favorable charge transport of the planar DPP unit, as there is no evidence of increased order in either DSC traces or GIWAXS data, shown is Figures 3-8 and 3-9, respectively. While shifts in Tg can be observed in the DCS traces, no polymer in this study produced a Tm peak prior to the decomposition temperature, suggesting these materials all form amorphous solid state structures. Similar results are seen in the GIWAXS data, where isotropic scattering

indicates the presence of π-π packing, but in no preferential direction. These isotropic scattering halos are consistent with other amorphous conjugated materials, including fullerenes. As can be seen in Figure 3-9, the BHJ film of **P5** and $PC_{71}BM$ appear nearly identical, as the amorphous scattering from π-π interactions in the polymer overlap with those found in $PC_{71}BM$. Interestingly, **P5** does not show strong field dependence, seen in Figure 3-7d, where the slope of 2 in the SCLC regime remains linear. This suggests that **P5** contains less trap states than the TPA-XDOT family, enabling higher mobility and field-independent charge transfer.

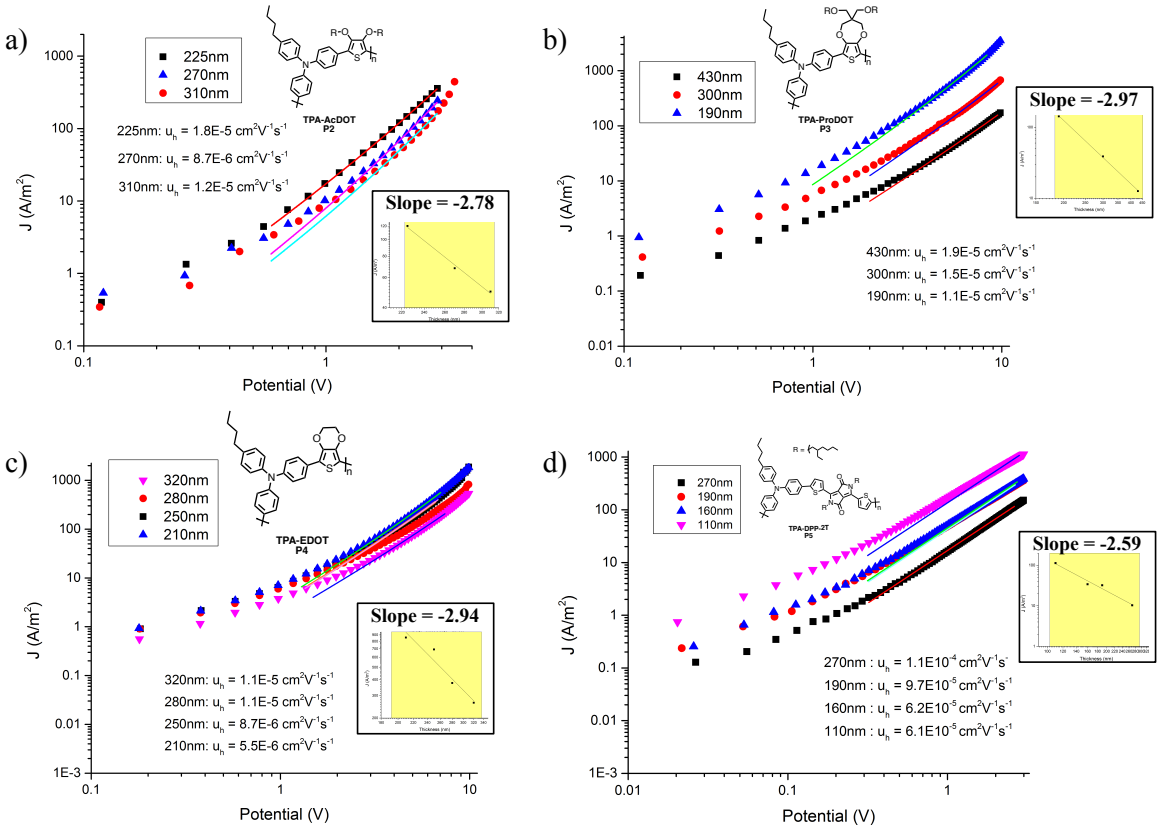

Figure 3-7. Hole only device J-V curves of **P2-P5** (a-d) of varying active layer thickness with mobility fits in the SCLC regime. Insets show thickness dependence tests to verify the relation $J \sim 1/L^3$.

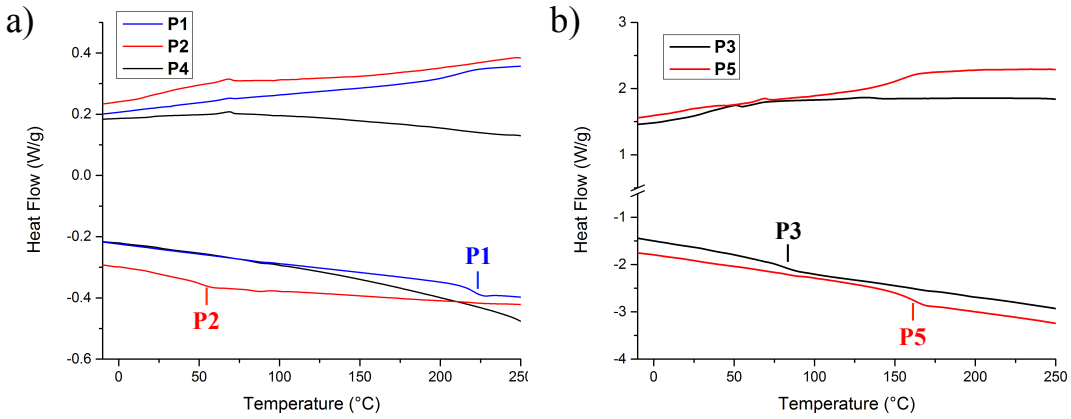

c)

Polymer	P1	P2	P3	P4	P5
T_g (^{0}C)	220	58	76	-	156

Figure 3-8. DSC traces of **P1,P2, P4** (a), **P3** and **P5** (b), and Tg values extracted from the curves (c).

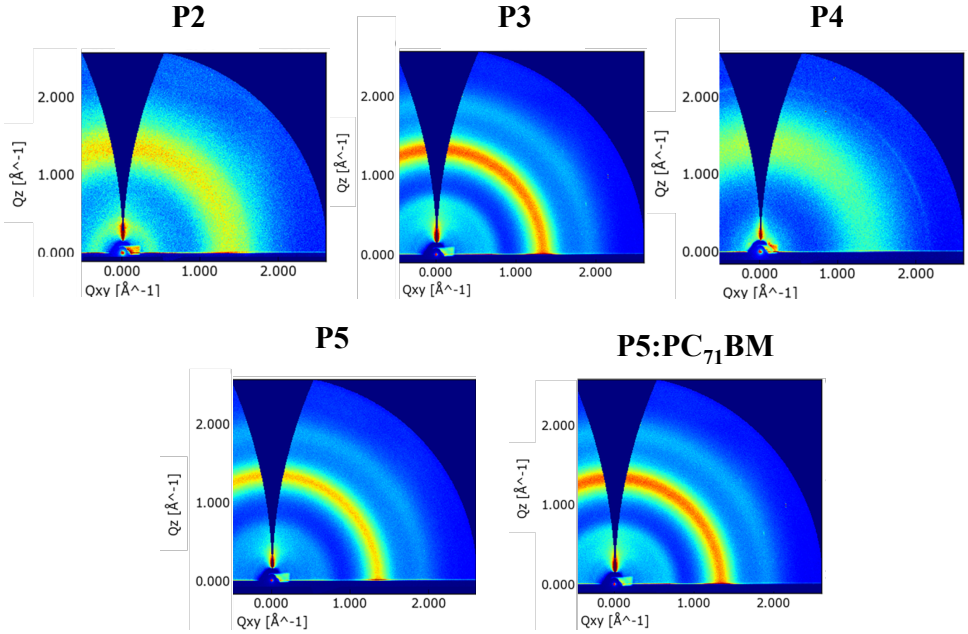

Figure 3-9. GIWAXS data of **P2-P5** showing isotropic scattering that is commonly found in amorphous conjugated polymers. BHJ of **P5:PC$_{71}$BM** shows an overlap of the isotropic scattering of the polymer and fullerene.

3.4 Triphenylamine Polymer Applications

3.4.1 Electrochromism

All three of the TPA-XDOT polymers were blade coated onto ITO glass and evaluated as EC materials as detailed in Chapter 2.4.4. As seen in Figure 3-10a and 3-10b, **P3** and **P4** were able to switch between yellow neutral states and less colored oxidized states in a voltage window of -0.5 V to 0.7 V; however, **P2** was incapable of reversibly switching. We hypothesize that **P2** does not switch reversibly because the film begins to lose adhesion to the electrode upon redox cycling. This instability may be the result of the highly twisted backbone caused by the combination of the sterically bulky AcDOT and TPA units. **P3** and **P4** share similar EC properties, reaching ~45% contrast with switching speeds of 2.3 and 1.5 seconds at their respective λ_{max}, as shown in Figure 3-10c and 3-10d. The colorimetry of both **P3** and **P4** in their neutral state, as seen in Figure 3-10e, have large positive b* (yellow) values and low negative a* (green) values, resulting in the overall appearance of yellow films. As the polymers are oxidized there is a gradual decrease in neutral absorbance and increase in polaron absorption leading to a green intermediate color, with colorimetry values approaching and then crossing the a* axis. Interestingly, the colorimetry reveals that the most color neutral states for both polymers are not the fully oxidized states. This is due to the steady increase in absorbance in the near IR region encroaching upon the visible region of the spectrum after the film has already become color neutral, leaving residual color in the fully oxidized state. Both polymers become most color neutral at 0.5 V, with a*/b* values of 1.1/2.2 and 2.2/0.6 for **P3** and **P4**, respectively.

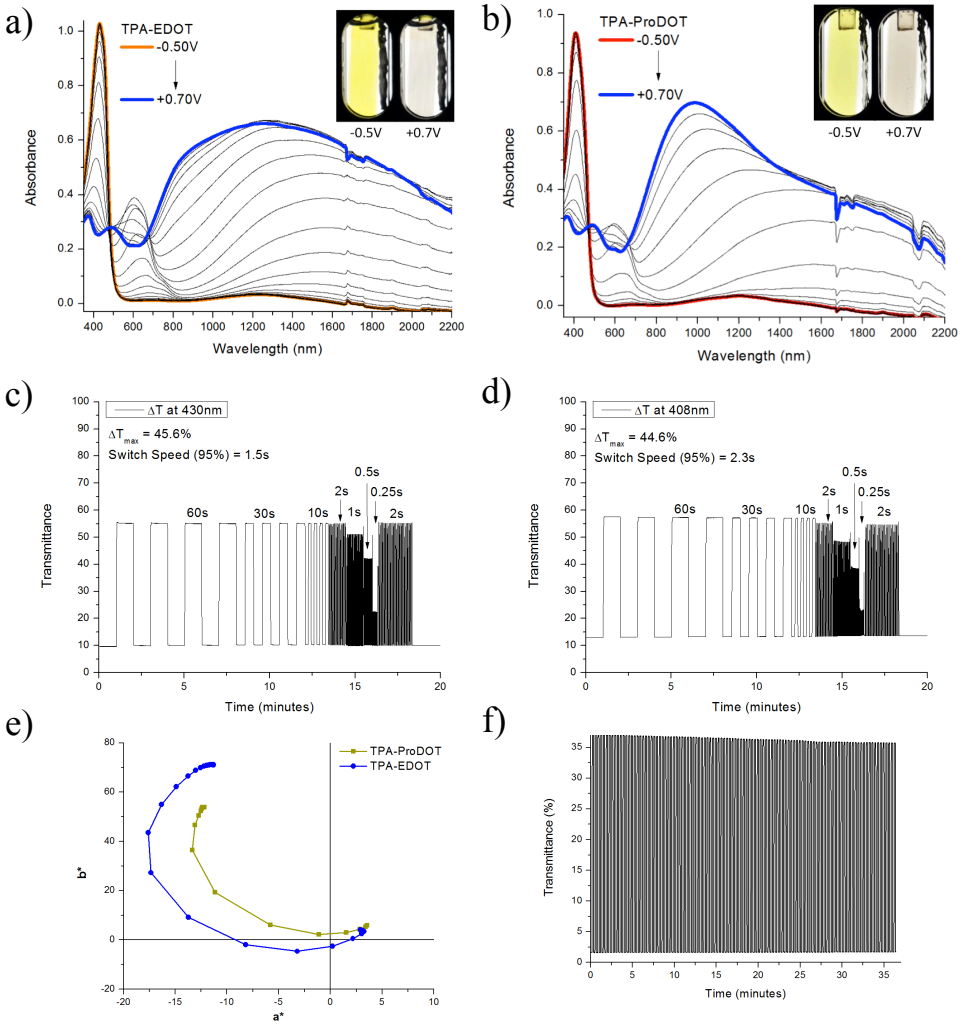

Figure 3-10. Spectroelectrochemical data of **P4** (a) and **P3** (b) with photographs of the film on ITO in both neutral (yellow) and oxidized (colorless) states. Switching speed data of **P4** (c) and **P3** (d) shown at various switching speeds at the polymers' λ_{max}. a*b* diagram showing the color change occurring during electrochemical oxidation of **P3** and **P4** from -0.5 V to 0.7 (e), and switching stability example of **P4** under 1000 switches between -0.5V to 0.7V in 10 second intervals.

Unlike typical EC polymers (e.g. PEDOT), **P3** and **P4** do not appear to form bipolaron bands, which can be attributed to the broken conjugation caused by the lone electron pairs on the nitrogen atoms along the backbone. This break in conjugation leaves each repeat unit in effective electronic isolation from the next, making bipolaron stabilization across the backbone inefficient, and resulting in TPA-XDOT polymers operating, in effect, as discrete chromophores which form cation radical and dication

states. In order to evaluate the stability of the TPA polymers to redox cycling, **P4** was electrochemically switched for 1000 cycles, as shown in Figure 3-10f. Only a small change in contrast (~2%) was observed, demonstrating the stability of these polymers. The stability of this polymer is unique, as the Reynolds group has typically observed stability issues when incorporating phenylene units into the polymer backbone, with contrast dropping off after just 20 cycles.[167] Crosslinking through the phenylene unit under redox cycling has been hypothesized to be the cause of this instability, but the stability observed in **P4** does not fit with this theory. One possible explanation for this increased stability is that the spin density of the radical cation is highly localized on the nitrogen center of TPA, making it less reactive to crosslinking through the phenyl rings compared to dioxythiophene-phenylene polymers. The D-A-D polymer, **P5**, is ineffective as an EC because the color change was minimal, moving from a deep blue (neutral) to a slightly more transparent blue (oxidized) state.

3.4.2 Polymer Light-Emitting Diodes

PLEDs were fabricated with TPA-XDOT polymers as the active layer in the architecture ITO/PEDOT:PSS/TPA-XDOT/Ca/Al, as detailed in Chapter 2.4.3, and the resulting J-V and Luminance curves can be found in Figure 3-11. While all three polymers emitted yellow-green light with peak intensities between 515-530 nm, **P3** exhibited the most stable performance, shown in Figure 4, with a turn-on voltage around 4V and a maximum luminance of ~250 cd/m2 at 6V. **P2** displays a higher max luminance of ~450 cd/m2 and has a much sharper turn-on threshold but a large amount of leakage current. **P4** is much less stable, showing large leakage currents and requiring larger currents to reach max luminance of ~450 cd/m2 at 8 V before quickly dying out. Since

P2 contains the sterically bulky AcDOT monomer, the decrease in intermolecular interactions would promote recombination over charge transfer, and therefore increased EL efficiency. However, as with the electrochromic results for **P2**, there is some inherent instability within the film, especially at higher voltages. For **P4**, the increased planarity between the XDOT unit and the phenyl unit of TPA may lead to more favorable intermolecular interactions, which would promote charge transfer over recombination and decrease EL efficiency. For **P5**, creating an internal donor-acceptor system leads to quenching of visible fluorescence, so the material could not operate in a PLED.

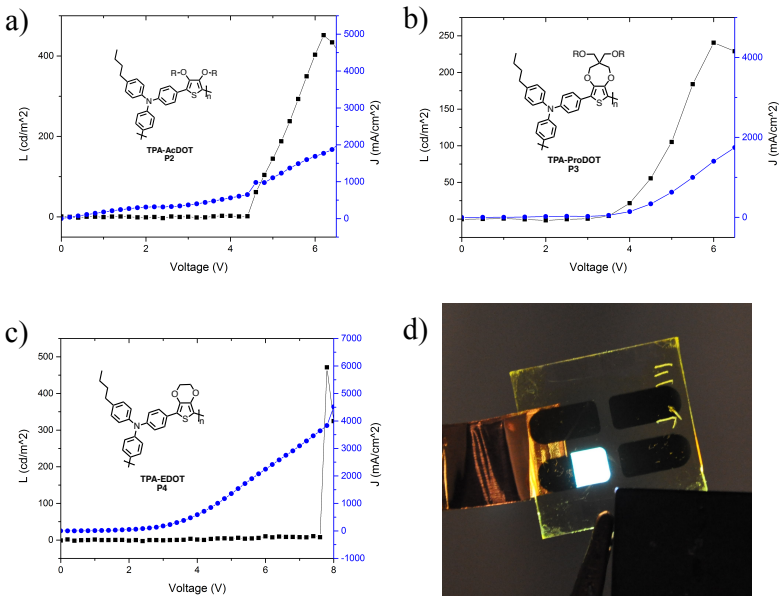

Figure 3-11. Luminance (L) and Current Density (D) vs. Voltage (V) plots of **P2-P4** PLED devices (a-c) and image of **P3** PLED in operation (d).

3.4.3 Organic Photovoltaic Devices

Although its donor-acceptor structure prevented **P5** from properly functioning as an EC or EL device, its strong visible light absorption and low bandgap led us to

investigate the polymer's ability to serve as a donor phase material in bulk heterojunction solar cells with the well-known acceptor $PC_{71}BM$ as illustrated by the device metrics in Figure 3-12. Device fabrication and testing details can be found in Chapter 2.4.1. Despite its amorphous qualities, solar cells with the architecture ITO/PEDOT:PSS/**P5**:$PC_{71}BM$ (1:3)/Ca/Al achieved an average PCE of 2.31%. Though these results are not state-of-the-art, the mobility and PCE is surprising for a polymer that lacks any detectable order in both pristine films and in blends with $PC_{71}BM$ as evidenced by GIWAXS results in Figure 3-9, suggesting that hopping across small polymer aggregates is sufficient for charge separation and transport. This type of transport within disordered polymers has been highlighted by Noriega *et al.* as a viable route to high mobility materials.[91] One route to improve the PCE of this structure is through side chain tuning, as this has been shown to have a significant impact on polymer/fullerene mixing.[168] Polymers **P1-P4** were not considered for OPV cells due to their high bandgaps.

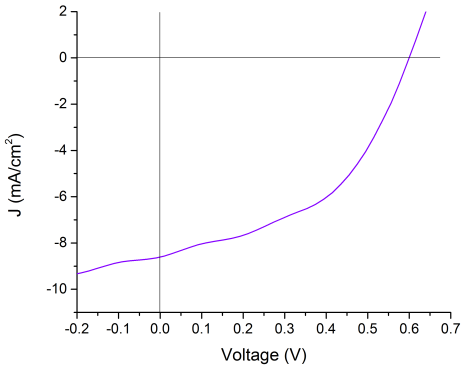

Device	**P5**:$PC_{71}BM$ (1:3)
J_{SC} ($mAcm^{-2}$)	8.18± 0.25
V_{OC} (V)	0.61
FF (%)	46.63 ± 1.23
PCE (%)	2.31 ± 0.15

Figure 3-12. J-V curve and associated device metrics of an OPV cell using **P5**:$PC_{71}BM$ as the active layer.

3.5 Summary of Results

This work demonstrates that TPA copolymers prepared by DHAP can be used to develop new multifunctional optical and electronic materials. TPA units are effective processing comonomers, providing favorable solubility and film forming attributes while serving as a conjugation breaking building block. This embedded break provides materials with controlled levels of conjugation, which results in the ability to tune redox potential, light absorption/emission, and charge transport depending on the comonomers used. While no signs of local aggregation are evident through DSC or GIWAXS, TPA-XDOT polymers have mobilities on the order of 10^{-5} $cm^2V^{-1}s^{-1}$, display luminance up to ~450 cd/m^2 in PLEDs, and can be switched between yellow and transparent in EC devices with contrasts up to 45%. By incorporating an electron-deficient unit into the pTPA backbone, amorphous TPA polymers can be used as active layers in OPVs, with **P5** reaching efficiencies of up to ~2.5%. Ultimately, varied functionality can be brought into amorphous TPA polymers by copolymerizing with either electron rich or electron poor aryl monomers. Though there is still a balance to be struck when designing multipurpose organic electronic materials, this work shows that highly soluble materials can be designed with multifunctionality in mind. However, a major drawback of this amorphous design through a TPA processing comonomer is the low charge mobility that likely arises from the high degree of disorder and broken conjugation, hindering both interchain and intrachain charge transport. While this work showed that with more planar comonomers, such as DPP-2T, charge mobility can be increased, it may prove difficult for this design to enable the high mobility materials required for OFET and OPV applications. On the other hand, these polymers exhibited promising EC properties,

especially in terms of stability. Further work on TPA copolymers may prove useful in new EC polymer designs, as well as materials for dual EC/EL devices.

3.6 Synthetic Methods

General Synthetic Materials and Methods:

The parent polymer, pTPA **(P1)** was purchased from 1-Material, analyzed by ^{1}H NMR and GPC, and used without further purification. The monomers used in this study, 4,4'-dibromo-4''-butyltriphenylamine (dibromo-TPA, **1**), 3,4-di(2-ethylhexyloxy)thiophene (AcDOT, **2**), 3,4-propylene (diethylhexyloxymethyl) dioxythiophene (ProDOT**,** **3**), and 2,5-di(2-ethylhexyl)-3,6-di(thiophen-2-yl)-diketopyrrolopyrrole (DPP-2T, **5**) were synthesized *via* literature procedures.[169-171] 3,4-ethylenedioxythiophene (EDOT, **4**) (97%) was purchased from Alfa Aesar and purified via vacuum distillation before use. Pivalic acid (99%, Sigma), $Pd(OAc)_2$ (98%, Strem Chemicals), Hermann's catalyst (98%, Sigma), K_2CO_3 (anhydrous, Oakwood Products), 18-Crown-6 (99%, Acros), diethyldithiocarbamic acid diethylammonium salt (97%, TCI America), P(*o*-anisyl)$_3$ (96%, Sigma), and Cs_2CO_3 (anhydrous, Oakwood Products) were all used as received. N,N-dimethylacetamide (DMAc) (HPLC grade, Alfa Aesar) was filtered through a pad of basic alumina (Sigma Aldrich) and degassed prior to use. Chloroform and chlorobenzene (BDH) were used without further purification to dissolve the polymers.

Polymerization of TPA-XDOT family

Dibromo-TPA **(1)** (1mmol), XDOT monomer **(2, 3, or 4)** (1 mmol), $Pd(OAc)_2$ (2 mol%), pivalic acid (0.33 mmol), and potassium carbonate (3 mmol) were added to an oven-dried 50 mL roundbottom flask. The flask was vacuum pumped and refilled with argon 3 times before adding 10 mL of DMAc to the reactants under argon. The flask was equipped with an oven-dried condenser, and the solution was stirred at 140 °C for a material dependent amount of time as detailed below. After completion, the solution was cooled to room temperature and then precipitated into methanol. Chloroform was used to dissolve any material remaining in flask, and was also precipitated into methanol. After 30 minutes of stirring in methanol, the solution was filtered over a 0.45 μm nylon filter. The filtered solid was collected into a Soxhlet thimble, and was purified *via* successive Soxhlet extractions in methanol, acetone, hexanes, dichloromethane, and chloroform for 24 hours each. Depending on the polymer, either the dichloromethane or chloroform fraction was taken and allowed to stir at 40 °C with a spatula tip of a palladium scavenger (diethylammonium diethyldithiocarbamate) and a potassium scavenger (18-crown-6) for 1 hour. The solution was then concentrated by rotary evaporation to < 10 mL and reprecipitated into methanol. After 30 minutes stirring in methanol, the solution was filtered and the final polymer solid was collected and dried under vacuum.

TPA-AcDOT (P2): The roundbottom flask was lowered into an oil bath preheated at 140 °C and was left to stir for 15 minutes until the solution seized up into a gel. Insoluble material was transferred to the Soxhlet thimble along with the precipitate. After Soxhlet extraction and precipitation (main fraction in dichloromethane), a yellow twine-like solid was afforded with a 23% yield. M_n: 33 kDa, Đ: 2.7 vs PS in THF @ 35 °C, ^{1}H NMR (300 MHz, $CDCl_3$@50 °C): δ: 7.59 (br, 4H), 7.07 (br, 8H), 3.92 (d, 4H), 2.60 (br, 2H), 1.64 (m, 4H), 1.20 –1.50 (m, 23H), 0.95 (t, 4H), 0.87 (t, 14H). Anal. calcd. for $C_{42}H_{55}NO_2S$: C (79.07) H (8.69) N (2.20) S (5.03), Found: C (79.19) H (8.64) N (2.11) S (4.85).

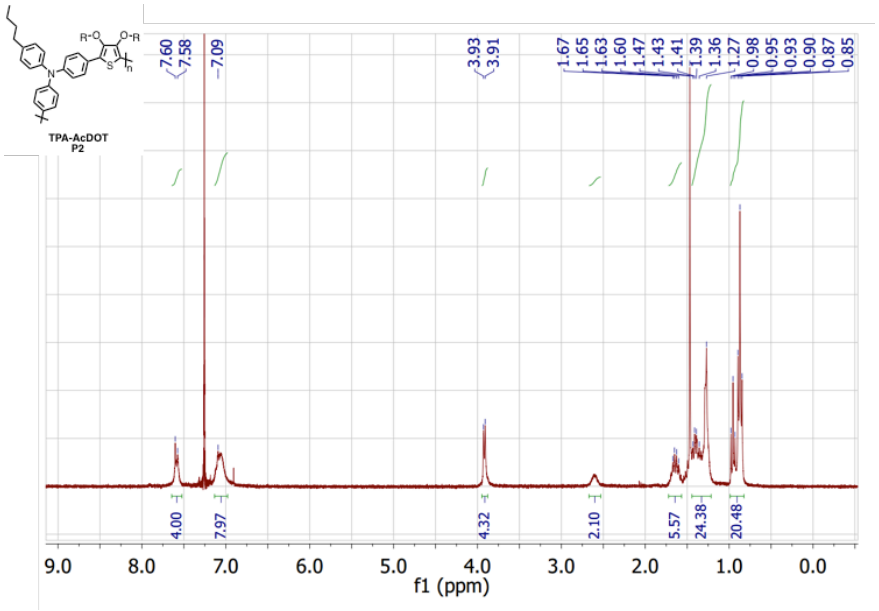

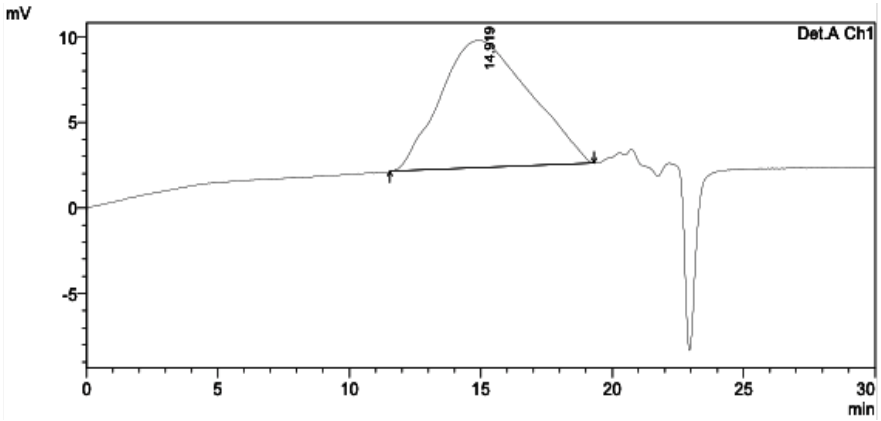

TPA-ProDOT (P3): The reaction was left to stir overnight. Insoluble material was transferred to the Soxhlet thimble along with the precipitate. After Soxhlet extraction and precipitation (main fraction in dichloromethane), a yellow powder was afforded with a 65% yield. M_n: 60 kDa, Đ: 2.0 vs PS in THF @ 35 °C, ^{1}H NMR (300 MHz, $CDCl_3$@50 °C): δ: 7.60 (br, 4H), 7.07 (br, 8H), 4.15 (s, 4H), 3.55 (s, 4H), 3.30 (d, 4H), 2.60 (t, br, 2H), 1.63 (m, 2H), 1.20 –1.50 (m, 28H), 0.90 (m, 17H). Anal. calcd. for $C_{47}H_{63}NO_4S$: C (76.48) H (8.60) N (1.90) S (4.34), Found: C (75.68) H (8.69) N (1.90) S (4.33).

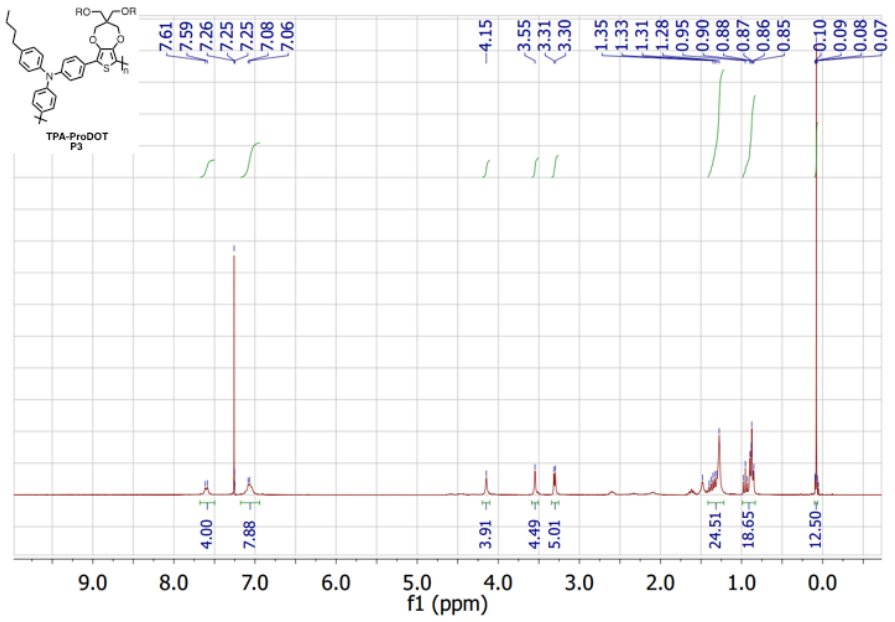

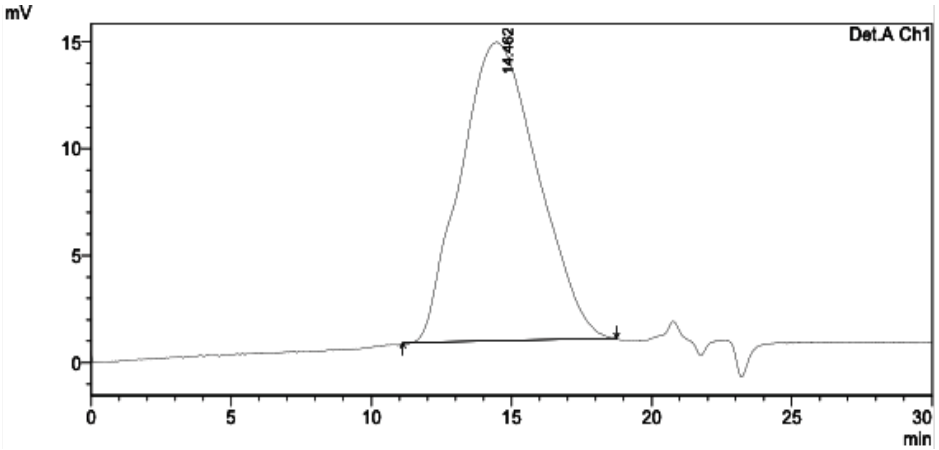

TPA-EDOT (P4): Reaction was left to stir for 8 hours. After Soxhlet extraction and precipitation (main fraction in chloroform), a yellow flaky solid was afforded with a 51% yield. M_n: 29 kDa, Đ: 2.2 vs PS in THF @ 35 °C, ^{1}H NMR (300 MHz, $CDCl_3$@50 °C): δ: 7.60 (br, 4H), 7.07 (br, 8H), 4.32 (s, 4H), 2.55 (t, br, 2H), 1.58 (m, 2H), 1.37 (m, 2H), 0.93 (t, 3H). Anal. calcd. for $C_{28}H_{25}NO_2S$: C (76.51) H (5.73) N (3.19) S (7.29), Found: C (76.33) H (5.68) N (3.22) S (7.80).

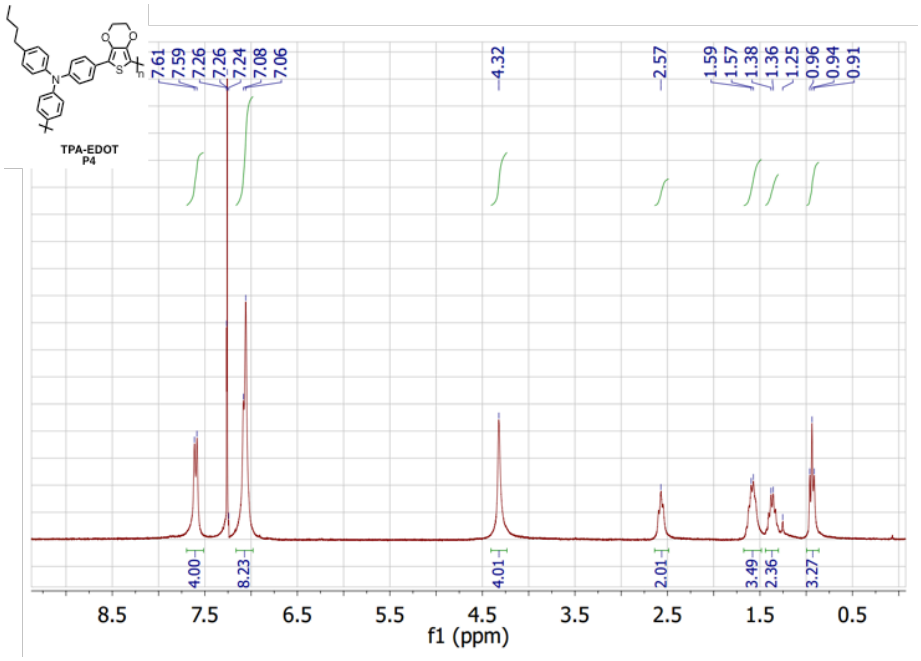

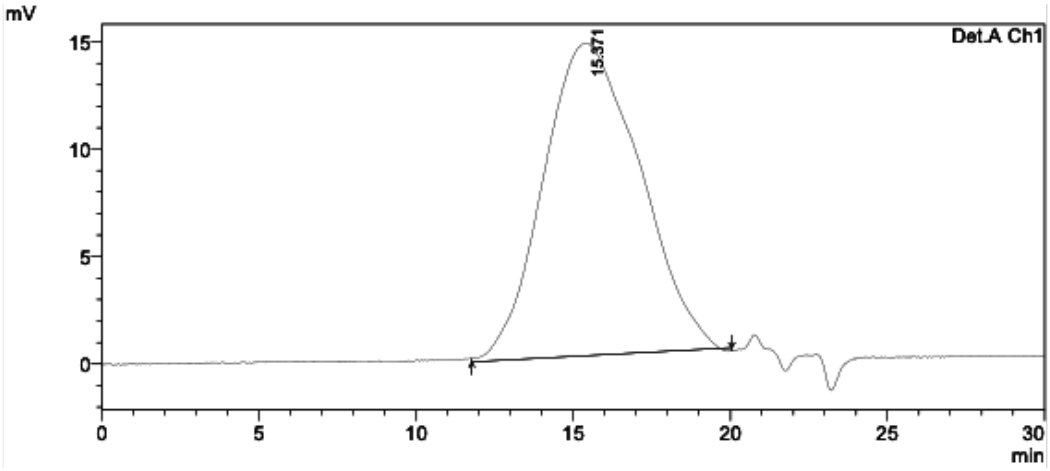

Synthesis of TPA-DPP-2T (P5)

Dibromo-TPA **(1)** (0.534 mmol), DPP-2T **(5)** (0.534 mmol), $Pd(OAc)_2$ (5 mol%), P(o-anisyl)$_3$ (10 mol%), pivalic acid (0.534 mmol), and cesium carbonate (1.60 mmol) were added to an oven-dried 50 mL roundbottom flask. The flask was vacuum pumped and refilled with argon 3 times before adding 10 mL dried, degassed toluene to the reactants under argon. The flask was equipped with an oven-dried condenser, and the solution was stirred at 110 °C for 20 hours. After completion, the solution was cooled to room temperature and then precipitated into methanol. Chloroform was used to dissolve any material remaining in flask, and was also precipitated into methanol. The solution was filtered over a 0.45 μm nylon filter, the solid was collected into a Soxhlet thimble, and was purified *via* successive Soxhlet extractions in methanol, acetone, hexanes, dichloromethane, and chloroform for 24 hours each. The chloroform fraction was taken and allowed to stir at 40 °C with a spatula tip of a palladium scavenger (diethylammonium diethyldithiocarbamate) for 1 hour. The solution was then condensed to < 10 mL and reprecipitated into methanol. The solution was filtered and the final polymer solid was collected and dried under high vacuum, resulting in 341 mg (78%) of **P5** as a fluffy purple solid. Mn: 20 kDa, Đ: 3.0 vs PS in 1,2,4-trichlorobenzene @ 140 °C. ^{1}H NMR (300 MHz, $CDCl_3$@50 °C): δ: 8.95 (d, 2H), 7.55 (d, 4H), 7.38 (d, 2H), 7.15 (q, br, 8H), 4.07 (d, br, 4H), 2.61 (tr, 2H), 1.95 (br, 2H), 1.65 (m, 2H), 1.27 (m, 18H), 0.98 (m, 15H). Anal. calcd. for $C_{28}H_{25}NO_2S$: C (75.97) H (7.23) N (5.11) S (7.80), Found: C (75.76) H (7.19) N (4.88) S (7.55).

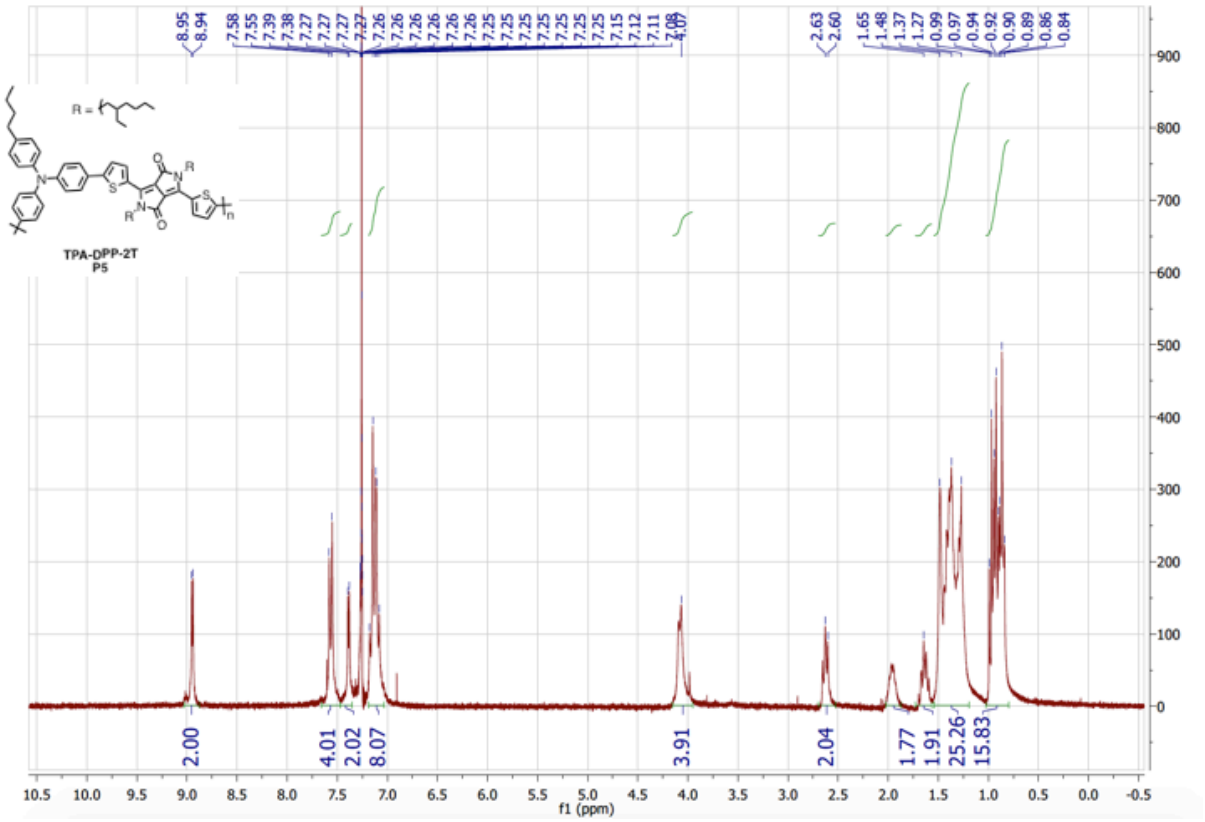
TPA-DPP-2T
P5
f1 (ppm)

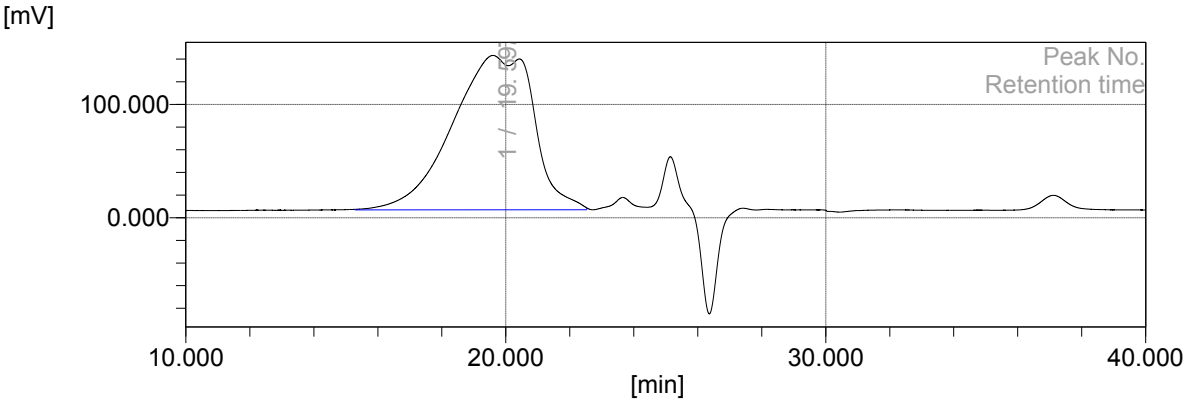
[mV]
100.000
0.000
10.000
20.000
30.000
40.000
[min]
Peak No.
Retention time

CHAPTER 4

ENABLING SMART AQUEOUS PRINTING WITH MULTISTAGE SIDE CHAINS

4.1 Background and Motivation

One of the core advantages of organic electronic devices is the ability to adapt their fabrication to continuous, large area, low-temperature, solution processing techniques; commonly referred to as roll-to-roll processing.[99, 172] However, most research labs conducting solution-processable organic electronics research make use of halogenated, aromatic solvents such as chlorobenzene to dissolve and coat thin films from their semiconducting materials. These solvents present many health and environmental risks, and in many cases would preclude the transition of organic electronics from research lab to industrial printing facilities. Estimates show that with current printing processes for organic photovoltaic (OPV) devices, 16 million liters of chlorobenzene (over 6 Olympic swimming pools) would be needed to print $1GW_p$ of solar panels.[173] Industries will not adopt this technology if large quantities of halogenated solvents are required as the carrier solvent; so developments are being made throughout the field to move towards continuous solution-processing techniques that make use of safe and environmentally benign "green" solvents.

Numerous groups have focused their attention on using alternate solvents such as xylene derivatives, THF, hexanes, and tetralin, which have led to photovoltaic and field-effect transistor performance comparable to chlorobenzene.[174-181] In many cases, the

materials are not redesigned for these solvents, and focus is placed on optimization of processing variables to replicate high mobility through different solvents. While these solvents are preferred over halogenated solvents, to fully address safety concerns and lower the barrier to industrial feasibility, efforts should be made to move towards environmentally benign solvents such as ketones, esters, alcohols, 2-methyl THF, and water.[182-183]

In this chapter, a novel multistage cleavable side chain approach is presented that provides aqueous solubility to conjugated polymer systems without sacrificing electroactivity. Using this method, conjugated polymers can be synthesized, purified, and characterized in organic solvents, hydrolyzed to obtain an aqueous soluble conjugated polyelectrolyte, and coated onto substrates using aqueous solutions. After thin film deposition, UV irradiation can be used to photocleave the side chain, leaving behind a solvent-resistant, electroactive polymer backbone that is free from insulating side chain mass. This chapter will cover prior and ongoing methods within the organic electronics community to develop water-soluble conjugated polymers, including polar and ionic side chains, and miniemulsion to create colloidal solutions. A brief review of conjugated polymers with cleavable side chains will also be presented as an introduction to the multistage side chain method. After a discussion about the concept and benefits of this process, the first proof-of-concept multistage side chain polymer, **P(T3-MS)**, will be introduced alongside methods of characterizing the material and its functionality in electrochromic (EC) films and OFET devices. Follow up work on a multistage polymer designed for high performance in OFET devices, **P(DPP-DTT-MS)**, will be presented along with the ability for this polymer to enable electrolyte-gated organic transistors

(EGOTs) that can be fully printed (electrodes, dielectric, semiconductor) using only green solvents (water, isopropanol, acetone).

4.2 Functional Side Chains as Processing Components

A central theme of this dissertation is the use of structural motifs within conjugated polymers to impart desirable processability. Polymer side chains have been a predominant handle for chemists to alter solubility, and therefore processability, in conjugated polymers, with aliphatic side chains providing organic solubility serving as a common example.[184] By utilizing side chains that incorporate functional and reactive groups, solubility can be affected in a variety of ways that go beyond organic solvents. Ionic and polar side chains can be used to impart aqueous solubility, and cleavable side chains can be used to create solvent resistance after thin film deposition.

4.2.1 Ionic and Polar Side Chains

Conjugated polymers with pendant ionic side chains, or conjugated polyelectrolytes, exhibit aqueous solubility and have been widely studied and are commonly used in electrode modification and solution-based redox applications, but have limitations in solid-state semiconductors due to their inherent conductivity and the ability of ions to screen a voltage bias.[185-186] For these reasons, there a few examples of conjugated polyelectrolytes used as active layers in solid-state applications, with the work presented in this chapter and a cationic conjugated polyelectrolyte by the Bazan group serving as the only examples of polyelectrolyte OFETs.[187] Outside of solid-state applications, conjugated polyelectrolytes processed from aqueous solutions have shown promise in organic electrochemical transistors (OECTs), where the presence of ions can

support the transport of electrolyte ions within semiconductor films.[188] Apart from ionic groups on the side chain, another method for obtaining aqueous processability is the use of ionic surfactants and conjugated polymers with aliphatic side chains in a miniemulsion process to create semiconductor colloids that can be dispersed in aqueous media.[189-190] However, even with this method the impact of ionic groups within the aqueous coated thin films can hinder electroactivity, as the Chung group showed that switching from an ionic surfactant to a non-ionic surfactant in conjugated polymer colloids can increase OFET mobility from 10^{-3} $cm^2V^{-1}s^{-1}$ to 2.5 $cm^2V^{-1}s^{-1}$.[191]

Using polar, nonionic side chains, such as oligoethers, remedies the effects of pendant ions and has been used to achieve water soluble polythiophenes for OFETs with mobility values on the order of 10^{-5} $cm^2V^{-1}s^{-1}$.[192] Similar to ionic side chains, polar side chains have shown promise in OECTs due to their ability to support ion transport within polymer films.[48] However, many oligoether functionalized CPs suffer from poor solubility in both organic and aqueous solvents, and while they can be coated from dispersions, they often cannot be characterized by common methods like gel permeation chromatography (GPC).[48].

4.2.2 Cleavable Side Chains

Cleavable side chains provide conjugated polymers with the ability to transition from organic solubility to aqueous solubility, or from solubility to insolubility. Examples can be found within the Frechet group, where thermo-cleavable ester side chains were incorporated into conjugated polymers as a route to post-processing functionality.[65-66] Shown in Figure 4-1a, these polymers could be cast from chlorobenzene and then heated

to ~200° C to cleave ester sidechains, resulting in solvent resistant polymers with pendant carboxylic acids that exhibited up to a 0.5 eV decrease in bandgap compared to their non-cleaved counterparts. In an alternate approach to esters, Reeves *et al.* synthesized conjugated polymers with heptanoate sidechains that were aerosol spray coated from toluene and subsequently saponified by submersion into KOH in methanol, as shown is Figure 4-1b.[193] After methanolysis, the alcohol functionalized polymer films became solvent resistant and retained their electrochromic properties. In these systems, long aliphatic sidechains were utilized for their solubilizing properties, but the ester linkage provided processing functionality that allows for their removal after deposition.

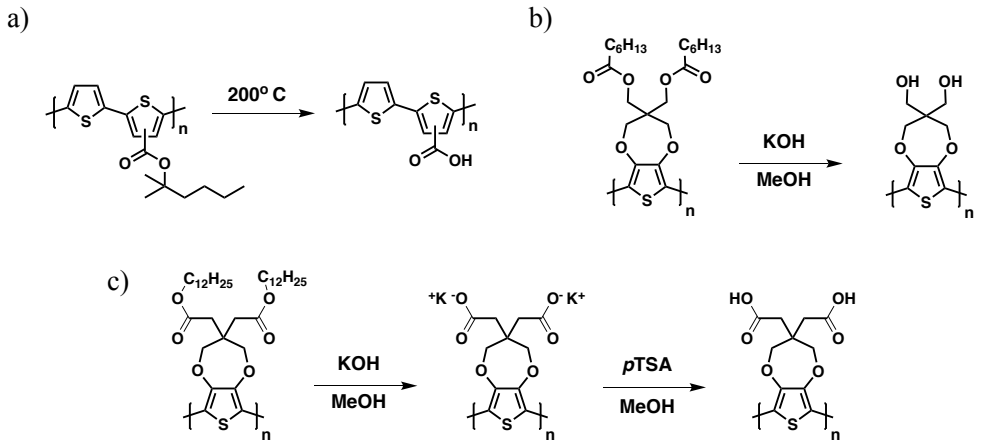

Figure 4-1. Examples of side chain cleavage reactions in conjugated polymers. Thermal cleavage of an organic soluble ester functionalized polymer to an insoluble polymer film (a)[65], hydrolysis of an organic soluble ester side functionalized polymer to an insoluble film (b)[67], and hydrolysis of an organic soluble ester functionalized polymer to a water soluble polyelectrolyte, followed by acidification to an insoluble polymer film (c).[63]

Conjugated polymers with ester side chains have also been saponified in bulk, providing access to aqueous solubility *via* carboxylate terminated side chains as shown in Figure 4-1c.[64, 194] These conjugated polyelectrolytes were spray cast from water and converted to solvent resistant films by acidification of carboxylates to carboxylic acids,

providing an environmentally benign method for producing robust films for electrochromic and supercapacitor applications. These systems make use of aliphatic side chains to achieve organic solubility for conventional polymerizations, characterization, and purification, while the ester linkage provides the processing functionality to bring aqueous solubility to the materials. In all of these examples, ester side chains can provide the processing functionality for a post-deposition cleavage or a pre-deposition solubility transition, depending on the orientation of the ester. Both functionalities are desirable for printed electronics processing, but in these systems the ester side chains can only provide one or the other.

4.3 Conjugated Polymers with Multistage Side Chains

In this work, we present design guidelines for integrating two orthogonal processing functionalities into conjugated polymers, enabling new routes for aqueous processing of organic electronic materials. The general concept is outlined in Figure 4-2. Multistage cleavable side chains are designed to provide conjugated polymers with three processing stages, with each being removed to transition to the following stage. In *Stage 1* the polymer is soluble in organic solvents, allowing for the use of traditional polymerization methods (Stille, Suzuki, Direct Arylation), Soxhlet purifications, and characterization in organic solvents. It should be noted that in application, this stage would be carried out by a chemical manufacturer in typical polymer production facilities. After production, the first responsive functional group can be triggered to transition into *Stage 2*. In this processing stage the polymer is soluble in aqueous solutions and can be printed onto substrates without the use of surfactants. Here, the processing may be done in a myriad of printing and coating facilities where the water solubility will limit toxic

exposure. After printing, the second responsive functionality can be triggered to remove the cleavable sidechains and transition to the *Core* polymer. The *Core* is primarily made up of the conjugated backbone alone, providing an insoluble electroactive film ready for application in an electronic device. As such, the final material will be composed as much as possible of electroactive, conjugated material. Using this concept, we demonstrate a proof of concept polymer, **P(T3-MS)** with multistage cleavable sidechains that can be processed from an aqueous solution and used as the active material in organic field-effect transistor (OFET) and electrochromic (EC) applications.

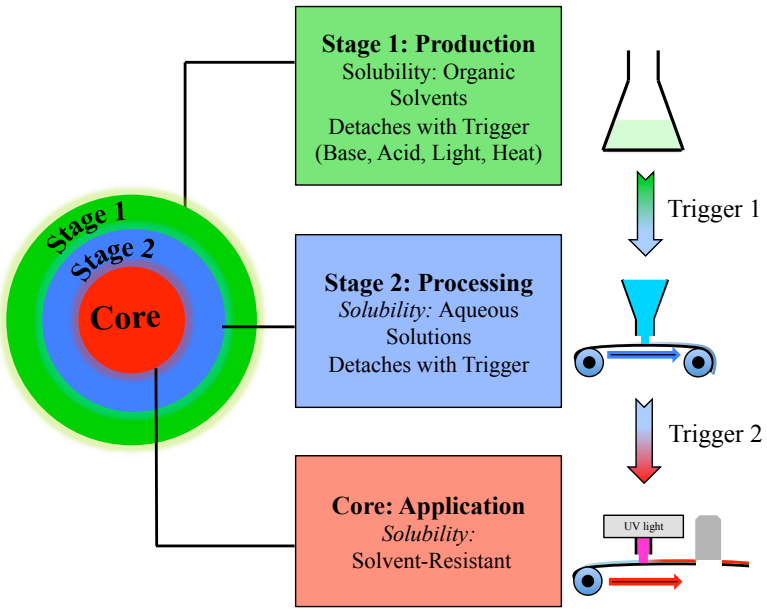

Figure 4-2. Design concept for polymers with multistage cleavable side chains. Polymers can be synthesized with organic solubility, converted to an aqueous soluble polymer through Trigger 1, and converted to an insoluble polymer through Trigger 2.

4.4 Proof of Concept Multistage Polymer P(T3-MS)

A polythiophene bearing multistage cleavable side chains, **P(T3-MS)-O**, was synthesized to demonstrate the use of this process. Shown in Figure 4-3, this regiorandom polythiophene contains two reactive functional groups: esters and an *o*-nitrobenzyl group.

The esters provide the ability to transition from an organic soluble polymer to an aqueous soluble polyelectrolyte through a post-polymerization reaction in base. Saponification of ester side chains to carboxylates has been previously used within the Reynolds group to allow for aqueous processing of conjugated, electrochromic polymers.[64, 194] The *o*-nitrobenzyl functionality embeds a mechanism for cleaving off the bulk of the side chain through UV induced formation of a radical on the nitro group. *O*-nitrobenzyl groups have been commonly used by polymer chemists to create controlled cleavage points[195], and have been used by the Thomas group to create UV patternable polythiophene photoresists.[70] In combination, these reactive functionalities provide the organic soluble **P(T3-MS)-O** with the ability to transition to an aqueous soluble polyelectrolyte, **P(T3-MS)-PE**, and then transition to an insoluble polymer **P(T3-MS)-I** following UV irradiation.

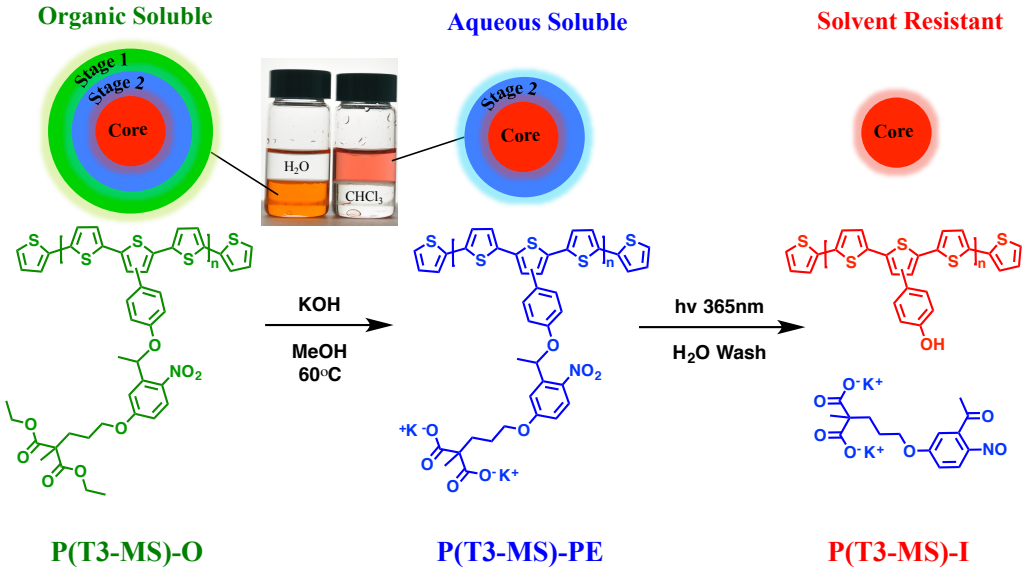

Figure 4-3. Process for preparation of regioirregular phenol functionalized polythiophene with multistage cleavable sidechains. **P(T3-MS)-O** is treated with base to transition to the polyelectrolyte **P(T3-MS)-PE**, visualized by the change in solubility from chloroform to water. After aqueous deposition, the thin film is irradiated with 365 nm UV light to form the insoluble **P(T3-MS)-I** and the ionic sidechain is removed through an aqueous wash.

4.4.1 P(T3-MS)-O Synthesis, Saponification, and Cleavage

P(T3-MS)-O was synthesized *via* a traditional Migita-Kosugi-Stille polymerization in toluene from a distannyl bithiophene with a dibromothiophene bearing the multistage cleavable side chain. The complete synthesis is described in Chapter 4.7.1. Following Soxhlet purification, a red polymer with M_n 11 kDa (Đ = 1.9) was yielded in 68% from the chloroform fraction. A portion of the polymer was stirred overnight in a solution of potassium hydroxide and methanol, described generally in Chapter 2.3.1 and detailed in Chapter 4.7.1, affording an aqueous soluble polyelectrolyte **P(T3-MS)-PE.** The transition from *Stage 1* to *Stage 2* was affirmed by the shift in solubility from organic soluble to aqueous soluble, illustrated by the biphasic solutions of chloroform and water in Figure 4-3, a change in water contact angle on thin films from 70° to 50° as seen in Figure 4-4, and by the observed loss of ethyl groups *via* ^{1}HNMR in Figure 4-5.

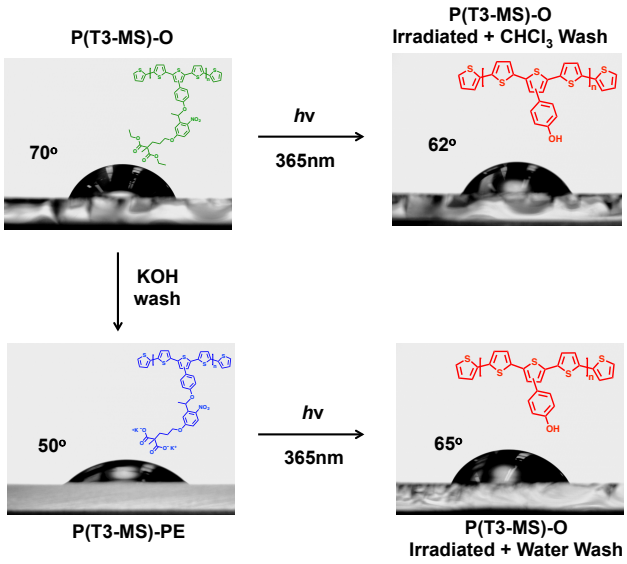

Figure 4-4. Water contact angle measurements on films of **P(T3-MS)-O** and **P(T3-MS)-PE** before and after irradiation. Films were tested, then irradiated for 150 minutes at 365 nm and washed in their casting solvent, allowed to air dry, then tested again. Changes in contact angle correspond to changes in the polymer structure.

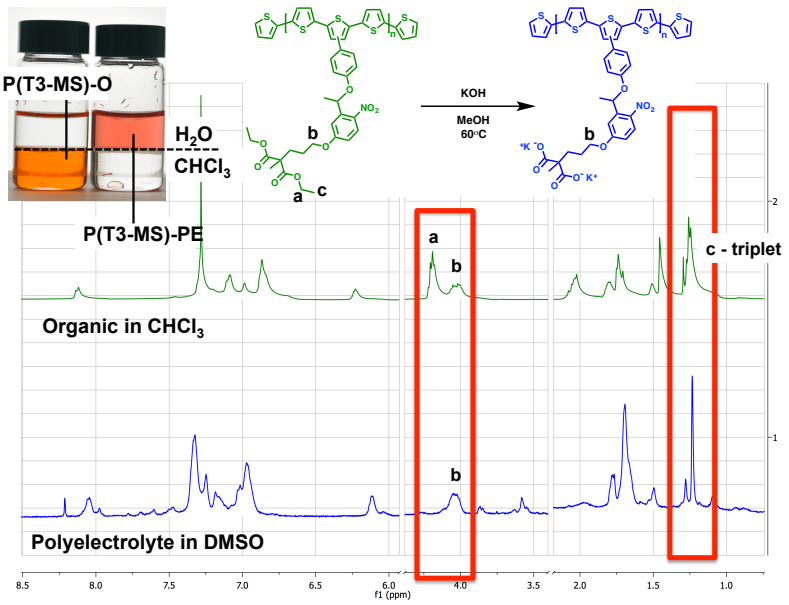

Figure 4-5. Polymer ^{1}H NMR of **P(T3-MS)-O** and **P(T3-MS)-PE** in $CDCl_3$ and DMSO-d_6, respectively. Conversion can be seen by the disappearance of the ethyl ester peaks, shown above as quartet **a** (CH_2) and triplet **c** (CH_3). Inset shows solutions of the two in a biphasic solution of chloroform and DI water, illustrating the shift in polymer solubility.

To test the effectiveness of the UV cleavable *o*-nitrobenzyl functionality, films of both **P(T3-MS)-O** and **P(T3-MS)-PE** were blade coated onto glass slides from chloroform and 1:1 water:isopropyl alcohol (H_2O:IPA), respectively, and irradiated in a UV chamber for 150 minutes at 365 nm and ~5 mW/cm^2. The cleavage mechanism and testing methods are further discussed in Chapter 2.3.3. For **P(T3-MS)-PE**, IPA was used as a co-solvent in order to reduce the surface tension of the deposition solution, allowing for enhanced wetting and film formation during blade coating, as detailed in Chapter 2.3.2.[138]. UV-vis spectra before and after irradiation are shown in Figure 4-6. The main features to be noted in the UV-vis data is the minimal change in the conjugated backbone's π to π* transition in conjunction with the loss of a peak around 312 nm for both polymer systems, which is characteristic of the transition from an *o*-nitrobenzyl group to the cleaved nitroso group[196]. In both cases, irradiation leads to loss of this peak,

while subsequent rinsing in the casting solvent leads to a negligible loss in peak absorption, indicating that the polymer has become solvent resistant.

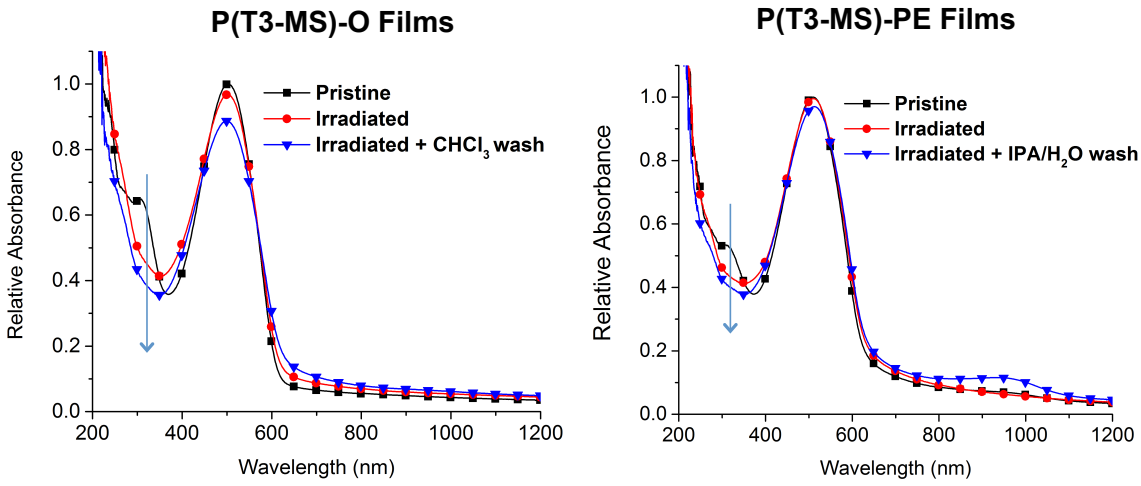

Figure 4-6. UV-vis solvent resistivity study of organic processed (left) and aqueous processed (right) multistage cleavable polymers. Blue arrows reveal the loss of a peak around 312nm that corresponds to the o-nitrobenzyl cleavable functionality.

Cleavage was also observed by ^{1}HNMR in filtered solutions of both **P(T3-MS)-O** and **P(T3-MS)-PE** after UV irradiation. As shown in Figures 4-7, irradiated solutions reveal the loss of a benzyl peak that is converted to a ketone during the cleaving process. Contact angle measurements, shown in Figure 4-4, also suggest that cleavage from either **P(T3-MS)-O** or **P(T3-MS)-PE** leads to the same anticipated polymer structure. **P(T3-MS)-O** shows a water contact angle of 70^{o} which is reduced to 62^{o} upon conversion to **P(T3-MS)-I** after irradiation and a chloroform wash. **P(T3-MS)-PE** films show a contact angle of 50^{o}, which increases to 65^{o} when converted to **P(T3-MA)-I** after irradiation and a 1:1 H_2O:IPA wash. The minimal differences in contact angles between films of **P(T3-MS)-I** indicate that a similar polymer surface structure is obtained whether the film is initially cast in its organic soluble form or in its polyelectrolyte form.

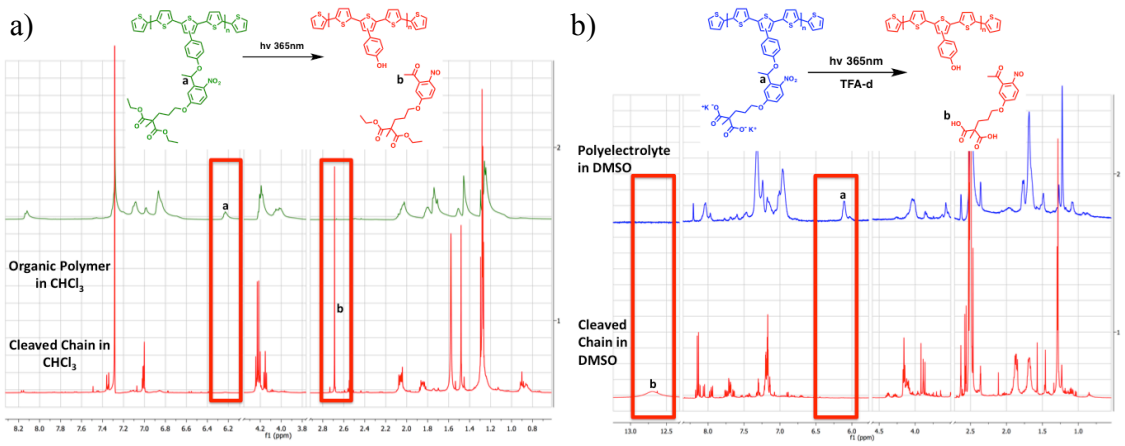

Figure 4-7. Polymer ^{1}H NMR of **P(T3-MS)-O** (a) and **P(T3-MS)-PE** (b) and their respective cleaved side chain after UV irradiation in solution. **P(T3-MS)-O** was dissolved in chloroform at 15 mg/mL and **P(T3-MS)-PE** was dissolved in 1:1 H_2O/IPA at 15 mg/mL, and the solutions were irradiated at 365nm in a UV chamber for 5 hours. The resulting solutions were filtered to remove insoluble material and concentrated by rotary evaporator. ^{1}H NMR of **P(T3-MS-O)** was recorded in $CDCl_3$. Since the polymer backbone becomes insoluble, the filtrate should mainly contain the cleaved side chain. As can be seen above, the benzyl peak **a** can no longer be found in the irradiated solution, while a new peak **b** grows in that corresponds to the methyl ketone of the side chain. ^{1}H NMR of **P(T3-MS)-PE** was recorded in DMSO-d_6. Since the polymer backbone becomes insoluble, the filtrate should mainly contain the cleaved side chain. As can be seen above, the benzyl peak **a** can no longer be found in the irradiated solution, but the methyl ketone peak cannot be resolved. As a solution, a few drops of deuterated trifluoroacetic acid (TFA-d) were added to the DMSO-d_6 to induce acidification of the carboxylates to form carboxylic acids. As seen in the spectrum above, this resulted in the growth of peak **b**, corresponding to a carboxylic acid on the side chain.

We next sought to answer whether or not the cleavable side chain was fully removed from the film, and what this removal does to the polymer's solid-state structure. Because the side chains of **P(T3-MS)-PE** contained two elements not found in the main polymer backbone, nitrogen (N) and potassium (K), XPS surface and depth profiling experiments on thin films of this polymer were used to quantify the amount of side chain within the film throughout the multistage process. Alongside these results, **P(T3-MS)-PE** was studied using Grazing-Incidence Wide-Angle X-Ray Scattering (GIWAXS) to monitor structural variations of the polymer throughout the multistage process.

Measurement specifics and 1D line cuts of the scattering plots can be found in Chapter 4.8. The results are summarized in Figure 4-8. Since sulfur (S) is unique to the polymer backbone, integrated peaks for N1s and K2p were normalized to the S2p peak area and compared to the expected repeat unit atomic ratios. Full XPS spectra and integration details can be found in Chapter 4.9. For the N1s peak, both the pristine and irradiated films show ratios close to the expected N:S ratio of 0.33. Slight deviation in the pristine sample may be caused by surface impurities or prematurely cleaved side chains. The K2p peaks show similar results, though the K:S ratio never reaches the expected value of 0.66. This difference could be caused by incomplete saponification of the side chains, premature side chain cleavage and/or a loss of the counterion during the deposition. In the GIWAXS scattering plots shown in Figure 4-8, irradiation leads to a large change (a→b), notably the formation of discrete crystallite scattering peaks. These peaks, which can be seen as small spots of intensity in Figure 4-8b, are commonly indicative of the presence of discrete molecular crystallites. The GIWAXS data suggests that side chains are being cleaved after irradiation, but remain in the film as discrete crystalline domains, which agrees with the minimal changes in atomic makeup seen in the XPS data.

Once irradiated and washed, the N:S ratio drops to 0.1, corresponding to a large loss in elemental nitrogen. These results show that, while irradiation cleaves the polymer side chains, about a third of the side chains are either not cleaved or not removed by the aqueous wash. Alternatively, the K2p peaks show complete removal of K after the aqueous wash. Unlike the nitrogen on the side chain, the potassium exists as the polyelectrolyte's counterion and therefore has a greater ability to diffuse out of the film in conjunction with ion exchange or weak acid protonation of the carboxylates to carboxylic

acids. The complete loss of potassium ions, but not side chains, could also result in the self-doping of the polythiophene backbone by the anionic carboxylates leftover on the side chains. Evidence for this self-doping can be observed in the irradiated and washed **P(T3-MS)-PE** UV-vis spectrum in Figure 4-6, where a peak around 1000 nm begins to appear, typically corresponding to polaronic charge carriers in conjugated polymers.[197].

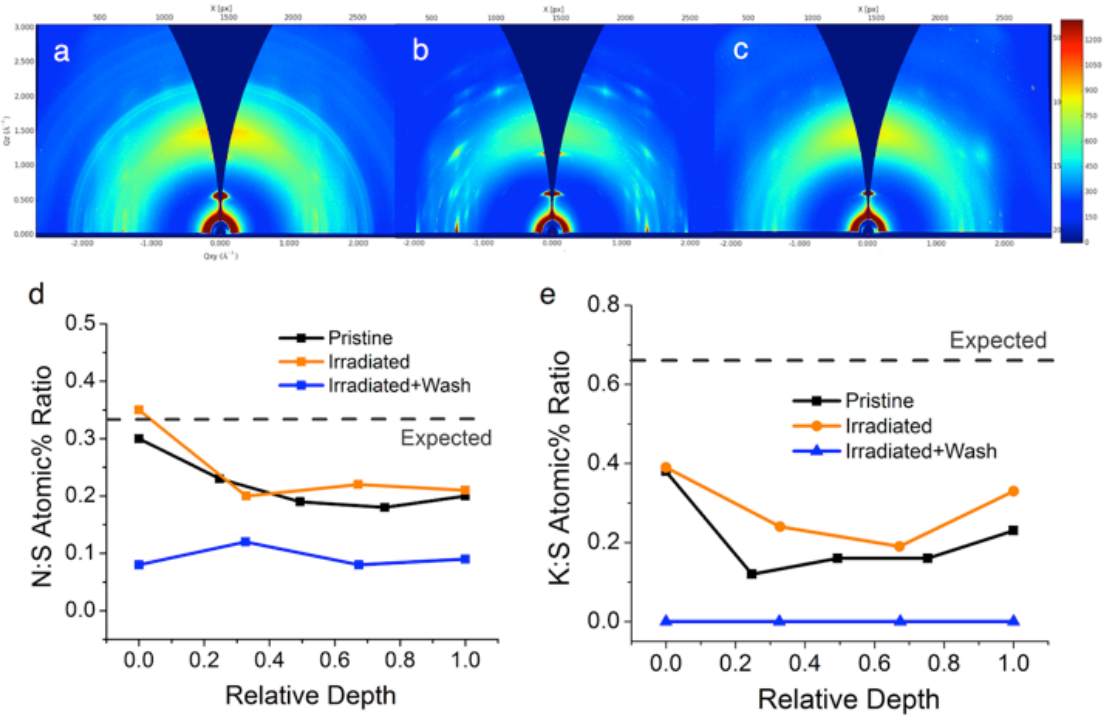

Figure 4-8. Grazing-Incidence Wide-Angle X-Ray Scattering (GIWAXS) plots of **P(T3-MS)-PE** thin films as-cast (a), irradiated (b), and irradiated and washed with 1:1 H_2O:IPA (c). Atomic ratios of N:S (d) and K:S (e) within **P(T3-MS)-PE** films calculated via XPS. Pristine, irradiated, and irradiated and washed films are shown at varying depths from the surface (relative depth =0) and through the thickness of the film (relative depth = 1) in comparison to the expected ratio of 0.33 (N:S) and 0.66 (K:S).

GIWAXS results of the film after the aqueous wash process (b→c) show a disappearance of most of the small crystallite peaks, aligning with the significant removal of sidechain mass seen in the XPS atomic ratios. It is also worth noting that the overall

(100) and (010) diffraction pattern seen for the polymer remains unchanged, with strong edge-on lamellar packing seen along the Q_z axis throughout the process. The XPS etching data reveals a similar progression to what is seen on the surface, suggesting that these transformations are taking place throughout the film. Films were etched using an argon ion gun and spectra were taken at intervals until the substrate was reached. Elemental ratios from the surface (Relative Depth = 0) to the interface with the glass substrate (Relative Depth = 1) are shown in Figure 4-8d and 4-8e. The lower ratios seen in the etched data for pristine and irradiated samples are likely due to the partial decomposition and evaporation of the polymer during the plasma etching process, which has been previously observed in conjugated polymer films.[198] Etching data contained higher carbon content, which may also suggest partial decomposition and evaporation.

4.4.2 P(T3-MS) Device Application Testing

To observe the effects of the multistage process on device applications, **P(T3-MS)-O** and **P(T3-MS)-PE** were tested for OFET mobility and electrochromism, representing solid-state applications and solution based redox applications, respectively. Charge carrier properties were investigated through p-type OFET devices with a bottom-gate/bottom-contact architecture. Device fabrication and testing details are provided in section Chapter 2.4.2. OFET transfer curves are shown in Figure 4-9 with calculated mobility values averaged across 3 **P(T3-MS)-O** devices and 9 **P(T3-MS)-PE** devices. The pristine **P(T3-MS)-O** films cast from chloroform exhibit an average mobility of 8.1 x 10^{-5} $cm^2V^{-1}s^{-1}$, on the same order of magnitude to the mobility observed by the Thomas group's polythiophene with photocleavable side chains (2.6 x 10^{-5} $cm^2V^{-1}s^{-1}$)[70] as well as

regiorandom P3HT (10^{-4} – 10^{-5} $cm^2V^{-1}s^{-1}$).[199] After irradiation and washing, the mobility drops to 3.7 x 10^{-5} $cm^2V^{-1}s^{-1}$.

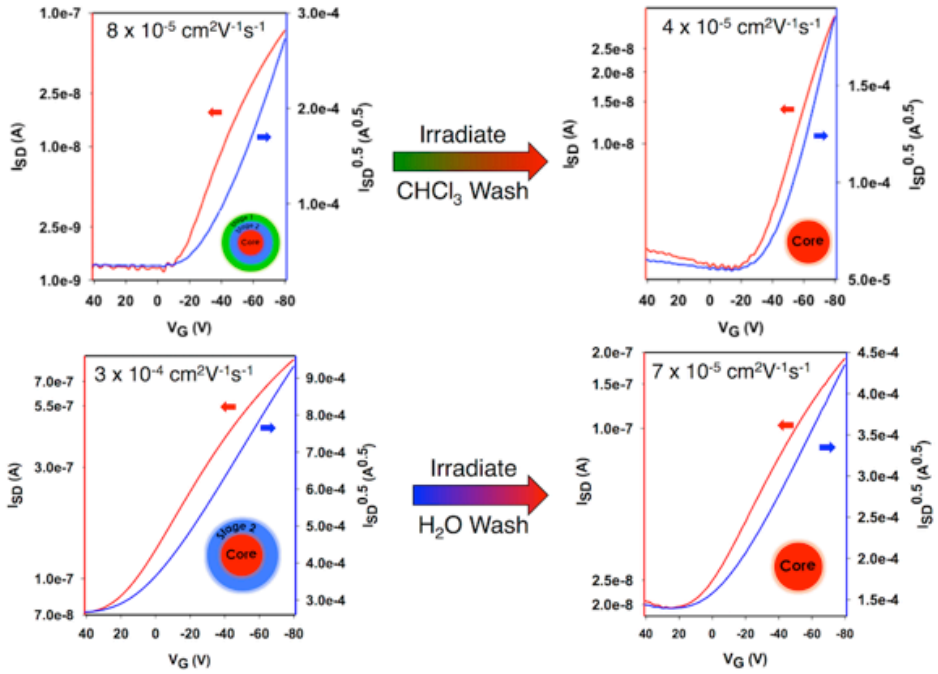

Figure 4-9. OFET transfer curves and average hole mobility values across 3 devices of **P(T3-MS)-O** (top) and 9 devices of **P(T3-MS)-PE** (bottom) films in their pristine state and after irradiation and washing.

The pristine **P(T3-MS)-PE** films cast from 1:1 H_2O:IPA obtain an average mobility of 2.5 x 10^{-4} $cm^2V^{-1}s^{-1}$. This result was unexpected, as conjugated polyelectrolytes do not typically function well in OFET devices due to the presence of mobile counterions and high off currents caused by intrinsic conductivity. At this time, there is no clear explanation for why these conjugated polyelectrolytes show OFET response while most do not. To our knowledge, the only other example reported for a polyelectrolyte OFET material is an n-type polymer from the Bazan group[187], making **P(T3-MS)-PE** novel in its ability to function as a polyelectrolyte p-type OFET. After irradiation and washing of this polymer, the mobility drops to 6.8 x 10^{-5} $cm^2V^{-1}s^{-1}$. For

both polymers, an intermediate stage was tested after irradiation but before washing, but neither showed an electrical response. We hypothesize that OFET mobility is disrupted by the presence of mobile side chains that have not yet been removed from the film.

While the mobility of the aqueous processed and cleaved **P(T3-MS)-PE** is not state-of-the-art for CPs, the results are promising when compared to other regiorandom polythiophenes that achieve similar mobility values. It is possible that higher mobility values will be achieved by applying the multistage concept to a regioregular, highly planar backbone similar to current high mobility polymers. However, the aqueous processed OFETs in this study show high OFF currents, leading to ON/OFF ratios on the order of 10^1. Likely caused by the presence of water and ions within the film, this represents a limitation for the multistage concept that will need to be addressed in future work.

Redox response and red to colorless electrochromism were observed in films of **P(T3-MS)-O** and **P(T3-MS)-PE** on ITO/glass before and after irradiation and washing. Broad, reversible oxidation peaks were recorded for both polymers by cyclic voltammetry (CV) and showed negligible changes after irradiation, with the onset of oxidation remaining around -0.1V relative to the ferrocene/ferrocenium redox couple throughout the multistage process. CV and differential pulse voltammetry (DPV) data is shown in Figure 4-10, and CV and DPV methods are described in Chapter 2.2.3.

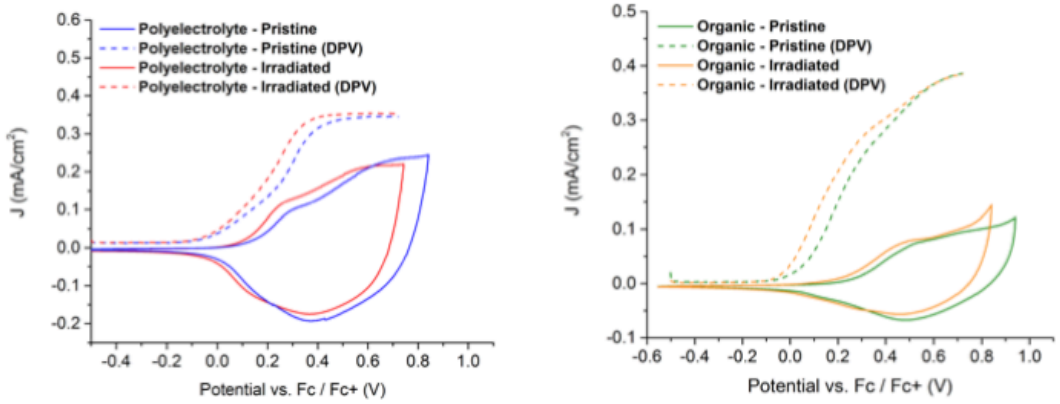

Figure 4-10**.** Cyclic Voltammetry (CV) and Differential Pulse Voltammetry (DPV) data of **P(T3-MS)-PE** (right) and **P(T3-MS)-O** (right) cast onto a glassy carbon button electrode which served as the working electrode, a platinum flag as the counter electrode, a reference electrode (Ag/Ag^+, 10 mM $AgNO_3$ in 0.5 M $TBAPF_6$-ACN, $E_{1/2}$ for ferrocene: 68 mV), and 0.5M $TBAPF_6$/PC as the supporting electrolyte. Scans were taken at 50 mV/s.

The oxidation of these polymers is accompanied by a color change from red in the neutral state and colorless in the oxidized state. Figure 4-11 shows the spectroelectrochemical series of a **P(T3-MS)-PE** film on ITO/glass along with photographs of the resulting color change. Electrochromic film fabrication and testing methods are described in Chapter 2.4.4. The electrochromic film demonstrates up to a 47% contrast for the pristine polymer and 40% contrast after irradiation, comparable to the ~50% contrast achievable in P3HT films.[200] Irradiated films show faster switching speeds, reaching 95% contrast in 6 seconds while the pristine films take 14 seconds. Switching speed data can be found in Figure 4-12. This may be the result of superior ion intercalation throughout the film and faster electronic response due to removed side chain mass. Similar results are seen for the chloroform processed **P(T3-MS)-O** and can be found in Figure 4-13. As with the OFET devices, these multistage polymers do not compare to state-of-the-art high contrast electrochromic polymers, but rather demonstrate

the ability for aqueous processed multistage polymers to be used in redox applications.

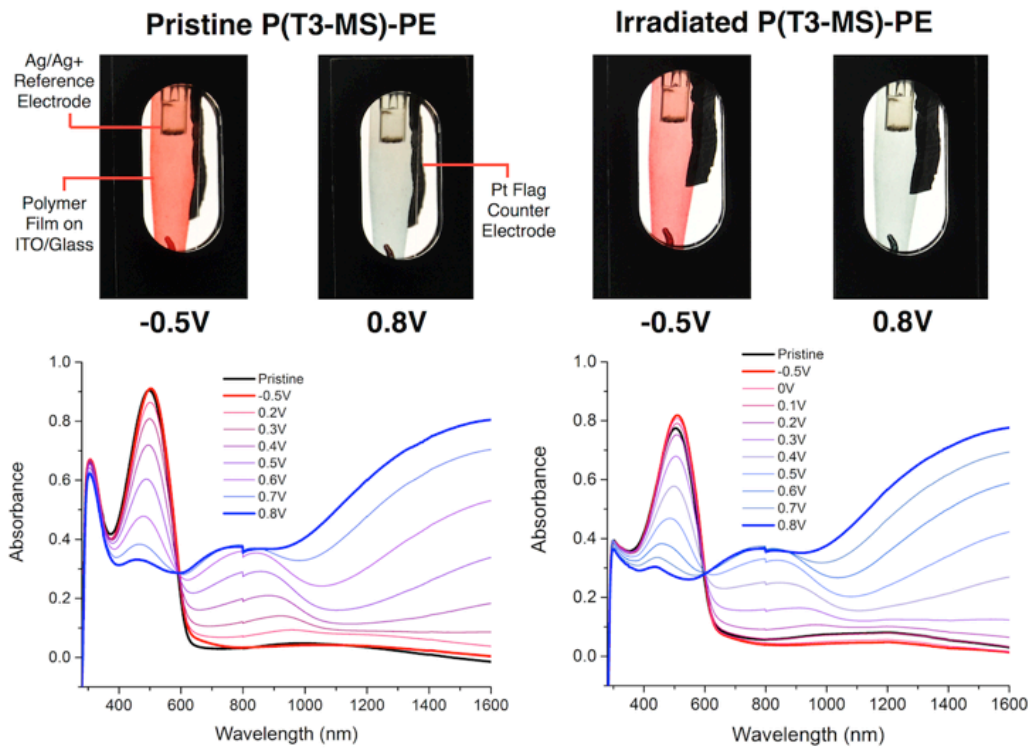

Figure 4-11. Spectroelectrochemical series for aqueous processed **P(T3-MS)-PE** films on ITO/glass in its pristine state (left) and after irradiation and washing (right) with photographs of the films in their neutral (red) and oxidized (colorless) states. Spectra and photos were taken in a three electrode cell setup with the ITO serving as the working electrode, a platinum flag as the counter electrode, a reference electrode (Ag/Ag^+, 10 mM $AgNO_3$ in 0.5 M $TBAPF_6$-ACN, $E_{1/2}$ for ferrocene: 68 mV), and 0.5M $TBAPF_6$/PC as the supporting electrolyte. The tapered lower end of the film is caused by an edge pooling effect when blade coating from aqueous solution.

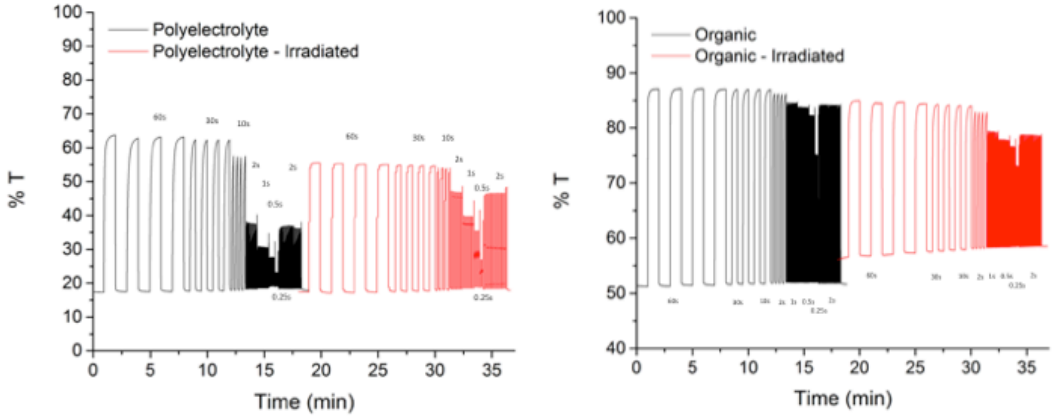

Figure 4-12. Switching speed results for **P(T3-MS)-O** (left) and **P(T3-MS)-PE** (right) films before and after irradiation. Polymers were used in the same setup as Spectroelectrochemistry experiments, and the transmittance at their λ_{max} was monitored as the potential was varied between -0.5 V and 0.8 V for defined time intervals.

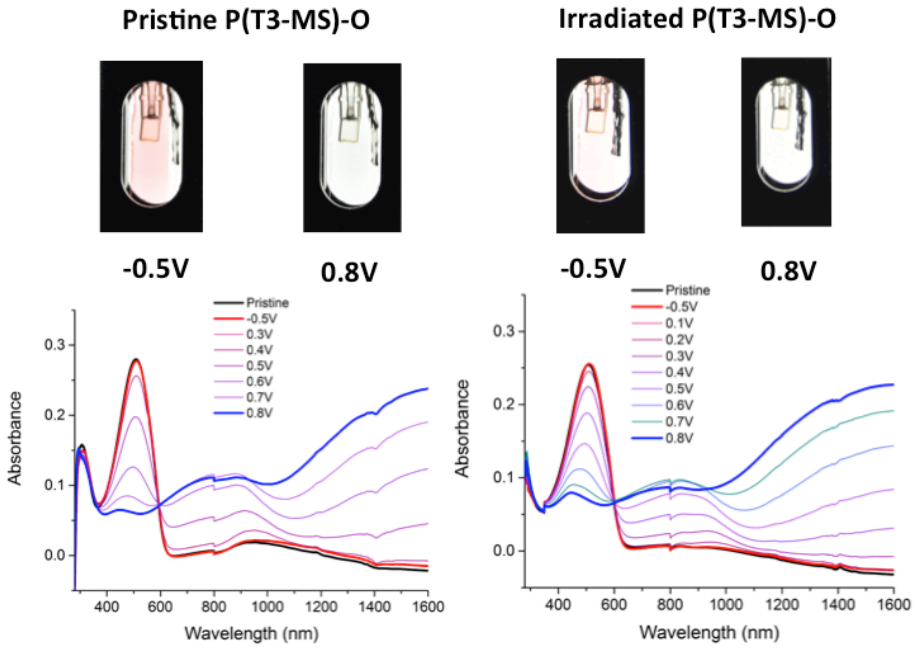

Figure 4-13. Spectroelectrochemical series for **P(T3-MS)-0** films on ITO/glass in its pristine state (left) and after irradiation and washing (right) with photographs of the films in their neutral (red) and oxidized (colorless) states. Spectra and photos were taken in a three electrode cell setup with the ITO serving as the working electrode, a platinum flag as the counter electrode, a reference electrode (Ag/Ag^+, 10 mM $AgNO_3$ in 0.5 M $TBAPF_6$-ACN, $E_{1/2}$ for ferrocene: 68 mV), and 0.5M $TBAPF_6$/PC as the supporting electrolyte.

4.5 Next Generation Multistage Polymer P(DPP-DTT-MS)

While the proof of concept polymer **P(T3-MS)** obtained the desired processing metrics, the following work focuses on increasing the performance of conjugated polymers with multistage cleavable side chains by translating the concept to current high performance polymer backbones. Aside from seeking high performance, we sought to investigate whether multistage side chains could be used as a universal method to modify the side chains on state-of-the-art conjugated polymers to achieve aqueous solubility. Herein, we present an extension of this concept by modifying a high mobility p-type conjugated polymer, **P(DPP-DTT)**, with multistage cleavable side chains to obtain high mobility in OFET devices processed from aqueous inks. **P(DPP-DTT)** has been shown to produce OFET mobility values on the order of 1-10 $cm^2V^{-1}s^{-1}$ with 2-octyldodecyl side chains when processed from chlorobenzene (CB).[101, 201] The polymer in this study, **P(DPP-DTT-MS)** maintains the same conjugated backbone as **P(DPP-DTT)**, but replaces the aliphatic side chains with the multistage cleavable side chains attached through a benzylphenoxy linker as shown in Figure 4-14. **P(DPP-DTT-MS)** was synthesized, purified, and characterized in organic solvents, hydrolyzed to the water soluble polyelectrolyte **P(DPP-DTT-MS)-PE** for aqueous processing, and photocleaved with UV light to afford the cleaved **P(DPP-DTT-MS)** polymer with benzylphenol side chains. Thin films of **P(DPP-DTT-MS)-PE** processed from aqueous inks were tested in bottom-gate bottom-contact OFETs and yielded hole mobility values on the order of 10^{-3} $cm^2V^{-1}s^{-1}$. **P(DPP-DTT-MS)-PE** was also used to realize electrolyte-gated organic transistors (EGOTs) that could be fully solution processed (electrodes, semiconductor,

dielectric) from environmentally benign solvents, affording devices with maximum transconductance (g_m) values of 1.1 mS at 1.07 V.

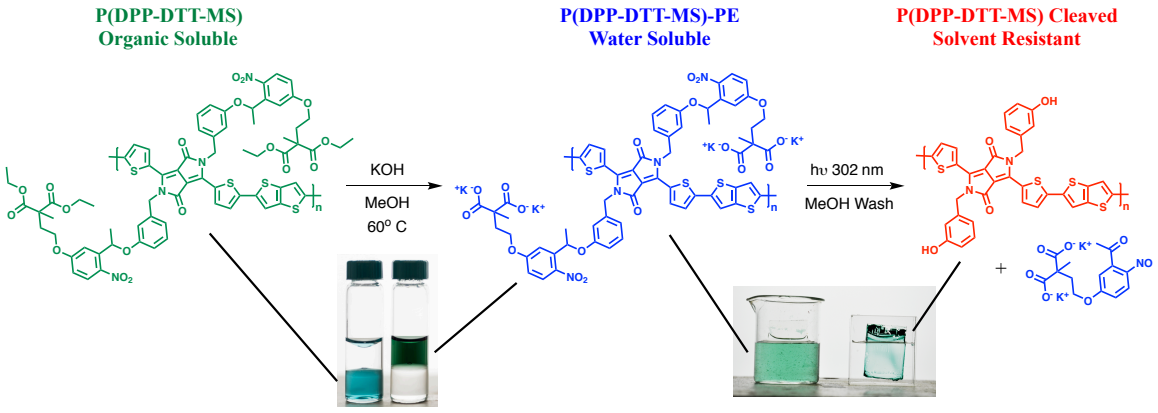

Figure 4-14. Multistage side chain process for **P(DPP-DTT-MS)**. The organic soluble precursor is treated with base to transition to the polyelectrolyte **P(DPP-DTT-MS)-PE**, visualized by the change in solubility from chloroform (bottom layer) to water (top layer). After aqueous deposition, the thin film is irradiated with 302 nm UV light to cleave the ionic side chain, which is washed away with methanol, leaving behind the cleaved **P(DPP-DTT-MS)** as a solvent resistant film. Solvent resistance is visualized by the retention of a thin film on glass within a beaker of water, whereas the as cast polyelectrolyte dissolves into the water.

4.5.1 P(DPP-DTT-MS) Synthesis, Saponification, and Cleavage

P(DPP-DTT-MS), shown in Figure 4-14, was synthesized *via* Migita-Kosugi-Stille polymerization from a dibromo bisthienyl-diketopyrrolopyrrole monomer with multistage side chains and a distannyl thieno[3,2-b]thiophene monomer. Monomer preparation and polymerization methods are presented in detail in Chapter 4.7.2**.** The polymer was purified through Soxhlet extraction, and the dichloromethane fraction yielded **P(DPP-DTT-MS)** with M_n of 62 kDa and $Đ$ of 5.2 vs. polystyrene standards in chloroform GPC. The high dispersity may be attributed to aggregation of the polymer in solution, which was also noted in previous reports of **P(DPP-DTT)** that exhibited

similarly broad molecular weight distributions.[101] The polymer could be solubilized in chlorinated organic solvents such as dichloromethane, chloroform, and chlorobenzene due to the ethyl ester groups affixed to the end of the multistage side chains. As shown in Figure 4-14, **P(DPP-DTT-MS)** was converted to the polyelectrolyte **P(DPP-DTT-MS)-PE** through a post-polymerization hydrolysis of the side chain terminal ester groups using KOH in methanol, as outlined in Chapter 2.3.1 and specifically detailed in Chapter 4.7.2. After hydrolysis, the resulting polyelectrolyte **P(DPP-DTT-MS)-PE** exhibited water solubility, which can be visualized by the shift in solubility within biphasic solutions of chloroform and water, shown in Figure 4-14. **P(DPP-DTT-MS)-PE** can be dissolved into water effectively up to concentrations of 10 mg/mL.

P(DPP-DTT-MS)-PE was blade coated onto glass slides using a 10 mg/mL concentration in a solution of 1:1 water:isopropylalcohol (H_2O:IPA). As outlined in Chapter 2.3.2, mixtures of water and IPA can be utilized to the surface tension of the deposition solution, allowing for enhanced wetting and film formation during blade coating. After coating, films were irradiated for 10 minutes at 302 nm (UVB light) with an intensity of 5 mW/cm^2 to initiate side chain cleavage through an intramolecular rearrangement of the *o*-nitrobenzyl unit.[195] The mechanism and process for UV cleavage is discussed in Chapter 2.3.3. As shown in Figure 4-14, the polymer became solvent resistant after side chain cleavage, allowing for films of **P(DPP-DTT-MS)-PE** to be submerged in water without dissolving. **P(DPP-DTT-MS)** could also be directly coated to thin films from chlorobenzene and subsequently irradiated to achieve solvent resistant films.

Solid-state photocleavage of the *o*-nitrobenzyl unit was monitored *via* UV-vis absorption experiments, the results of which are summarized in Figure 4-15. The absorption peak centered at 310 nm corresponds to the *o*-nitrobenzyl unit, and so using a UVB light source, which is centered around 302 nm, allows for effective photocleavage without significantly affecting the conjugated backbone that primarily absorbs in the range of 600-1000 nm. Figure 4-15a shows the absorbance of **P(DPP-DTT-MS)-PE** films as cast and after 5, 10, and 15 minutes of UV irradiation. After 5 minutes, the peak at 310 nm diminishes while a new, red-shifted peak grows in as the *o*-nitrobenzyl unit cleaves and forms a nitrosobenzaldehyde molecule. This new peaks continues to grow with increased irradiation time and saturates at 10 minutes, with almost no changes occurring between 10 and 15 minutes. After irradiation is complete the film is dipped into a bath of methanol to remove the cleaved side chain molecule, causing the new peak at 375 nm to diminish. After this process, the film becomes solvent resistant, and no further changes in absorption are observed after dipping the film in a water bath. It is important to note that delamination often occurs if the film is immediately dipped into water after irradiation, but if methanol is used first to remove the cleaved side chain, the films remain robust in subsequent water washes.

In an effort to decrease the steps involved in the photocleavage process, films of **P(DPP-DTT-MS)-PE** were irradiated directly in a methanol bath, allowing for immediate removal of the cleaved side chain during irradiation. As can be seen in Figure 4-15b, while the *o*-nitrobenzyl peak at 310 nm diminishes, the red-shifted peak corresponding to the cleaved side chain can no longer be observed throughout the irradiation process. Similar to the dry irradiation process, the changes in absorption

saturate after 10 minutes, with almost no changes occurring between 10 and 15 minutes. In contrast to the dry irradiation process, photocleavage within a methanol bath leads to a greater drop in absorbance at 310 nm, which may indicate a more efficient removal of the cleaved side chain.

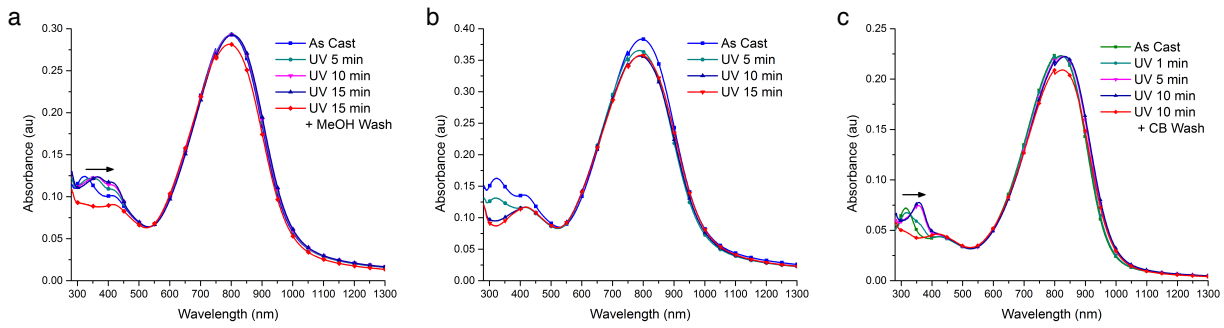

Figure 4-15. UV-vis absorption spectra throughout the photocleavage process. Photocleavage of **P(DPP-DTT-MS)-PE** films followed by a methanol wash (a), photocleavage of **P(DPP-DTT-MS)-PE** films within a methanol bath (b), and photocleavage of **P(DPP-DTT-MS)** films followed by a chlorobenzene wash. Arrows denote red-shifting of *o*-nitrobenzyl peak during irradiation.

The organic soluble **P(DPP-DTT-MS)** could also be directly cast from chlorobenzene and brought through the photocleavage process. The absorption spectra throughout irradiation, shown in Figure 4-15c, follow a similar trend as the polyelectrolyte films but with changes saturating at 5 minutes of irradiation, demonstrating a more rapid and efficient cleavage process compared to **P(DPP-DTT-MS)-PE**. After irradiation, the film was dipped into a bath of chlorobenzene, causing the removal of the cleaved side chain peak at 375 nm but retention of the backbone absorption peak from 600-1000 nm. While the 5 mW/cm^2 UV light source was used throughout this study, the ability to decrease irradiation time through a higher power light source was also investigated. Shown in Figure 4-16, by moving to a 80 mW/cm^2 UV light

source the films of **P(DPP-DTT-MS)-PE** can be cleaved to the same extent within 10 seconds. UV light sources with intensities over 100 mW/cm^2 are common within industrial UV curing processing lines, so this experiment demonstrates the potential for the photocleavage of **P(DPP-DTT-MS)-PE** to be performed in the sub-second timeframes preferred for continuous processing.

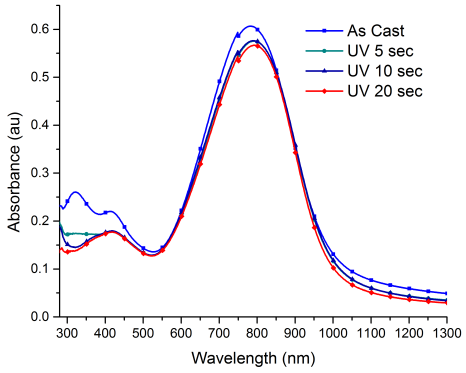

Figure 4-16. **P(DPP-DTT-MS)-PE** film coated from a 1:1 solution of H_2O:IPA irradiated using a 80 mW/cm^2 UVA (365 nm) light source within a methanol bath to induce photocleavage of side chains in shorter times.

While UV light can cause degradation in conjugated polymers, irradiated and washed films of both **P(DPP-DTT-MS)** and **P(DPP-DTT-MS)-PE** show only a slight decrease in λ_{max}, and the decrease takes place only after the washing step, which more likely indicates that some of the material is still soluble after cleavage rather than an impact of UV degradation. To avoid a combination of UV light and oxygen, which has been shown to degrade conjugated polymer films[202], irradiation steps were performed within an argon atmosphere. However, no absorbance differences were observed between films irradiated in argon and films irradiated in an ambient atmosphere.

Aside from retention of their optical properties, cleaved films of **P(DPP-DTT-MS)** and **P(DPP-DTT-MS)-PE** also retain electroactivity. Electrochemical cyclic voltammetry (CV) and differential pulse voltammetry (DPV) measurements were recorded for **P(DPP-DTT-MS)** and **P(DPP-DTT-MS)-PE** before and after photocleavage, and the results are shown in Figure 4-17.

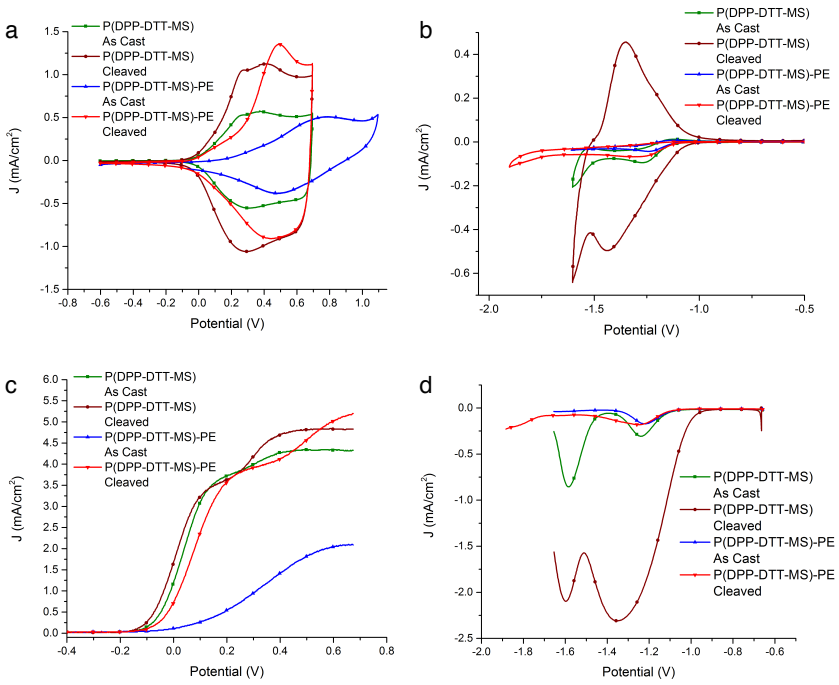

Figure 4-17. Electrochemical Cyclic Voltammetry (CV) oxidation (a) and reduction (b) and Differential Pulse Voltammetry (DPV) oxidation (c) and reduction (d) data of **P(DPP-DTT-MS)** and **P(DPP-DTT-MS)-PE** in their as cast and photocleaved states, cast onto a glassy carbon button electrode which served as the working electrode, a platinum flag as the counter electrode, a reference electrode (Ag/Ag^+, 10 mM $AgNO_3$ in 0.5 M $TBAPF_6$-ACN, $E_{1/2}$ for ferrocene: 68 mV), and 0.5M $TBAPF_6$/PC as the supporting electrolyte. CV scans were taken at 50 mV/s. DPV scans were performed with step size 2 mV, step time 50 ms, pulse amplitude 100 mV.

DPV oxidation measurements show negligible differences between the onsets of oxidation of **P(DPP-DTT-MS)**, **P(DPP-DTT-MS)-PE**, and photocleaved films of both, revealing that the multistage process of hydrolysis and photocleavage do not significantly

impact the energy levels of the polymer. CV oxidation scans for cleaved films of both polymers reach higher current values than as cast films, which may signify a higher capacity for the conjugated backbone to interact with the electrolyte due to lower amounts of side chain mass. These results are in line with our previous work on **P(T3-MS)**, in which cleaved films exhibited faster electrochromic switching speeds than their as cast counterparts, likely caused by the increased ability for ions to interact with the polymer backbone after removal of side chain mass.

4.5.2 P(DPP-DTT-MS) Organic Field-Effect Transistors

Bottom-Gate Bottom-Contact (BG/BC) OFET devices using **P(DPP-DTT-MS)** and **P(DPP-DTT-MS)-PE** blade coated from chlorobenzene and 1:1 H_2O:IPA, respectively, were fabricated to investigate the hole mobility properties of these polymers before and after photocleavage. OFET device fabrication and testing methods are presented in Chapter 2.4.2. **P(DPP-DTT-MS)** was stirred overnight at 10 mg/mL in chlorobenzene, and films were blade coated at 20 mm/s on an 80^o C stage with a blade gap of 200 mm. **P(DPP-DTT-MS)-PE** was stirred overnight at 10 mg/mL in 1:1 H_2O:IPA, and films were blade coated at 20 mm/s on a 40^o C stage with a blade gap of 200 mm. All films were coated to a thickness in the range of 60 nm ± 10 nm as measured by profilometry. Transfer curves for these devices are shown in Figure 4-18 and resulting device metrics are summarized in Table 4-1. Overall, there was a trend of cleaved films exhibiting higher mobility values than their as cast versions. **P(DPP-DTT-MS)-PE** had an as cast maximum mobility of 9.80 x 10^{-4} $cm^2V^{-1}s^{-1}$ that increased to a maximum mobility of 2.03 x 10^{-3} $cm^2V^{-1}s^{-1}$ after 10 minutes of UV irradiation and washing in methanol. However, both as cast and cleaved films produced low current on to off ratios

($I_{ON/OFF}$) on the order of 10^1 – 10^2. **P(DPP-DTT-MS)** films cast from chlorobenzene had an as cast maximum mobility of 2.40 x 10^{-3} $cm^2V^{-1}s^{-1}$ that increases by an order of magnitude to a maximum mobility of 1.69 x 10^{-2} $cm^2V^{-1}s^{-1}$ after 10 minutes of UV irradiation and washing in chlorobenzene. The $I_{ON/OFF}$ values are also higher for these films, ranging from 10^3 – 10^4 for as cast films and 10^2 – 10^3 for cleaved films.

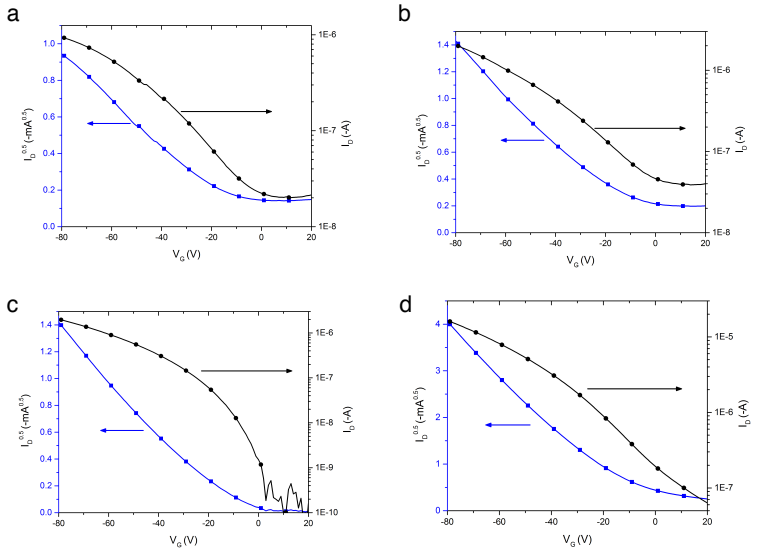

Figure 4-18. Transfer curves for bottom-gate bottom-contact (BG/BC) OFET devices of **P(DPP-DTT-MS)-PE** as cast (a) and after 10 minutes of UV irradiation and methanol washing (b), and **P(DPP-DTT-MS)** as cast (c) and after 10 minutes of UV irradiation and chlorobenzene washing (d).

In both cases, mobility increases after side chain cleavage, which may result from enhanced interactions between polymer backbones after removal of the insulating side chain bulk. Lack of ionic groups within the film could explain the higher performance for the chlorobenzene cast films of **P(DPP-DTT-MS)** compared to aqueous cast films of **P(DPP-DTT-MS)-PE**. **P(DPP-DTT-MS)-PE** contains ionic groups affixed to the side chain, and even after irradiation, some of these chains may still be attached to the polymer backbone, or the cleaved ionic side chain could be trapped within the film. In

our prior work with **P(T3-MS)**, we observed retention of ~1/3 of the side chain mass within the films after cleavage *via* elemental mapping by X-ray photoelectron spectroscopy (XPS), as shown in Figure 4-8. Whether still affixed to the polymer backbone or trapped within the film as cleaved molecules, these ionic groups can act as charge traps, or serve to screen the applied gate voltage, leading to lower charge mobility.

Active Layer	μ_h average ($cm^2V^{-1}s^{-1}$)	μ_h maximum ($cm^2V^{-1}s^{-1}$)	V_{th} (V)	$I_{ON/OFF}$
P(DPP-DTT-MS)-PE as cast	$9.60 \times 10^{-4} \pm 1.90 \times 10^{-5}$	9.80×10^{-4}	-8.28 ± 0.63	$10^1 - 10^2$
P(DPP-DTT-MS)-PE cleaved	$1.99 \times 10^{-3} \pm 2.70 \times 10^{-5}$	2.03×10^{-3}	-11.60 ± 0.13	$10^1 - 10^2$
P(DPP-DTT-MS) as cast	$2.39 \times 10^{-3} \pm 3.00 \times 10^{-6}$	2.40×10^{-3}	-16.66 ± 0.31	$10^3 - 10^4$
P(DPP-DTT-MS) cleaved	$1.67 \times 10^{-2} \pm 1.59 \times 10^{-4}$	1.69×10^{-2}	-12.88 ± 0.08	$10^2 - 10^3$
P(DPP-DTT)	0.726 ± 0.087	0.843	-0.94 ± 0.57	$10^3 - 10^4$

Table 4-1. Bottom-gate bottom-contact (BG/BC) OFET device metrics for **P(DPP-DTT-MS)-PE** and **P(DPP-DTT-MS)** as cast and cleaved, and the control polymer **P(DPP-DTT)**. Calculated from transfer curves of 10 devices each.

While the OFET hole mobility of ~10^{-3} $cm^2V^{-1}s^{-1}$ for aqueous coated films is two orders of magnitude higher than what was previously achieved in our group with the multistage polythiophene cast from aqueous solution (~10^{-5} $cm^2V^{-1}s^{-1}$), the mobility is still significantly lower than the control polymer with the same backbone and 2-octyldodecyl side chains, **P(DPP-DTT)**. As shown in Table 4-1 and in the OFET transfer curve in Figure 4-19, **P(DPP-DTT)** achieved a maximum hole mobility of 0.84 $cm^2V^{-1}s^{-1}$, similar to the value of 0.94 $cm^2V^{-1}s^{-1}$ first reported for this polymer.[201] **P(DPP-DTT)** was stirred overnight at 5 mg/mL in chlorobenzene, and films were blade coated at 20

mm/s on an 80° C stage with a blade gap of 200 mm. All films were coated to a thickness in the range of 60 nm ± 10 nm as measured by profilometry.

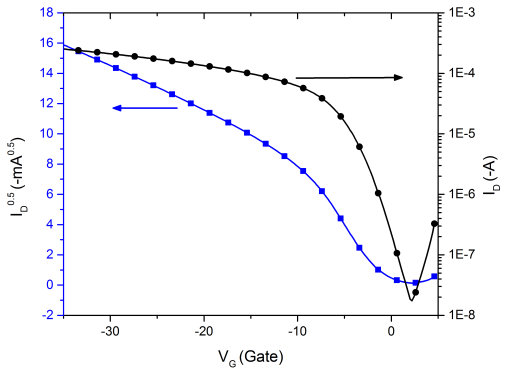

Figure 4-19. OFET transfer curve data of control polymer **P(DPP-DTT)**, swept from +5 V to -35 V with a source-drain bias (V_D) of -80 V.

While the presence of ionic groups may be a factor causing lower mobility, there are other factors involved that are unrelated to the use of aqueous solutions, as the chlorobenzene cast **P(DPP-DTT-MS)** films also exhibit significantly lower mobility values than **P(DPP-DTT)**. The discrepancy is likely a result of a morphology and solid-state structure less conducive to charge transport. Atomic force microscopy (AFM) images of **P(DPP-DTT-MS)** and **P(DPP-DTT-MS)-PE**, shown in Figure 4-20 and 4-21 respectively, do not exhibit the nanofibrillar ordered features previously reported for **P(DPP-DTT-MS)**.[101] Unlike aliphatic chains that can interdigitate and facilitate lamellar stacking, the multistage side chains are complex, bulky, and can lead to increased disorder throughout the polymer film. While side chain cleavage removes these bulky groups from the polymer backbone, and there is evidence that this process leads to a smoothening of the film morphology in AFM images, the polymer chains may not have the ability to redistribute into a higher order structure. However, apparent in both **P(DPP-**

DTT-MS) and **P(DPP-DTT-MS)-PE** is that removal of side chain mass does not produce pinholes or cracking within the films. In both cases, a possible explanation for how this cleaved volume is filled is through polymer chain rearrangement facilitated by energy provided by the UV light and the cleaved chain molecule acting as a plasticizer. Even if chain rearrangement is occurring, it is also possible that aliphatic side chains promote the nanofibrillar morphology observed in films of **P(DPP-DTT)** that contribute to the material's high charge mobility. A potential solution to this problem in multistage side chains is to redesign the chain to allow for enhanced solid-state packing prior to the photocleavage, possibly through the use of longer aliphatic chains on the terminal esters.

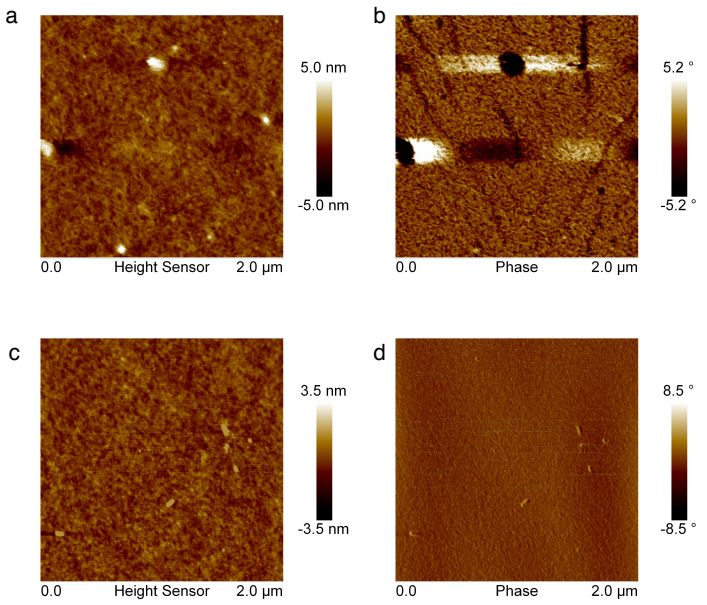

Figure 4-20. AFM height and phases images of **P(DPP-DTT-MS)** films as cast from chlorobenzene (a,b) and after photocleavage and washing in chlorobenzene (c,d). Roughness values (rms) reduce from 0.71 nm to 0.42 nm after cleavage and washing. Irregularities in the as cast films are also removed after cleavage. These irregularities, seen in (a) and (b), were present in AFMs of all as cast films of **P(DPP-DTT-MS)** and may indicate premature photocleavage and subsequent aggregation of side chains in solution.

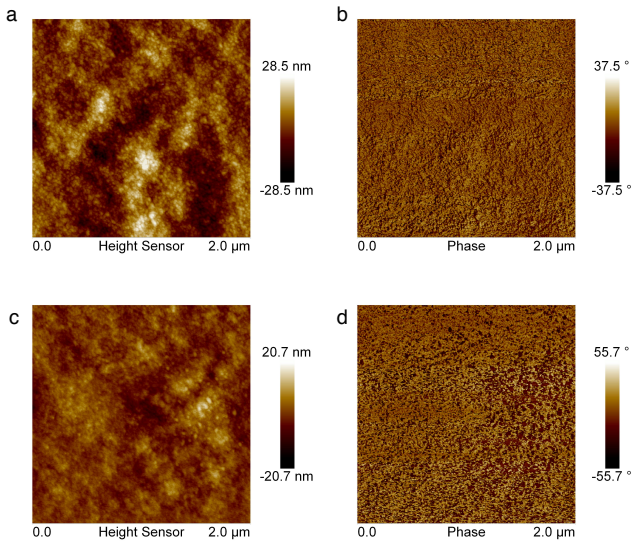

Figure 4-21. AFM height and phases images of **P(DPP-DTT-MS)-PE** films as cast from 1:1 H_2O:IPA (a,b) and after photocleavage and washing in methanol (c,d). Roughness values (rms) reduce from 7 nm to 3.1 nm after cleavage and washing. Otherwise, no significant feautures are present within these images, and aside from smoothening of the morphology after cleavage, no changes are observed in the irradiation and washing process.

4.5.3 P(DPP-DTT-MS) Electrolyte-Gated Organic Transistors

While there are benefits in moving to aqueous solutions for coating the semiconducting layer of OFETs, the architecture used still relies on doped silicon gates, silicon dioxide dielectrics, and gold source and drain electrodes that were fabricated in a cleanroom and not solution processed. In efforts to move towards completely solution processed transistors, we incorporated **P(DPP-DTT-MS)-PE** into electrolyte-gated organic transistors (EGOTs) where the electrodes, dielectric, and semiconductor are all solution processed from environmentally benign solvents. The Frisbie group has demonstrated fully aerosol jet printed EGOTs using PEDOT:PSS electrodes, poly(3-hexylthiophene) as the semiconductor, and an ion gel electrolyte as the dielectric.[203] The high capacitance of electrolyte dielectrics (> 10 $\mu F/cm^2$) allows for high charge-carrier

densities to be reached in semiconducting materials over a small voltage window, typically between +1V and -1V, enabling high mobility transistor devices that operate at low voltages. Following this approach, EGOTs were fabricated using PEDOT:PSS source, drain, and gate electrodes inkjet printed from water, **P(DPP-DTT-MS)-PE** blade coated from 1:1 H_2O:IPA and irradiated at 302 nm for 10 minutes within a methanol bath, and an ion gel electrolyte, 1-ethyl-3-methylimidazolium bis(trifluoromethylsulfonyl)imide, [EMI][TFSI] in poly(vinylidene fluoride-co-hexafluoropropylene), P(VDF-HFP), drop-cast from acetone. A schematic of the device is presented in Figure 4-22a, and device preparation and testing methods are presented in Chapter 2.4.5.

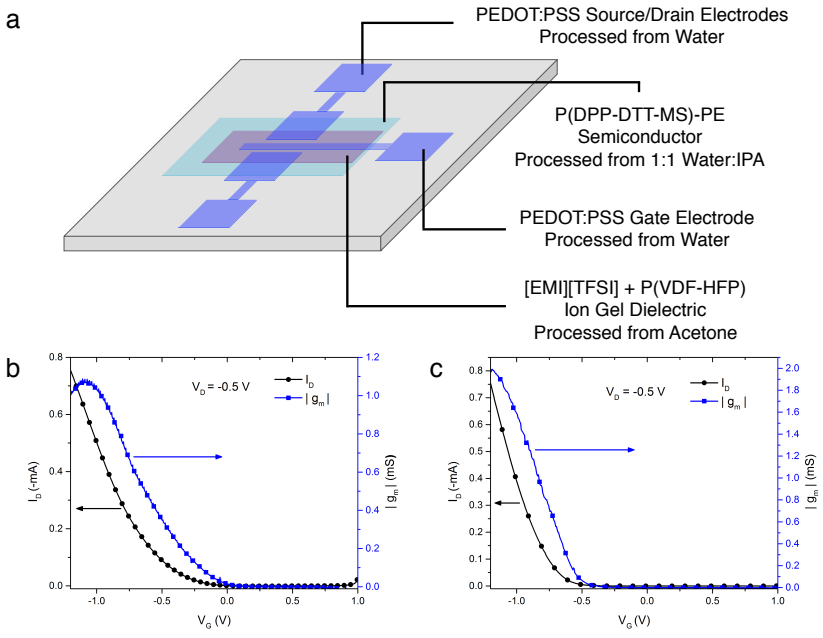

Figure 4-22. Schematic of the architecture for fully solution processed electrolyte-gated organic transistors (EGOTs) (a). Transfer curves and corresponding transconductance values of EGOT devices using **P(DPP-DTT-MS)-PE** processed from 1:1 H_2O:IPA as the semiconductor (b), and with **P(DPP-DTT)** processed from chlorobenzene as the semiconductor (c). Channel length and width were 200 μm and 2000 μm, respectively. Devices were tested with a source-drain bias (V_D) of 0.5V and a sweep rate of 50 mV/sec.

EGOT devices were tested using a source-drain bias (V_D) of 0.5V and a sweep rate of 50 mV/sec, sweeping from +1 V to -1.5 V. The transfer curves of the devices are shown in Figure 4-22b, and the low degree of hysteresis can be seen in the forward and reverse sweep data shown in Figure 4-23. Reporting accurate material mobility values from EGOTs is not as straightforward as in OFET devices, because unlike solid-state dielectrics used in OFETs, ions from the electrolyte dielectric penetrate the semiconductor film through the process.[204-205] These ions effectively dope the semiconductor, leading to significantly larger charge-carrier densities than what occurs in OFET operation. Applying standard mobility calculations leads to mobility values for **P(DPP-DTT-MS)-PE** EGOT devices in the range of 10 and 100 $cm^2V^{-1}s^{-1}$, which are likely inflated above the intrinsic mobility of the polymers due to electrochemical doping from the electrolyte. For these reasons, we have chosen to report transconductance (g_m) as the metric for these devices. Transconductance is calculated as the absolute value of $\Delta I_D/\Delta V_G$ from device transfer curves, and is the commonly used metric in organic electrochemical transistors (OECTs), which feature a similar operation of electrolyte ions penetrating the semiconductor leading to doping and dedoping of the material.[206] Device metrics of EGOT devices are presented in Table 4-2. **P(DPP-DTT-MS)-PE** EGOT devices reached maximum g_m values of 1.1 mS at a V_G of -1 V, with the transfer curve and corresponding transconductance curve shown in Figure 4-22b. In comparison, chlorobenzene cast **P(DPP-DTT)** EGOT devices reached maximum g_m values of 2.0 mS at a V_G of -1.1 V, with the transfer curve and corresponding transconductance curve shown in Figure 4-22c.

Active Layer	g_m average (mS)	g_m maximum (mS)	V_G at maximum g_m (V)	g_m maximum / (W·d/L) (S/m)
P(DPP-DTT-MS)-PE cleaved	0.8 ± 0.2	1.1	-1.01 ± 0.11	2,200
P(DPP-DTT)	1.2 ± 0.5	2.0	-1.07 ± 0.12	4,000

Table 4-2. EGOT device metrics for aqueous processed, cleaved films of **P(DPP-DTT-MS)-PE** and chlorobenzene processed **P(DPP-DTT)**. Calculated from transfer curves of 10 devices each. Device channel dimensions (L x W) were (200 μm x 2000 μm) and film thickness (d) for both devices were 50 nm.

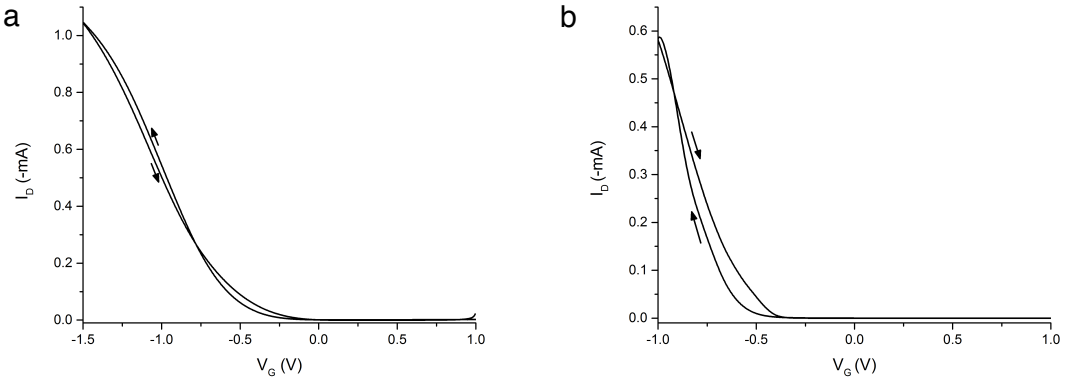

Figure 4-23. EGOT forward and reverse transfer curves for cleaved **P(DPP-DTT-MS)-PE** (a) and **P(DPP-DTT)** (b). Both devices show minimal hysteresis at sweep rates of 50 mV/sec.

While the control polymer **P(DPP-DTT)** still outperforms the aqueous cast **P(DPP-DTT-MS)-PE**, the difference is only a factor of 2, while OFET mobility differed by a factor of ~400. The closing of this performance gap may be attributed to the cleaved **P(DPP-DTT-MS)-PE** film having a greater ability to interact with ions from the electrolyte, as illustrated previously in Figure 4-17 by the broadening of the CV after cleavage. In work with **P(T3-MS)-PE**, the cleaved film exhibited electrochromic

switching speeds of 6 seconds, compared to the speed of 14 seconds for as cast films, shown in Figure 4-12. The EGOT operating mechanism is similar to electrochromic switching in electrolyte, both are influenced by the ability for the polymer backbone to interact with electrolyte ions to electrochemically oxidize and neutralize the polymer. Removal of side chains, which are not electrochemically active, provides a faster response between ions and the polymer backbone. Although **P(DPP-DTT)** films achieve higher hole mobility values, it contains bulky aliphatic side chains that can hinder these interactions. The association of aliphatic side chains in **P(DPP-DTT)** films promote increased crystallinity, which can also hinder the transport of ions. These polymer-electrolyte interactions are likely the driver for the closing of the performance gap between **P(DPP-DTT-MS)-PE** and **P(DPP-DTT)** in EGOT devices.

Both **P(DPP-DTT-MS)-PE** operate in accumulation mode, meaning they are natively in their OFF state and can be turned ON through application of a gate voltage. Since the active layer dimensions play a role in transconductance values, g_m was divided by the active layer dimensionality (W·d/L), where W is channel width, d is film thickness, and L is channel length, in order to compare these results to other accumulation mode organic transistors. For printed EGOT devices the channel dimensions (L x W) were 200 μm x 2000 μm and film thickness (d) for both devices were 50 nm. This led to values of 2,200 S/m for cleaved **P(DPP-DTT-PE)** devices and 4,000 S/m for **P(DPP-DTT)**. In comparison, P3HT EGOTs with gold electrodes and an ion gel dielectric achieve values ~ 20 S/m[207], OECTs using crosslinked films of a polythiophene polyelectrolyte with gold electrodes reach values of ~ 6,700 S/m[208], and OECTs using a polythiophene with glycol side chains and gold electrodes obtain values

up to ~ 13,000 S/m.[48] **P(DPP-DTT-MS)-PE** EGOT devices achieve transconductance values in a similar range as state-of-the-art OECTs, and devices are fully solution processed using only environmentally benign solvents (water, IPA, and acetone).

4.6 Summary and Outlook

In summary, **P(DPP-DTT-MS)** has been designed as a high performance multistage side chain conjugated polymer to build off proof-of-concept work on multistage **P(T3-MS)**. Both of these polymers can be synthesized, purified, and characterized using organic solvents, which is preferred for both producing high molecular weight polymers and characterizing their molecular weight using traditional GPC techniques. The polymers can be hydrolyzed to afford water-soluble conjugated polyelectrolytes, which can be coated into thin films using a 1:1 H_2O:IPA solution. Multistage polymer thin films can be irradiated under UVB light to cleave the polymer side chain, leaving behind a solvent-resistant, electroactive film. This process was harnessed to fabricate OFETs with aqueous processed active layers that reach maximum hole mobility values of 2.03 x 10^{-3} $cm^2V^{-1}s^{-1}$ using **P(DPP-DTT-MS)-PE**. Electrochromic (EC) films can also be processed from aqueous solutions, and as shown with **P(T3-MS)-PE**, side chain cleavage leads to faster switching speeds. The aqueous processability of **P(DPP-DTT-MS)-PE** was also leveraged to fabricate EGOT devices completely through environmentally benign solution processing methods, leading to devices that operated at a maximum transconductance of 1.1 mS at a gate voltage of -1 V. To our knowledge, this is the first example of an organic transistor completely fabricated through solution processing methods that only make use of environmentally benign solvents. This process also has the potential to further increase solid-state interactions

between conjugated polymer backbones and electrolyte by removing inactive side chain mass from the film. While our initial intent was to fabricate solid-state operating devices such as OFETs and OPVs using aqueous solutions, our work shows that these multistage materials may be more beneficial to devices that operate through redox activity, such as ED devices, EGOTs, and OECTs, due to their enhanced ability to interact with ionic media after side chain cleavage. Through further optimization of polymer backbones, multistage side chains, and the methods of chemically linking the two, conjugated polymers with multistage side chains can become a leading design strategy for fabricating high performance EC devices, EGOTs and OECTs in safe and environmentally benign solution-processing methods.

Summarized in Figure 4-24, the use of conjugated polymers with multistage side chains benefit the field of organic electronics from production, to processing, and to final applications. On the production side, traditional polymerization techniques for conjugated polymers (Stille, Suzuki, Direct Arylation) can continue to be performed within organic solvents. These methods have been thoroughly developed to synthesize high molecular weight conjugated polymers. Purification and fractionation techniques can also continue to be performed within organic solvents. Additionally, this process is highly adaptable to varying conjugated polymer backbones. Most soluble conjugated polymers make use of side chains, and can be readily modified in incorporate multistage side chains using similar synthetic organic reactions. On the processing side, multistage side chains enable safe and environmentally benign coating methods to be utilized due to their ability to provide aqueous solubility. Not only can this increase workplace safety and reduce the environmental footprint of coating, but can also lower the barrier of entry into industrial

coating facilities where solvents like chlorobenzene cannot be used. Finally, on the application side this process can provide solvent-resistant, robust, and electroactive conjugated polymer films for a variety of organic electronic devices. Solvent-resistance can be a useful property for orthogonal processing, and can also enable use in aqueous and biological applications. Additionally, side chain cleavage can enhance performance by removing insulating material from the film, as shown in redox applications within this work. Altogether, there are numerous benefits to using conjugated polymers with multistage side chains within the field of printed organic electronics.

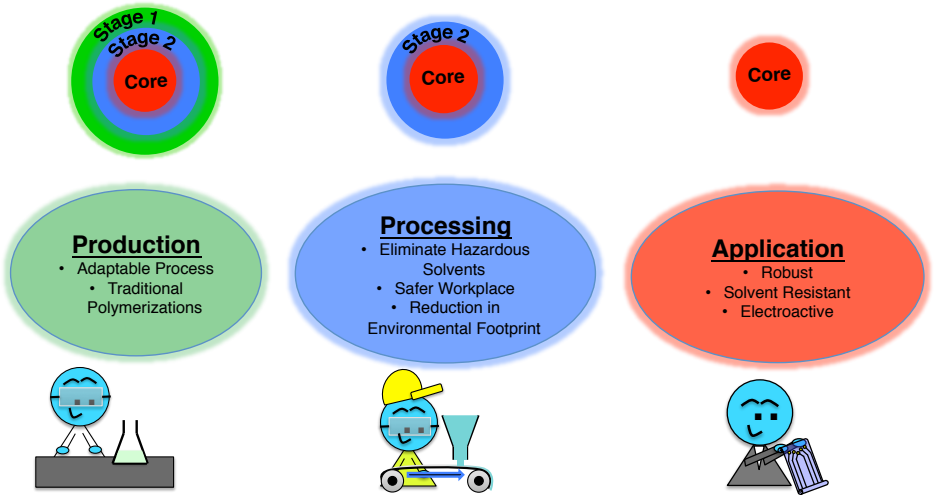

Figure 4-24. Summary of the benefits provided by the development of conjugated polymers with multistage side chains from production to processing and to final organic electronic applications.

4.7 Synthetic Methods

4.7.1 Synthetic Methods for P(T3-MS)

General Synthetic Materials, Methods, and Characterization:

4-(2,5-dibromothiophen-3-yl)phenol (**M1)** and 5,5'-bis(trimethylstannyl)-2,2'-bithiophene were synthesized according to literature procedures.[70, 209] Diethyl methylmalonate (99%, Alfa Aesar), K_2CO_3 (anhydrous, Oakwood Products), sodium hydride (95%, Sigma), 1,3-propanediol di-p-tosylate (98%, Sigma), titanium (IV) chloride (99%, Alfa Aesar), 5-hydroxy-2-nitrobenzaldehyde (95%, Matrix), N-bromosuccinimide (99%, Alfa Aesar), methylmagnesium bromide (3M in diethyl ether, Sigma), triphenylphosphine (99%, Alfa Aesar), $Pd_2(dba)_3$*$CHCl_3$ adduct (Sigma), diethyldithiocarbamic acid diethylammonium salt (97%, TCI America), P(*o*-tolyl)$_3$ (96%, Sigma), 2-bromothiophene (98%, Sigma) and 2-(tributylstannyl)thiophene (97%, Alfa Aesar) were all used as received. N,N-dimethylformamide (anhydrous, Alfa Aesar) and chloroform (BDH) were used as received. Propylene carbonate (Acros Organics), diethyl ether (BDH), tertahydrofuran (BDH), and toluene (BDH) were purified and dried using a solvent purification system. Tetrabutylammonium hexafluorophosphate ($TBAPF_6$, Alfa Aesar, 98%) was recrystallized from ethanol and dried under high vacuum prior to use. ^1H and ^{13}C NMR spectra were taken on a 500MHz Bruker NMR for 32 and 1024 scans, respectively. Chloroform peaks were reference to 7.26 ppm for ^1H spectra and 77.16 ppm for ^{13}C spectra.

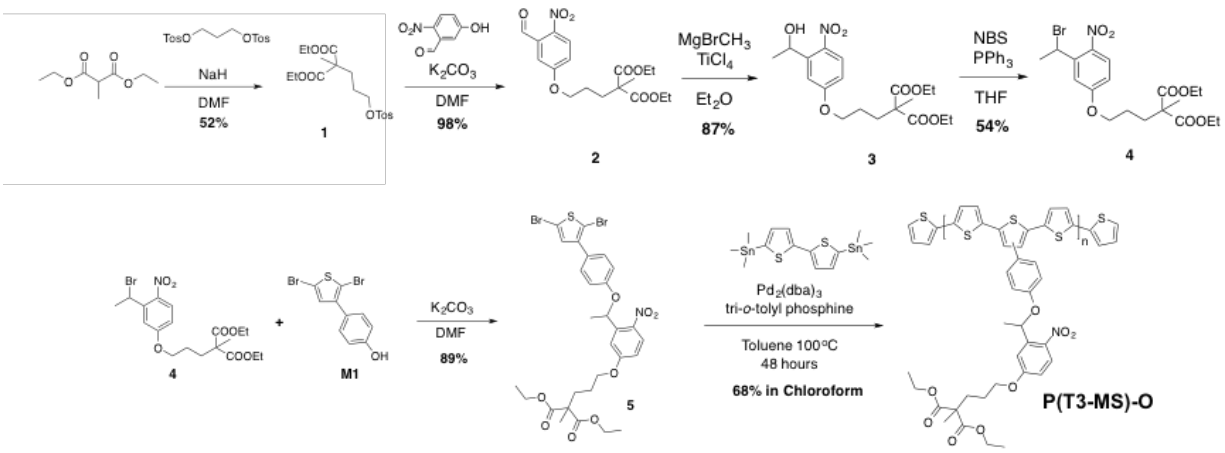

Scheme 4-1. Outline of synthetic route to **P(T3-MS-O)**.

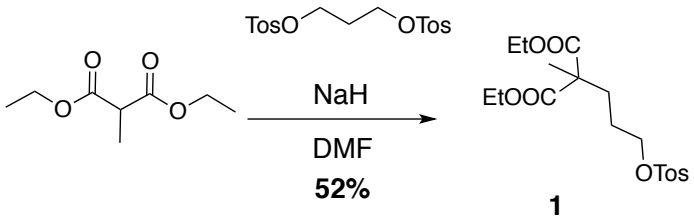

Diethyl 3-methyl-3-(3-(tosyloxy)propoxy)pentanedioate (1): In an argon atmosphere glovebox, 993 mg (86.16 mmol) NaH was added to an oven-dried 3-neck roundbottom flask equipped with a condenser and sealed. The flask was taken out of the glovebox, and 200 mL of anhydrous, degassed DMF was added to the flask. 6 g (34.46 mmol) of diethyl methylmalonate was slowly added to the solution and the solution was allowed to stir at room temperature for 30 minutes, after which 33 g (86.16 mmol) of propane-1,3-ditosylate was added to the solution as a solid. The solution was stirred at 50^{o} C overnight and was then quenched with 25 mL of 1M HCl and 100 mL H_2O. The solution was extracted with EtOAc and the organic layers were washed with H_2O and brine, dried with $MgSO_4$, filtered, and concentrated by rotary evaporator. The compound was purified by column chromatography using 1:9 EtOAc/hexanes to afford 6.92 g (52%) of **1** as a

colorless oil. ^{1}H NMR (500 MHz, $CDCl_3$): δ: 7.77 (d, J = 8.0 Hz, 2H), 7.34 (d, J = 8.0 Hz, 2H), 4.15 (q, J = 7.1 Hz, 4H), 4.01 (t, J = 6.3 Hz, 2H), 2.44 (s, 3H), 1.84 (m, 2H), 1.62 (m, 2H), 1.35 (s, 3H), 1.22 (t, J = 7.1 Hz, 6H). ^{13}C NMR (500 MHz, $CDCl_3$): 171.98, 144.91, 133.12, 129.97, 128.02, 70.41, 61.46, 53.20, 31.74, 24.34, 21.75, 20.04, 14.13. HRMS (ESI MS) *m/z*: theor: 409.1291 found: 409.1288 (+ Na ion found)

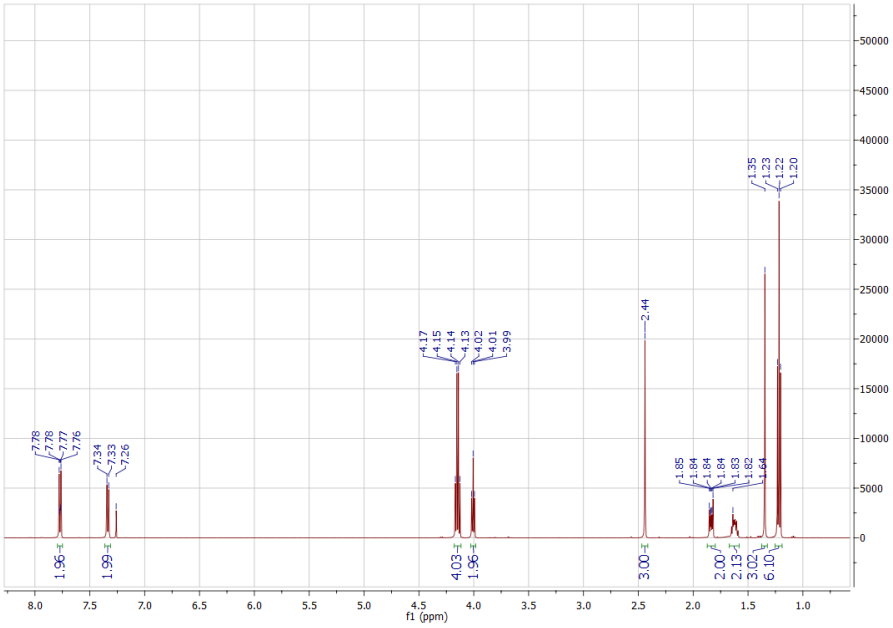

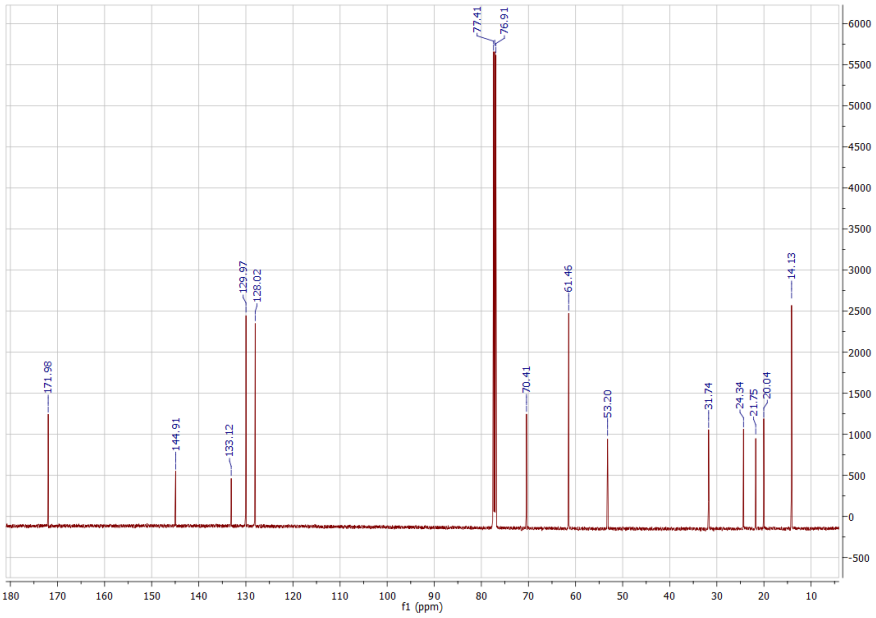

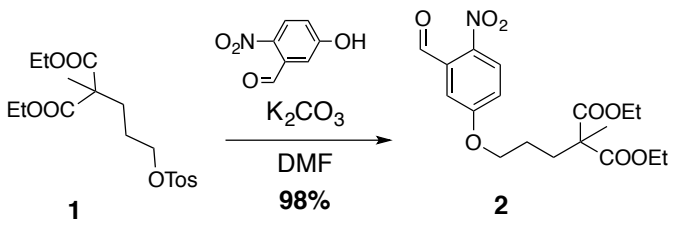

Diethyl 2-(3-(3-formyl-4-nitrophenoxy)propyl)-2-methylmalonate (2): To an oven-dried 2-neck roundbottom flask, 1.56 g (9.32 mmol) of 5-hydroxy-2-nitrobenzaldehyde and 3.51 g (25.40 mmol) of potassium bicarbonate was added, sealed, and evacuated and refilled with argon 3 times. 3.29 g (8.47 mmol) of **1** was dissolved in 10 mL anhydrous, degassed DMF and transferred to the reaction flask. 50 mL anhydrous, degassed DMF was added to the flask, and the reaction was stirred at 70^{o} C overnight. The reaction was allowed to return to room temperature, then the solution was filtered to remove salts and the filtrate was concentrated by rotary evaporation. The compound was purified by column chromatography using 1:9 EtOAc/hexanes as the eluent to afford 3.16 g (98%) of **2** as a colorless oil. ^{1}H NMR (500 MHz, $CDCl_3$): δ: 10.47 (s, 1H), 8.14 (d, J = 9.1 Hz, 1H), 7.29 (d, J = 2.8 Hz, 1H), 7.12 (dd, J = 9.1 Hz, 2.8 Hz, 1H), 4.19 (q, J = 7.1 Hz, 4H), 4.10 (t, J = 6.2 Hz, 2H), 2.03 (m, 2H), 1.81 (m, 2H), 1.45 (s, 3H), 1.25 (t, J = 7.1 Hz, 6H). ^{13}C NMR (500 MHz, $CDCl_3$): 188.34, 171.85, 163.17, 142.02, 134.15, 127.09, 118.70, 113.52, 68.88, 61.20, 53.06, 31.91, 23.97, 19.79, 13.88. HRMS (ESI MS) *m/z*: theor: 382.1496 found: 382.1496.

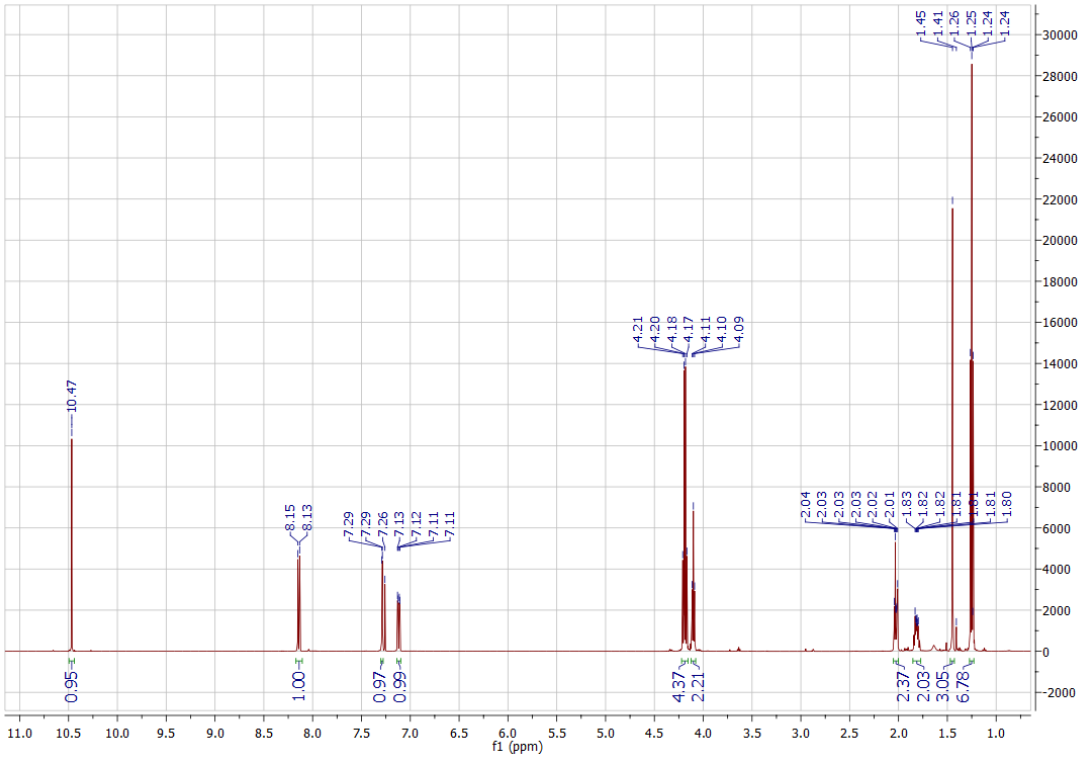
10.47
8.15
8.13
7.29
7.29
7.26
7.13
7.12
7.11
7.11
4.21
4.20
4.18
4.17
4.11
4.10
4.09
2.04
2.03
2.03
2.03
2.02
2.01
1.83
1.82
1.82
1.81
1.81
1.80
1.45
1.41
1.26
1.25
1.24
1.24
0.95
1.00
0.97
0.99
4.37
2.21
2.37
2.03
3.05
6.78
f1 (ppm)

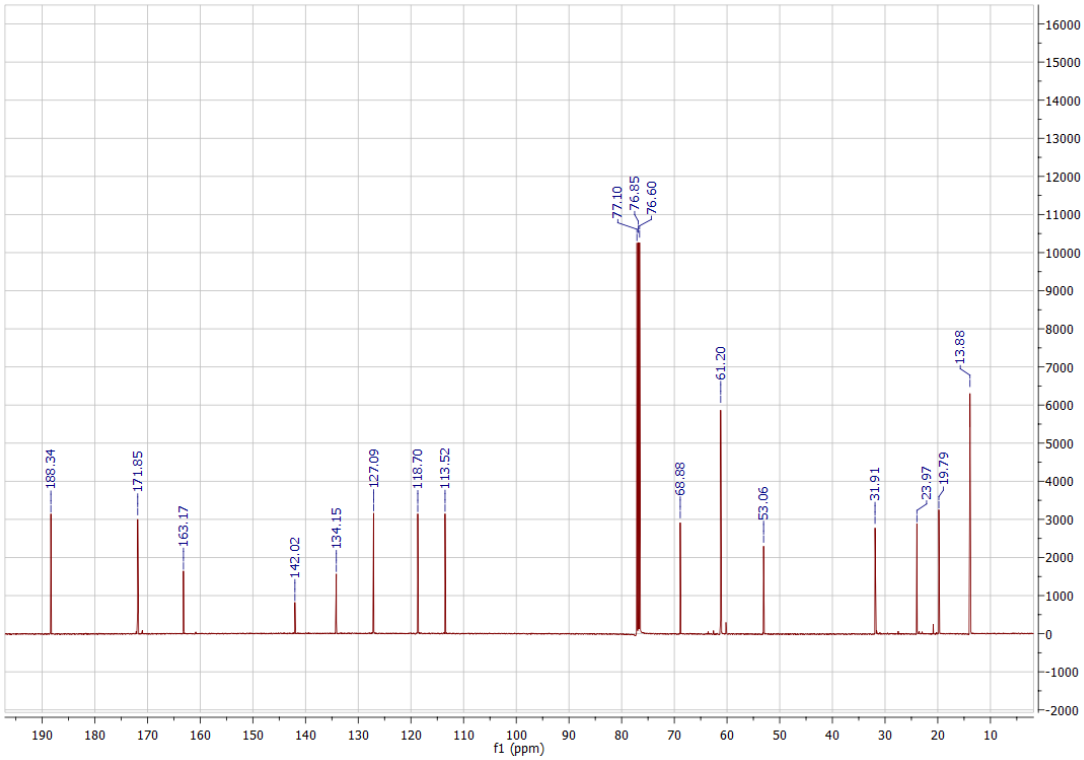
188.34
171.85
163.17
142.02
134.15
127.09
118.70
113.52
77.10
76.85
76.60
68.88
61.20
53.06
31.91
23.97
19.79
13.88
f1 (ppm)

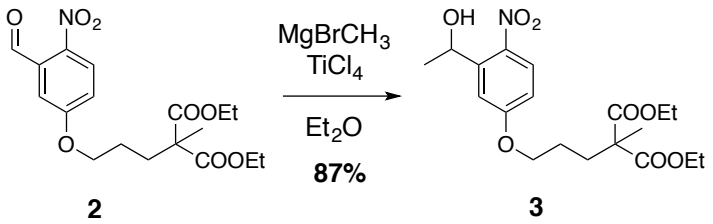

2 **3**

Diethyl 2-(3-(3-(1-hydroxyethyl)-4-nitrophenoxy)propyl)-2-methylmalonate (3): To an oven-dried 2-neck roundbottom flask, 240 mL anhydrous, degassed diethyl ether was added and cooled to -78^{o} C. 4.03 g (21.24 mmol) of $TiCl_4$ was then added to the reaction flask followed by slow addition of 2.60 mL (7.79 mmol) of 3M CH_3MgBr in diethyl ether. After 30 minutes of stirring at -78^{o} C, 2.7 g (7.08 mmol) of **2** dissolved in 10 mL diethyl ether was added to the reaction. The solution was stirred for 3 hours and allowed to gradually return to room temperature. The reaction mixture was poured into 400 mL H_2O and extracted with EtOAc. The organic layers were washed with H_2O and brine, dried over $MgSO_4$, filtered and concentrated by rotary evaporation. The compound was purified *via* column chromatography using 1:4 EtOAc/Hexanes as the eluent to afford 2.44 g (87%) of **3** as a pale yellow oil. ^{1}H NMR (500 MHz, $CDCl_3$): δ: 8.03 (d, J = 9.1 Hz, 1H), 7.30 (d, J = 2.8 Hz, 1H), 6.82 (dd, J = 9.1 Hz, 2.8 Hz, 1H), 5.55 (q, J = 6.3 Hz, 1H), 4.19 (q, J = 7.1 Hz, 4H), 4.07 (t, J = 6.3 Hz, 2H), 2.03 (m, 2H), 1.80 (m, 2H), 1.54 (d, J = 6.3 Hz, 3H), 1.45 (s, 3H), 1.25 (t, J = 7.1 Hz, 6H). ^{13}C NMR (500 MHz, $CDCl_3$): 172.27, 163.43, 144.99, 140.52, 127.73, 113.52, 112.59, 68.58, 66.07, 61.50, 53.42, 32.27, 24.35, 24.32, 20.10, 14.20. HRMS (ESI MS) *m/z*: theor: 420.1629 found: 420.1625.

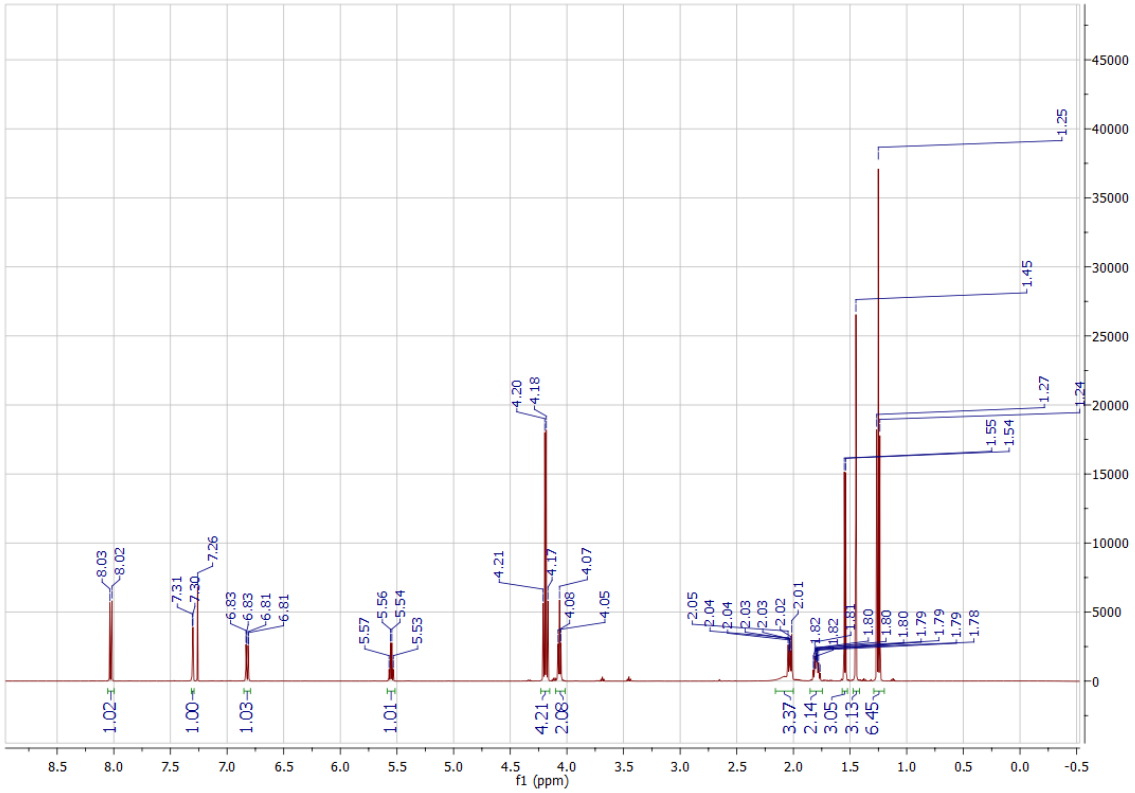
8.03
8.02
7.31
7.30
7.26
6.83
6.81
6.81
5.57
5.56
5.54
5.53
4.21
4.20
4.18
4.17
4.08
4.07
4.05
2.05
2.04
2.04
2.03
2.03
2.02
2.01
1.82
1.81
1.80
1.80
1.80
1.79
1.79
1.78
1.55
1.54
1.45
1.27
1.25
1.24
1.02
1.00
1.03
1.01
4.21
2.08
3.37
2.14
3.05
3.13
6.45
f1 (ppm)

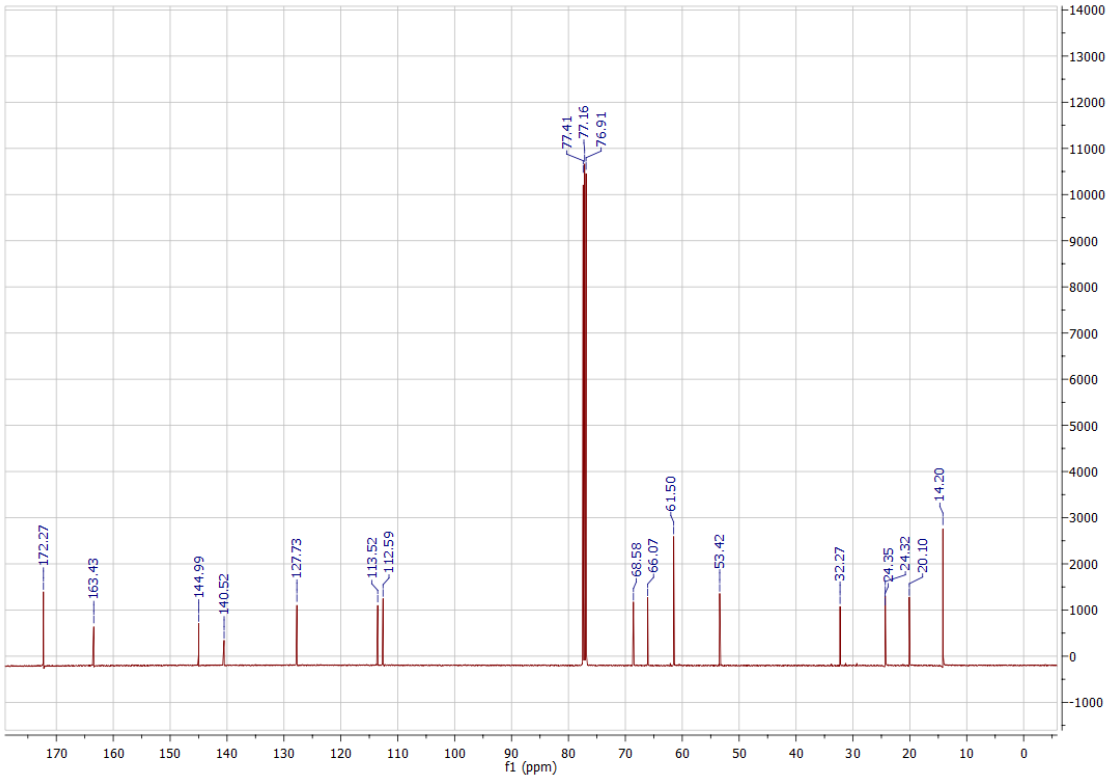
172.27
163.43
144.99
140.52
127.73
113.52
112.59
77.41
77.16
76.91
68.58
66.07
61.50
53.42
32.27
24.35
24.32
20.10
14.20
f1 (ppm)

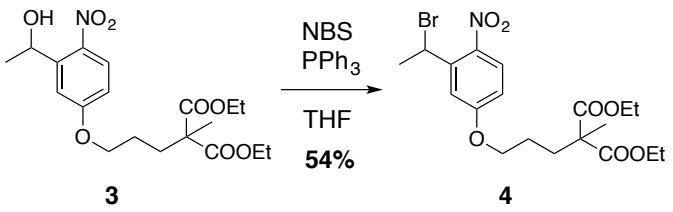

3 4

Diethyl 2-(3-(3-(1-bromoethyl)-4-nitrophenoxy)propyl)-2-methylmalonate (4): To an oven-dried roundbottom flask 740 mg (2.82 mmol) of PPh_3 and 470 mg (2.64 mmol) of N-bromosuccinimide were added and the flask was evacuated and refilled with argon 3 times. The flask was cooled to 0°C and 700 mg (1.76 mmol) of **3** dissolved in 30 mL THF was added to the reaction. The reaction was allowed to stir for 3 hours while gradually returning to room temperature, after which the reaction was quenched with 20 mL H_2O. The mixture was extracted with EtOAc, and the organic layer was washed with H_2O and brine, dried over $MgSO_4$, filtered and concentrated by rotary evaporation. The compound was purified by column chromatography using 1:4 EtOAc/Hexanes as the eluent, affording 437 mg (54%) **4** as a pale yellow oil. ^{1}H NMR (500 MHz, $CDCl_3$): δ: 7.95 (d, J = 9.1 Hz, 1H), 7.31 (d, J = 2.7 Hz, 1H), 6.84 (dd, J = 9.1 Hz, 2.7 Hz, 1H), 6.00 (q, J = 6.8 Hz, 1H), 4.20 (q, J = 7.1 Hz, 4H), 4.07 (td, J = 6.3 Hz, 1.5 Hz, 2H), 2.05 (m, 5H), 1.82 (m, 2H), 1.46 (s, 3H), 1.26 (t, J = 7.1 Hz, 6H). ^{13}C NMR (500 MHz, $CDCl_3$): 172.24, 162.92, 141.05, 140.35, 127.57, 115.75, 113.99, 68.71, 61.52, 53.41, 42.68, 32.29, 27.38, 24.34, 20.11, 14.22. HRMS (ESI MS) *m/z*: theor: 460.0965 found: 460.0960.

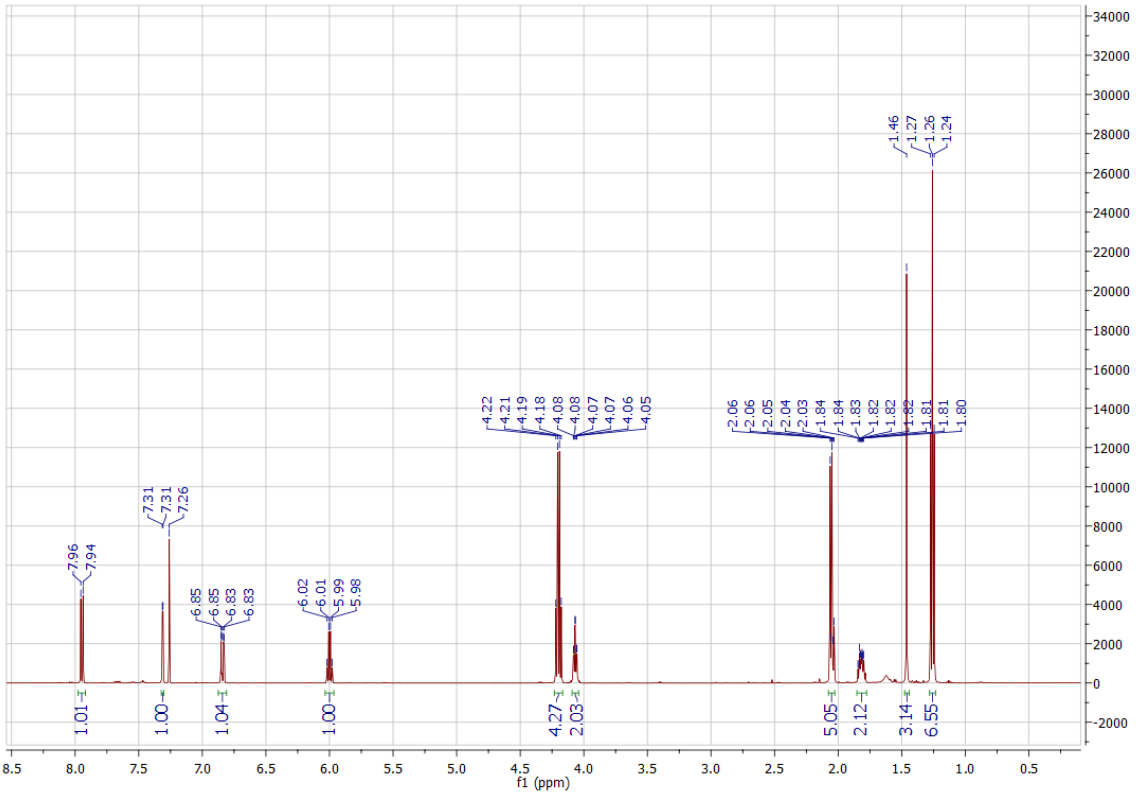
7.96
7.94
7.31
7.31
7.26
6.85
6.85
6.83
6.83
6.02
6.01
5.99
5.98
4.22
4.21
4.19
4.18
4.08
4.08
4.07
4.07
4.06
4.05
2.06
2.06
2.05
2.04
2.03
1.84
1.84
1.83
1.82
1.82
1.82
1.81
1.81
1.80
1.46
1.27
1.26
1.24
1.01
1.00
1.04
1.00
4.27
2.03
5.05
2.12
3.14
6.55
f1 (ppm)

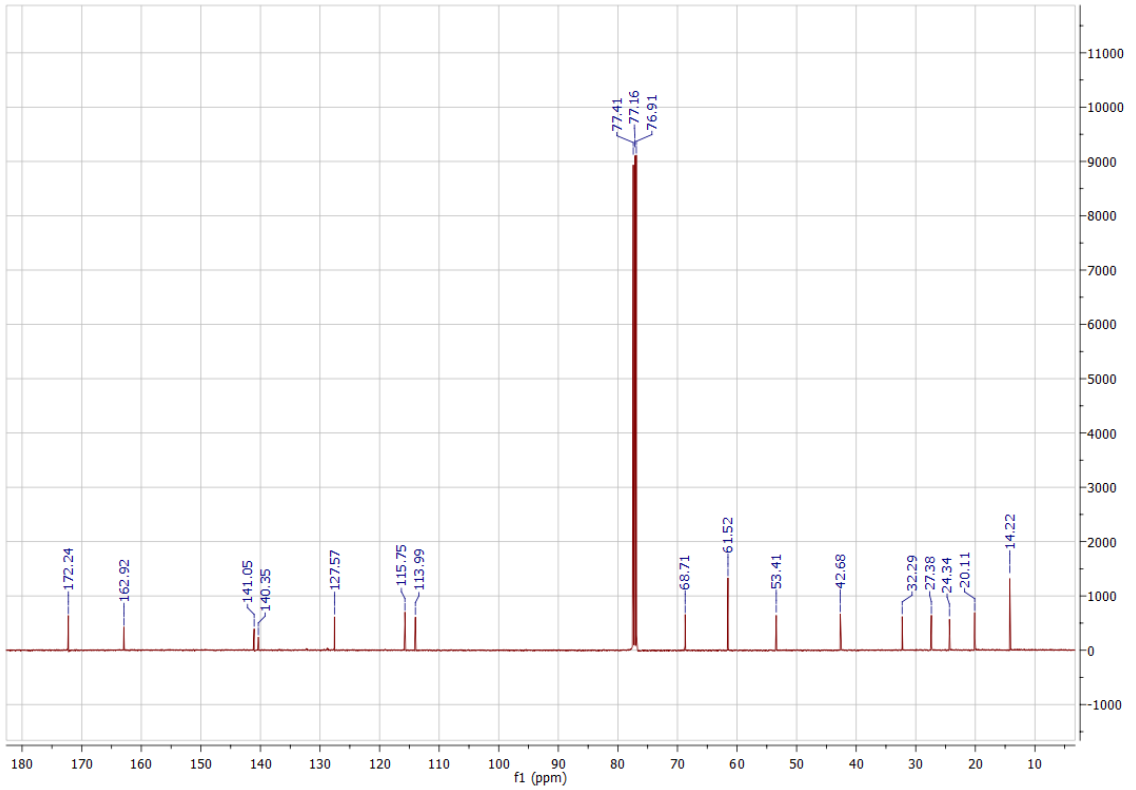
172.24
162.92
141.05
140.35
127.57
115.75
113.99
77.41
77.16
76.91
68.71
61.52
53.41
42.68
32.29
27.38
24.34
20.11
14.22
f1 (ppm)

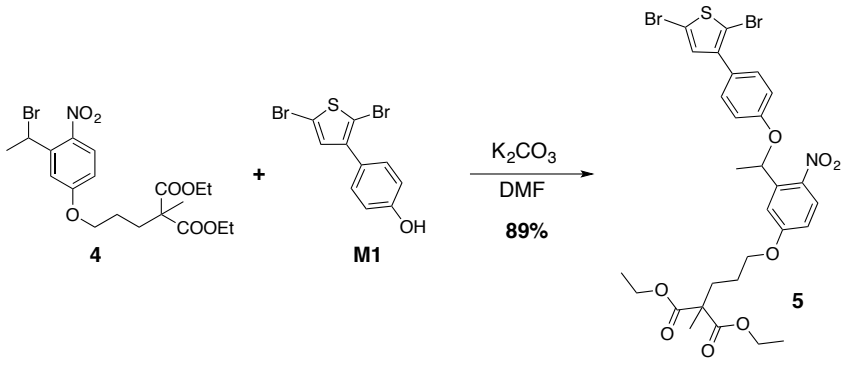

Diethyl-2-(3-(3-(1-(4-(2,5-dibromothiophen-3-yl)phenoxy)ethyl)-4 nitropheno xy)propyl)-2-methylmalonate (5): To an oven-dried 2-neck roundbottom flask 207 mg (0.45 mmol) of **4** and 186 mg (1.35 mmol) of potassium bicarbonate were added and the flask was evacuated and refilled with argon 3 times. 165 mg (0.49 mmol) of **M1** dissolved in 10 mL anhydrous, degassed DMF was added to the flask, followed by an additional 30 mL of anhydrous, degassed DMF. The reaction was stirred overnight at 60^{o} C and quenched with 5 mL of 1M HCl followed by 30 mL H_2O. The mixture was extracted with EtOAc and the organic layers were washed with H_2O and brine, dried over $MgSO_4$, filtered and concentrated by rotary evaporation. The compound was purified by column chromatography using dichloromethane as the eluent to afford 287 mg (89%) of **5** as a pale yellow oil. ^{1}H NMR (500 MHz, $CDCl_3$): δ: 8.14 (d, J = 9.1 Hz, 1H), 7.35 (d, J = 8.5 Hz, 2H), 7.21 (d, J = 2.4 Hz, 1H), 6.94 (s, 1H), 6.84 (m, 3H), 6.18 (q, J = 6.2 Hz, 1H), 4.18 (q, J = 7.0 Hz, 4H), 3.99 (m, 2H), 2.00 (m, 2H), 1.76 (m, 2H), 1.70 (d, J = 6.2 Hz, 3H), 1.42 (s, 3H), 1.24 (t, J = 7.1 Hz, 6H). ^{13}C NMR (500 MHz, $CDCl_3$): 172.23, 163.79, 157.24, 142.90, 141.54, 140.11, 131.73, 129.93, 128.11, 127.12, 115.54, 113.77, 112.56, 111.17, 107.03, 71.98, 68.61, 61.49, 53.39, 32.23, 24.29, 23.68, 20.06, 14.21. HRMS (ESI MS) *m/z*: theor: 734.0029 found: 734.0029.

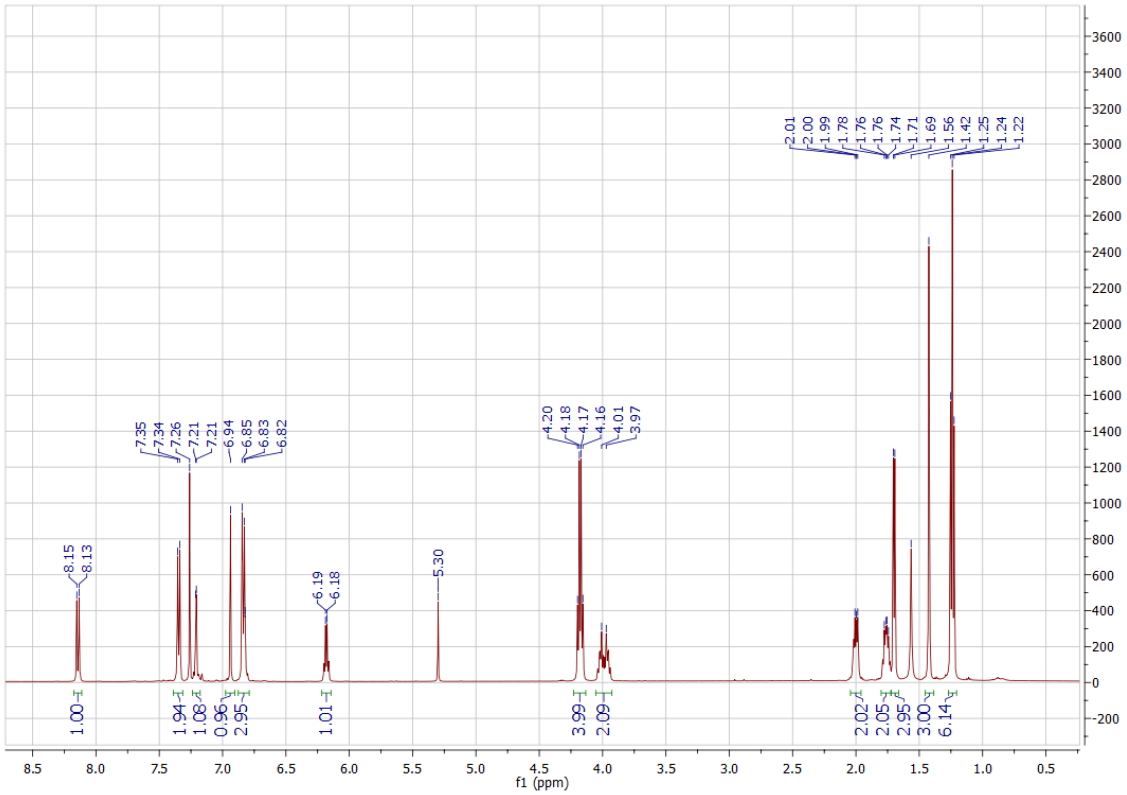
8.15
8.13
7.35
7.34
7.26
7.21
7.21
6.94
6.85
6.83
6.82
6.19
6.18
5.30
4.20
4.18
4.17
4.16
4.01
3.97
2.01
2.00
1.99
1.78
1.76
1.76
1.74
1.71
1.69
1.56
1.42
1.25
1.24
1.22
1.00
1.94
1.08
0.96
2.95
1.01
3.99
2.09
2.02
2.05
2.95
3.00
6.14
f1 (ppm)

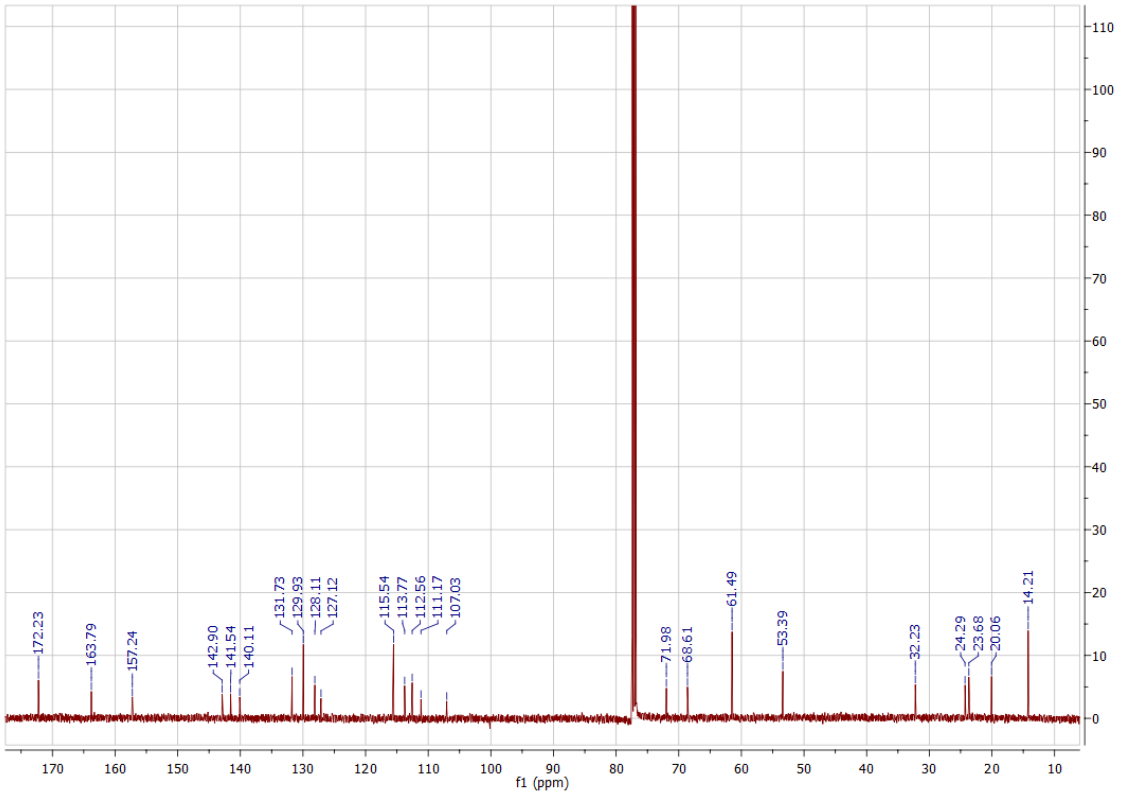
172.23
163.79
157.24
142.90
141.54
140.11
131.73
129.93
128.11
127.12
115.54
113.77
112.56
111.17
107.03
71.98
68.61
61.49
53.39
32.23
24.29
23.68
20.06
14.21
f1 (ppm)

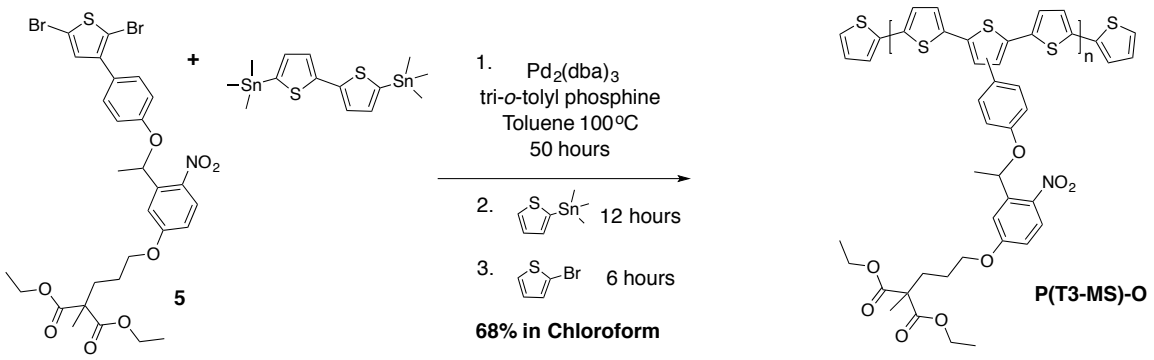

P(T3-MS)-O: To an oven-dried 3-neck flask 198 mg (0.40 mmol) of 5,5'-bis(trimethylstannyl)-2,2'-bithiophene was added and the flask was evacuated and refilled with argon 3 times. 287 mg (0.40 mmol) of **5** dissolved in 10 mL dry, degassed toluene was added to the flask. In an argon atmosphere glovebox, 13 mg (0.012 mmol) of $Pd_2(dba)_3$ chloroform adduct and 15 mg (0.048 mmol) of P(o-tolyl)$_3$ were weighed out into a vial, dissolved in 15 mL dry, degassed toluene and added to the reaction flask. The reaction was stirred at 110^o C for 50 hours, after which 0.1 mL of 2-(tributylstannyl)thiophene was added as an end-capper and allowed to stir overnight. 0.1 mL of 2-bromothiophene was added as an end-capper and allowed to stir for 6 hours, after which the reaction was cooled and precipitated into methanol. The precipitate was filtered and purified by successive Soxhlet extractions in methanol, acetone, hexanes, and chloroform. The chloroform fraction was taken and allowed to stir at 40° C with a spatula tip of a palladium scavenger (diethylammonium diethyldithiocarbamate) for 1 hour, after which it was concentrated to <10 mL and precipitated into methanol. The precipitate was filtered and dried over high vacuum to afford 185mg (68%) of **P(T3-MS)-O** as a red powder. Mn: 11 kDa, Mw: 21 kDa, *Đ:* 1.9 (GPC in THF vs. Polystyrene). Anal. calcd. for $C_{37}H_{35}NO_8S_3$: C (61.91) H (4.91) N (1.95) S (13.40), Found: C (60.48) H (5.05) N (1.85) S (13.61).

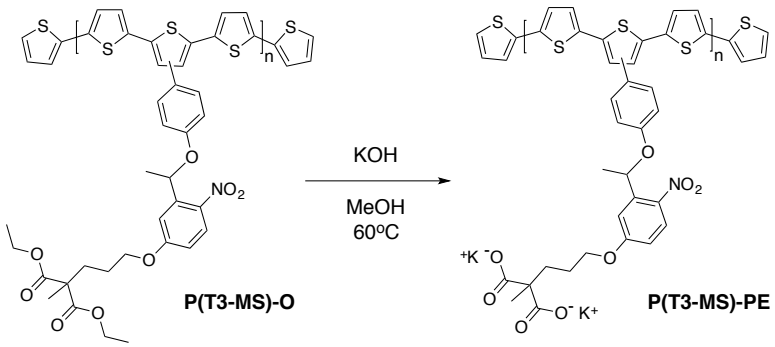

P(T3-MS)-PE: In an oven-dried roundbottom flask 52 mg of **P(T3-MS)-O** and 15 mL of a 1M KOH in methanol solution were added. The reaction was stirred at 60° C overnight, filtered and washed with methanol, and dried to afford 46 mg of **P(T3-MS)-PE** as a red powder.

4.7.2 Synthetic Methods for P(DPP-DTT-MS)

General Synthetic Materials, Methods, and Characterization:

5,5'-bis(trimethylstannyl)-2,2'-bithiophene[210] was synthesized according to literature procedures. **P(DPP-DTT)** was purchased from 1-Material with a reported M_n of 100 kDa vs. polystyrene standards with *Đ* of 5.2. Diethyl methylmalonate (99%, Alfa Aesar), K_2CO_3 (anhydrous, Oakwood Products), sodium hydride (95%, Sigma), 1,2-dibromoethane (98%, Sigma), titanium (IV) chloride (99%, Alfa Aesar), 5-hydroxy-2-nitrobenzaldehyde (95%, Matrix), N-bromosuccinimide (99%, Alfa Aesar), methylmagnesium bromide (3M in diethyl ether, Sigma), triphenylphosphine (99%, Alfa Aesar), $Pd_2(dba)_3$*$CHCl_3$ adduct (Sigma), diethyldithiocarbamic acid diethylammonium salt (97%, TCI America), P(*o*-tolyl)$_3$ (96%, Sigma), were all used as received. N,N-dimethylformamide (anhydrous, Alfa Aesar) and chloroform (BDH) were used as

received. Propylene carbonate (Acros Organics), diethyl ether (BDH), tertahydrofuran (BDH), and toluene (BDH) were purified and dried using a solvent purification system.

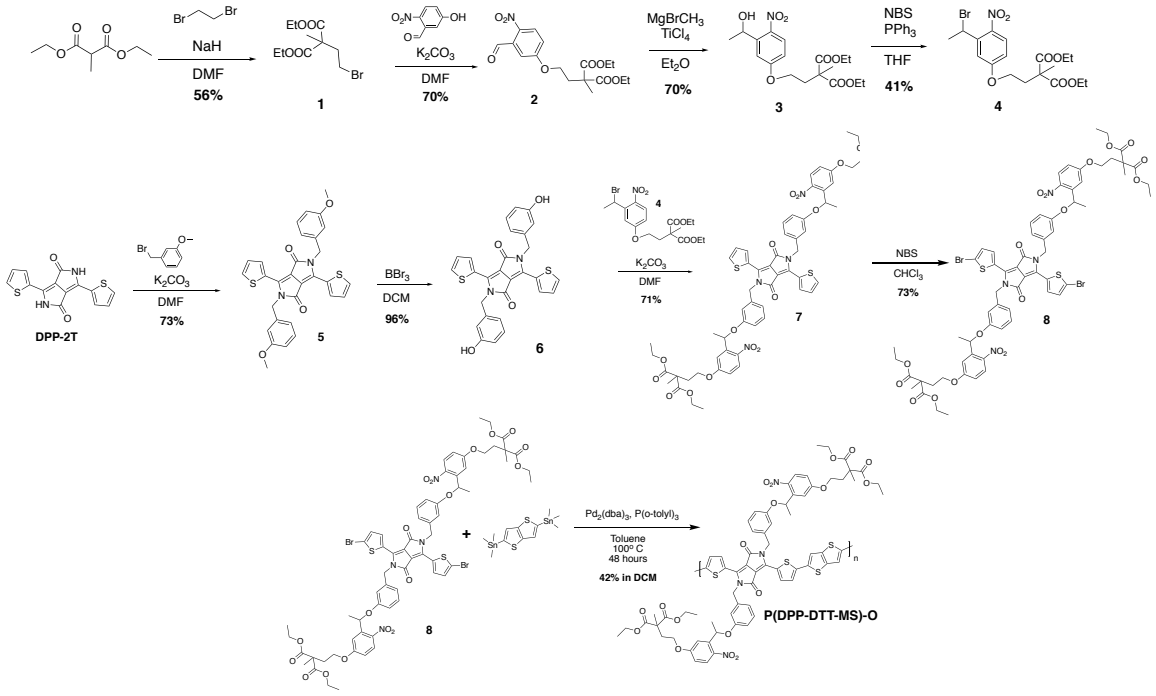

Scheme 4-2. Outline of synthetic route to **P(DPP-DTT-MS)**.

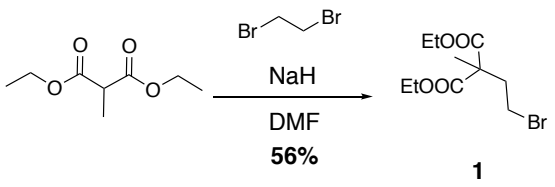

Diethyl 2-(2-bromoethyl)-2-methylmalonate (1): In an argon atmosphere glovebox, 1.45 g (60.57 mmol) NaH was added to an oven-dried 3-neck roundbottom flask equipped with a condenser and sealed. The flask was taken out of the glovebox, and 200 mL of anhydrous, degassed DMF was added to the flask. 8.79 g (50.48 mmol) of diethyl methylmalonate was slowly added to the solution and the solution was allowed to stir at room temperature for 30 minutes, after which 23.7 g (126.20 mmol) of 1,2-dibromoethane was added to the solution as a solid. The solution was stirred at 50^{o} C overnight and was then quenched with 25 mL of 1M HCl and 100 mL H_2O. The solution was extracted with EtOAc and the organic layers were washed with H_2O and brine, dried with $MgSO_4$, filtered, and concentrated by rotary evaporator. The compound was purified by column chromatography using 1:9 EtOAc/hexanes to afford 7.9 g (56%) of **1** as a colorless oil. ^{1}H NMR (300 MHz, $CDCl_3$): δ: 4.20 (q, J = 7.1 Hz, 4H), 3.40 (dd, J = 9.6 Hz, 6.8 Hz, 2H), 2.45 (dd, J = 9.6 Hz, 6.8 Hz, 2H), 1.45 (s, 3H), 1.27 (t, J = 7.2 Hz, 6H). ^{13}C NMR (500 MHz, $CDCl_3$): δ: 211.36, 208.55, 44.21, 34.78, 29.57, 26.14, 25.57. HRMS (ESI MS) *m/z*: theor: 303.0207 found: 303.0211 (+ Na ion found)

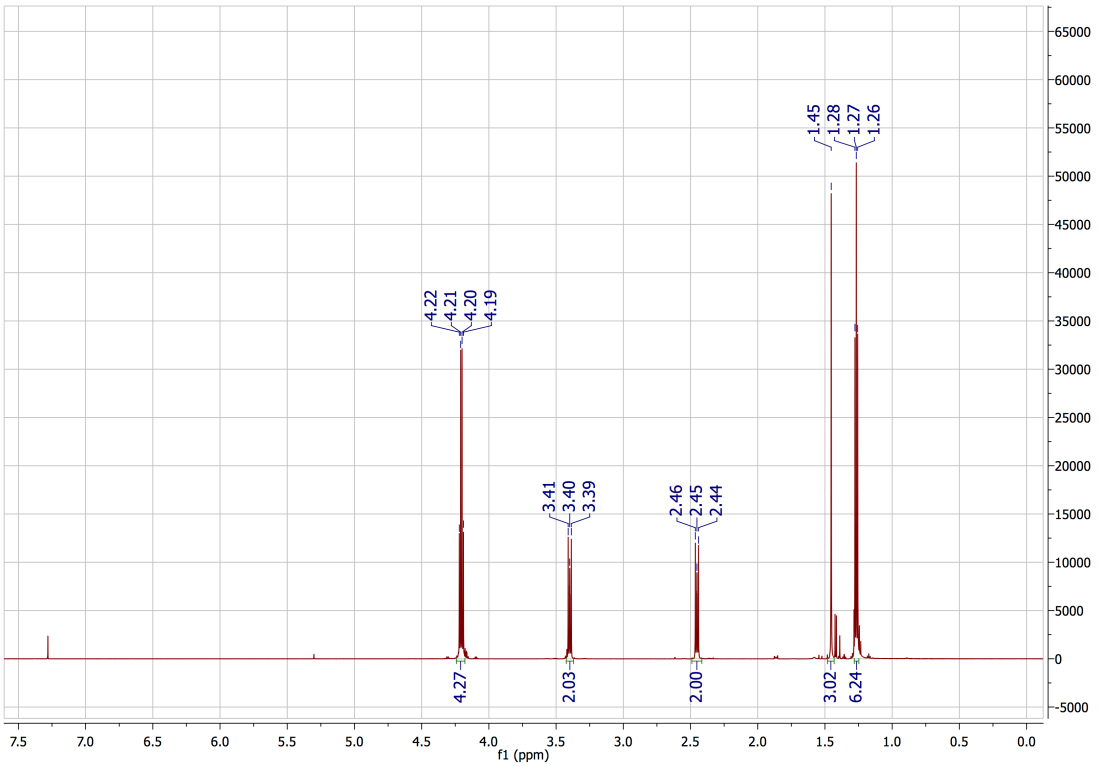
4.22
4.21
4.20
4.19
3.41
3.40
3.39
2.46
2.45
2.44
1.45
1.28
1.27
1.26
4.27
2.03
2.00
3.02
6.24
f1 (ppm)

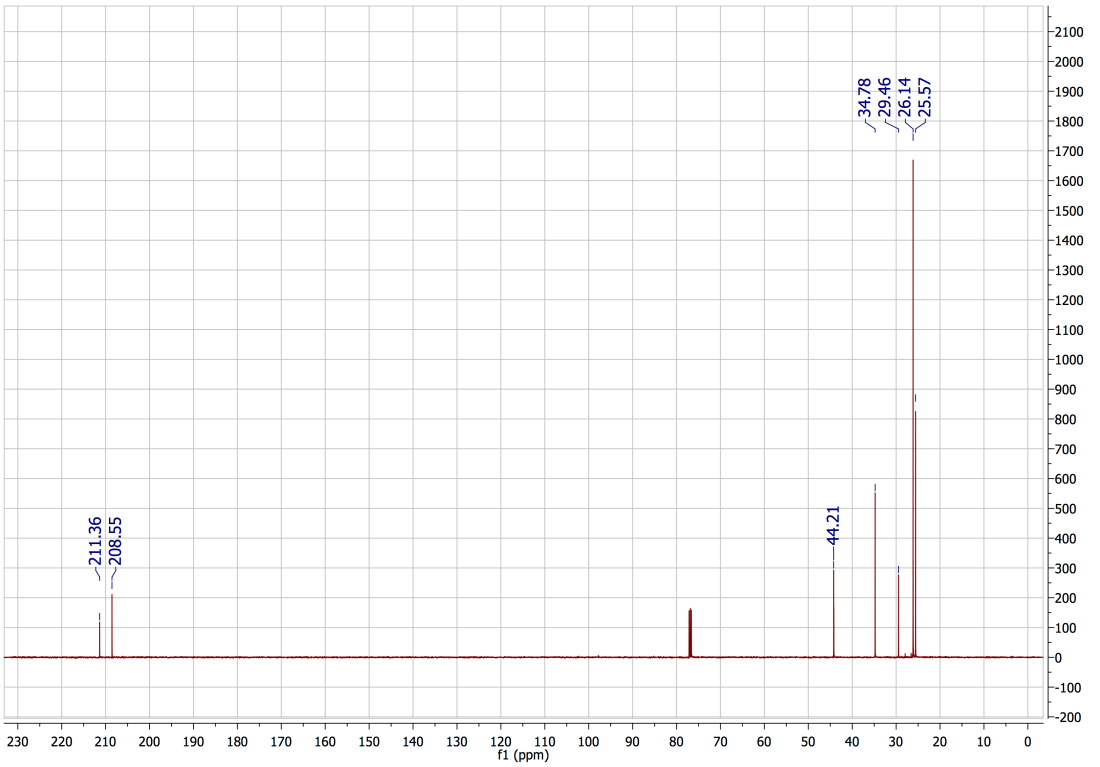
211.36
208.55
44.21
34.78
29.46
26.14
25.57
f1 (ppm)

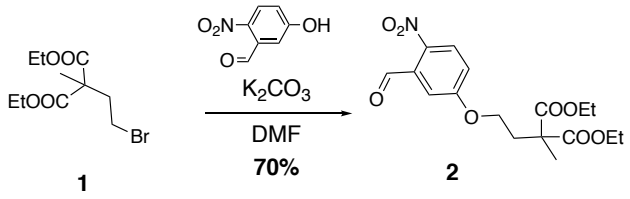

Diethyl 2-(3-(3-formyl-4-nitrophenoxy)ethyl)-2-methylmalonate (2): To an oven-dried 2-neck roundbottom flask, 5.16 g (30.91 mmol) of 5-hydroxy-2-nitrobenzaldehyde and 11.65 g (84.29 mmol) of potassium bicarbonate was added, sealed, and evacuated and refilled with argon 3 times. 7.90 g (28.09 mmol) of **1** was dissolved in 20 mL anhydrous, degassed DMF and transferred to the reaction flask. 180 mL anhydrous, degassed DMF was added to the flask, and the reaction was stirred at 70^{o} C overnight. The reaction was allowed to return to room temperature, then the solution was filtered to remove salts and the filtrate was concentrated by rotary evaporation. The compound was purified by column chromatography using 1:9 EtOAc/hexanes as the eluent to afford 7.17 g (70%) of **2** as a colorless oil. ^{1}H NMR (300 MHz, $CDCl_3$): δ: 10.49 (s, 1H), 8.17 (d, J = 9.1 Hz, 1H), 7.30 (d, J = 2.8 Hz, 1H), 7.13 (dd, J = 9.8 Hz, 2.8 Hz, 1H), 4.23 (m, 6H), 2.44 (t, J = 6.5 Hz, 2H), 1.52 (s, 3H), 1.27 (t, J = 7.1 Hz, 6H). ^{13}C NMR (500 MHz, $CDCl_3$): δ: 188.26, 171.48, 162.79, 142.14, 134.16, 127.11, 118.65, 113.58, 65.39, 61.43, 51.67, 34.35, 20.21, 13.83. HRMS (ESI MS) *m/z*: theor: 367.1267 found: 367.1263.

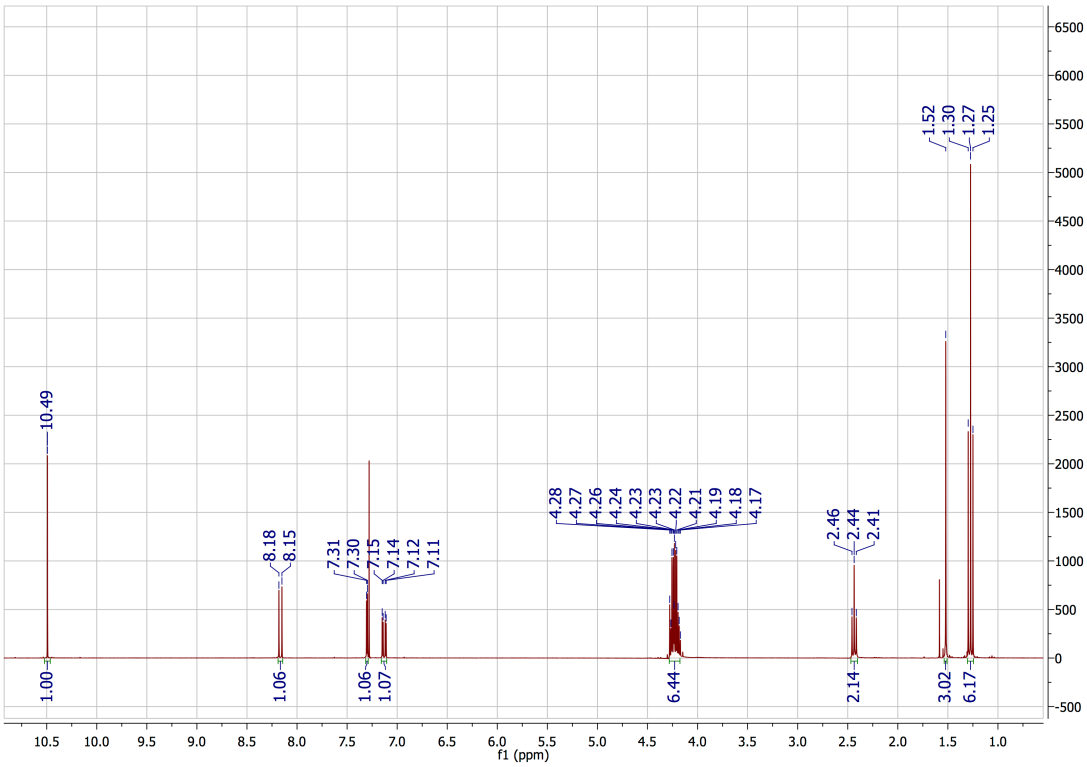
10.49
8.18
8.15
7.31
7.30
7.15
7.14
7.12
7.11
4.28
4.27
4.26
4.24
4.23
4.23
4.22
4.21
4.19
4.18
4.17
2.46
2.44
2.41
1.52
1.30
1.27
1.25
1.00
1.06
1.06
1.07
6.44
2.14
3.02
6.17
f1 (ppm)

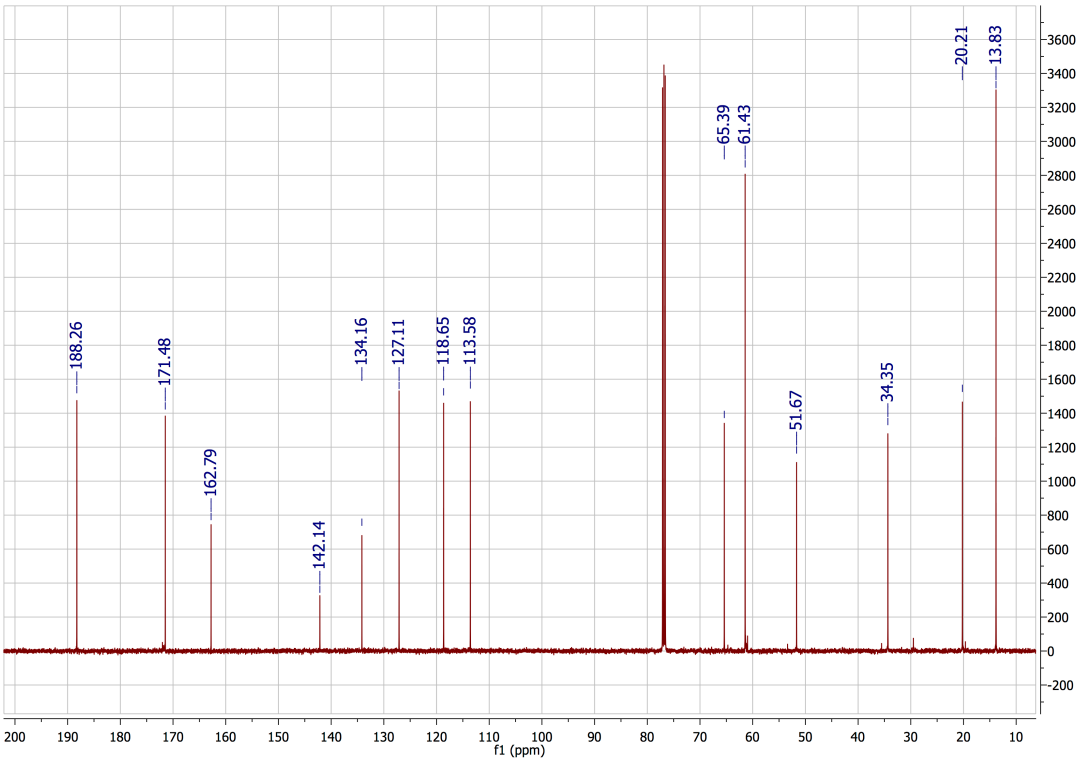
188.26
171.48
162.79
142.14
134.16
127.11
118.65
113.58
65.39
61.43
51.67
34.35
20.21
13.83
f1 (ppm)

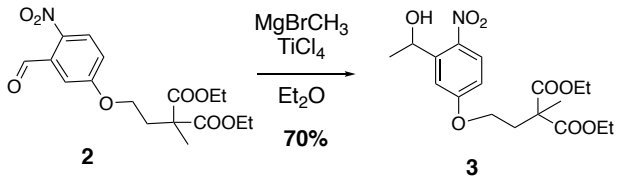

Diethyl 2-(3-(3-(1-hydroxyethyl)-4-nitrophenoxy)ethyl)-2-methylmalonate (3): To an oven-dried 2-neck roundbottom flask, 550 mL anhydrous, degassed diethyl ether was added and cooled to -78° C. 11.11 g (58.55 mmol) of $TiCl_4$ was then added to the reaction flask followed by slow addition of 7.20 mL (21.47 mmol) of 3M CH_3MgBr in diethyl ether. After 30 minutes of stirring at -78° C, 7.17 g (19.52 mmol) of **2** dissolved in 50 mL diethyl ether was added to the reaction. The solution was stirred for 3 hours and allowed to gradually return to room temperature. The reaction mixture was poured into 500 mL H_2O and extracted with EtOAc. The organic layers were washed with H_2O and brine, dried over $MgSO_4$, filtered and concentrated by rotary evaporation. The compound was purified *via* column chromatography using 1:4 EtOAc/Hexanes as the eluent to afford 5.24 g (70%) of **3** as a pale yellow oil. ^{1}H NMR (300 MHz, $CDCl_3$): δ: 8.04 (d, J = 9.1 Hz, 1H), 7.30 (d, J = 2.8 Hz, 1H), 6.83 (dd, J = 9.1 Hz, 2.8 Hz, 1H), 5.56 (m, 1H), 4.22 (m, 6H), 2.42 (t, J = 6.5 Hz, 2H), 2.40 (s, 1H), 1.56 (d, J = 6.3 Hz, 3H), 1.52 (s, 3H), 1.27 (t, J = 7.1 Hz, 6H). ^{13}C NMR (500 MHz, $CDCl_3$): δ: 171.61, 162.72, 144.63, 140.37, 127.43, 113.25, 112.24, 65.77, 64.73, 61.38, 51.74, 34.45, 23.99, 20.20, 13.83. HRMS (ESI MS) *m/z*: theor: 383.1580 found: 383.1586.

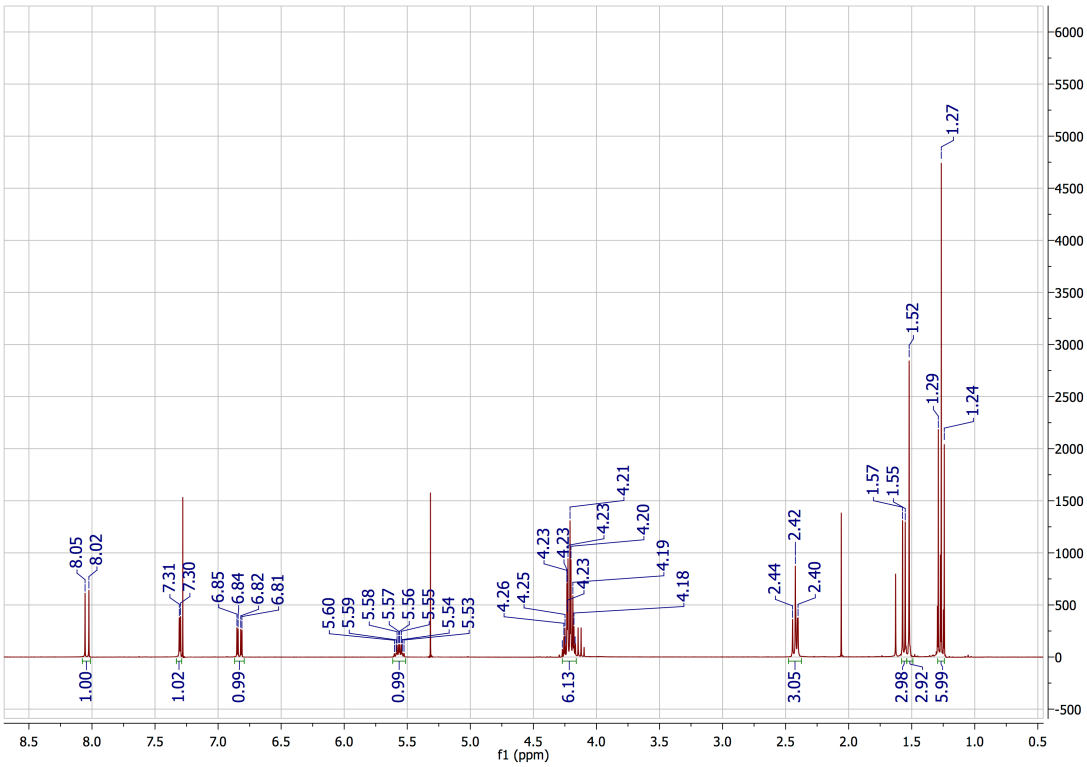
8.05
8.02
7.31
7.30
6.85
6.84
6.82
6.81
5.60
5.59
5.58
5.57
5.56
5.55
5.54
5.53
4.26
4.25
4.23
4.23
4.23
4.23
4.21
4.20
4.19
4.18
2.44
2.42
2.40
1.57
1.55
1.52
1.29
1.27
1.24
1.00
1.02
0.99
0.99
6.13
3.05
2.98
2.92
5.99
f1 (ppm)

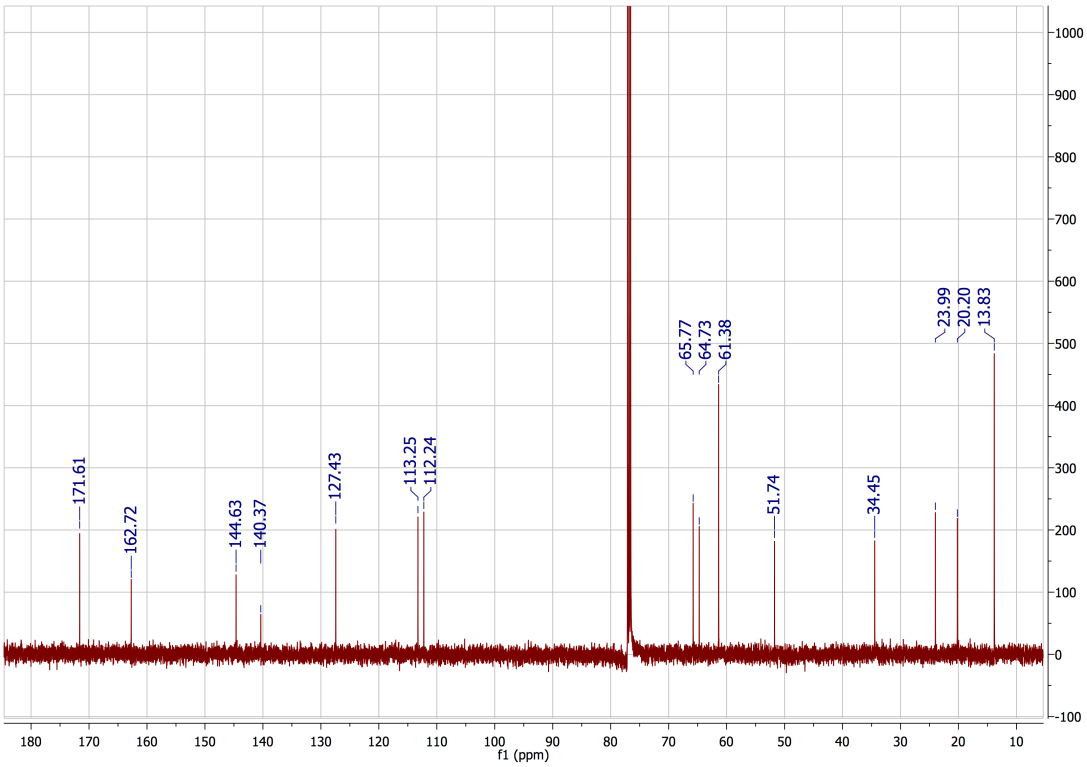
171.61
162.72
144.63
140.37
127.43
113.25
112.24
65.77
64.73
61.38
51.74
34.45
23.99
20.20
13.83
f1 (ppm)

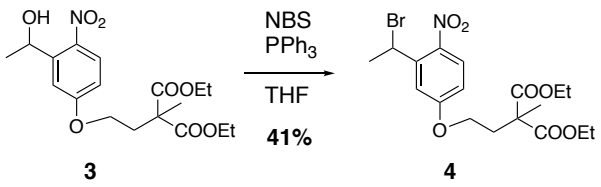

3 4

Diethyl 2-(3-(3-(1-bromoethyl)-4-nitrophenoxy)ethyl)-2-methylmalonate (4): To an oven-dried roundbottom flask 5.10 g (19.44 mmol) of PPh_3 and 3.25 g (18.26 mmol) of N-bromosuccinimide were added and the flask was evacuated and refilled with argon 3 times. The flask was cooled to 0^o C and 4.65 g (12.13 mmol) of **3** dissolved in 300 mL THF was added to the reaction. The reaction was allowed to stir for 3 hours while gradually returning to room temperature, after which the reaction was quenched with 20 mL H_2O. The mixture was extracted with EtOAc, and the organic layer was washed with H_2O and brine, dried over $MgSO_4$, filtered and concentrated by rotary evaporation. The compound was purified by column chromatography using 1:4 EtOAc/Hexanes as the eluent, affording 2.22 g (41%) **4** as a pale yellow oil. ^{1}H NMR (500 MHz, $CDCl_3$): δ: 7.96 (d, J = 9.1 Hz, 1H), 7.31 (d, J = 2.7 Hz, 1H), 6.86 (dd, J = 9.1 Hz, 2.7 Hz, 1H), 6.00 (q, J = 6.8 Hz, 1H), 4.22 (m, 6H), 2.43 (t, J = 6.5 Hz, 2H), 2.07 (d, 6.9 Hz, 3H), 1.53 (s, 3H), 1.27 (td, J = 7.1 Hz, 3.1Hz, 6H). ^{13}C NMR (500 MHz, $CDCl_3$): 171.59, 162.20, 140.75, 140.15, 127.27, 115.53, 113.59, 64.85, 61.42, 51.68, 42.27, 34.47, 27.04, 20.31, 13.85. HRMS (ESI MS) *m/z*: theor: 445.0736 found: 445.0753.

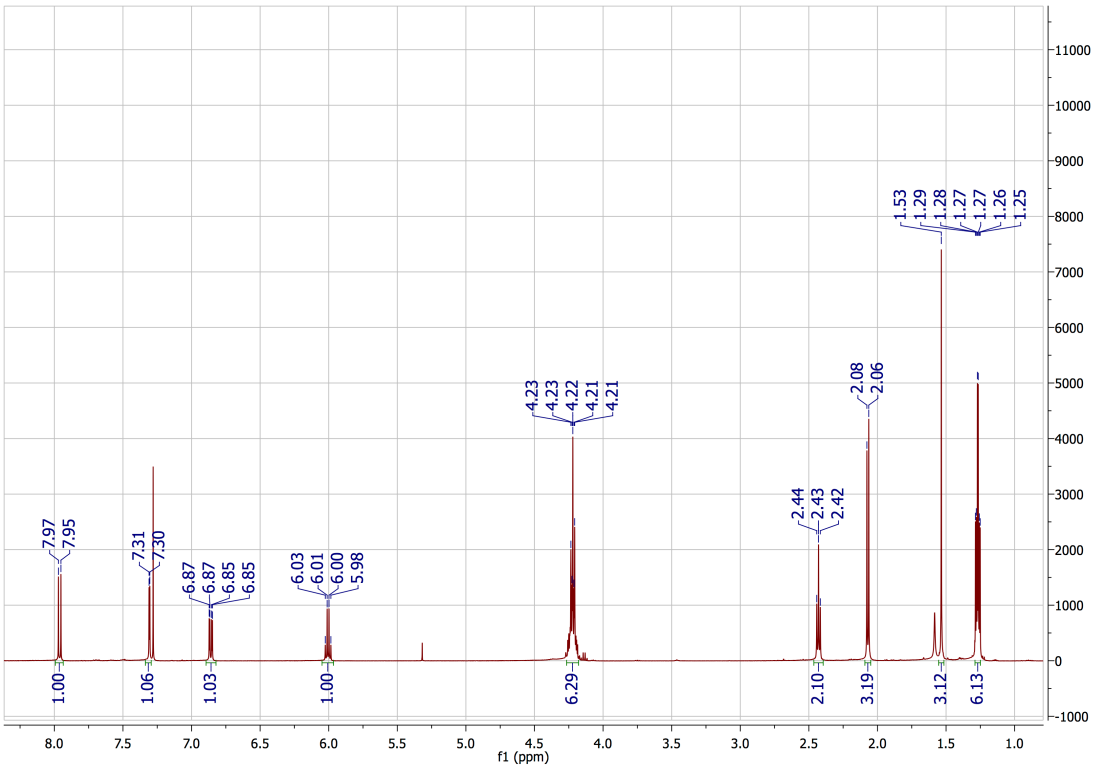
7.97
7.95
7.31
7.30
6.87
6.87
6.85
6.85
6.03
6.01
6.00
5.98
4.23
4.23
4.22
4.21
4.21
2.44
2.43
2.42
2.08
2.06
1.53
1.29
1.28
1.27
1.27
1.26
1.25
1.00
1.06
1.03
1.00
6.29
2.10
3.19
3.12
6.13
f1 (ppm)

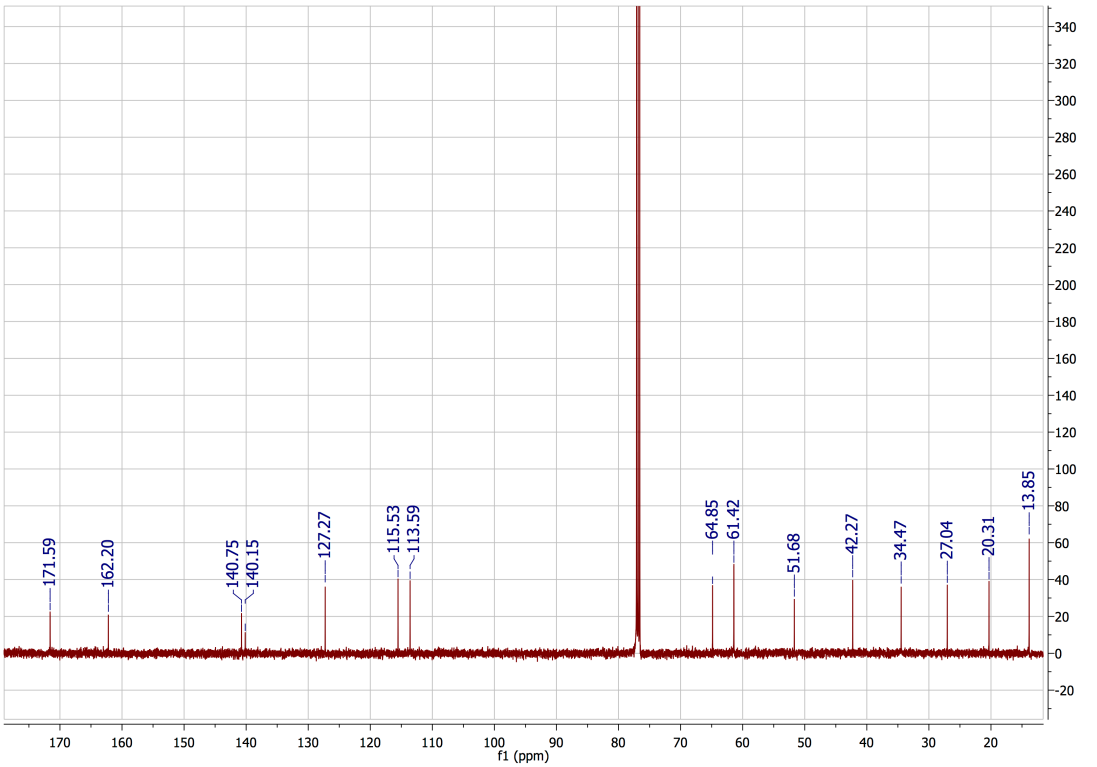
171.59
162.20
140.75
140.15
127.27
115.53
113.59
64.85
61.42
51.68
42.27
34.47
27.04
20.31
13.85
f1 (ppm)

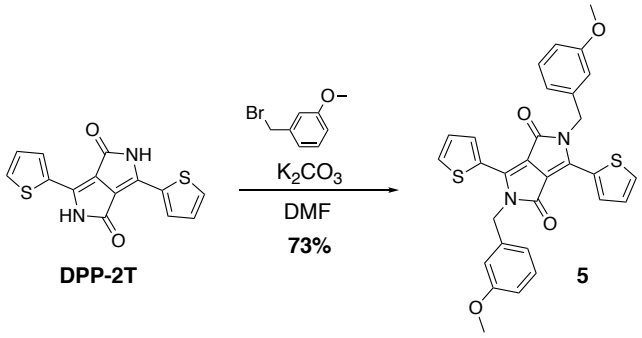

2,5-bis(3-methoxybenzyl)-3,6-di(thiophen-2-yl)-2,5-dihydropyrrolo[3,4-*c*]pyrrole-1,4-dione (5): To an oven-dried 2-neck roundbottom flask, 5 g (16.65 mmol) of 5- 3,6-di(thiophen-2-yl)-2,5-dihydropyrrolo[3,4-*c*]pyrrole-1,4-dione (**DPP-2T)** and 9.20 g (66.58 mmol) of potassium bicarbonate was added, sealed, and evacuated and refilled with argon 3 times. 7.36 g (36.62 mmol) of 1-(bromomethyl)-3-methoxybenzene was dissolved in 20 mL anhydrous, degassed DMF and transferred to the reaction flask. 150 mL anhydrous, degassed DMF was added to the flask, and the reaction was stirred at 80^{o} C overnight. The reaction was allowed to return to room temperature, quenched with 100 mL H_2O, then the solution was filtered to remove salts and the filtrate was concentrated by rotary evaporation. The compound was purified by column chromatography using dichloromethane as the eluent to afford 6.6 g (73%) of **5** as a dark red powder. ^{1}H NMR (500 MHz, $CDCl_3$): δ: 8.71 (dd, J = 3.9 Hz, 1.1 Hz, 2H), 7.57 (dd, J = 5 Hz, 1.1 Hz, 2H), 7.26 (t, J = 7.9 Hz, 2H), 7.20 (dd, J = 5 Hz, 3.9 Hz, 2H), 6.87 (m, 2H), 6.81 (m, 4H), 5.36 (s, 4H), 3.79 (s, 6H). ^{13}C NMR (500 MHz, $CDCl_3$): 161.35, 159.85, 140.28, 138.35, 134.76, 131.13, 129.68, 129.42, 128.26, 118.36, 112.23, 112.13, 107.49, 55.03, 45.13. HRMS (ESI MS) *m/z*: theor: 540.1177 found: 540.1189.

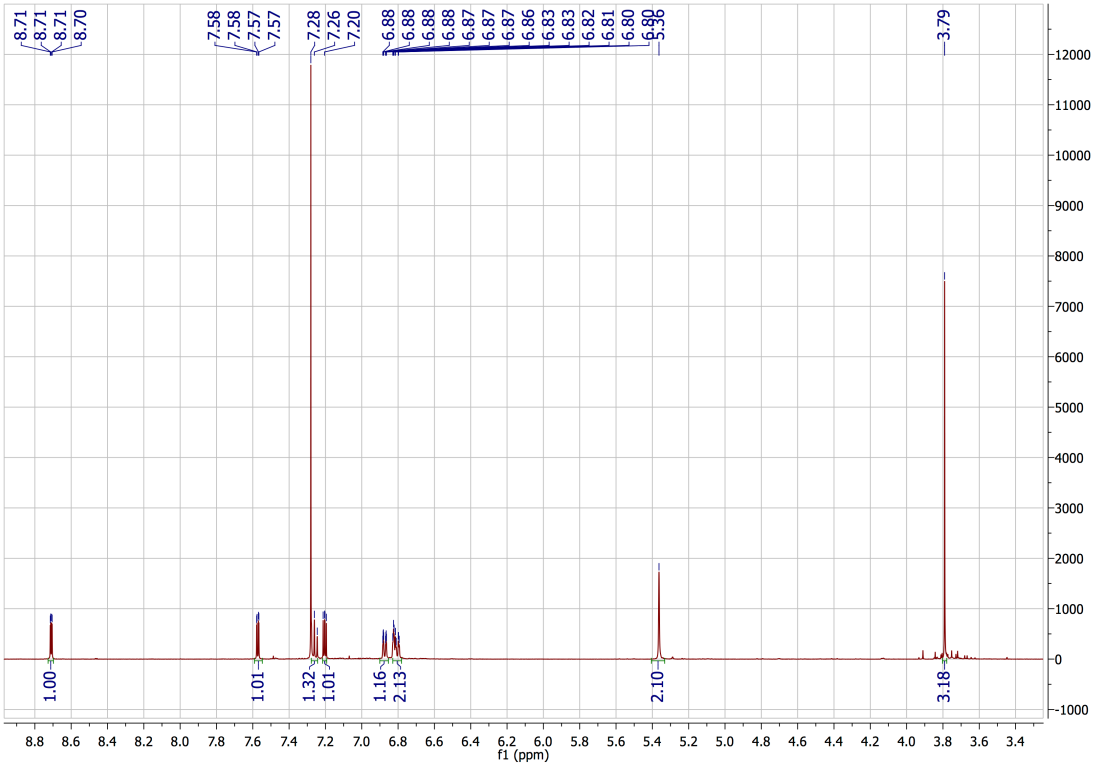
8.71
8.71
8.71
8.70
7.58
7.58
7.57
7.57
7.28
7.26
7.20
6.88
6.88
6.88
6.88
6.87
6.87
6.87
6.86
6.83
6.83
6.82
6.81
6.80
6.80
5.36
3.79
1.00
1.01
1.32
1.01
1.16
2.13
2.10
3.18
f1 (ppm)

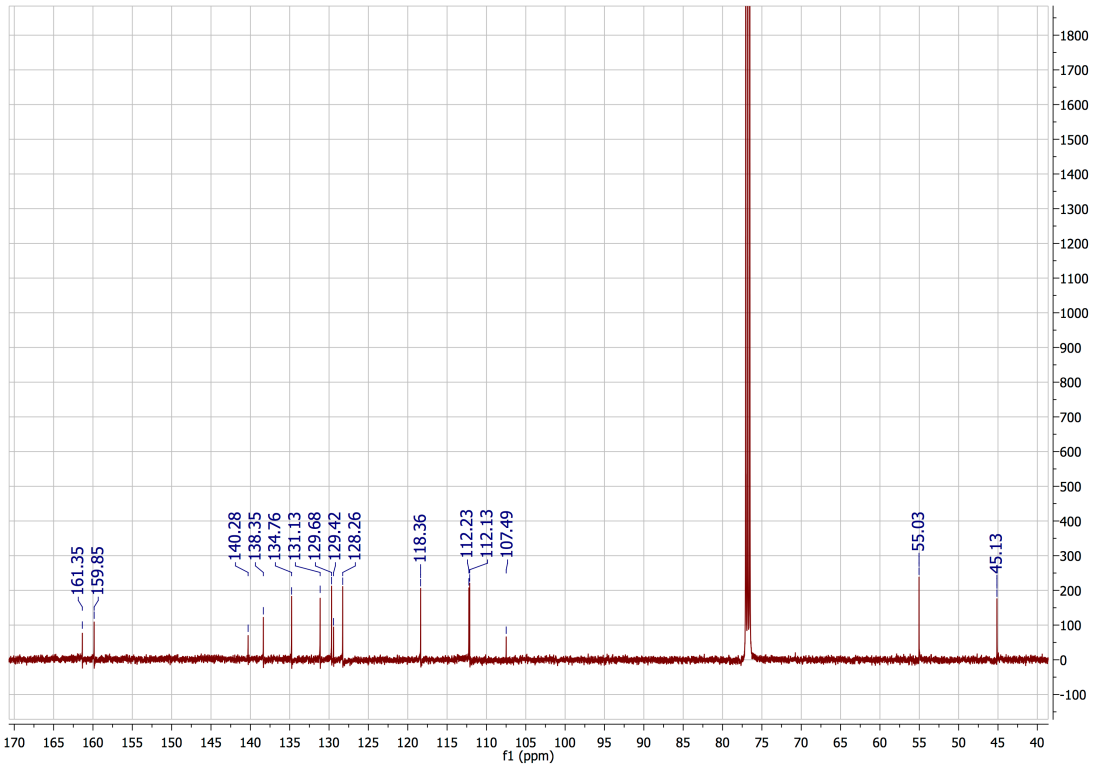
161.35
159.85
140.28
138.35
134.76
131.13
129.68
129.42
128.26
118.36
112.23
112.13
107.49
55.03
45.13
f1 (ppm)

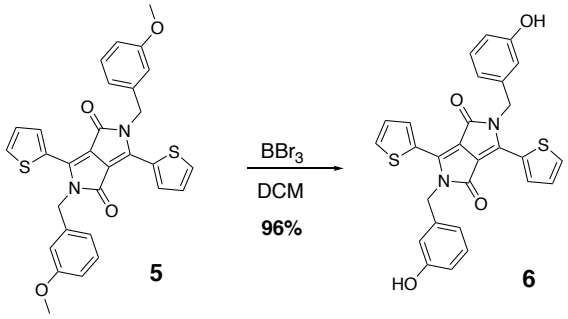

2,5-bis(3-hydroxybenzyl)-3,6-di(thiophen-2-yl)-2,5-dihydropyrrolo[3,4-*c*]pyrrole-1,4-dione (6): To an oven-dried roundbottom flask, 2.10 g (3.88 mmol) of **5** was added, sealed, and evacuated and refilled with argon 3 times. 150 mL of dry dichloromethane was added to the flask, and the solution was cooled to -78^{o} C. 11.1 mL (11.10 mmol) of a 1M solution of BBr_3 in dichloromethane was slowly added to the reaction, after which the reaction was warmed to room temperature and stirred overnight. The reaction was slowly quenched with 25 mL of H_2O, and the solution was filtered. The precipitate was washed over the filter paper with dichloromethane and water, affording 1.91 g (96%) of **6** as a red powder. ^{1}H NMR (300 MHz, DMSO-d6): δ: 9.42 (s, 2H), 8.67 (dd, J = 3.9 Hz, 1.2 Hz, 2H), 8.02 (dd, J = 5 Hz, 1.2 Hz, 2H), 7.34 (dd, J = 5 Hz, 3.9 Hz, 2H), 7.14 (t, J = 7.8 Hz 2H), 6.63 (m, 6H), 5.26 (s, 4H). ^{13}C NMR (500 MHz, DMSO-d6): δ: 160.86, 157.99, 140.06, 138.75, 134.72, 133.82, 130.13, 129.33, 128.84, 116.74, 114.44, 112.69, 106.71, 44.86. HRMS (ESI MS) *m/z*: theor: 512.0864 found: 512.0857.

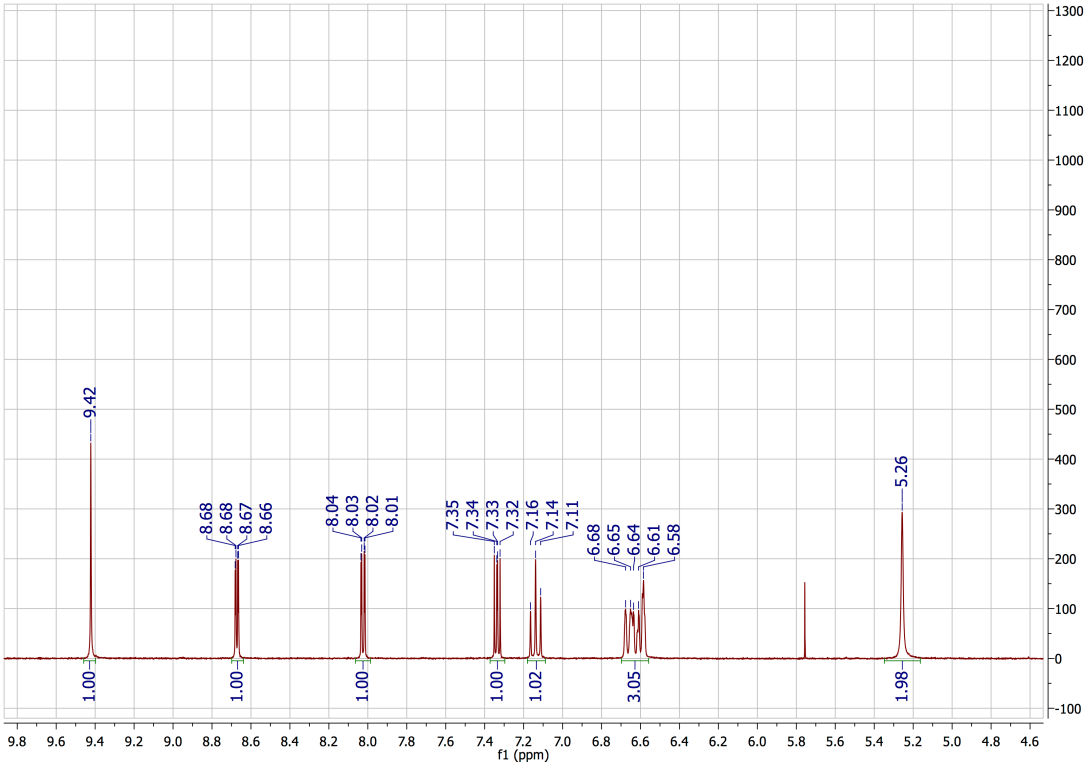
9.42
8.68
8.68
8.67
8.66
8.04
8.03
8.02
8.01
7.35
7.34
7.33
7.32
7.16
7.14
7.11
6.68
6.65
6.64
6.61
6.58
5.26
1.00
1.00
1.00
1.00
1.02
3.05
1.98
f1 (ppm)

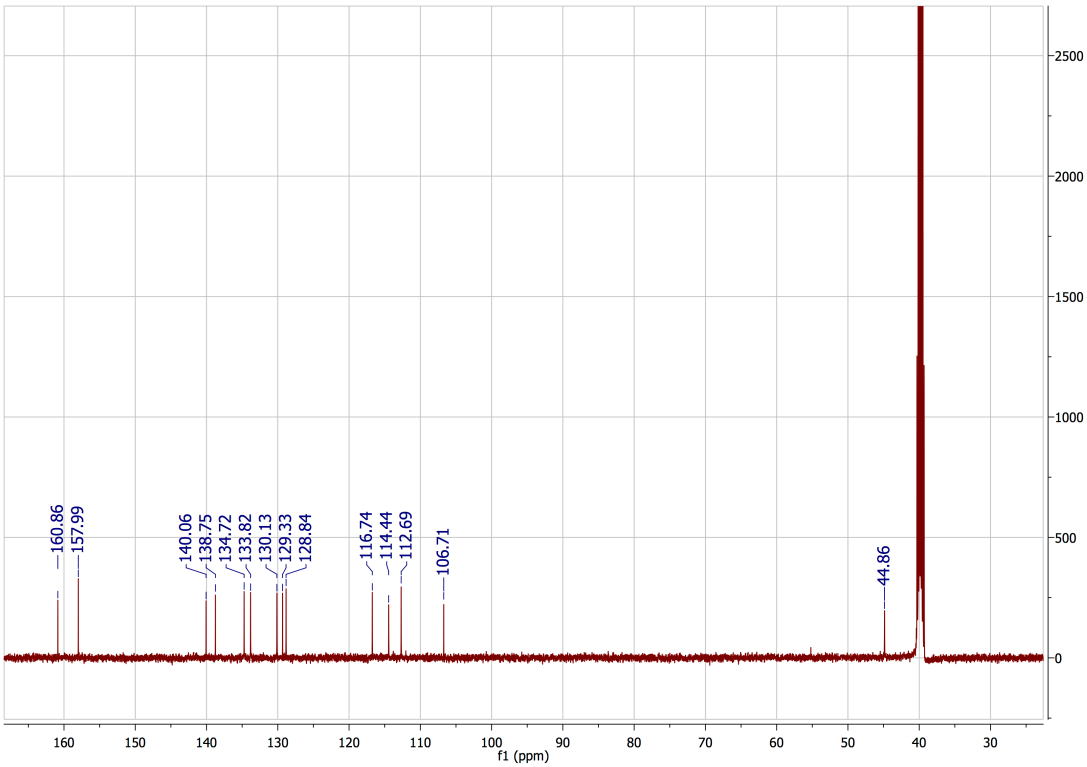
160.86
157.99
140.06
138.75
134.72
133.82
130.13
129.33
128.84
116.74
114.44
112.69
106.71
44.86
f1 (ppm)

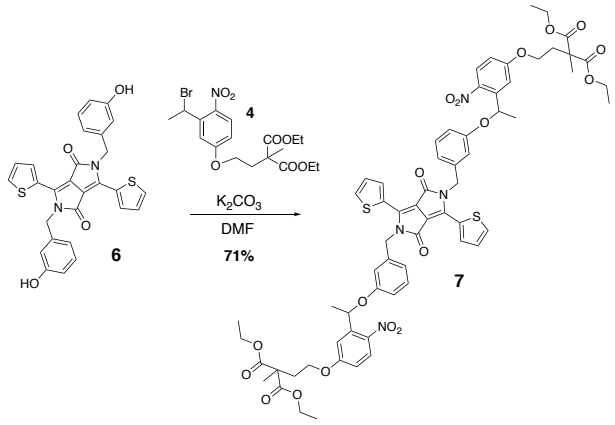

tetraethyl 2,2'-(((((((((1,4-dioxo-3,6-di(thiophen-2-yl)pyrrolo[3,4-*c*]pyrrole-2,5(1*H*,4*H*)-diyl)bis(methylene))bis(3,1-phenylene))bis(oxy))bis(ethane-1,1-diyl))bis(4-nitro-3,1-phenylene))bis(oxy))bis(ethane-2,1-diyl))bis(2-methylmalonate) (7): To an oven-dried 2-neck roundbottom flask, 1.08 g (2.11 mmol) of **6** and 1.02 g (7.37 mmol) of potassium bicarbonate was added, sealed, and evacuated and refilled with argon 3 times. 150 mL anhydrous, degassed DMF was added to the flask, followed by the addition of 2.07 g (4.64 mmol) of **4** dissolved in 20 mL anhydrous, degassed DMF. The reaction was stirred at 60^{o} C overnight. The reaction was allowed to return to room temperature, quenched with 100 mL H_2O, then the solution was filtered to remove salts and the filtrate was concentrated by rotary evaporation. The compound was purified by column chromatography using 1:99 EtOAc/Hexanes as the eluent to afford 1.85 g (71%) of **7** as a dark red solid. ^{1}H NMR (700 MHz, $CDCl_3$): δ: 8.61 (d, J = 3.7 Hz, 1H), 8.57 (d, J = 3.7 Hz, 1H), 7.98 (d, J = 9.1 Hz, 1H), 7.96 (d, J = 9.1 Hz, 1H), 7.55 (d, J = 5.1 Hz, 1H), 7.54 (d, J = 5.1 Hz, 1H), 7.19 (m, 4H), 7.04 (d, J = 2.5 Hz, 1H), 6.99 (d, J = 2.5 Hz, 1H), 6.87 (t, J = 8.1 Hz, 2H), 6.74 (d, J = 8.1 Hz, 1H), 6.72 (d, J = 8.1 Hz, 1H), 6.68 (dd, J = 9.1 Hz, 2.5 Hz, 1H), 6.63 (dd, J = 9.1 Hz, 2.5 Hz, 1H), 6.59 (s, 1H), 6.53 (s, 1H), 6.11 (q, J = 6.2 Hz, 1H), 6.09 (q, J = 6.2 Hz, 1H), 5.44 (d, J = 17.4 Hz, 1H), 5.35 (d, J = 17.4 Hz, 1H),

5.24 (d, J = 17.4 Hz, 1H), 5.15 (d, J = 17.4 Hz, 1H), 4.18 (m, 8H), 4.04 (m, 2H), 3.96 (m, 2H), 2.31 (q, J = 6.2 Hz, 4H), 1.62 (d, J = 6.2 Hz, 3H), 1.61 (d, J = 6.2 Hz, 3H), 1.46 (s, 6H), 1.22 (m, 12H). ^{13}C NMR (700 MHz, $CDCl_3$): 171.85, 171.73, 171.70, 163.03, 162.99, 161.26, 161.21, 157.68, 142.62, 142.55, 140.24, 140.04, 139.80, 139.70, 138.62, 138.43, 135.04, 134.98, 132.86, 131.38, 130.00, 129.37, 129.32, 128.34, 128.35, 127.97, 127.94, 118.90, 118.85, 114.70, 113.26, 113.04, 112.64, 112.60, 112.36, 112.28, 110.22, 107.40, 107.20, 71.58, 71.54, 64.83, 64.72, 61.51, 51.90, 51.79, 45.08, 45.00, 34.57, 23.41, 23.33, 20.53, 20.39, 14.00. HRMS (ESI MS) *m/z*: theor: 1242.3813 found: 1242.3826.

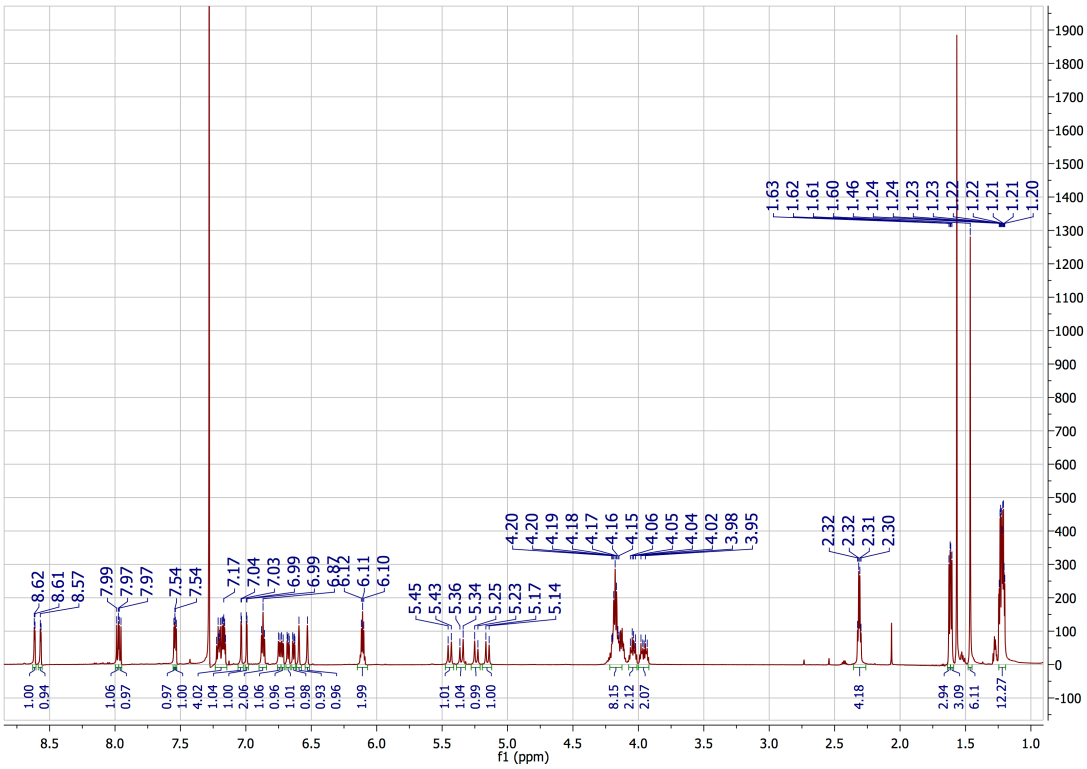
8.62
8.61
8.57
7.99
7.97
7.97
7.54
7.54
7.17
7.04
7.03
6.99
6.99
6.87
6.12
6.11
6.10
5.45
5.43
5.36
5.34
5.25
5.23
5.17
5.14
4.20
4.20
4.19
4.18
4.17
4.16
4.15
4.06
4.05
4.04
4.02
3.98
3.95
2.32
2.32
2.31
2.30
1.63
1.62
1.61
1.60
1.46
1.24
1.24
1.23
1.23
1.22
1.22
1.21
1.21
1.20
f1 (ppm)

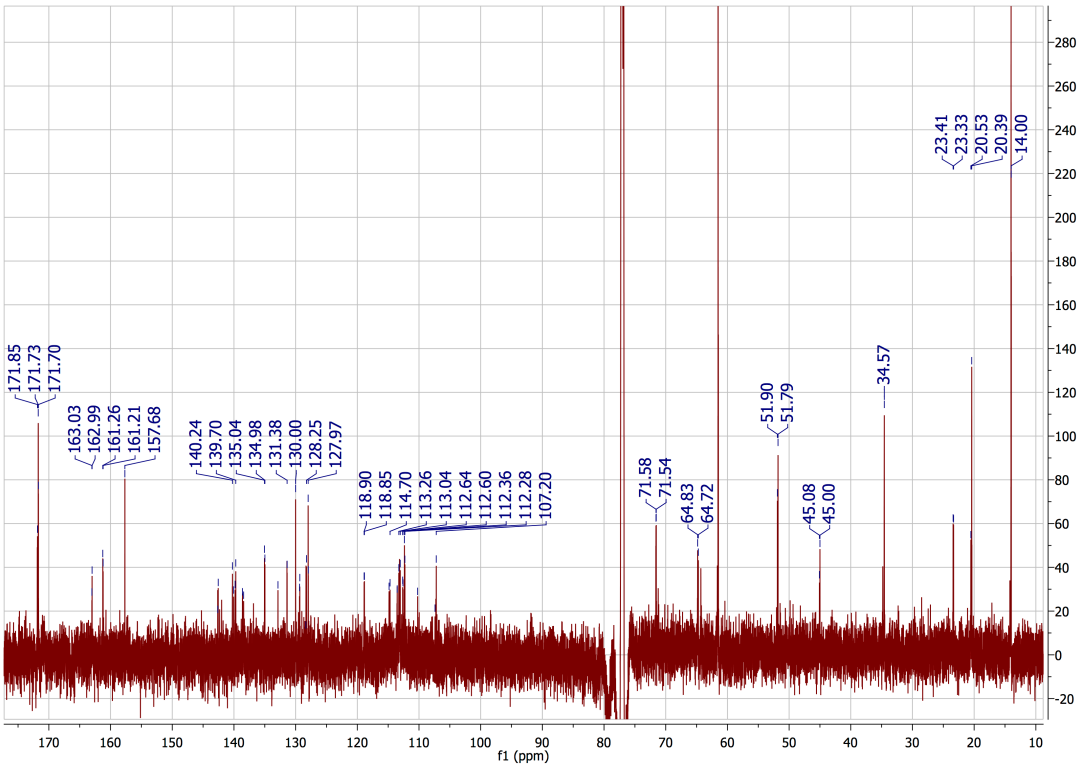
171.85
171.73
171.70
163.03
162.99
161.26
161.21
157.68
140.24
139.70
135.04
134.98
131.38
130.00
128.25
127.97
118.90
118.85
114.70
113.26
113.04
112.64
112.60
112.36
112.28
107.20
71.58
71.54
64.83
64.72
51.90
51.79
45.08
45.00
34.57
23.41
23.33
20.53
20.39
14.00
f1 (ppm)

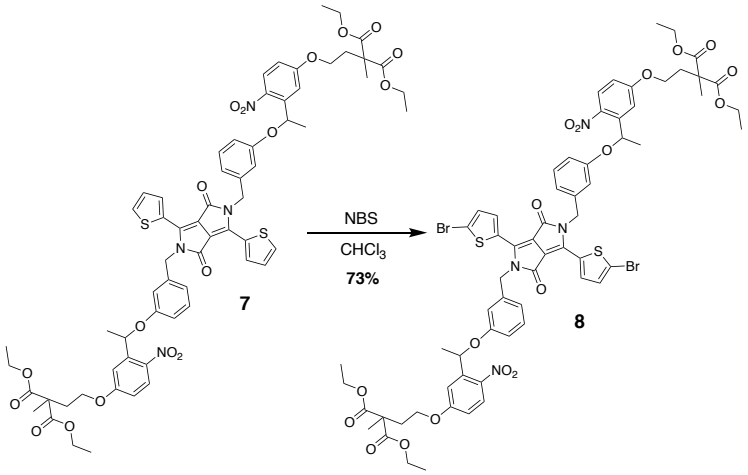

tetraethyl 2,2'-(((((((((3,6-bis(5-bromothiophen-2-yl)-1,4-dioxopyrrolo[3,4-*c*]pyrrole-2,5(1*H*,4*H*)-diyl)bis(methylene))bis(3,1-phenylene))bis(oxy))bis(ethane-1,1-diyl))bis(4-nitro-3,1-phenylene))bis(oxy))bis(ethane-2,1-diyl))bis(2-methylmalonate) (8): To an oven-dried roundbottom flask, 1.85 g (1.48 mmol) of **7** was added, sealed, and evacuated and refilled with argon 3 times. 100 mL $CHCl_3$ was added to the flask, and the solution was brought to 0^o C. 556 mg (3.12 mmol) of N-bromosuccinimide was added as a solid to the reaction, and the reaction was allowed to return to room temperature while stirring overnight. The solution was extracted three times each with H_2O and brine, and the organic layers were collected and concentrated. The compound was purified by column chromatography using 1:99 EtOAc/Hexanes as the eluent to afford 1.52 g (73%) of **8** as a dark red solid. ^{1}H NMR (700 MHz, $CDCl_3$): δ: 8.26 (d, J = 4.2 Hz, 1H), 8.19 (d, J = 4.2 Hz, 1H), 7.95 (d, J = 9.1 Hz, 1H), 7.92 (d, J = 9.1 Hz, 1H), 7.26 (t, J = 8 Hz, 1H), 7.23 (t, J = 8 Hz, 1H), 7.12 (d, J = 4.2 Hz, 1H), 7.10 (d, J = 4.2 Hz, 1H), 7.03 (d, J = 2.8 Hz, 1H), 6.96 (d, J = 2.8 Hz, 1H), 6.88 (d, J = 7.7 Hz, 1H), 6.86 (d, J = 7.7 Hz, 1H), 6.80 (dd, J = 8.2 Hz, 2.1 Hz, 1H), 6.76 (dd, J = 8.2 Hz, 2.1 Hz, 1H), 6.67 (dd, J = 9.1 Hz, 2.8 Hz, 1H), 6.62 (dd, J = 9.1 Hz, 2.8 Hz, 1H), 6.53 (s, 1H), 6.42 (s, 1H), 6.12 (q, J = 6.3 Hz,

1H), 6.10 (q, J = 6.3 Hz, 1H), 5.45 (d, J = 17.6 Hz, 1H), 5.31 (d, J = 17.6 Hz, 1H), 5.14 (d, J = 17.6 Hz, 1H), 5.00 (d, J = 17.6 Hz, 1H), 4.17 (m, 8H), 4.05 (m, 2H), 3.97 (m, 2H), 2.33 (q, J = 6.3 Hz, 4H), 1.62 (d, J = 6.3 Hz, 3H), 1.60 (d, J = 6.3 Hz, 3H), 1.47 (d, J = 2.5 Hz, 6H), 1.23 (m, 12H). ^{13}C NMR (700 MHz, $CDCl_3$): 171.73, 171.70, 171.69, 163.06, 163.03, 160.90, 160.81, 157.81, 157.78, 142.54, 142.44, 139.74, 139.58, 139.10, 138.09, 138.04, 134.88, 134.79, 131.43, 131.32, 130.23, 130.20, 128.00, 127.93, 119.77, 119.69,118.74, 118.67, 115.30, 115.04, 113.07, 112.93, 112.42, 112.33, 111.48, 107.41, 107.30, 71.48, 71.40, 64.82, 64.79, 61.51, 51.80, 51.79, 45.07, 44.93, 34.57, 34.56, 23.37, 23.31, 20.41, 20.40, 14.03. HRMS (ESI MS) *m/z*: theor: 1398.2023 found: 1398.2040.

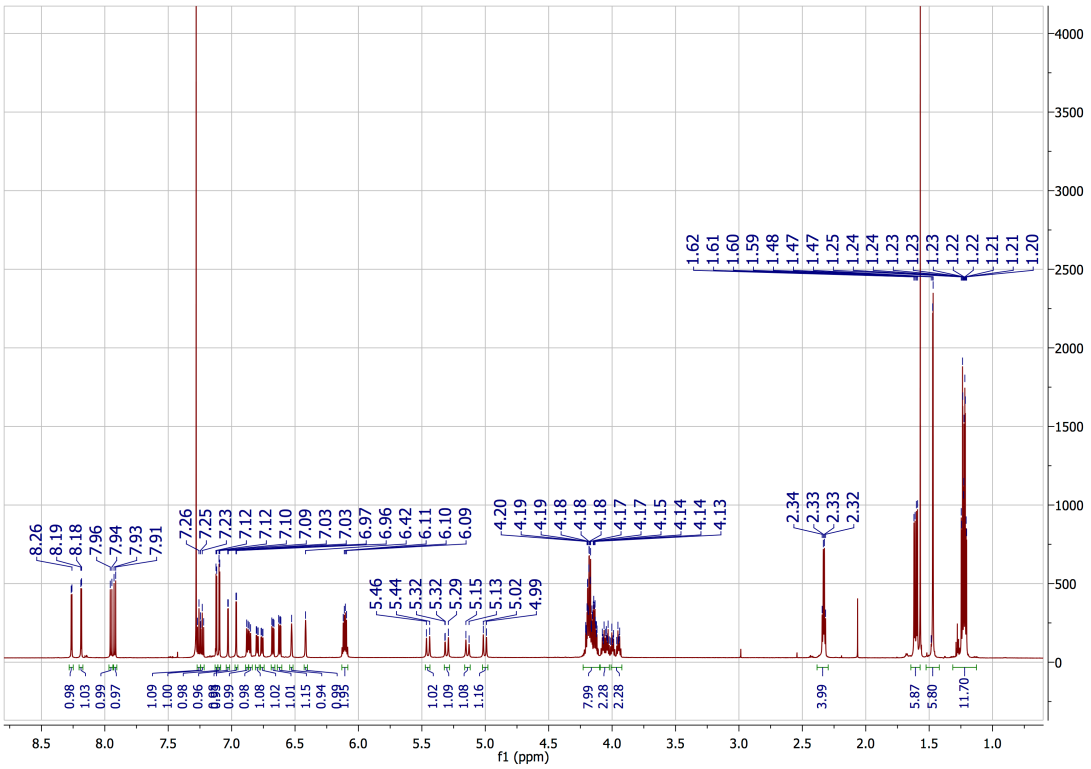
8.26
8.19
8.18
7.96
7.94
7.93
7.91
7.26
7.25
7.23
7.12
7.12
7.10
7.09
7.03
7.03
6.97
6.96
6.42
6.11
6.10
6.09
5.46
5.44
5.32
5.32
5.29
5.15
5.13
5.02
4.99
4.20
4.19
4.19
4.18
4.18
4.18
4.17
4.17
4.15
4.14
4.14
4.13
2.34
2.33
2.33
2.32
1.62
1.61
1.60
1.59
1.48
1.47
1.47
1.25
1.24
1.24
1.23
1.23
1.23
1.22
1.22
1.21
1.21
1.20
0.98
1.03
0.99
0.97
1.09
1.00
0.98
0.96
0.99
0.98
1.08
1.02
1.01
1.15
0.94
1.02
1.09
1.08
1.16
7.99
2.28
2.28
3.99
5.87
5.80
11.70
f1 (ppm)

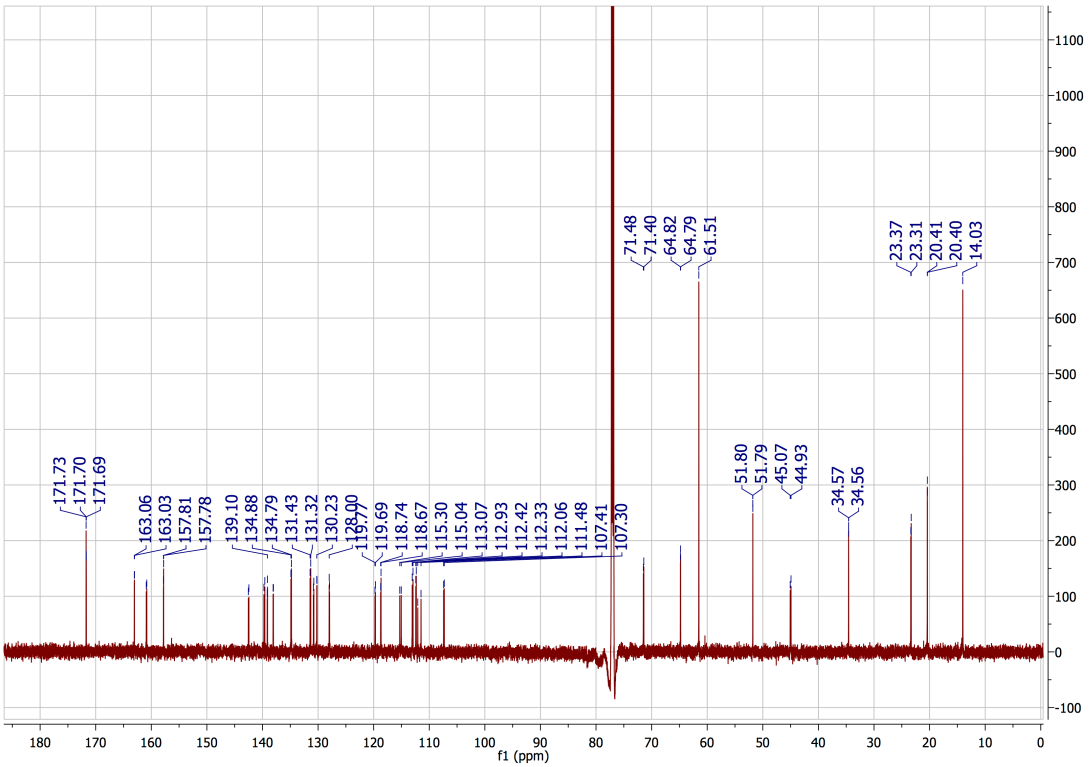
171.73
171.70
171.69
163.06
163.03
157.81
157.78
139.10
134.88
134.79
131.43
131.32
130.23
128.00
119.77
119.69
118.74
118.67
115.30
115.04
113.07
112.93
112.42
112.33
112.06
111.48
107.41
107.30
71.48
71.40
64.82
64.79
61.51
51.80
51.79
45.07
44.93
34.57
34.56
23.37
23.31
20.41
20.40
14.03
f1 (ppm)

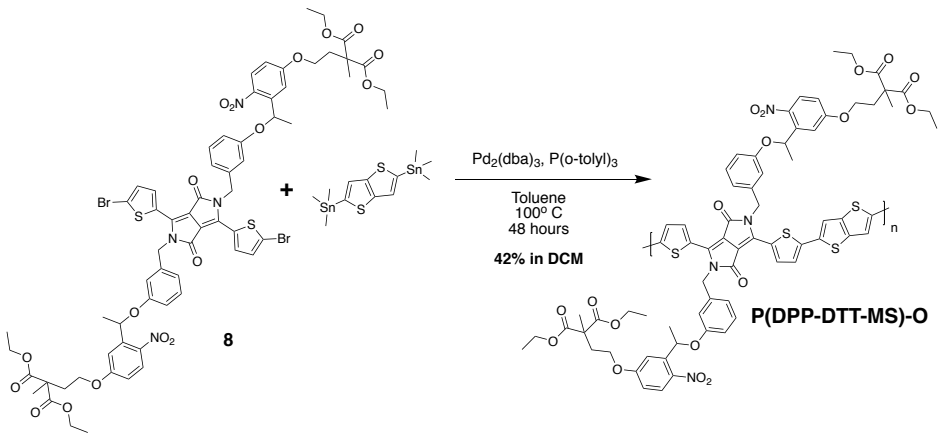

P(DPP-DTT-MS)-O: To an oven-dried 3-neck flask 1.50 g (1.06 mmol) of **8**, 500 mg (1.06mmol) of 2,5-bis(trimethylstannyl)thieno[3,2-*b*]thiophene, 34 mg of $Pd_2(dba)_3$ chloroform adduct, 40 mg of P(*o*-tolyl)$_3$, and 20 mL of dry toluene were added in an argon glovebox. The reaction was stirred at 100^{o}C for 48 hours, after which the reaction was cooled and precipitated into methanol. The precipitate was filtered and purified by successive Soxhlet extractions in methanol, acetone, hexanes, and dichloromethane. The dichloromethane fraction was taken and allowed to stir at 40°C with a spatula tip of a palladium scavenger (diethylammonium diethyldithiocarbamate) for 1 hour, after which it was concentrated to <10 mL and precipitated into methanol. The precipitate was filtered and dried over high vacuum to afford 627 mg (42%) of **P(DPP-DTT-MS)-O** as a dark purple powder. Mn: 62 kDa, Mw: 326 kDa, *Đ:* 5.2 (GPC in $CHCl_3$ vs. Polystyrene). Anal. calcd. for $C_{37}H_{35}NO_8S_3$: C (60.95) H (4.82) N (4.06) S (9.30), Found: C (60.06) H (5.12) N (3.87) S (9.03).

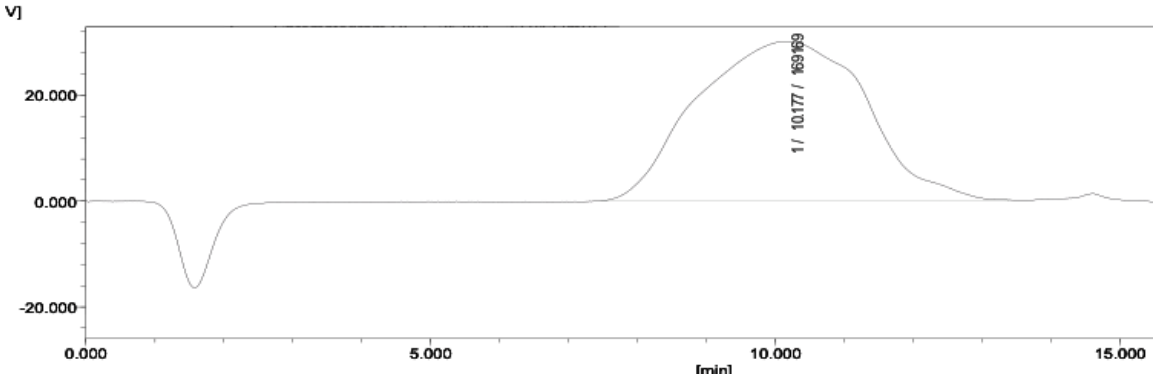

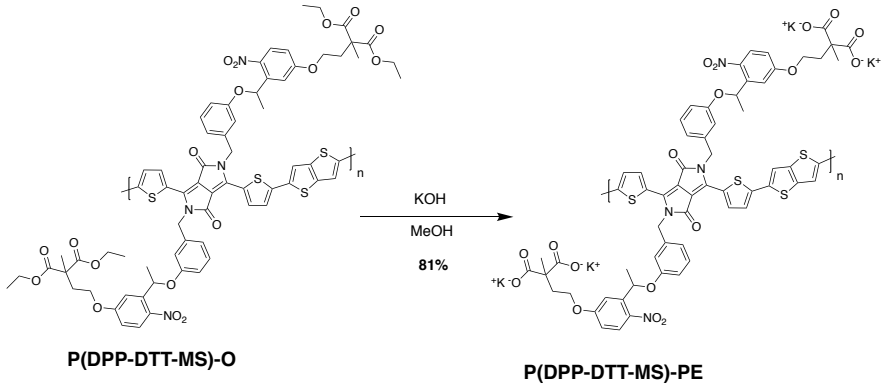

P(DPP-DTT-MS)-O **P(DPP-DTT-MS)-PE**

P(DPP-DTT-MS)-PE: In an oven-dried roundbottom flask 150 mg of **P(DPP-DTT-MS)-O** and 100 mL of a 1M KOH in methanol solution were added. The reaction was stirred at 70^{o}C overnight, filtered and washed with methanol and chloroform, and dried to afford 122 mg of **P(DPP-DTT-MS)-PE** as a dark purple powder.

4.8 Grazing Incidence Wide Angle X-Ray Scattering Methods and 1D Line Cuts

Grazing incidence wide angle X-ray scattering (GIWAXS) was performed at the Stanford synchrotron radiation light source (SSRL) on beamline 11-3. The beam energy was 12.7 keV. The angle of incidence was 0.13°, whereas the nominal critical angle for the films at the used energy is about 0.08°. A LaB6 standard sample was used to calibrate

the instrument and the software WxDiff2 version 1.20 was used for data reduction. The sample to detector distance was set to 250 mm.

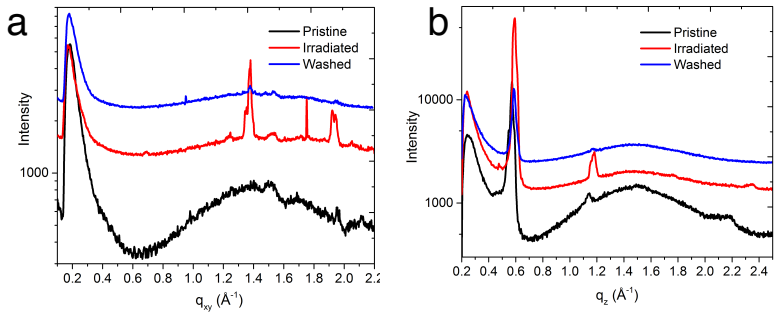

Figure 4-25. Offset 1D line cuts in the q_{xy} (a) and q_z (b) direction of **P(T3-MS)-PE** pristine, irradiated, and irradiated and washed.

4.9 X-Ray Photoelectron Spectroscopy Methods and Analysis

X-ray photoelectron spectroscopy experiments were performed on dried polymer films using a Thermo K-Alpha spectrometer equipped with a monochromated Aluminum K-α x-ray source (1486 eV) and a hemispherical 180˚ detector. The X-ray spot size used for all samples was 400 µm with a charge compensating flood gun to eliminate sample charging. Survey scans were performed with 1 eV binding energy resolution and 200 eV pass energy Elemental scans with 0.1 eV resolution were performed for N1s (392-410 eV), K2p (287-305 eV), and S2p (157-175 eV) electron binding energies. Depth profiling experiments were performed to analyze chemical makeup of the polymer films throughout their thickness. An argon ion gun was used to etch the polymer film using an energy of 1000 eV at medium current for 40 seconds. The raster size used was 1 mm. After each etching step, survey scans and high-resolution elemental scans were performed as above. Depth profiles were performed through the thickness of the film

determined by a large growth of O1s and Si 2p intensity (Figure 4-26). XPS spectra were analyzed and fitted using CasaXPS software in order to determine N:S and K:S atomic percent ratios shown in Figures 4-8d and 4-8e. Integrated areas were calculated according to the following equation:

$$at\% = \frac{A_{rel}}{KE^{0.6}(RSF)}$$

Where A_{rel} is the integrated area for each XPS peak, KE is the kinetic energy, and RSF is the relative sensitivity factor for the element (S:1.68, N:18, and K: 3.97). Example fits for the S2p, N1s, and K2p peaks measured on the surface of the **P(T3-MS)-PE** films are shown in Figure 4-27. Raw data for N1s and K2p peaks at the surface and at a depth of 15 nm for **P(T3-MS)-PE** as cast, irradiated, and irradiated and washed films are shown in Figure 4-28.

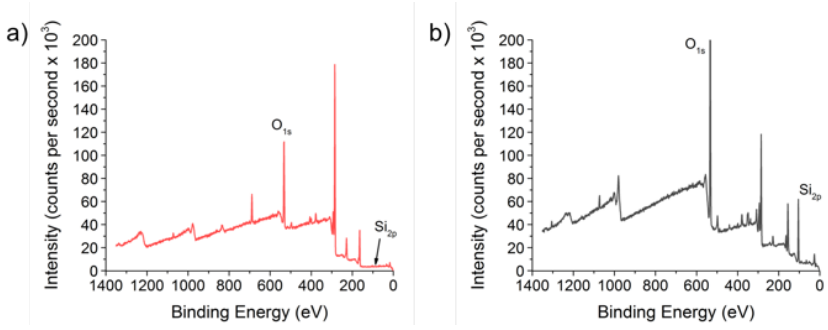

Figure 4-26. XPS survey spectra for **P(T3-MS)-PE** at the surface (a), and through the thickness of the film (b).

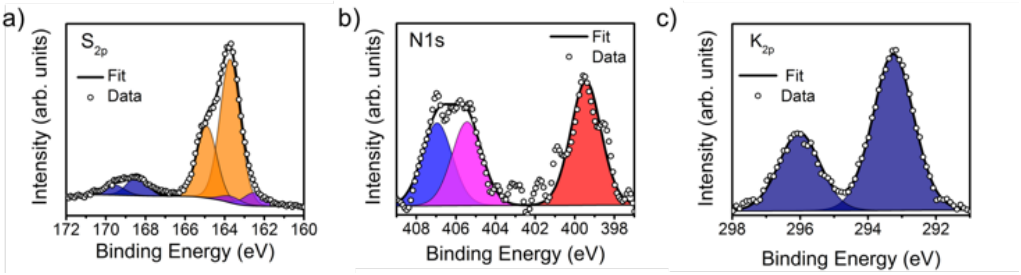

Figure 4-27. Representative peak decomposition for spectra taken at the **P(T3-MS)-PE** surface in the S2p region (a), N1s region (b), and the K2p region (c).

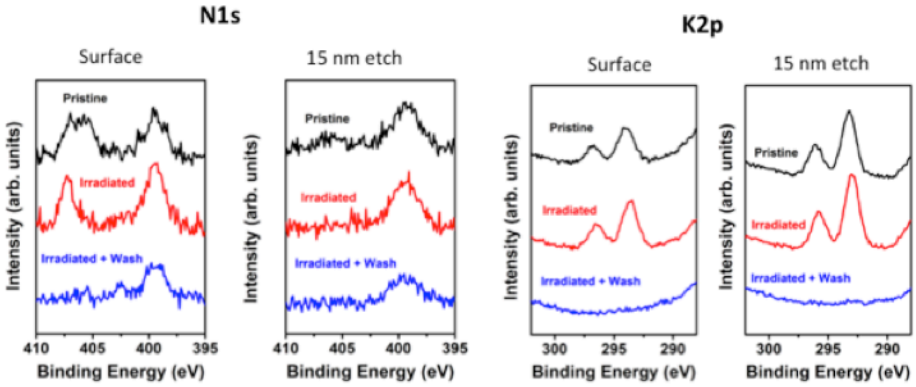

Figure 4-28. N1s and K2p XPS spectra for pristine (black), irradiated (orange), and irradiated and water/IPA washed (blue) films of **P(T3-MS)-PE** at the surface and bottom surface.

CHAPTER 5

PROBING THE IMPACT OF MINIMALLY SUBSTITUTED ACCEPTOR MOIETIES IN DONOR-ACCEPTOR POLYMERS FOR ORGANIC PHOTOVOLTAIC ACTIVE LAYER BLENDS

5.1 Background and Motivation

Organic photovoltaics (OPVs) are an actively studied class of renewable energy devices due to their ability to provide high power conversion efficiencies (PCE > 10%) from solution-processed materials, potentially enabling low-cost processing of large area solar cells. The light-absorbing active layers in these devices typically make use of a bulk-heterojunction (BHJ) thin film of a conjugated electron-donor material and a conjugated electron-acceptor material, where the interface between these two materials plays a crucial role in the separation of photogenerated excitons to free charges.[211-212] In this chapter, a novel family of conjugated donor-acceptor (D-A) copolymers designed with minimally substituted acceptor units are investigated for their ability to enhance this interface with electron-accepting molecular acceptors (MAs). These polymers make use of common acceptor moieties thieno[3,4-c]pyrrole-4,6- dione (TPD), diketopyrrolopyrrole (DPP), and isoindigo (iI) with methyl side chains to provide sterically unhindered sites for enhanced interactions with a MA, either $PC_{71}BM$ or ITIC in this study. The chapter will begin with a brief overview of D-A polymer design, mainly focusing on structural methods employed to enhance interactions between a D-A polymer and a MA. Based on these design principles, the rationale behind the use of

methyl side chain polymers will be presented, and the synthesis, optoelectronic characterization, and OPV device metrics in BHJ blends will be reported and discussed.

5.1.1 Donor-Acceptor Polymer and Molecular Acceptor Interactions

Briefly taught in Chapter 1.2.1.4, a common design motif for electron-donor materials is a conjugated polymer with a donor-acceptor (D-A) architecture, in which the repeat unit consists of an electron-donating portion (donor) and an electron-withdrawing portion (acceptor). The D-A approach serves to lower the energetic gap (E_g) in conjugated polymers and push absorption out to the photon-rich near-IR region.[47] The built-in dipole created from the donor to the acceptor aids in the delocalization of electron density in the backbone, which has made these systems popular for BHJ OPV active layers in which the polymer is excited by ambient light and the resulting electron can be shuttled from the donor moiety to the acceptor moiety, and finally transferred to the LUMO of a molecular acceptor (MA), such as $PC_{71}BM$, in the blend.

Because the LUMO levels of D-A polymers are localized around the acceptor portion of the repeat unit, several researchers in the field have hypothesized that increasing the probability for a MA to "dock" adjacent to the acceptor portion of the D-A polymer in the solid-state will lead to more efficient charge transfer from the polymer LUMO to the MA LUMO, leading to higher device efficiencies.[53, 213-214] This concept is illustrated in the schematic presented in Figure 5-1, where electrons are shuttled towards the acceptor moiety on the D-A polymer and can be efficiently transferred to the MA when they are close in proximity.

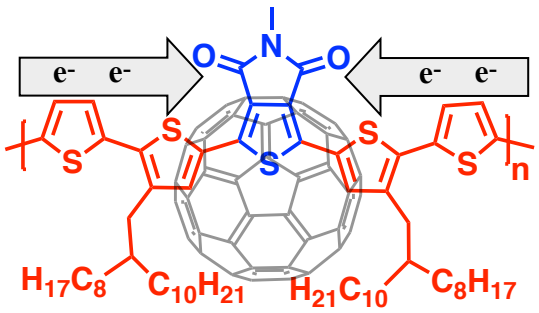

Figure 5-1. Schematic of a donor (red) – acceptor (blue) conjugated polymer and the potential impact of side chain sterics on the ability to control the interface with a molecular acceptor (MA), using the polymer from this study **P(T4-TPD-M)** and a C_{60} MA as an example. Through the design of bulky side chains on the donor and a small methyl chain on the acceptor, the probability of C_{60} "docking" closer to the acceptor moiety can be increased.

After observing that many high performing D-A polymers had sterically bulky alkyl substituents on the donor moiety and less bulky or an absence of alkyl substituents on the acceptor moiety, Graham *et al.* put forward the idea that preferential MA "docking" to the D-A polymer acceptor moiety could lead to enhanced photovoltaic performance.[53] Alongside their literature observations, the authors synthesized a family of benzo[1,2-b:4,5-b′]dithiophene−thieno[3,4-c]pyrrole-4,6- dione polymers (BDT-TPD) polymers with varied positioning of linear and branched alkyl side chains on the donor and acceptor moieties. Their work found that the BDT-TPD derivative with branched alkyl side chains of the donor moiety (BDT) and linear alkyl side chains on the acceptor moiety (TPD) resulted in the highest device efficiency when blended with $PC_{71}BM$, as summarized in Figure 5-2. Through a combination of device metrics, probing of intermolecular interactions through solid-state nuclear magnetic resonance (NMR) spectroscopy, and analysis of energetic disorder *via* charge transfer (CT) absorbance experiments, the authors attributed the enhanced device efficiencies to a higher probability of $PC_{71}BM$ molecules arranging in close proximity of the acceptor

portion of the D-A polymer in the solid-state. These results fit alongside their observational hypothesis that high OPV performance D-A polymers consist of sterically hindered donor moieties and sterically unhindered acceptor moieties. Several follow-up studies have investigated the effect of side chain steric hindrance in these BDT-TPD systems[213, 215-217] as well as in alternative D-A polymer systems.[214, 218]

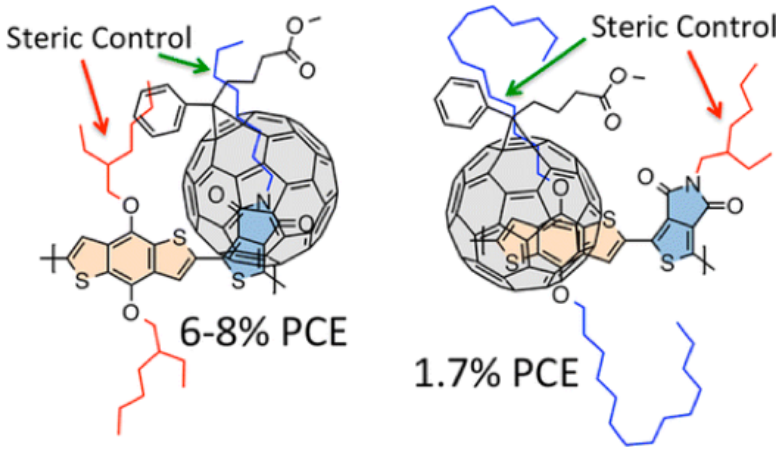

Figure 5-2. BDT-TPD polymers with varying degrees of steric bulk on the donor moiety side chain and the acceptor moiety side chain. Illustrates the effect of bulky branched side chains on the donor portion and linear side chains on the acceptor unit leading to high performance OPV blends with $PC_{71}BM$, and the opposite configuration leading to low performance. Image reproduced from reference [53].

5.1.2 Minimally Substituted Acceptor Design

Looking at current OPV D-A polymers through the lens of the steric control hypothesis put forward by Graham *et al.,* we had noted that PffBT4T-2OD (PCE-11, shown in Figure 5-3), a polymer that achieves PCE > 10% in $PC_{71}BM$ BHJ devices, fits the structural mold of minimal steric bulk on the acceptor moiety alongside a donor with bulky substituents.[125] We sought to modify this structure by replacing the 5,6-difluoro-2,1,3-benzothiadiazole acceptor unit with other minimally substituted acceptors that could ultimately be synthesized with bulkier side chains to isolate the effects of sterics on

D-A polymer / MA interactions. Thieno[3,4-c]pyrollo-4,6-dione (TPD)[219-227], diketopyrrolopyrrole (DPP)[101, 228-233], and isoindigo (iI)[51, 234-237] were chosen as acceptors due to their prevalence in D-A polymers within the OPV field. While these acceptor units are commonly functionalized with long aliphatic side chains, their methyl side chain derivatives have not been widely explored in conjugated polymer systems.[238-239] By leveraging solubility from the branched side chains on the donor moiety, methyl side chains can be incorporated into TPD, DPP, and iI copolymers without sacrificing solubility at high molecular weights. Shown in Figure 5-3 alongside PCE-11, this family of D-A polymers contains acceptor moieties with methyl side chains and a quaterthiophene donor with branched side chains directed away from the acceptor.

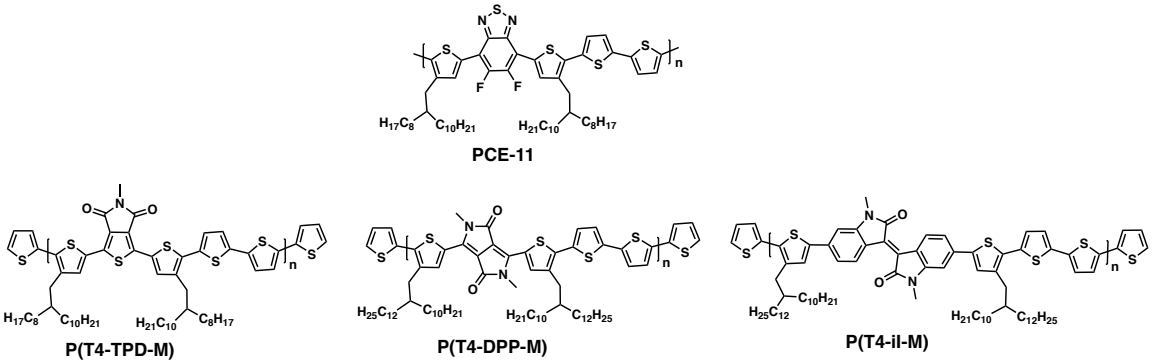

Figure 5-3. Repeat unit structures of minimally substituted acceptor D-A polymers compared to PCE-11.

As an initial study, these three D-A polymers have been synthesized and their optical, electrochemical, and SCLC hole mobility properties have been characterized. The photovoltaic capabilities of these polymers were investigated through their incorporation into BHJ OPV devices, exhibiting PCE > 5% with $PC_{71}BM$ as the MA and PCE > 2% with the non-fullerene MA ITIC. While **P(T4-DPP-M)** and **P(T4-iI-M)** provided similar photovoltaic properties with $PC_{71}BM$ (~5%) and ITIC (~2%), it was

found that the TPD derivative **P(T4-TPD-M)** yielded the highest PCE values with both $PC_{71}BM$ (7.5%) and ITIC (4.0%). These results show that methyl side chain derivatives of TPD, DPP, and iI can be useful acceptor moieties in D-A polymer systems, and the impact of sterics on the acceptor moiety can be elucidated in future studies through modification of the methyl side chain to bulkier aliphatic substituents.

5.2 Synthesis of Minimally Substituted Donor-Acceptor Polymers

The three minimally substituted D-A copolymers in this study, **P(T4-TPD-M)**, **P(T4-DPP-M)**, and **P(T4-iI-M)**, were synthesized *via* Migita-Kosugi-Stille polymerization from a distannyl bithiophene and the corresponding dibromo bithienyl acceptor moiety as outlined in Figure 5-4a. Monomer synthesis and polymerization methods are detailed in section Chapter 5.6. All three polymers were obtained in high molecular weight, as shown in Table 5-1, and were soluble in chlorobenzene and *o*-dichlorobenzene. While **P(T4-TPD-M)** was soluble at high molecular weight using 2-octyldodecyl side chains, both **P(T4-DPP-M)** and **P(T4-iI-M)** required 2-decyltetradecyl side chains to yield high molecular weight polymers that could still be solubilized and processed. A 2-decyltetradecyl analogue of **P(T4-TPD-M)** was synthesized to standardize the side chains used in the study, but the resulting polymer could not form a BHJ with either $PC_{71}BM$ or ITIC due to a high degree of phase separation in blend films, and therefore the 2-octyldodecyl derivative was used for comparison in this work.

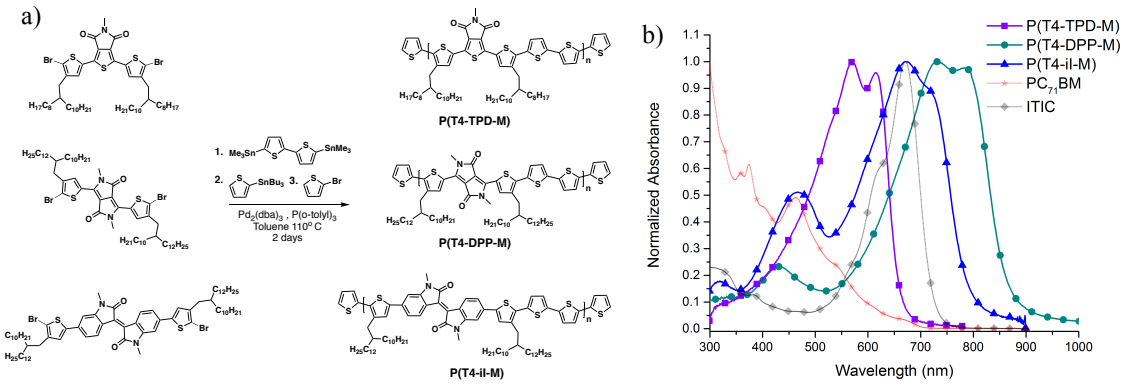

Figure 5-4. **P(T4-TPD-M)**, **P(T4-DPP-M)**, and **P(T4-iI-M)** polymerization conditions (a) and thin film UV-vis absorption spectra in comparison to $PC_{71}BM$ and ITIC solution spectra (b).

Polymer	Mn [a] (kDa)	Đ [a]	E_g [b] (eV)
P(T4-TPD-M)	59	1.8	1.84
P(T4-DPP-M)	63	2.1	1.40
P(T4-iI-M)	54	2.8	1.55

Table 5-1. Molecular weight and optical energy gap data for **P(T4-TPD-M)**, **P(T4-DPP-M)**, and **P(T4-iI-M)**. [a] Calculated from 1,2,4-trichlorobenzene GPC at 140° C vs. polystyrene standards. [b] Measured from onset of optical absorption.

5.3 Characterization of Minimally Substituted Donor-Acceptor Polymers

5.3.1 Absorption Properties

The UV-vis absorption spectra for thin films of these polymers are shown in Figure 5-4b alongside the solution absorption spectra of $PC_{71}BM$ and ITIC. Measurements were taken following procedures in Chapter 2.2.2. The variation in acceptor moiety leads to significant changes in the absorption spectra, with the low energy absorption peak red shifting ~100 nm from **P(T4-TPD-M)** to **P(T4-iI-M)**, and

another ~100 nm from **P(T4-iI-M)** to **P(T4-DPP-M)**, with energy gap (E_g) likely decreasing with a combination of increasing acceptor strength and increasing planarization between the donor and acceptor units. All three polymers absorb at higher wavelengths and have a low degree of spectral overlap with $PC_{71}BM$, which is favorable for broad absorption across the solar spectrum. With ITIC, the three polymers have a varying degree of spectral overlap, with **P(T4-TPD-M)** absorbing primarily at lower wavelengths, **P(T4-iI-M)** directly overlapping, and **P(T4-DPP-M)** absorbing at higher wavelengths. With **P(T4-TPD-M)** performing as the optimal D-A polymer for both $PC_{71}BM$ and ITIC in this study, the ability to absorb to the near-IR region of the visible spectrum may not be necessary for yielding high PCE devices. Instead, the higher performance may be attributed to more efficient light-harvesting of higher energy photons compared to **P(T4-DPP-M)** and **P(T4-iI-M)**.

5.3.2 Electrochemical Properties

Electrochemical cyclic voltammetry (CV) and differential pulse voltammetry (DPV) measurements are shown in Figure 5-5, and were used to calculate the HOMO energy levels of the three polymers shown in Figure 5-5d according to the formula $E_{HOMO} = - (E_{onset,ox\ vs\ Fc/Fc+} + 5.1)$.[137] Measurements were carried out according to procedures in Chapter 2.2.3. The deepest HOMO level of -5.63 eV is obtained by **P(T4-TPD-M)**, followed by -5.48 eV for **P(T4-iI-M)**, and -5.37 eV for **P(T4-DPP-M)**. Using E_g to calculate the LUMO from these HOMO values leads to values of -3.79 eV, -3.93 eV, and -3.97 eV for **P(T4-TPD-M)**, **P(T4-iI-M)**, and **P(T4-DPP-M)**, respectively. Compared to the LUMO levels of $PC_{71}BM$[240] and ITIC[241], -4.2 eV and -4.1 eV respectively, **P(T4-TPD-M)** has the most favorable LUMO energy offset to efficiently transfer excited

electrons, while **P(T4-DPP-M)** and **P(T4-iI-M)** have LUMO levels that have a smaller offset with ITIC (~0.1 – 0.2 eV) and with $PC_{71}BM$ (~0.2 – 0.3 eV). Additionally, the deeper HOMO level observed for **P(T4-TPD-M)** provides the largest offset between the D-A polymer HOMO and the MA LUMO, which directly impacts the open circuit voltage (V_{OC}) of OPV devices.[242] The combination of a higher LUMO and deeper HOMO make **P(T4-TPD-M)** the most compatible for BHJ OPV layers with both $PC_{71}BM$ and ITIC compared to the other two polymers, which is likely why it outperforms them in OPV devices.

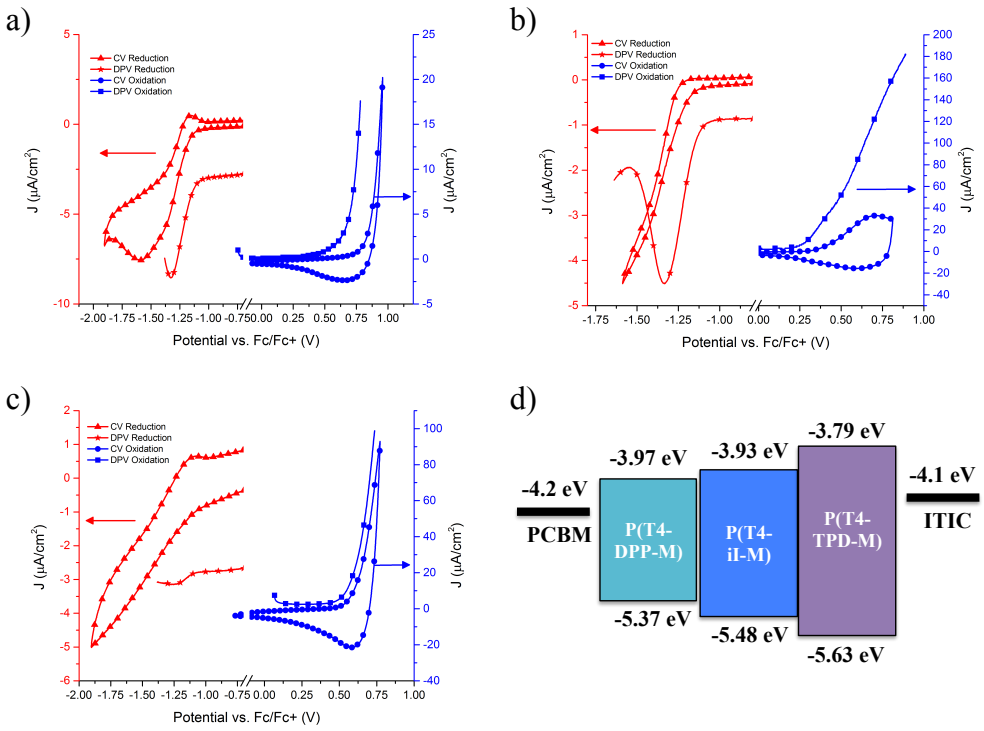

Figure 5-5. **P(T4-TPD-M)**, **P(T4-DPP-M)**, and **P(T4-iI-M)** Cyclic Voltammetry (CV) and Differential Pulse Voltammetry (DPV) scans for **P(T4-TPD-M)** (a), **P(T4-DPP-M)** (b), and **P(T4-iI-M)** (c), and an energy level diagram comparing these polymers to $PC_{71}BM$ and ITIC (d). HOMO values calculated from onset of oxidation in DPV measurements. LUMO values calculated as HOMO + E_g.

5.3.3 Space Charge Limited Current Hole Transport

Space-charge limited current (SCLC) experiments were performed on hole-only devices with the architecture ITO/MoO_3/Polymer/MoO_3/Ag to assess the bulk hole mobility of the three polymers as neat materials. SCLC methodology is presented in Chapter 2.4.6, and J-V curves for the hole-only devices are shown in Figure 5-6.

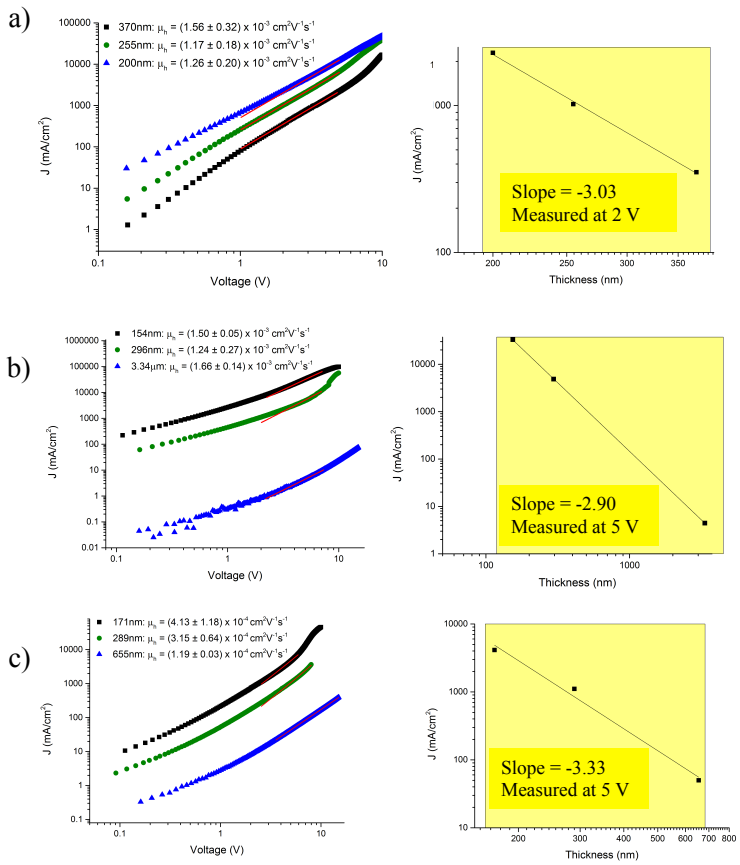

Figure 5-6. J-V curves and fits in SCLC regime for hole-only devices of **P(T4-TPD-M)** (a), **P(T4-DPP-M)** (b), and **P(T4-iI-M)** (c) at three different thicknesses. Plots on the right confirm the thickness dependence of SCLC measurements in which $J \sim 1/L^3$, meaning a slope of -3 should ideally be obtained when plotting J/L at a constant voltage between devices of multiple thicknesses.

For all three polymers, SCLC measurements were performed on three different thicknesses each in order to assess the validity of the results. Thickness dependence

experiments should always be performed for SCLC mobility measurements to assure the relationship $J \sim 1/L^3$, where L is the active layer thickness, at a fixed voltage in the SCLC regime. The slope of ~ -3 in the L vs. J plot for all three polymers affirms the mobility results accurately fit the model mobility equation presented in Chapter 2.4.2. Both **P(T4-TPD-M)** and **P(T4-DPP-M)** exhibited comparable mobility values on the order of 10^{-3} $cm^2V^{-1}s^{-1}$, while **P(T4-iI-M)** obtained mobility values an order of magnitude lower at 10^{-4} $cm^2V^{-1}s^{-1}$. The lower mobility for the isoindigo derivative can potentially indicate weaker π–π interactions between polymer backbones in the solid-state.

5.4 Organic Photovoltaic Devices

In order to investigate the photovoltaic properties of the three polymers, inverted OPV devices with the architecture ITO/ZnO/Active Layer/MoO_3/Ag. Inverted device architectures were utilized due to their enhanced stability in ambient atmosphere compared to conventional architecture devices. Conventional architectures typically make use of the PEDOT:PSS, which is hygroscopic, and calcium, which has a low work function, both of which cause degradation in ambient environments.[243] By avoiding these interlayers, inverted OPV devices achieve prolonged lifetimes and ambient stability. OPV device fabrication methods are described in Chapter 2.4.1. Active layers were blade coated from either 1:1.2 Polymer:$PC_{71}BM$ with 3% of the additive 1,8-diiodooctane (DIO) or 1:1 Polymer:ITIC with 3% of the additive 1-chloronaphthalene (CN). All blends were tested with varying amounts of DIO or CN, and varying thicknesses controlled by coating temperature, and the presented conditions were found to provide optimal PCE. Optimized BHJ active layer coating methods are described in Chapter 5.7.

Device metrics are summarized in Table 5-2 with corresponding J-V curves shown in Figure 5-7. **P(T4-TPD-M)** devices obtained the highest efficiencies with both $PC_{71}BM$ (7.5%) and ITIC (4.0%), while **P(T4-DPP-M)** and **P(T4-iI-M)** performed similarly with both $PC_{71}BM$ (5.4% and 5.3% respectively) and ITIC (2.2% and 2.4% respectively). Averages and standard deviations were calculated from 8 devices each.

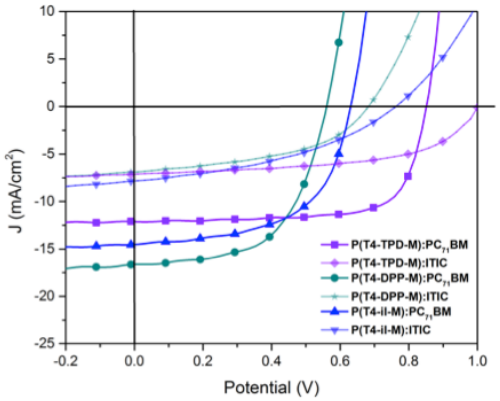

Figure 5-7. J-V curves for **P(T4-TPD-M)**, **P(T4-DPP-M)**, and **P(T4-iI-M)** based OPV BHJ devices with both $PC_{71}BM$ and ITIC in an inverted architecture consisting of ITO/ZnO/Active Layer/MoO_3/Ag.

Active Layer	V_{OC} (V)	J_{SC} (mA/cm^2)	FF (%)	PCE (%) best (average)	Active Layer Thickness (nm)
P(T4-TPD-M):$PC_{71}BM$ (1:1.2) + 3% DIO	0.83 ± 0.01	12.0 ± 0.2	69 ± 1	7.5 (6.8 ± 0.3)	145 ± 5
P(T4-TPD-M):ITIC (1:1) + 3% CN	1.00	6.8 ± 0.3	57 ± 1	4.0 (3.8 ± 0.2)	175 ± 5
P(T4-DPP-M):$PC_{71}BM$ (1:1.2) + 3% DIO	0.56 ± 0.01	16.4 ± 0.4	58 ± 2	5.4 (5.2 ± 0.1)	210 ± 5
P(T4-DPP-M):ITIC (1:1) + 3% CN	0.69 ± 0.01	6.7 ± 0.2	46 ± 1	2.2 (2.1 ± 0.1)	170 ± 5
P(T4-iI-M):$PC_{71}BM$ (1:1.2) + 3% DIO	0.64 ± 0.01	13.6 ± 0.6	57 ± 1	5.3 (4.9 ± 0.2)	180 ± 5
P(T4-iI-M):ITIC (1:1) + 3% CN	0.76	7.3 ± 0.6	40 ± 1	2.4 (2.2 ± 0.2)	170 ± 5

Table 5-2. Device statistics for **P(T4-TPD-M)**, **P(T4-DPP-M)**, and **P(T4-iI-M)** based OPV BHJ devices with both $PC_{71}BM$ and ITIC in an inverted architecture consisting of ITO/ZnO/Active Layer/MoO_3/Ag.

There are a few key points to be elaborated on concerning Table 5-2:

1. For both $PC_{71}BM$ and ITIC devices, **P(T4-TPD-M)** excels over the other polymers due to substantially higher open circuit voltage (V_{OC}) values. The higher V_{OC} values with $PC_{71}BM$ and ITIC, 0.83 V and 1.00 V respectively, can be attributed to the deeper HOMO level of **P(T4-TPD-M)**, leading to a larger energy offset between the HOMO of the D-A polymer and LUMO of the MA.[242] The same reasoning can be made for **P(T4-iI-M)** obtaining larger V_{OC} values in comparison to **P(T4-DPP-M)**.

2. P(T4-TPD-M) devices also benefit from significantly higher fill factors (FF). Higher FF values may arise due to a variety of reasons including morphology, solid-state structure, charge mobility, and an ability to form ohmic contacts with the hole and electron transport layers.[244] The surface morphology of all BHJ blends were probed through atomic force microscopy (AFM), and the resulting images are presented in Figure 5-8, 5-9, and 5-10. However, there are no stark differences visible in the AFM images that could correlate to the higher FFs in **P(T4-TPD-M)** devices. In fact, **P(T4-TPD-M)** films are generally rougher than the other polymers, and blends with ITIC reveal spherulite looking textures that may suggest higher phase separation present in the films. The hole mobility obtained through SCLC measurements is comparable between **P(T4-TPD-M)** and **P(T4-DPP-M)**, and therefore cannot explain the ~10% difference in FF seen between devices with these two polymers. Another possible cause for the higher FF values is the deep HOMO level, which may impart a more favorable energetic interface between the polymer and hole transport layer.

3. Short circuit current (J_{SC}) values were highest with the **P(T4-DPP-M)** and **P(T4-iI-M)** devices, leveraging additional photocurrent from absorption in the near-IR, which is not present in the **P(T4-TPD-M)** devices as shown in the external quantum efficiency (EQE) spectra shown in Figure 5-11. **P(T4-DPP-M)** obtains some of the highest J_{SC} values with $PC_{71}BM$ due to the combination of its ability to extract more photocurrent from the near-IR as well as its high SCLC mobility of ~10^{-3} $cm^2V^{-1}s^{-1}$. Looking at the EQE spectra in Figure 5-11, **P(T4-iI-M)** appears to extract the most photocurrent across the visible spectrum, but may not reach the highest J_{SC} values due to its lower SCLC mobility of ~10^{-4} $cm^2V^{-1}s^{-1}$. Devices made from **P(T4-DPP-M)** and **P(T4-iI-M)** also performed optimally with thicker films, providing additional photocurrent and increased J_{SC} values.

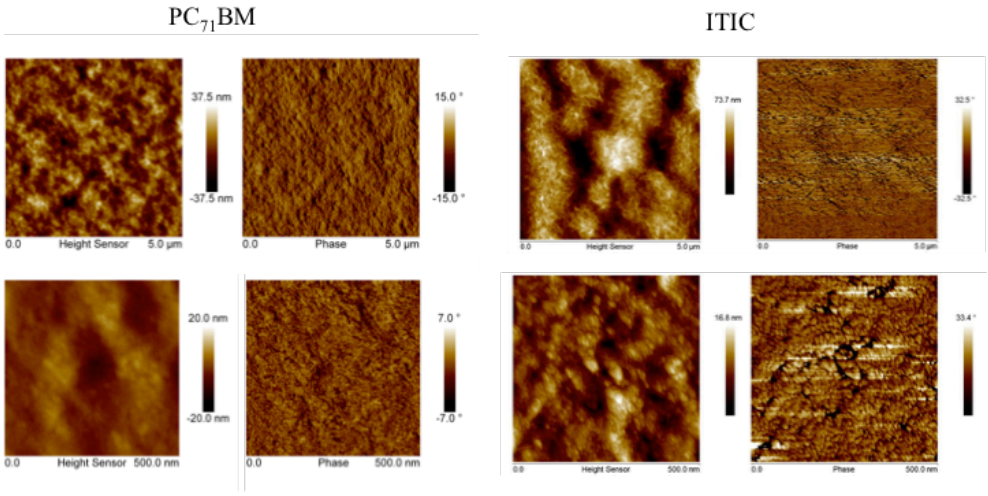

Figure 5-8. AFM height and phase images at both 5 μm and 500nm scales for **P(T4-TPD-M)** BHJ active layers with both $PC_{71}BM$ and ITIC.

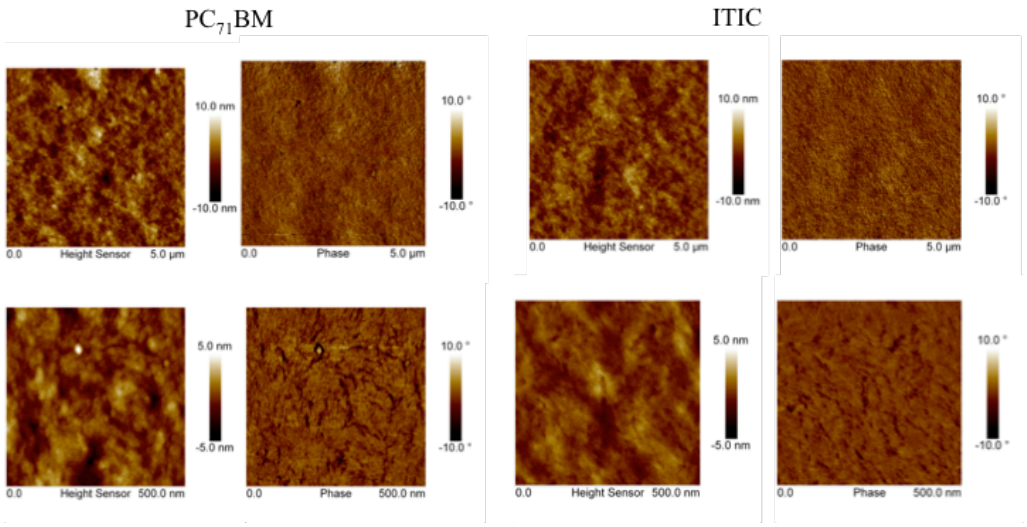

Figure 5-9. AFM height and phase images at both 5 mm and 500nm scales for **P(T4-DPP-M)** BHJ active layers with both $PC_{71}BM$ and ITIC.

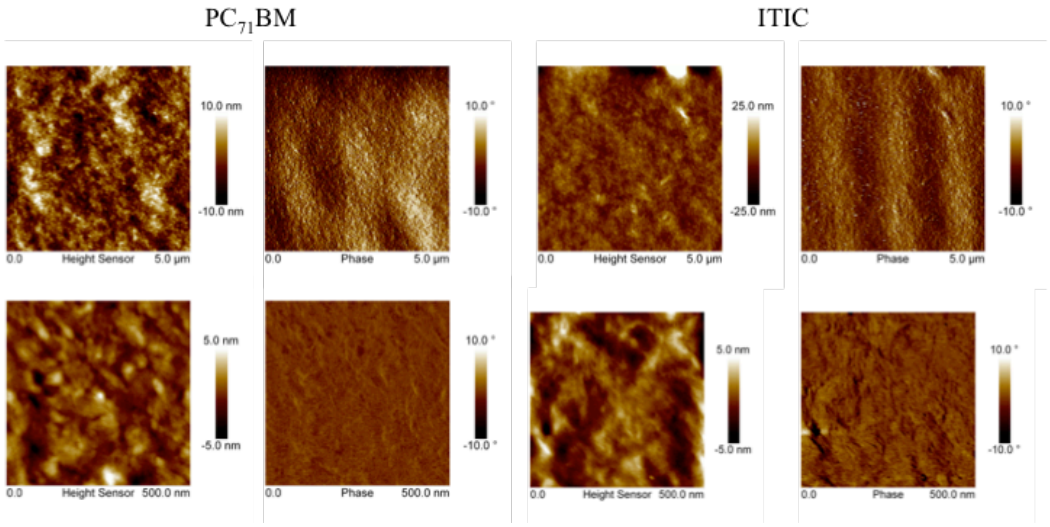

Figure 5-10. AFM height and phase images at both 5 mm and 500nm scales for **P(T4-iI-M)** BHJ active layers with both $PC_{71}BM$ and ITIC.

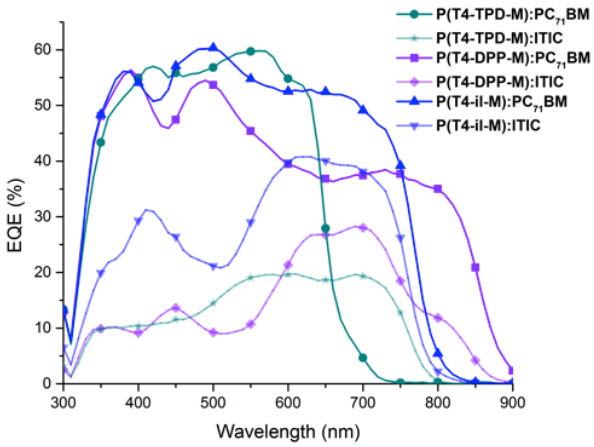

Figure 5-11. External quantum efficiency (EQE) spectra of **P(T4-TPD-M)**, **P(T4-DPP-M)**, and **P(T4-iI-M)** devices with both $PC_{71}BM$ and ITIC.

5.5 Summary and Outlook

In summary, a family of D-A polymers with minimally substituted acceptor moieties, **P(T4-TPD-M)**, **P(T4-DPP-M)**, and **P(T4-iI-M)** were designed and synthesized for use in OPV devices with $PC_{71}BM$ and ITIC. Optimal device efficiencies with $PC_{71}BM$ (7.5%) and ITIC (4.0%) were both obtained using **P(T4-TPD-M)**, while **P(T4-DPP-M)** and **P(T4-iI-M)** obtained lower efficiencies with $PC_{71}BM$ (5.4% and 5.3% respectively) and ITIC (2.1% and 2.2% respectively). The differences in OPV device efficiency primarily stem from higher V_{OC} and FF values in the **P(T4-TPD-M)** devices. Due to the higher device performance with both MAs, **P(T4-TPD-M)** will be utilized for follow up studies within the Reynolds group aimed at replacing the methyl side chain with a longer alkyl chain (n-octyl) and a bulkier alkyl chain (2-ethylhexyl) to assess the impact of sterics on D-A polymer:MA interactions and ultimately OPV device performance. The project flow of this study is represented in Figure 5-12, where this initial work was aimed at determining the optimal acceptor unit for the minimally

substituted side chain study, and future work will focus on side chain modification to assess the impact of side chain sterics on D-A polymer:MA interactions. With the polymer **P(T4-TPD-M)** setting the TPD moiety as the optimal acceptor for OPV devices using both $PC_{71}BM$ and ITIC, future work on side chain modification can start at a high baseline for PCE.

Future work on **P(T4-TPD-M)**, the n-octyl derivative **P(T4-TPD-O)**, and the 2-ethylhexyl derivative **P(T4-TPD-EH)** aims to develop an understanding of the impact of steric bulk on the D-A polymer acceptor moiety in terms of BHJ device efficiency and D-A polymer:MA interactions. Aside from the experiments presented in this work including synthesis, optoelectronic characterization, and devices testing and optimization, the key experiments will target changes in D-A polymer:MA interactions imparted through side chain modification. The first set of experiments will focus on the impact of side chains on the energetic disorder of BHJ blends. Lower energetic disorder is favorable for decreased recombination in BHJ blends, and can indicate that D-A polymer:MA interactions are more consistent throughout the film.[53, 217, 245] Energetic disorder will be probed through temperature dependent SCLC hole and electron mobility measurements, sub-bandgap EQE measurements, and transient photoluminescence measurements.[217]

The second set of experiments will focus on the impact of side chain sterics on structural interactions between the D-A polymers and MAs. Grazing incidence wide angle X-ray scattering (GIWAXS) can be used to determine the impact of side chain sterics on the π–π stacking of D-A polymers in BHJ blends.[246] If the D-A polymer:MA interactions are more consistent, as would be the case if MA docking is actively promoted and not random occurrences through the film, then a smaller distribution of

stacking distances should be observed by GIWAXS. Solid-state 2D ^{13}C:^{1}H heteronuclear correlation (HETCOR) NMR measurements will also be performed to determine the through-space interactions between the D-A polymers and MAs. This technique has been used to provide insight into polymer-fullerene interactions by probing coupling between ^{1}H and ^{13}C nuclei that are in close proximity.

This comprehensive study will elucidate the impact of side chain sterics in D-A polymer:MA interactions and test the validity of the MA docking hypothesis, for both fullerene and non-fullerene MAs. Building on this understanding will play an important role in the future design of conjugated D-A polymers for OPV applications.

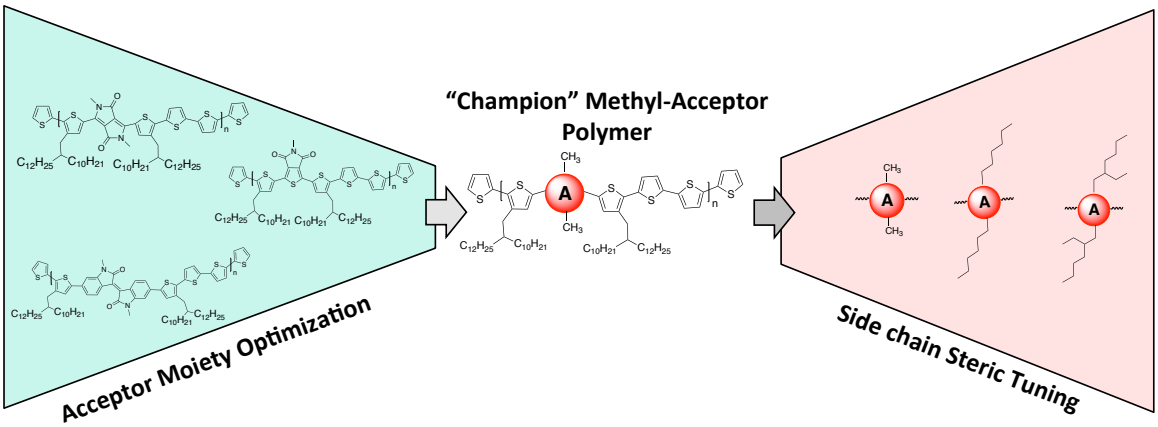

Figure 5-12. Schematic illustrating the project flow for investigating the role of side chain sterics on D-A polymer:MA interactions, where this work represents an optimization of acceptor moiety to obtain the highest baseline PCE with both $PC_{71}BM$ and ITIC. Future work will aim to tune the steric interactions of the acceptor moiety by swapping the methyl side chain for n-octyl and 2-ethylhexyl side chains.

5.6 Synthetic Methods

General Synthetic Materials, Methods, and Characterization:

4H-thieno[3,4-c]pyrrole-4,6(5H)-dione (**1**)[221], 6,6'-dibromoisoindigo[247], (4-(2-octyldodecyl)thiophen-2-yl)trimethylstannane, (4-(2-decyltetradecyl)thiophen-2-yl)trimethylstannane, 3-(2-decyltetradecyl)thiophene, and 5,5'-bis(trimethylstannyl)-2,2'-bithiophene[210] were synthesized according to literature procedures. Iodomethane (99%, Alfa Aesar), K_2CO_3 (anhydrous, Oakwood Products), N-bromosuccinimide (99%, Alfa Aesar), $Pd_2(dba)_3$*$CHCl_3$ adduct (Sigma), diethyldithiocarbamic acid diethylammonium salt (97%, TCI America), P(*o*-tolyl)$_3$ (96%, Sigma), 2-bromothiophene (98%, Sigma) and 2-(tributylstannyl)thiophene (97%, Alfa Aesar), diisopropyl succinate (99%, TCI America), potassium *tert*-butoxide (97%, Alfa Aesar), *tert*-amyl alcohol (99%, Sigma Aldrich), sodium azide (99%, Alfa Aesar), and n-butyl lithium (2.M in hexanes, Sigma Aldrich) were all used as received. Diisoproylamine (99%, Alfa Aesar) was distilled prior to use. N,N-dimethylformamide (anhydrous, Alfa Aesar) and chloroform (BDH) were used as received. Propylene carbonate (Acros Organics), diethyl ether (BDH), tertahydrofuran (BDH), and toluene (BDH) were purified and dried using a solvent purification system.

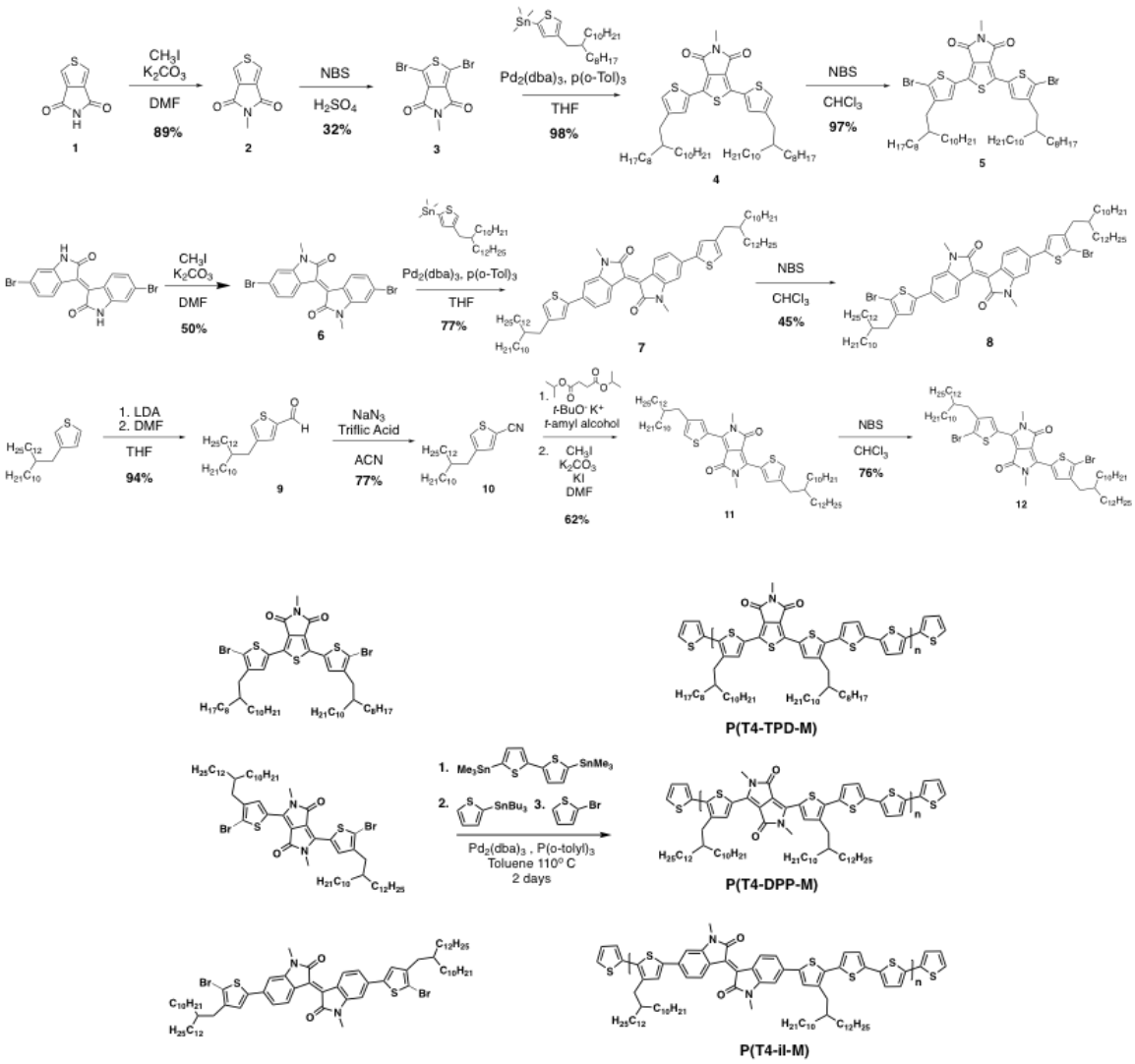

Scheme 5-1. Outline of synthetic route to **P(T4-TPD-M)**, **P(T4-DPP-M)**, and **P(T4-iI-M)**

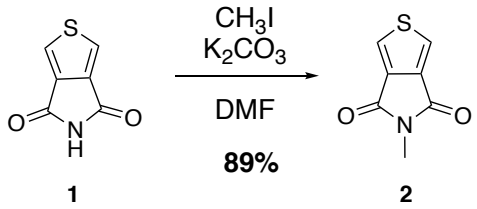

5-methyl-4H-thieno[3,4-c]pyrrole-4,6(5H)-dione (2)[1]: To an oven-dried 3-necked round bottom flask, **1** (900 mg, 5.88 mmol) and potassium bicarbonate (2.10 g, 12.21 mmol) were added, sealed, evacuated, and refilled with argon 3 times. 25 mL of dry DMF was added to the flask. Iodomethane (1.48 g, 10.46 mmol) was slowly added to the solution and the solution allowed to stir at room temperature for two days. The solution was then quenched with 1 mL of 1M HCl, poured into a 300-mL round bottom flask, and concentrated by rotary evaporation. The compound was dissolved in ethyl acetate and filtered to remove the remaining salts. The solids were collected and purified by column chromatography (silica gel, DCM) to yield **2** (870 mg, 79% yield) as a crystalline white solid. ^{1}H NMR (500 MHz, $CDCl_3$): δ: 7.84 (s, 2H), 3.15 (s, 3H). ^{13}C NMR (500 MHz, $CDCl_3$): δ: 162.55, 136.45, 125.41, 24.21. HRMS (ESI MS) *m/z*: theor: 167.0041 found: 167.0037.

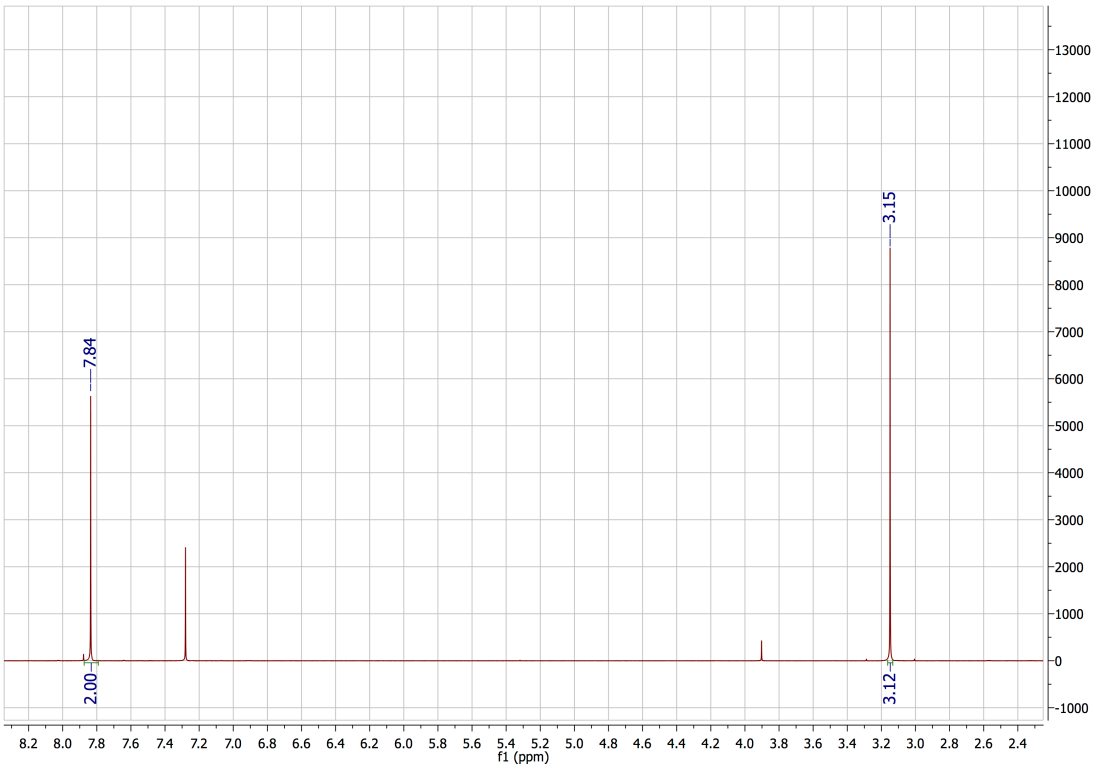
7.84
3.15
2.00
3.12
f1 (ppm)

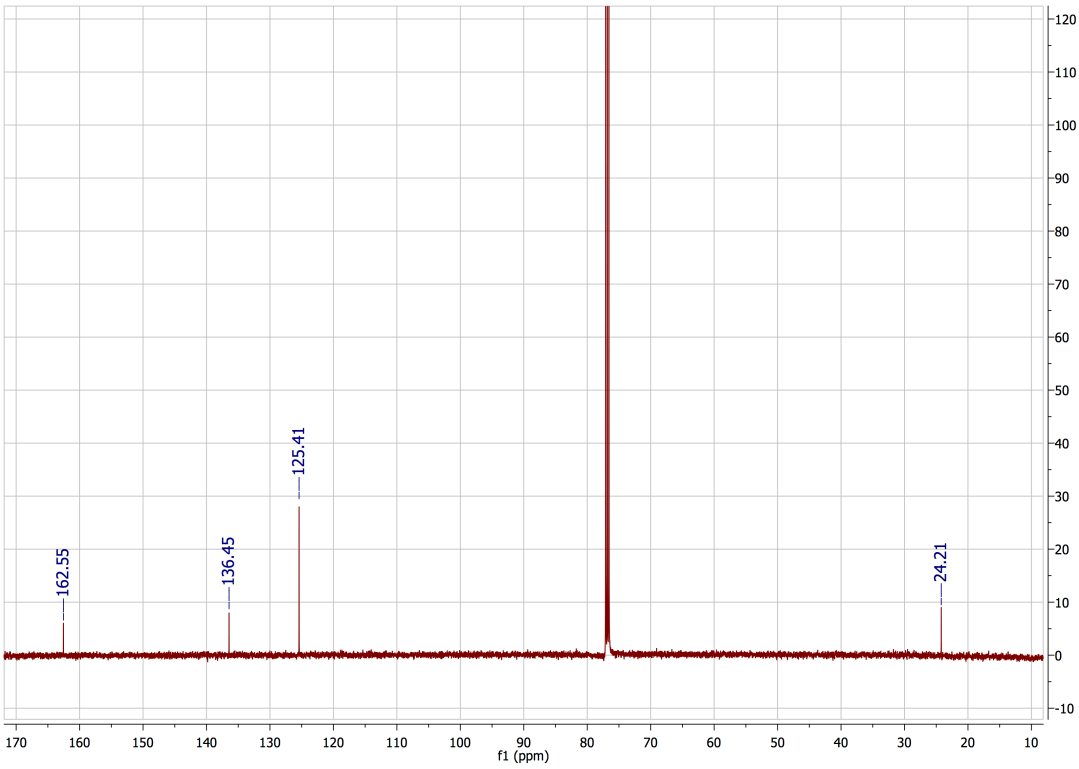
162.55
136.45
125.41
24.21
f1 (ppm)

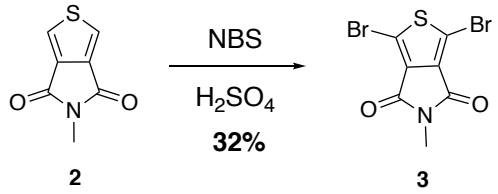

2 3

1,3-dibromo-5-methyl-4H-thieno[3,4-c]pyrrole-4,6(5H)-dione (3): To an oven-dried round bottom flask, **2** (530 mg, 3.17 mmol), N-bromosuccinimide (1.52 g, 8.55 mmol), and concentrated sulfuric acid (17.8-18.4 M H_2SO_4) (25 mL) was added. The reaction was stirred under an argon atmosphere overnight at room temperature. The reaction mixture was quenched with 100 mL H_2O and extracted with ethyl acetate; the organic layer was collected and concentrated by rotary evaporation. The compound was re-dissolved in ethyl acetate and extracted a second time with a solution of concentrated potassium carbonate in water to remove the orange color. The organic layer was collected and concentrated by rotary evaporation. The compound was purified by chromatography (silica gel, 1:3 EtOAc:hexanes) to yield **3** (330 mg, 32% yield) as a beige crystalline solid. ^{1}H NMR (500 MHz, $CDCl_3$): δ: 3.13 (s, 3H). ^{13}C NMR (500 MHz, $CDCl_3$): δ: 160.23, 134.61, 112.91, 24.51. HRMS (ESI MS) *m/z*: theor: 322.8251 found: 322.8267.

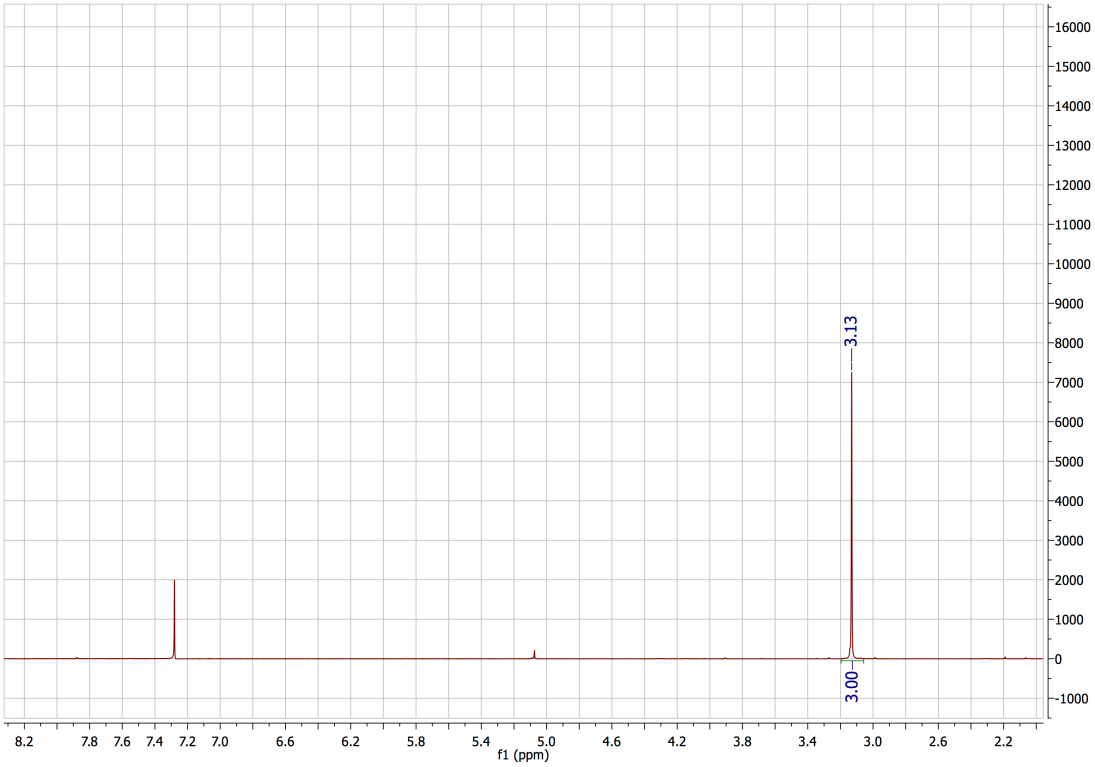
3.13
3.00
f1 (ppm)

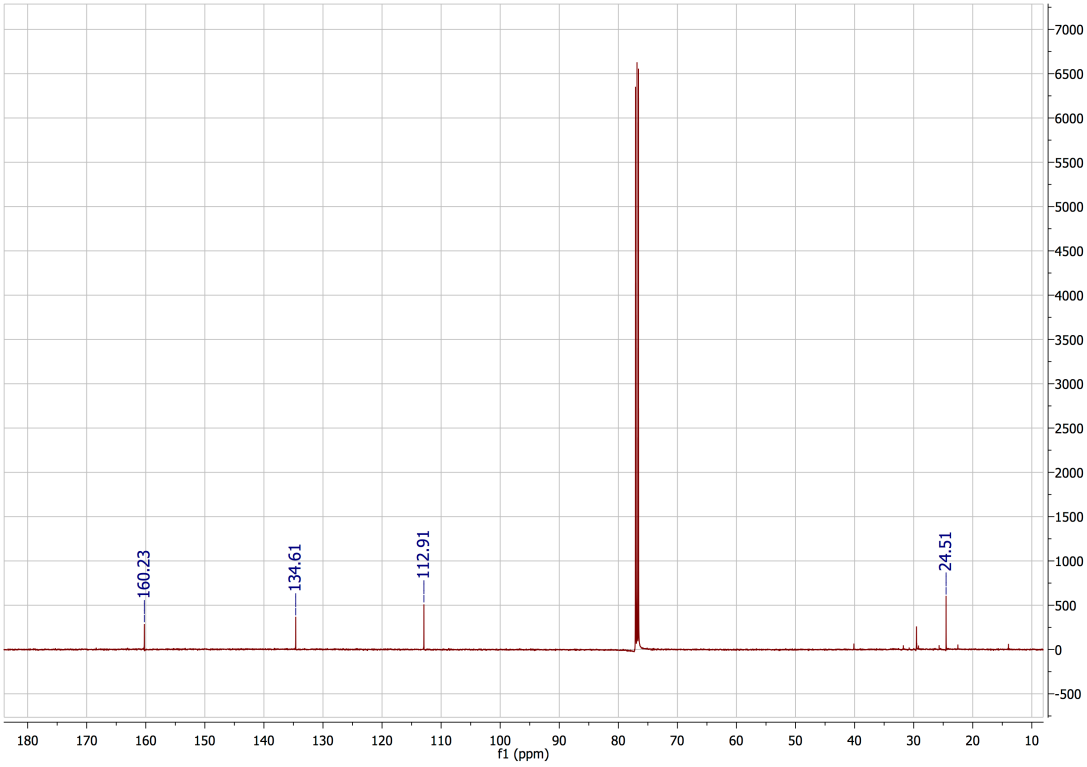
160.23
134.61
112.91
24.51
f1 (ppm)

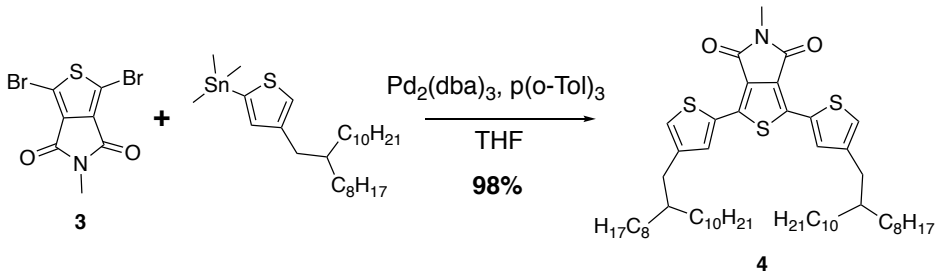

5-methyl-1,3-bis(4-(2-octyldodecyl)thiophen-2-yl)-4*H*-thieno[3,4-c]pyrrole-4,6(5*H*)-dione (4): To an oven-dried round bottom flask was added **3** (0.330 g, 1.01 mmol), (4-(2-octyldodecyl)thiophen-2-yl)trimethylstannane (1.34 g, 2.34 mmol), and 10 mL dry degassed THF. A condenser was added and the set-up was placed under inert conditions. In an argon glove box, $Pd_2(dba)_3$ (21 mg, 0.02 mmol) and P(o-Tol)$_3$ (25 mg, 0.08 mmol) were weighed into a 10-mL vial. The vial was sealed to maintain inert conditions. Upon removal from the glove box, the contents of the 10-mL vial were dissolved in a small amount of dry degassed THF (<5 mL) and transferred to the multi-necked vessel. The reaction was refluxed overnight at 70 °C. The compound was purified by column chromatography (silica gel, hexanes) to yield **4** (890 mg, 98% yield) as a waxy yellow solid. ^{1}H NMR (500 MHz, $CDCl_3$): δ: 7.85 (s, 2H), 7.02 (s, 2H), 3.19 (s, 3H), 2.58 (d, J = 6.8 Hz, 4H), 1.67 (m, 2H), 1.27 (m, 64H), 0.89 (t, J = 6.5 Hz, 12H). ^{13}C NMR (500 MHz, $CDCl_3$): δ: 162.55, 143.51, 136.73, 131.76, 131.38, 127.76, 124.28, 38.67, 34.71, 33.07, 31.75, 29.82, 29.54, 29.52, 29.49, 29.20, 26.38, 24.15, 22.52, 13.95. HRMS (ESI MS) *m/z*: theor: 891.6055 found: 891.6053.

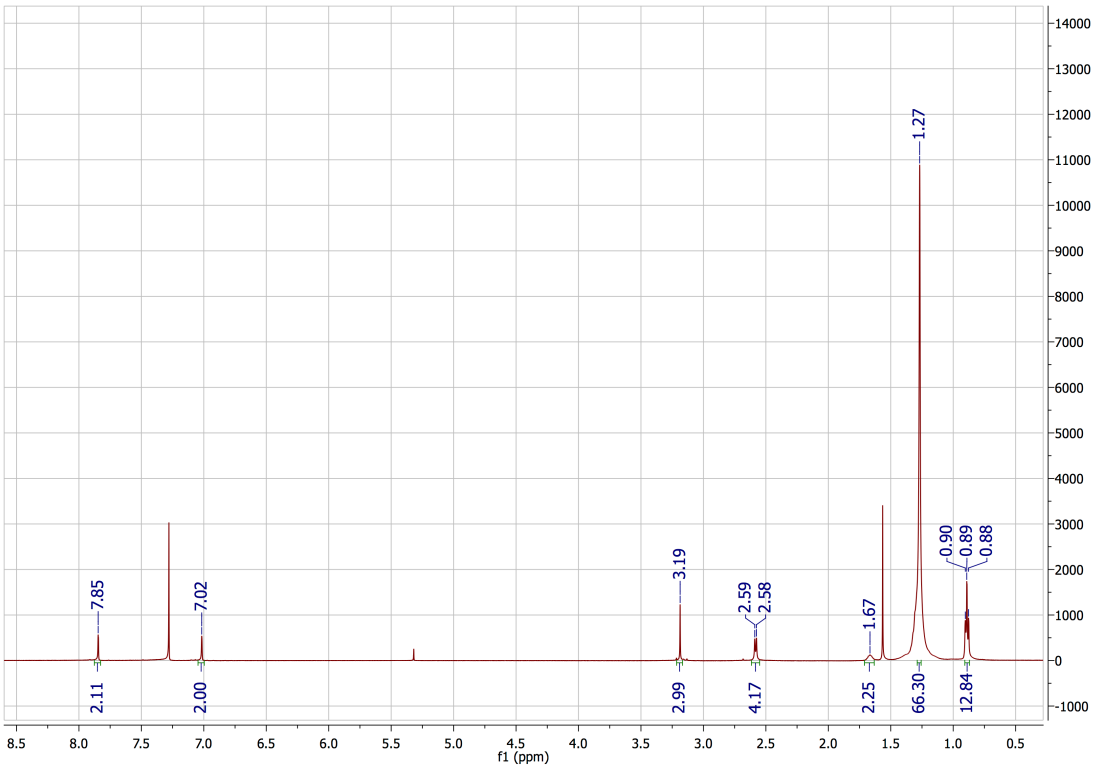
7.85
7.02
3.19
2.59
2.58
1.67
1.27
0.90
0.89
0.88
2.11
2.00
2.99
4.17
2.25
66.30
12.84
f1 (ppm)

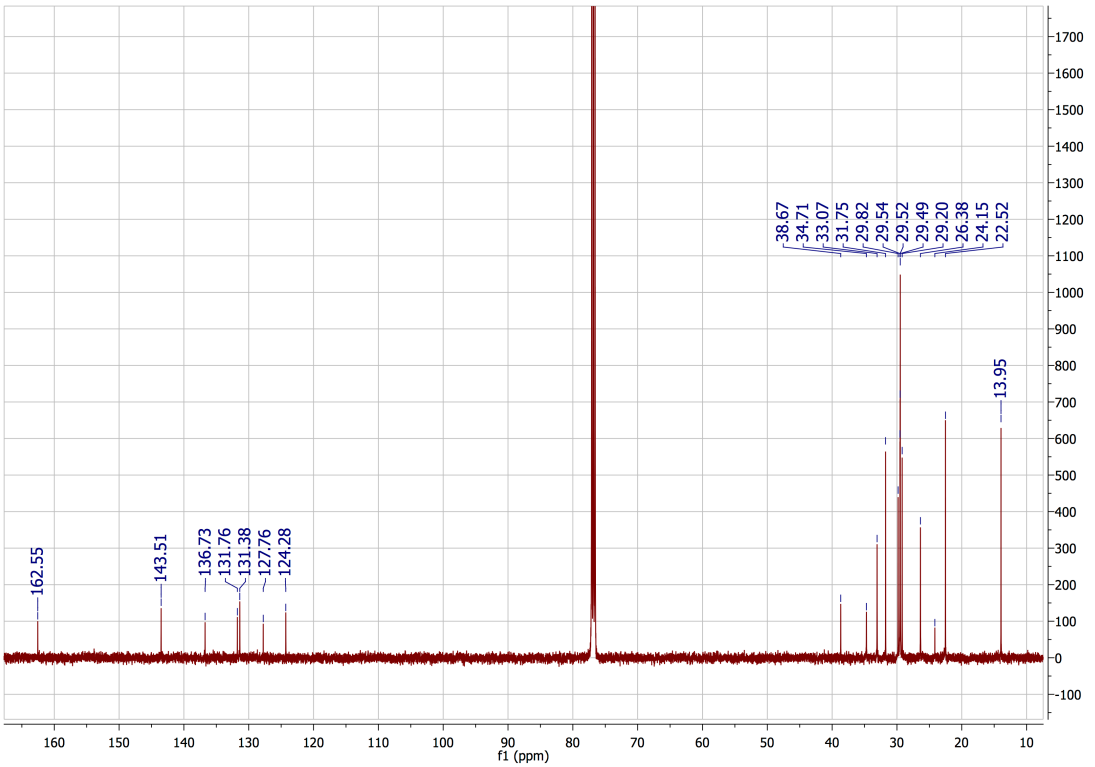
38.67
34.71
33.07
31.75
29.82
29.54
29.52
29.49
29.20
26.38
24.15
22.52
13.95
162.55
143.51
136.73
131.76
131.38
127.76
124.28
f1 (ppm)

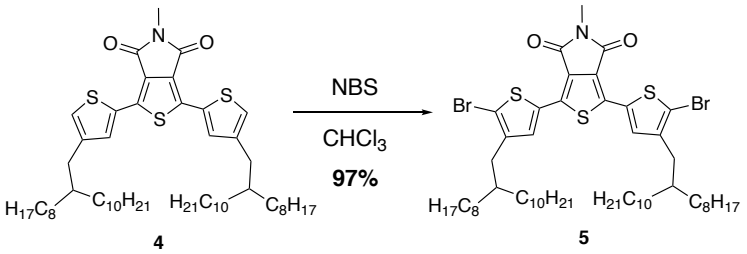

4 5

1,3-bis(5-bromo-4-(2-octyldodecyl)thiophen-2-yl)-5-methyl-4*H*-thieno[3,4-c]pyrrole-4,6(5*H*)-dione (5): To an oven-dried round bottom flask was added **4** (620 mg, 0.695 mmol), SiO_2 (20 mg), and $CHCl_3$ (20 mL) at 0°C. N-bromosuccinimide (272 mg, 1.529 mmol) was added to the reaction vessel. The reaction was brought to room temperature and stirred overnight. The reaction was extracted with H_2O, and the organic layers were collected and removed by rotary evaporation. The compound was purified by column chromatography (silica gel, 0.5:9.5 EtOAc:hexanes). The resulting compound was precipitated in methanol and filtered to yield **8** (710 mg, 97% yield) as a waxy yellow solid. ^{1}H NMR (500 MHz, $CDCl_3$): δ: 7.60 (s, 2H), 3.16 (s, 3H), 2.52 (d, J = 7.1 Hz, 4H), 1.71 (m, 2H), 1.27 (m, 64H), 0.89 (t, J = 6.9 Hz, 12H). ^{13}C NMR (500 MHz, $CDCl_3$): δ: 162.19, 142.78, 135.33, 131.48, 130.64, 128.06, 114.00, 38.31, 33.96, 33.13, 31.77, 29.83, 29.56, 29.54, 29.52, 29.50, 29.22, 26.33, 24.19, 22.53, 13.96. HRMS (ESI MS) *m/z*: theor: 1047.4265 found: 1047.4261.

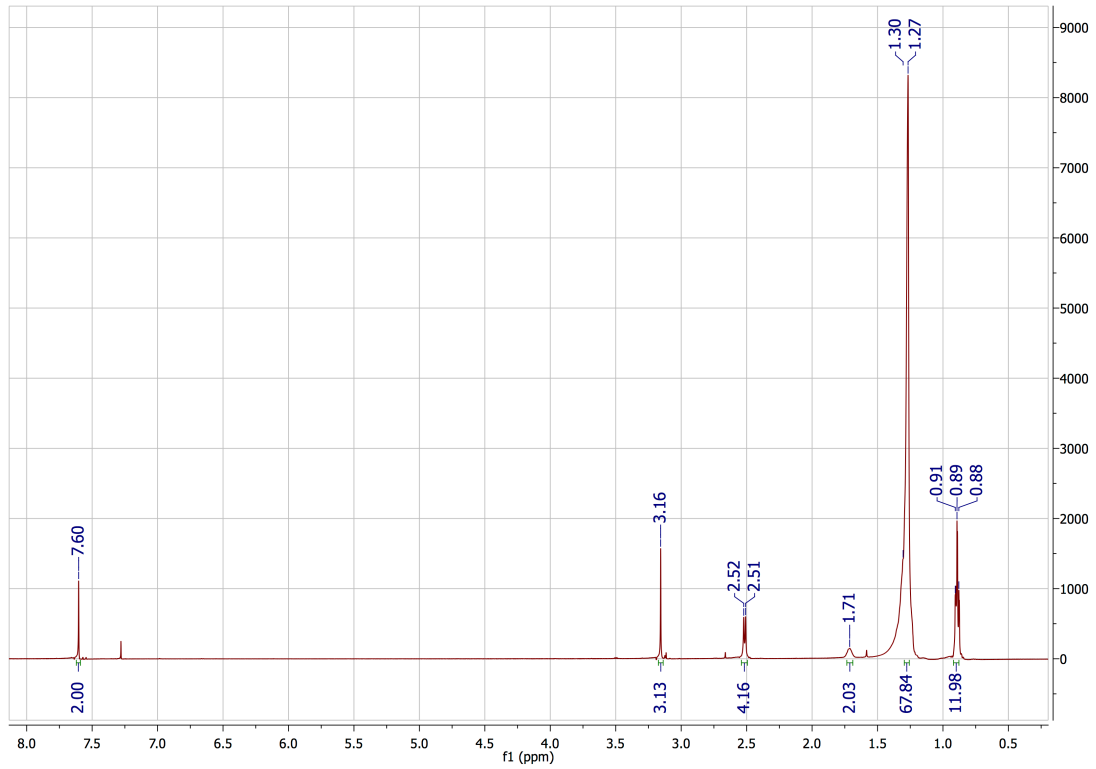
1.30
1.27
7.60
3.16
2.52
2.51
1.71
0.91
0.89
0.88
2.00
3.13
4.16
2.03
67.84
11.98
f1 (ppm)

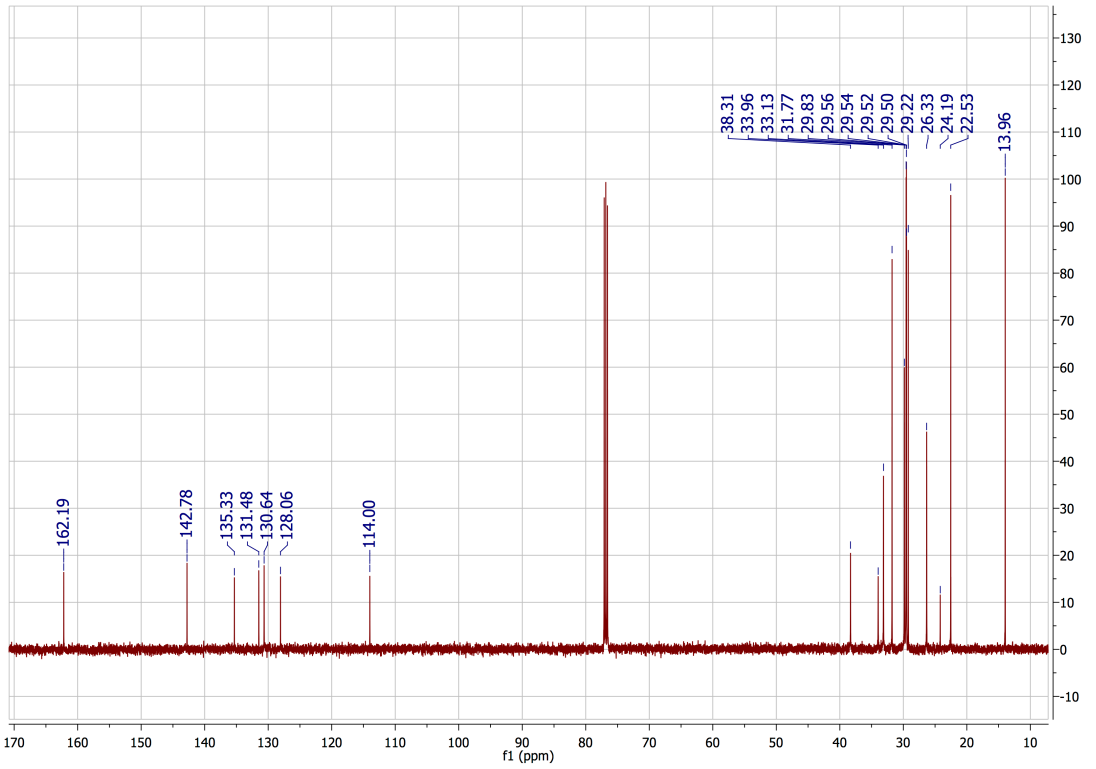
38.31
33.96
33.13
31.77
29.83
29.56
29.54
29.52
29.50
29.22
26.33
24.19
22.53
13.96
162.19
142.78
135.33
131.48
130.64
128.06
114.00
f1 (ppm)

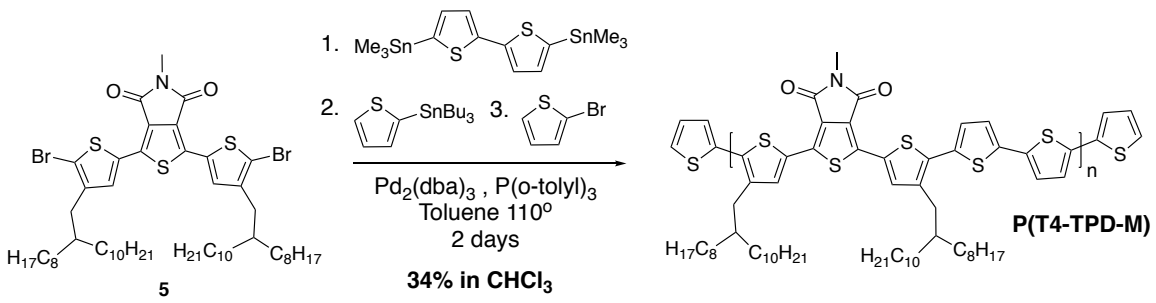

P(T4-TPD-M): To a 3-necked oven-dried round bottom flask was added **5** (340 mg, 0.323 mmol). The vessel was brought into an argon glove box, where 5,5'-bis(trimethylstannyl)-2,2'-bithiophene (159 mg, 0.323 mmol), $Pd_2(dba)_3$ (10 mg, 0.009 mmol), and $P(o\text{-}tol)_3$ (12 mg, 0.038 mmol) was added to the vessel. The flask was equipped with a condenser, sealed, and removed from the glove box. Dry, degassed toluene (5 mL) was added. The reaction was stirred for 48 hours at 110 °C. Tributyl(thiophen-2-yl) stannane (0.1 mL) was added at 48 hours; 2-bromothiophene (0.1 mL) was added at 54 hours. The reaction was cooled to 60° C, after which a spatula tip of palladium scavenger (diethylammonium diethyldithiocarbamate) was added at 60 hours and stirred for an additional hour. After the reaction was cooled to room temperature, the product was precipitated into methanol and filtered. The precipitate was purified by Soxhlet extraction (solvents used: methanol, acetone, hexane, dichloromethane, chloroform). Product in the chloroform fraction was condensed to ~5 mL, precipitated into methanol, and dried by vacuum filtration to yield polymer **P(T4-TPD-M)** (115 mg, 34% yield) as a dark red solid. Mn: 59 kDa, Mw: 105 kDa, Đ: 1.77 vs. polystyrene standard in 1,2,4-trichlorobenzene at 140°C. Anal. calcd. for $C_{63}H_{91}NO_2S_5$: C (71.74) H (8.70) N (1.33) S (15.20), Found: C (71.58) H (8.61) N (1.39) S (14.92).

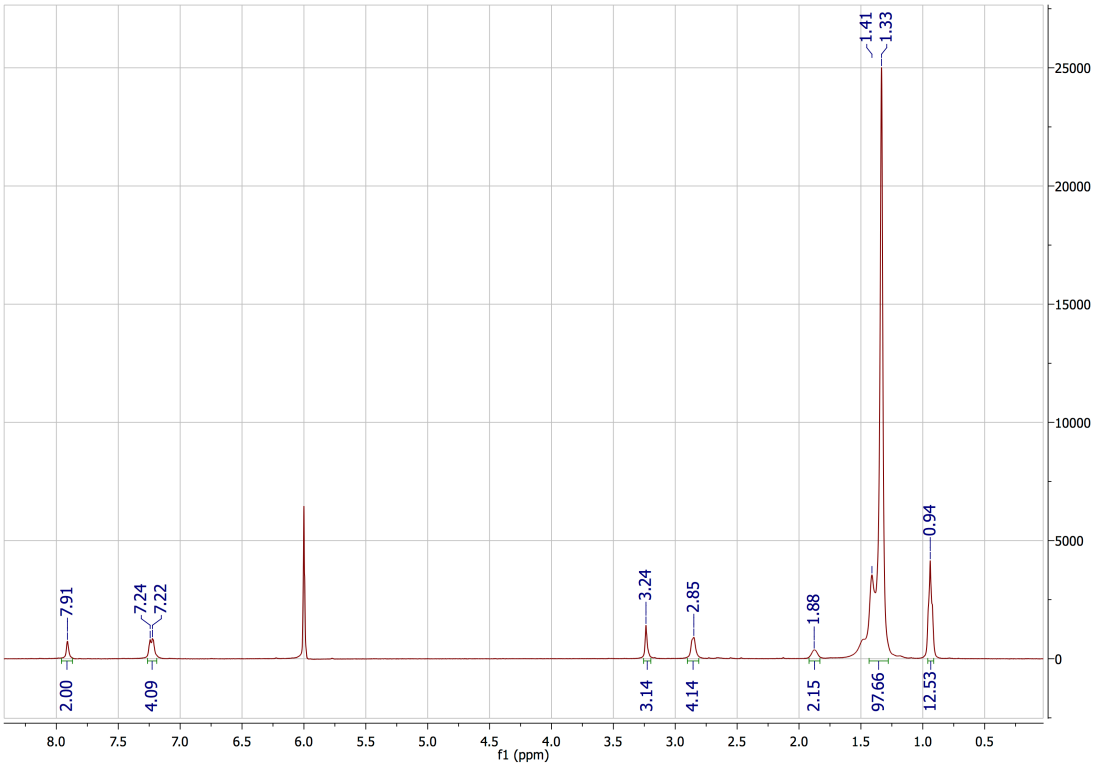
1.41
1.33
25000
20000
15000
10000
5000
0
0.94
7.91
7.24
7.22
3.24
2.85
1.88
2.00
4.09
3.14
4.14
2.15
97.66
12.53
8.0
7.5
7.0
6.5
6.0
5.5
5.0
4.5
4.0
3.5
3.0
2.5
2.0
1.5
1.0
0.5
f1 (ppm)

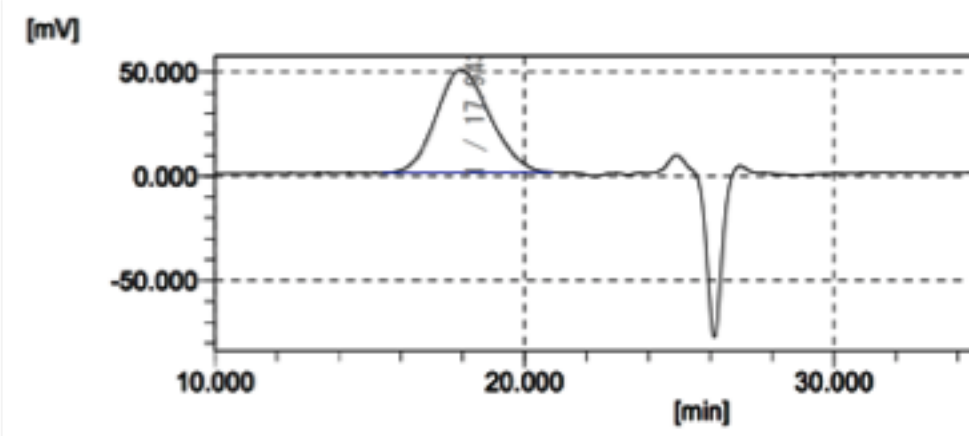
[mV]
50.000
0.000
-50.000
10.000
20.000
30.000
[min]

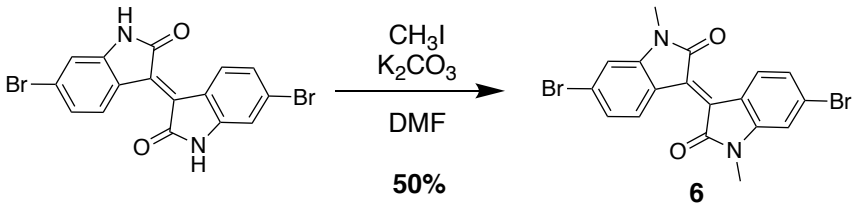

(*E*)-6,6'-dibromo-1,1'dimethyl-[3,3'-biindolinylidene]-2,2'-dione (6): To an oven-dried pressure vessel was added 6,6'-dibromoisoindigo (2.00 g, 4.76 mmol) and potassium carbonate (3.29 g, 23.8 mmol). Anhydrous DMF (70 mL) was added followed by dropwise addition of methyl iodide (1.48 mL, 23.8 mmol). The reaction was stirred at 80°C for 24 hours. The reaction was quenched with 1M HCl (1 mL) and stirred for 2 hours. The DMF was removed *via* rotary evaporation, and the compound was dissolved in chloroform and extracted with H_2O. The organic layers were collected and condensed. The compound was purified by column chromatography (silica gel, 1:4 EtOAc:hexanes) to yield **6** (1.10 g, 50% yield) as a dark brown crystalline powder. ^{1}H NMR (300 MHz, $CDCl_3$): δ: 9.13 (d, J = 8.6 Hz, 2H), 7.22 (dd, J = 8.6 Hz, 1.9 Hz, 2H), 6.97 (d, J = 1.9 Hz, 2H), 3.29 (s, 2H). HRMS (ESI MS) *m/z*: theor: 445.9265 found: 445.9272.

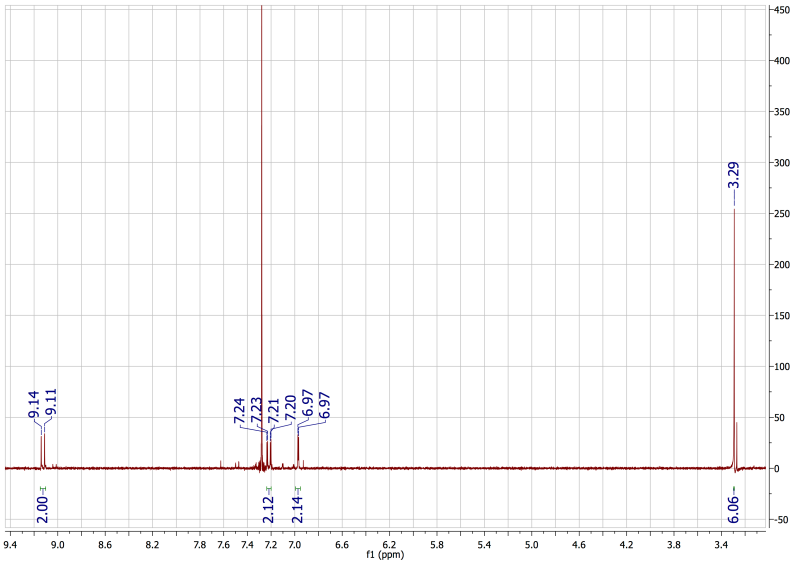

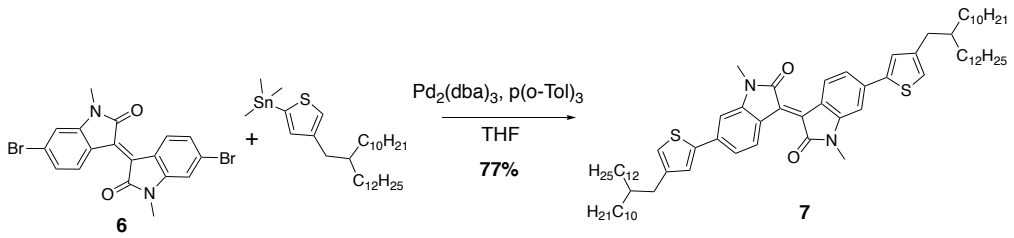

(E)-6,6'-bis(4-(2-decyltetradecyl)thiophen-2-yl)-1,1'-dimethyl-[3,3'-biindolinylidene] -2,2'-dione (7): To a 2-necked oven-dried round bottom flask was added **6** (628 mg, 1.40 mmol). The flask was brought into an argon glove box where $Pd_2(dba)_3$ (29 mg, 0.028 mmol) and P(o-tol)$_3$ (34 mg, 0.112 mmol) were added to the reaction flask. The flask was equipped with a condenser, sealed, and removed from the glove box. The vessel/condenser set-up was placed in an oil-bath and attached to a water condenser system. Under argon, a small amount of dry, degassed THF was used to transfer (4-(2-decyltetradecyl)thiophen-2-yl)trimethylstannane (2.04 g, 3.5 mmol) to the reaction vessel. The rest of the dry, degassed THF [14 mL total (0.1 M with respect to **6**)] was added. The reaction was refluxed overnight in the dark at 100 °C. The compound was purified by column chromatography (silica gel, 1:9 EtOAc:hexanes) to yield **7** (1.22 g, 77% yield) as a purple waxy solid. ^{1}H NMR (500 MHz, $CDCl_3$): δ: 9.23 (d, J = 8.4 Hz, 2H), 7.33 (d, J = 8.4 Hz, 2H), 7.27 (s, J = 2H), 6.99 (s, J = 2H), 6.95 (s, 2H), 3.38 (s, 6H), 2.59 (d, J = 6.7 Hz, 4H), 1.67 (m, 2H), 1.28 (m, 80H), 0.9 (t, J = 6.7 Hz, 12H). ^{13}C NMR (500 MHz, $CDCl_3$): δ: 168.25, 145.99, 143.65, 143.13, 138.09, 131.68, 130.10, 126.33, 121.97, 120.79, 118.91, 104.25, 38.88, 37.63, 35.04, 33.65, 33.28, 31.94, 30.12, 30.01, 29.71, 29.69, 29.67, 29.37, 26.67, 26.66, 26.56, 26.05, 22.70, 13.88. HRMS (ESI MS) *m/z*: theor: 1126.8321 found: 1126.8332.

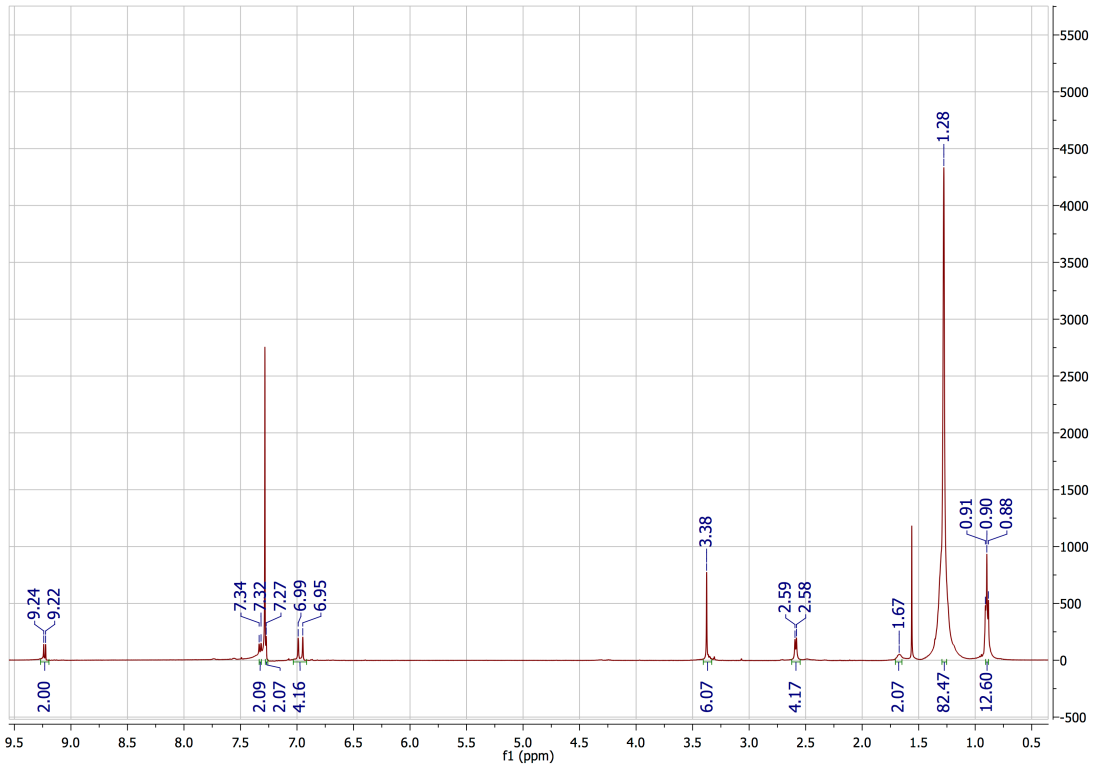
9.24
9.22
7.34
7.32
7.27
6.99
6.95
3.38
2.59
2.58
1.67
1.28
0.91
0.90
0.88
2.00
2.09
2.07
4.16
6.07
4.17
2.07
82.47
12.60
f1 (ppm)

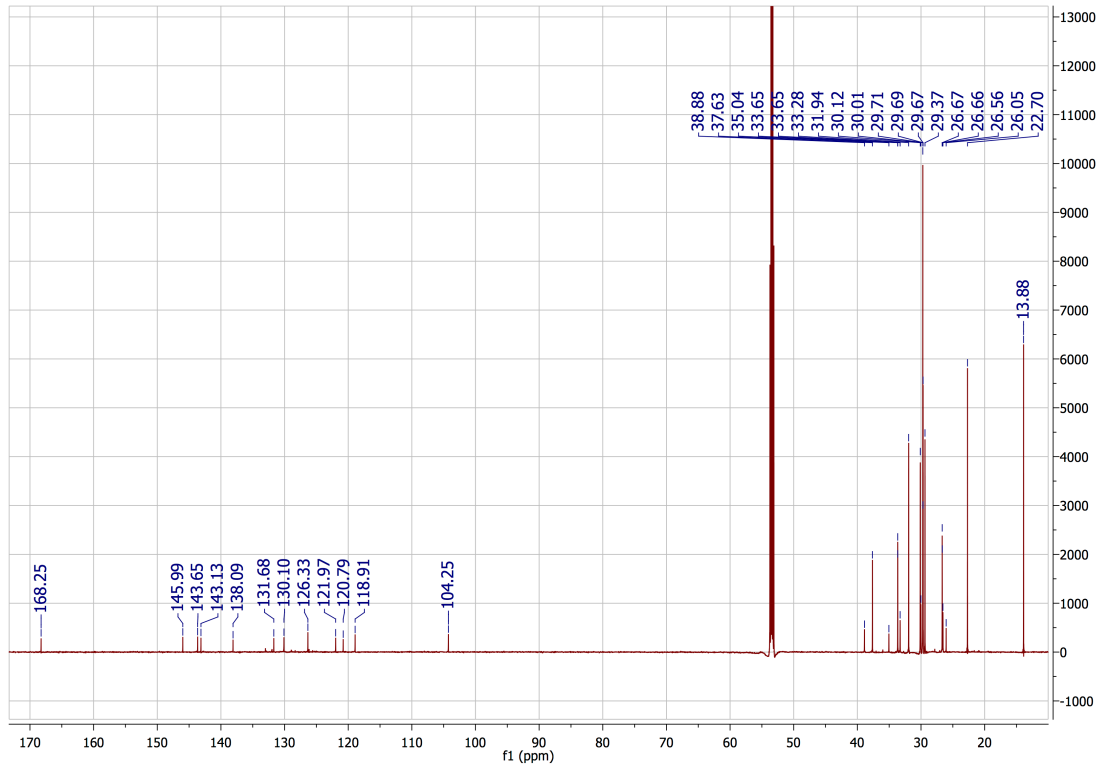
38.88
37.63
35.04
33.65
33.65
33.28
31.94
30.12
30.01
29.71
29.69
29.67
29.37
26.67
26.66
26.56
26.05
22.70
13.88
168.25
145.99
143.65
143.13
138.09
131.68
130.10
126.33
121.97
120.79
118.91
104.25
f1 (ppm)

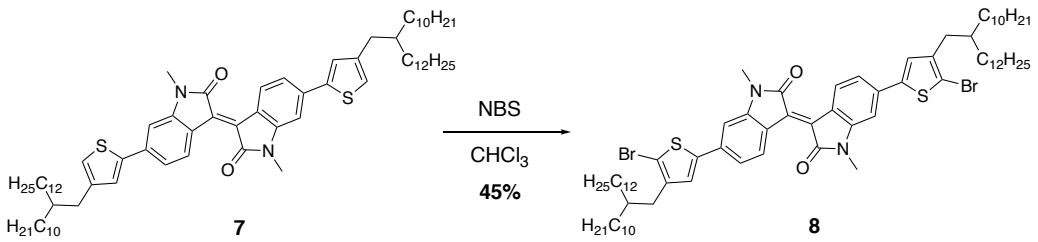

(E)-6,6'-bis(5-bromo-4-(2-decyltetradecyl)thiophen-2-yl)-1,1'-dimethyl-[3,3'-biindolinylidene]-2,2'-dione (14): To an oven-dried round bottom flask cooled to 0°C was added **7** (350 mg, 0.310 mmol) and $CHCl_3$ (35 mL). N-bromosuccinimide (110 mg, 0.620 mmol) was added. The ice bath was removed, and the reaction was stirred in the dark overnight. The reaction was extracted with water, and the organic layers were collected and condensed by rotary evaporation. The compound was purified by column chromatography (silica gel, 1:3 DCM:hexanes) to yield **8** (180 mg, 45% yield) as a purple-black waxy solid. ^{1}H NMR (500 MHz, $CDCl_3$): δ: 9.22 (d, J = 8.4 Hz, 2H), 7.33 (d, J = 8.4 Hz, 2H), 7.23 (dd, J = 8.4 Hz, 1.7 Hz, 2H), 7.11 (s, J = 2H), 6.88 (d, J = 1.7 Hz, 2H), 3.33 (s, 6H), 2.53 (d, J = 7.2 Hz, 4H), 1.73 (m, 2H), 1.27 (m, 80H), 0.89 (t, J = 6.9 Hz, 12H). ^{13}C NMR (500 MHz, $CDCl_3$): δ: 168.13, 145.69, 142.70, 142.64, 137.10, 131.68, 130.24, 125.51, 120.90, 118.85, 110.51, 103.83, 38.40, 34.19, 33.17, 31.75, 29.84, 29.54, 29.52, 29.50, 29.19, 26.35, 26.04, 22.52, 13.95. HRMS (ESI MS) *m/z*: theor: 1282.6531 found: 1282.6529.

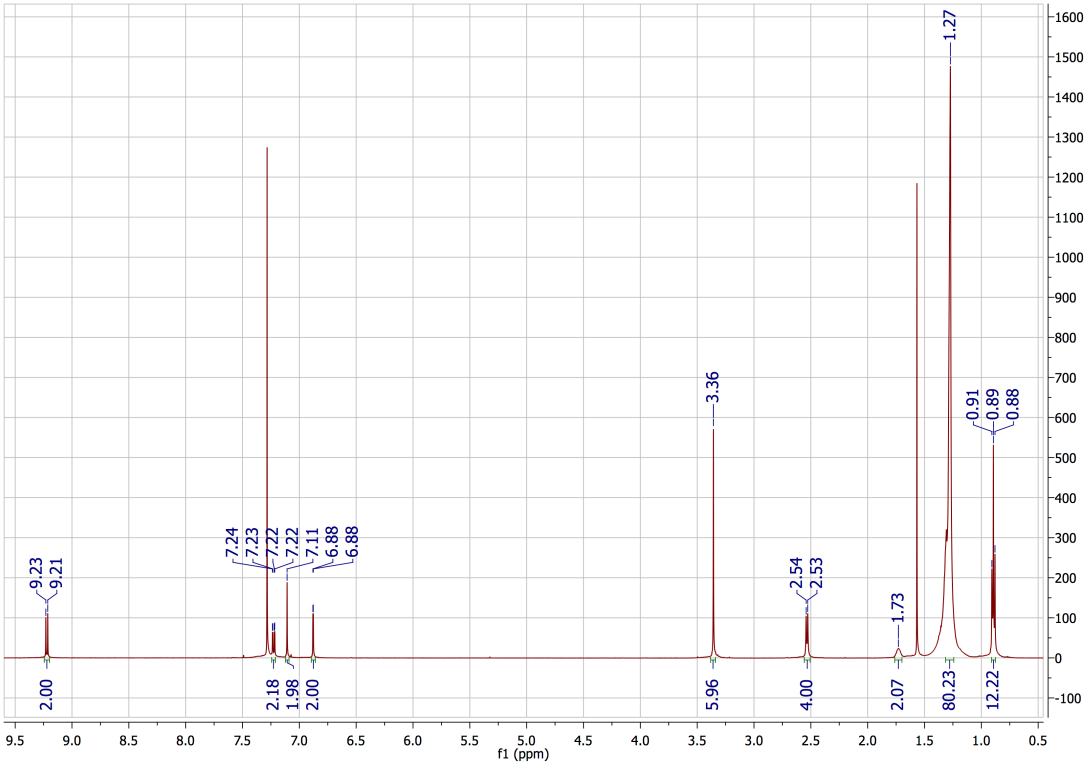
9.23
9.21
7.24
7.23
7.22
7.22
7.11
6.88
6.88
3.36
2.54
2.53
1.73
1.27
0.91
0.89
0.88
2.00
2.18
1.98
2.00
5.96
4.00
2.07
80.23
12.22
f1 (ppm)

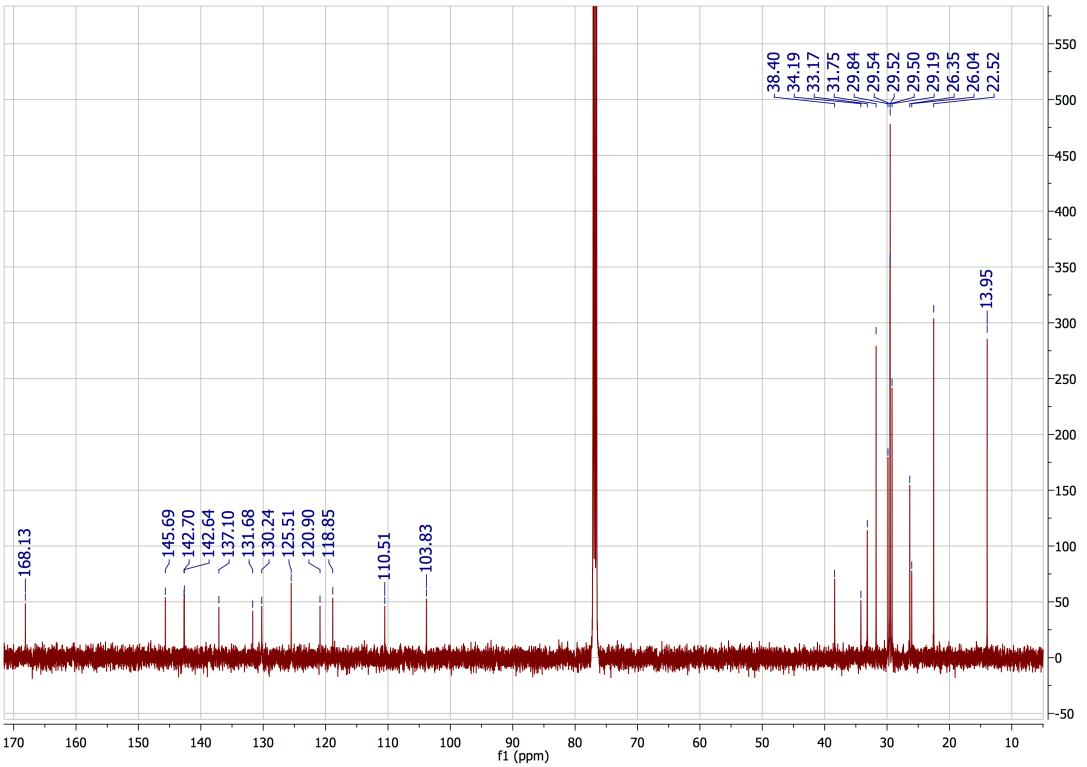
168.13
145.69
142.70
142.64
137.10
131.68
130.24
125.51
120.90
118.85
110.51
103.83
38.40
34.19
33.17
31.75
29.84
29.54
29.52
29.50
29.19
26.35
26.04
22.52
13.95
f1 (ppm)

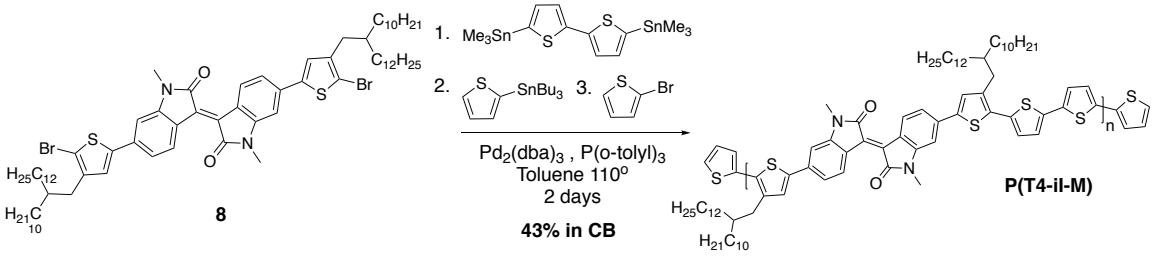

P(T4-iI-M): To a 3-necked oven-dried 25-mL round bottom flask was added **8** (304 mg, 0.236 mmol). The vessel was brought into an argon glove box, where 5,5'-bis(trimethylstannyl)-2,2'-bithiophene (116 mg, 0.236 mmol), $Pd_2(dba)_3$ (7.3 mg, 0.007 mmol), and $P(o\text{-}tol)_3$ (8.6 mg, 0.028 mmol) was added to the vessel. The flask was equipped with a condenser, sealed, and removed from the glove box. Dry, degassed toluene (5 mL) was added. The reaction was stirred for 48 hours at 110 °C. Tributyl(thiophen-2-yl) stannane (0.1 mL) was added at 48 hours; 2-bromothiophene (0.1 mL) was added at 54 hours. The reaction was cooled to 60° C, after which a spatula tip of palladium scavenger (diethylammonium diethyldithiocarbamate) was added at 60 hours and stirred for an additional hour. After the reaction was cooled to room temperature, the product was precipitated into methanol and filtered. The precipitate was purified by Soxhlet extraction (solvents used: methanol, acetone, hexane, dichloromethane, chloroform, chlorobenzene). Product in the chlorobenzene fraction was condensed to ~5 mL, precipitated into methanol, and dried by vacuum filtration to yield polymer **P(T4-iI-M)** (132 mg, 43% yield) as a dark purple solid. Mn: 54 kDa, Mw: 151 kDa, Đ: 2.78 vs. polystyrene standard in 1,2,4-trichlorobenzene at 140°C. Anal. calcd. for $C_{82}H_{116}N2O_2S_4$: C (76.34) H (9.06) N (2.17) S (9.94), Found: C (76.05) H (9.14) N (2.20) S (9.87).

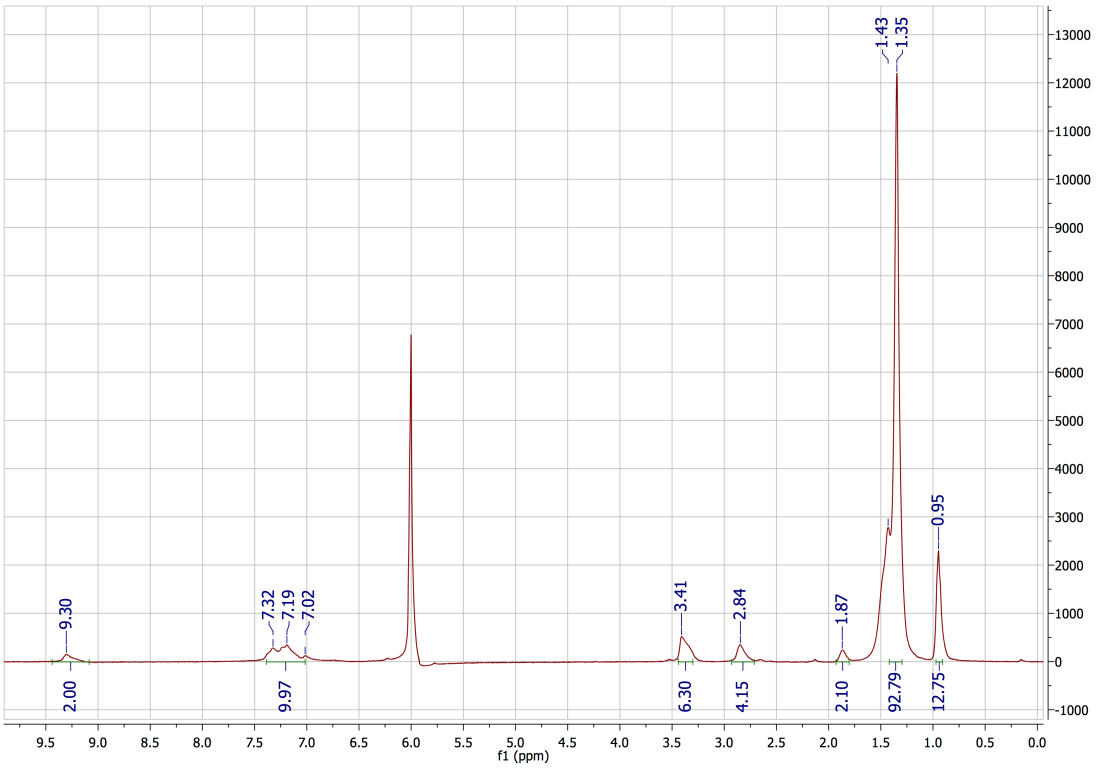
1.43
1.35
0.95
9.30
7.32
7.19
7.02
3.41
2.84
1.87
2.00
9.97
6.30
4.15
2.10
92.79
12.75
f1 (ppm)

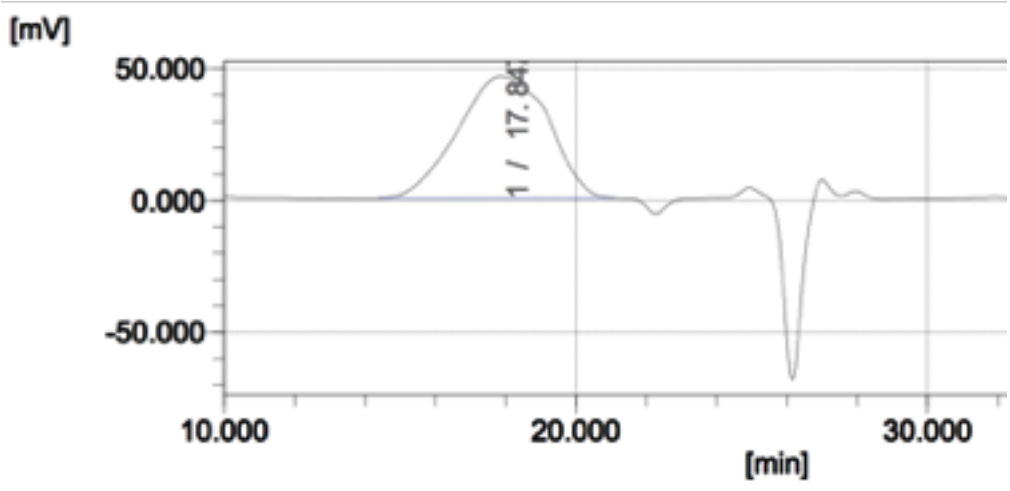
[mV]
50.000
0.000
-50.000
10.000
20.000
30.000
[min]

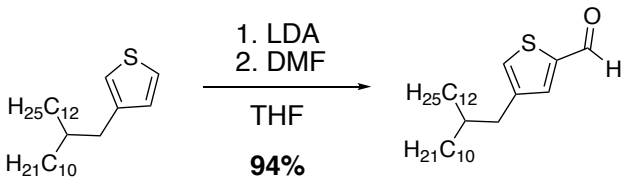

9

4-(2-decyltetradecyl)thiophene-2-carbaldehyde (9): To an oven-dried round bottom flask was added 3-(2-decyltetradecyl)thiophene (3.63 g, 8.65 mmol) and THF (60 mL), and the flask was brought to -78^{o} C (**Flask 1**). To a separate oven-dried round bottom flask was added diisopropylamine (0.96 g, 9.51 mmol) and THF (8 mL), and the flask was brought to -78^{o} C (**Flask 2**). N-butyllithium (2.5 M in hexanes, 3.6 mL, 9.07 mmol) was added dropwise to **Flask 2** under argon at -78^{o} C to generate lithium diisopropylamide (LDA). The solution was allowed to stir for 10 minutes at -78^{o} C, then brought to 0^{o} C for 10 minutes, and finally returned to -78^{o} C. **Flask 2** was added dropwise into **Flask 1** under argon at -78^{o} C, after which the solution was stirred for 10 minutes. The solution was warmed to 0^{o} C for 10 minutes, and then returned to -78^{o} C, at which point DMF (5 mL) was added to the solution. The solution was allowed to stir overnight, after which the THF was removed *via* rotary evaporation. The compound was purified through column chromatography (silica gel, 1:9 EtOAc:hexanes) to afford **9** (3.28 g, 94%) as a clear oil. ^{1}H NMR (500 MHz, $CDCl_3$): δ: 9.90 (d, J = 1.2 Hz, 1H), 7.59 (d, J = 1.2 Hz, 1H), 7.36 (s, 1H), 2.59 (d, J = 6.8 Hz, 2H), 1.62 (m, 1H), 1.27 (m, 40H), 0.90 (t, J = 7 Hz, 6H). ^{13}C NMR (500 MHz, $CDCl_3$): δ:.182.88, 143.39, 143.27, 137.53, 131.09, 38.77, 34.43, 33.00, 31.74, 31.72, 29.77, 29.48, 29.46, 29.42, 29.18, 29.14, 26.41, 22.51, 13.95. HRMS (ESI MS) *m/z*: theor: 448.3738 found: 448.3735.

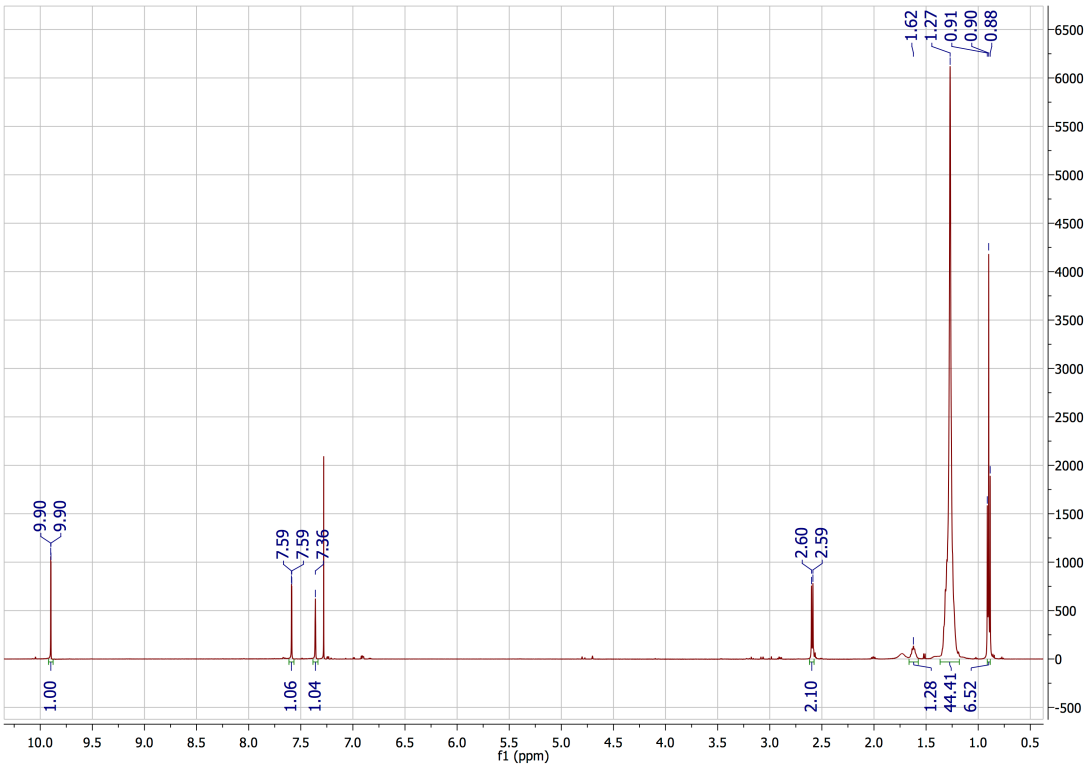
9.90
9.90
7.59
7.59
7.36
2.60
2.59
1.62
1.27
0.91
0.90
0.88
1.00
1.06
1.04
2.10
1.28
44.41
6.52
f1 (ppm)

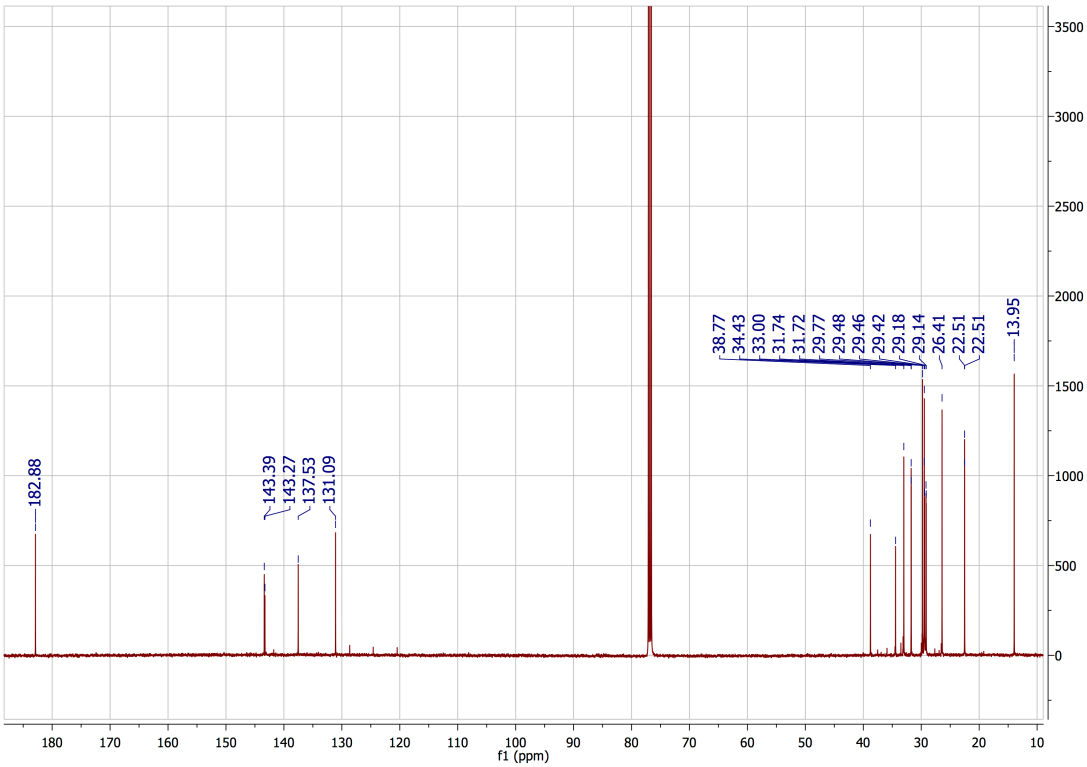
182.88
143.39
143.27
137.53
131.09
38.77
34.43
33.00
31.74
31.72
29.77
29.48
29.46
29.42
29.18
29.14
26.41
22.51
22.51
13.95
f1 (ppm)

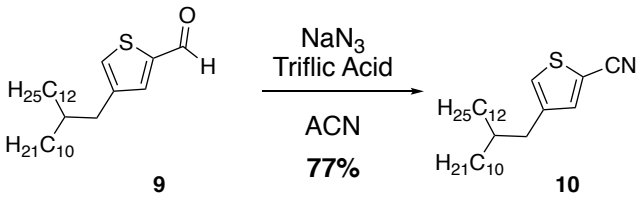

4-(2-decyltetradecyl)thiophene-2-carbonitrile (10): To an oven-dried round bottom was added **9** (3.25 g, 7.24 mmol), sodium azide (706 mg, 10.86 mmol) and acetonitrile (15 mL), and the solution was allowed to stir at room temperature for 5 minutes. Triflic acid (3.26 g, 21.72 mmol) was slowly added to the solution under argon, after which the solution was stirred for 10 minutes. The reaction was quenched with a solution of K_2CO_3 in H_2O and extracted with DCM. The organic layers were collected and extracted with H_2O, and the organic layers were collected and condensed. The compound was purified through column chromatography (silica gel, hexanes) to afford **10** (2.48 g, 77%) as a clear oil. ^{1}H NMR (500 MHz, $CDCl_3$): δ: 7.43 (s, 1H), 7.18 (s, 1H), 2.57 (d, J = 6.8 Hz, 2H), 1.60 (m, 1H), 1.28 (m, 40H), 0.91 (t, J = 6.9 Hz, 6H). ^{13}C NMR (500 MHz, $CDCl_3$): δ: 142.75, 138.63, 128.06, 114.44, 109.06, 38.71, 34.24, 32.96, 31.74, 31.72, 29.75, 29.47, 29.46, 29.41, 29.17, 29.13, 26.37, 22.52, 22.50, 13.95. HRMS (ESI MS) *m/z*: theor: 445.3742 found: 445.3755.

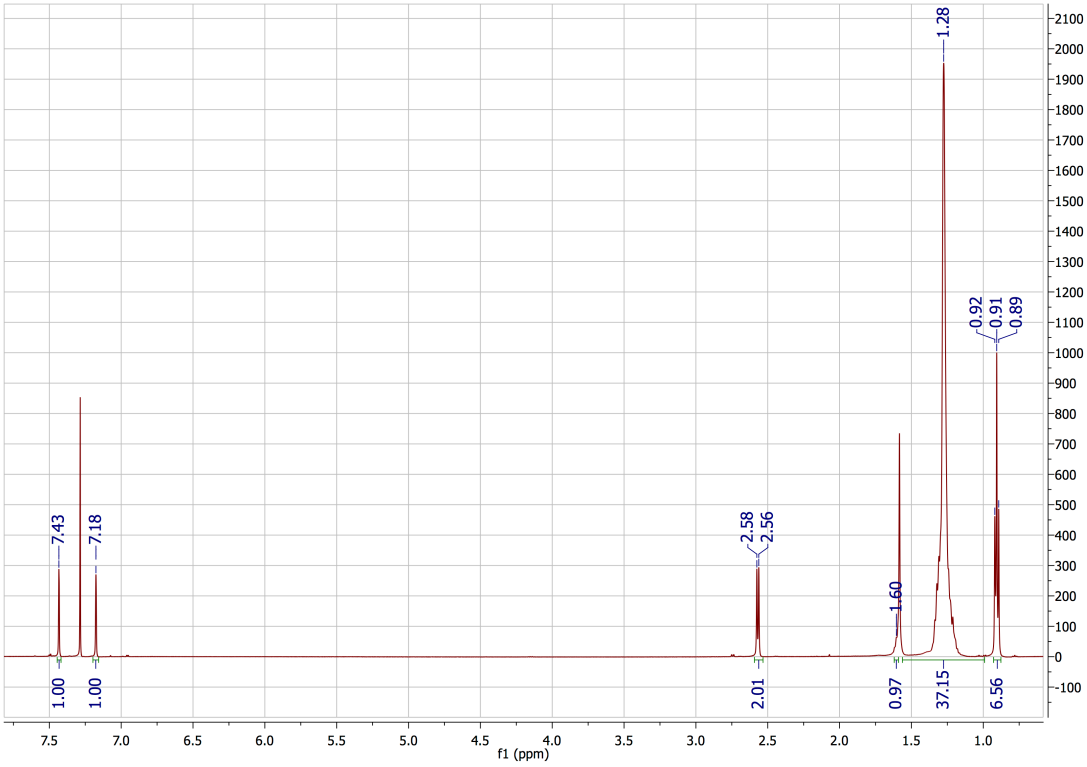
7.43
7.18
2.58
2.56
1.60
1.28
0.92
0.91
0.89
1.00
1.00
2.01
0.97
37.15
6.56
f1 (ppm)

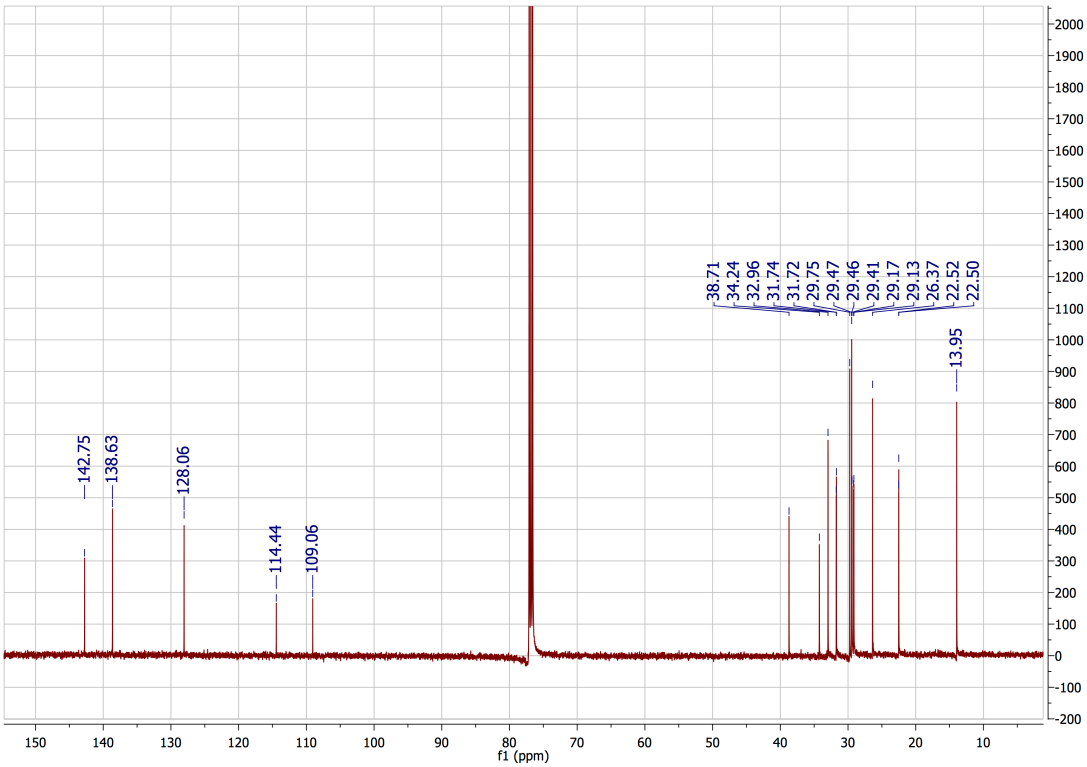
38.71
34.24
32.96
31.74
31.72
29.75
29.47
29.46
29.41
29.17
29.13
26.37
22.52
22.50
13.95
142.75
138.63
128.06
114.44
109.06
f1 (ppm)

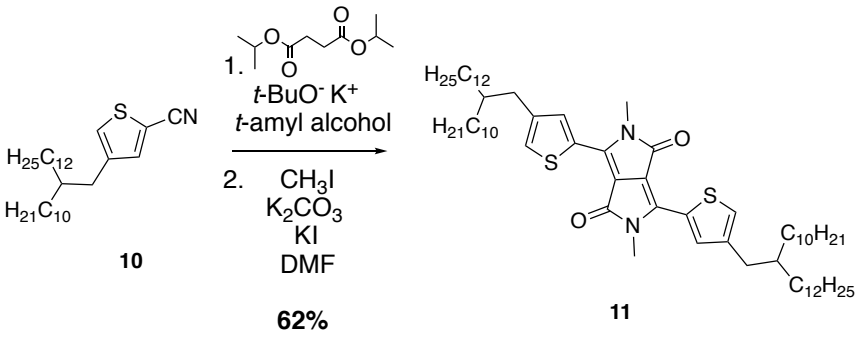

3,6-bis(4-(2-decyltetradecyl)thiophen-2-yl)-2,5-dimethyl-2,5-dihydropyrrolo[3,4-*c*]pyrrole-1,4-dione (11): To an oven-dried round bottom was added **10** (1.30 g, 2.91 mmol), potassium *t*-butoxide (490 mg, 1.45 mmol) and *t*-amyl alcohol (10 mL), and the solution was heated to 110° C. Diisopropyl succinate (295 mg, 1.45 mmol) dissolved in *t*-amyl alcohol (2 mL) was added dropwise to the reaction, and the solution was allowed to stir at 110° C overnight. The reaction was cooled to room temperature, then slowly quenched with acetic acid (1 mL). The reaction was poured into methanol (50 mL) and stirred for 1 hour, after which the solution was filtered. The resulting precipitate was washed with methanol and H_2O, and the red powder was dried under vacuum overnight. After drying, the red powder was added to an oven-dried round bottom flask along with methyl iodide (816 mg, 5.75 mmol), K_2CO_3 (800 mg, 5.75 mmol), potassium iodide (200 mg, 1.43 mmol), and DMF (15 mL). The solution was stirred overnight at 60° C, after which the DMF was removed *via* rotary evaporation. The product was dissolved into DCM and extracted with H_2O and brine. The organic layers were collected and condensed. The compound was purified through column chromatography (silica gel, DCM) to afford **11** (880 mg, 62%) as a red solid. ^{1}H NMR (500 MHz, $CDCl_3$): δ: 8.76 (d, J = 1.3 Hz, 2H), 7.26 (d, J = 1.3 Hz, 2H), 3.64 (s, 6H), 2.77 (d, J = 6.9 Hz, 4H), 1.74 (m, 2H), 1.27 (m, 80H), 0.89 (t, J = 6.3 Hz, 12H). ^{13}C NMR (500 MHz, $CDCl_3$): δ: 161.17,

144.10, 140.30, 136.65, 129.86, 127.18, 106.82, 38.87, 34.81, 33.24, 31.94, 30.05, 29.70, 29.68, 29.64, 29.38, 29.36, 29.17, 26.52, 22.70, 14.14. HRMS (ESI MS) *m/z*: theor: 1000.7852 found: 1000.7850.

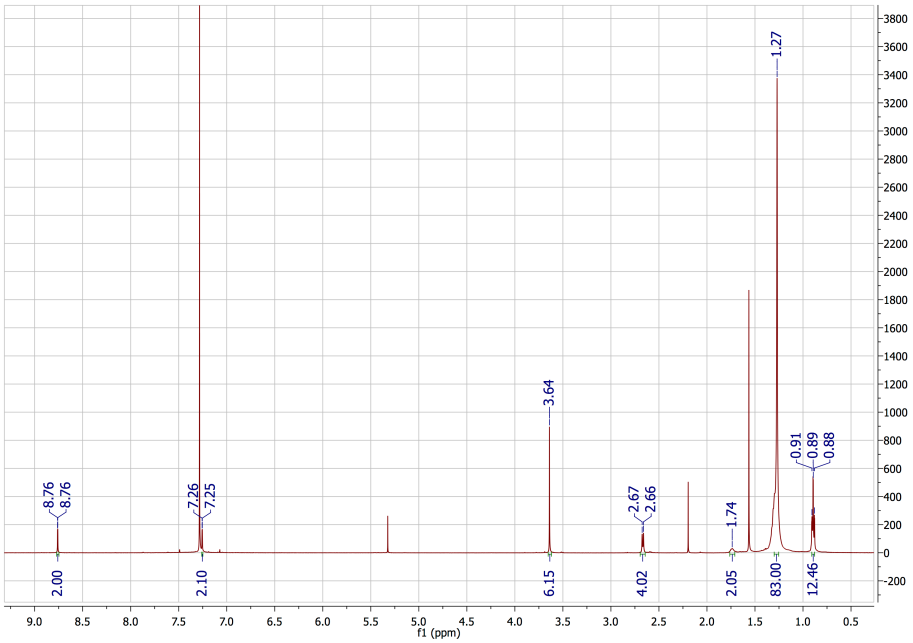

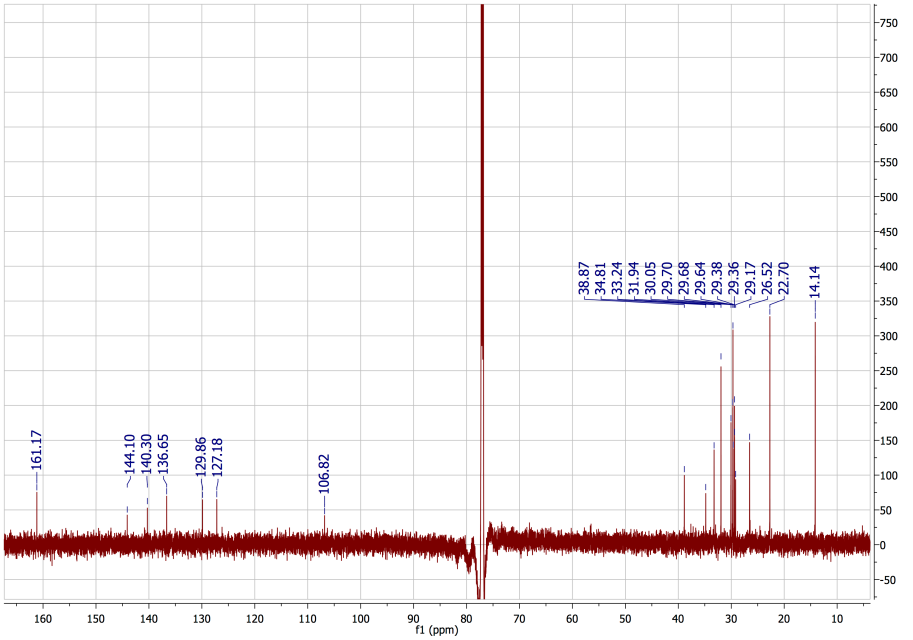

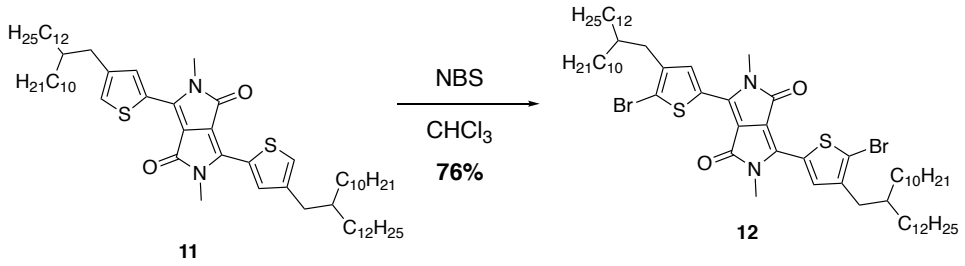

3,6-bis(5-bromo-4-(2-decyltetradecyl)thiophen-2-yl)-2,5-dimethyl-2,5-dihydropyrrolo[3,4-*c*]pyrrole-1,4-dione (12): To an oven-dried round bottom flask cooled to 0°C was added **11** (880 mg, 0.878 mmol) and $CHCl_3$ (25 mL). N-bromosuccinimide (313 mg, 1.75 mmol) was added. The ice bath was removed, and the reaction was stirred in the dark overnight. The reaction was extracted with H_2O, and the organic layers were collected and condensed by rotary evaporation. The compound was purified by column chromatography (silica gel, DCM) to yield **12** (180 mg, 45% yield) as a red solid. ^{1}H NMR (500 MHz, $CDCl_3$): δ: 8.63 (s, 2H), 3.58 (s, 6H), 2.61 (d, J = 7.2 Hz, 4H), 1.80 (m, 2H), 1.27 (m, 80H), 0.90 (t, J = 7.0 Hz, 12H). ^{13}C NMR (500 MHz, $CDCl_3$): δ: 160.63, 143.48, 139.15, 135.89, 129.36, 117.17, 106.79, 38.27, 33.91, 33.13, 31.76, 29.84, 29.54, 29.52, 29.49, 29.48, 29.20, 28.83, 26.28, 22.52, 13.95. HRMS (ESI MS) *m/z*: theor: 1156.6062 found: 1156.6069.

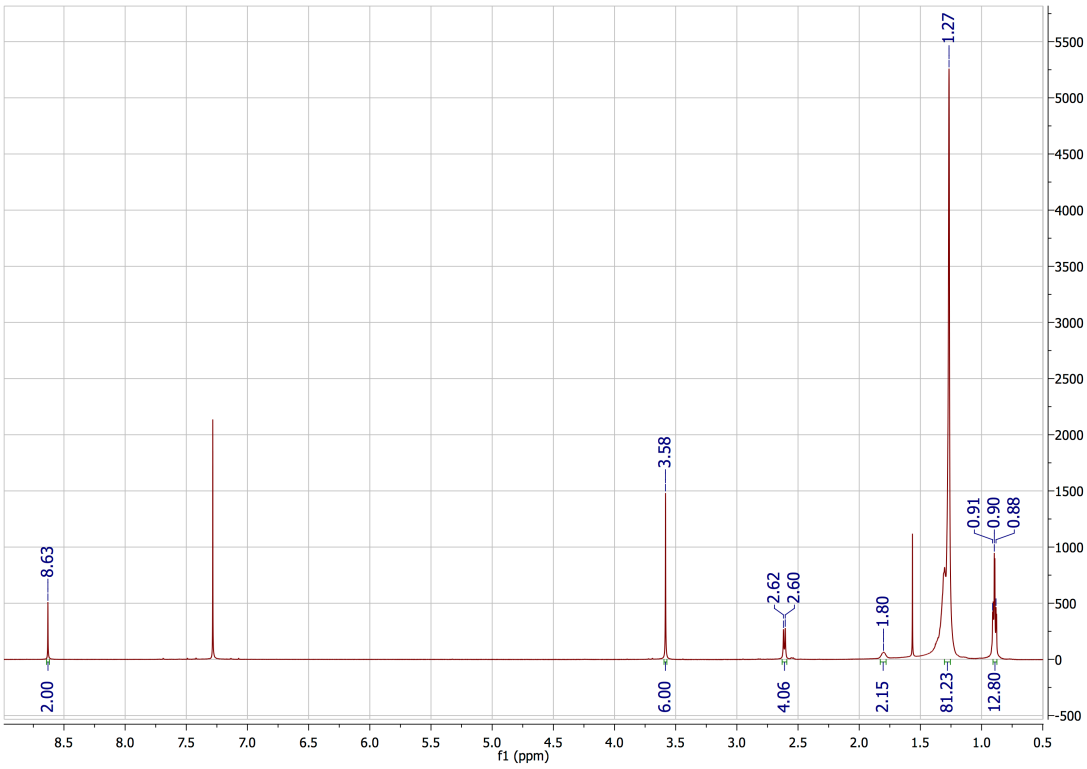
8.63
3.58
2.62
2.60
1.80
1.27
0.91
0.90
0.88
2.00
6.00
4.06
2.15
81.23
12.80
f1 (ppm)

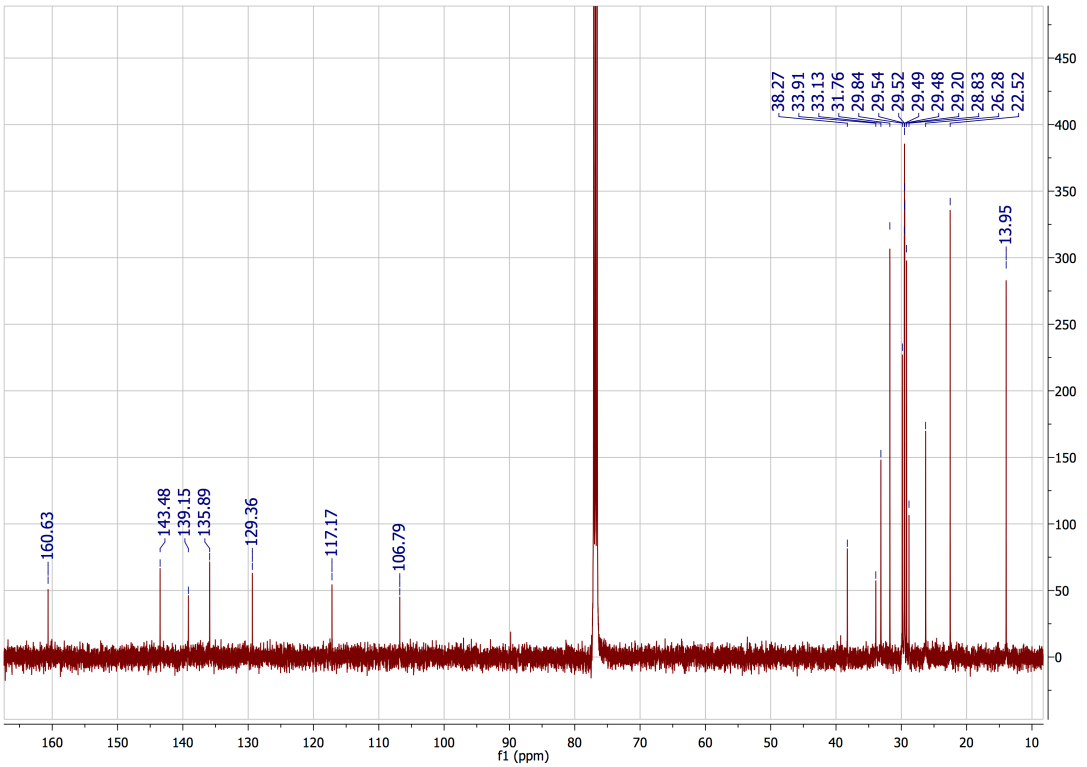
160.63
143.48
139.15
135.89
129.36
117.17
106.79
38.27
33.91
33.13
31.76
29.84
29.54
29.52
29.49
29.48
29.20
28.83
26.28
22.52
13.95
f1 (ppm)

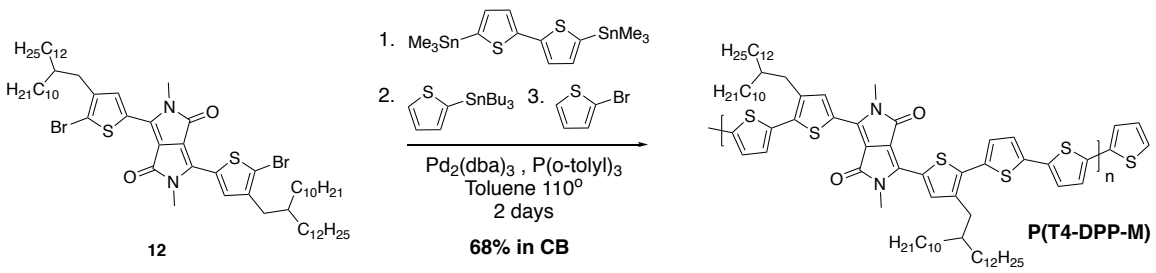

P(T4-DPP-M): To a 3-necked oven-dried 25-mL round bottom flask was added **12** (105 mg, 0.091 mmol). The vessel was brought into an argon glove box, where 5,5'-bis(trimethylstannyl)-2,2'-bithiophene (45 mg, 0.091 mmol), $Pd_2(dba)_3$ (3 mg, 0.003 mmol), and $P(o\text{-}tol)_3$ (4 mg, 0.011 mmol) was added to the vessel. The flask was equipped with a condenser, sealed, and removed from the glove box. Dry, degassed toluene (2 mL) was added. The reaction was stirred for 48 hours at 110 °C. Tributyl(thiophen-2-yl) stannane (0.1 mL) was added at 48 hours; 2-bromothiophene (0.1 mL) was added at 54 hours. The reaction was cooled to 60° C, after which a spatula tip of palladium scavenger (diethylammonium diethyldithiocarbamate) was added at 60 hours and stirred for an additional hour. After the reaction was cooled to room temperature, the product was precipitated into methanol and filtered. The precipitate was purified by Soxhlet extraction (solvents used: methanol, acetone, hexane, dichloromethane, chloroform, chlorobenzene). Product in the chlorobenzene fraction was condensed to ~5 mL, precipitated into methanol, and dried by vacuum filtration to yield polymer **P(T4-DPP-M)** (72 mg, 68% yield) as a dark purple solid. Mn: 63 kDa, Mw: 132 kDa, Đ: 2.08 vs. polystyrene standard in 1,2,4-trichlorobenzene at 140°C. Anal. calcd. for $C_{82}H_{116}N2O_2S_4$: C (74.30) H (9.53) N (2.41) S (11.02), Found: C (73.68) H (9.47) N (2.36) S (11.15).

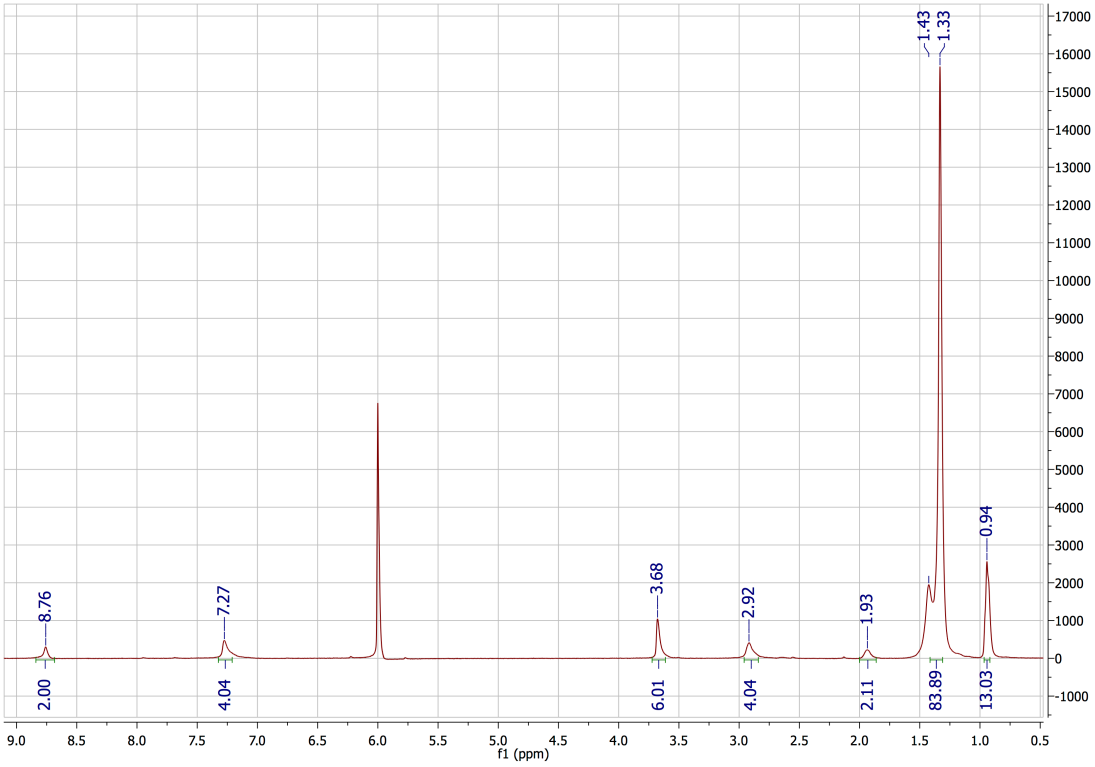
1.43
1.33
0.94
3.68
2.92
1.93
8.76
7.27
2.00
4.04
6.01
4.04
2.11
83.89
13.03
f1 (ppm)

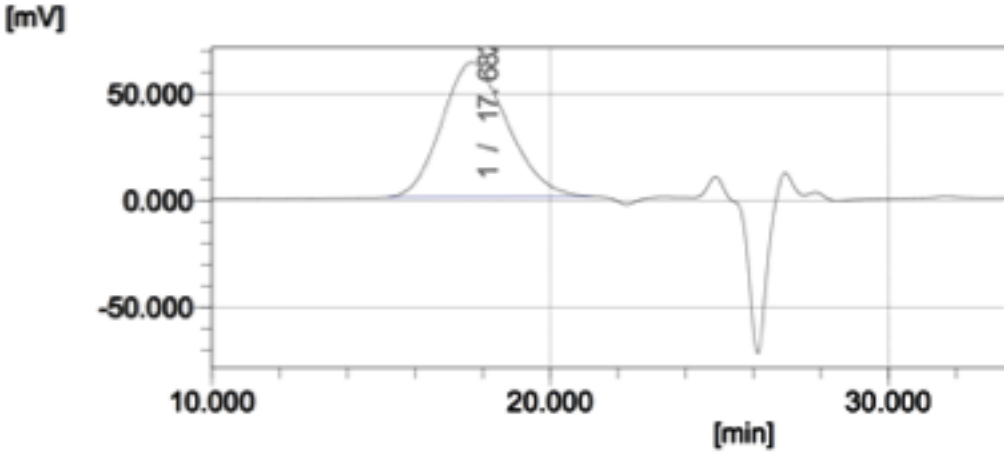
[mV]
50.000
0.000
-50.000
10.000
20.000
30.000
[min]

5.7 Blade Coating Conditions for Organic Photovoltaic Active Layers

P(T4-TPD-M):$PC_{71}BM$ (1:1.2): A 40 mg/mL solution of a 1:1.2 blend of **P(T4-TPD-M)**:$PC_{71}BM$ in 1:1 chlorobenzene:o-dichlorobenzene was stirred overnight at 85° C. 3% by volume of DIO was added to the solution and allowed to stir for ~30 minutes prior to coating. From the 85° C solution, films were blade coated at a speed of 20 mm/s, with a blade height of 200 μm, and a room temperature stage.

P(T4-TPD-M):ITIC (1:1): A 40 mg/mL solution of a 1:1 blend of **P(T4-TPD-M)**:ITIC in 1:1 chlorobenzene:o-dichlorobenzene was stirred overnight at 85° C. 3% by volume of CN was added to the solution and allowed to stir for ~30 minutes prior to coating. From the 85° C solution, films were blade coated at a speed of 20 mm/s, with a blade height of 200 μm, and a room temperature stage.

P(T4-DPP-M):$PC_{71}BM$ (1:1.2): A 30 mg/mL solution of a 1:1.2 blend of **P(T4-DPP-M)**:$PC_{71}BM$ in 1:1 chlorobenzene:o-dichlorobenzene was stirred overnight at 85° C. 3% by volume of DIO was added to the solution and allowed to stir for ~30 minutes prior to coating. From the 85° C solution, films were blade coated at a speed of 20 mm/s, with a blade height of 200 μm, and an 80° C stage.

P(T4-DPP-M):ITIC (1:1): A 30 mg/mL solution of a 1:1 blend of **P(T4-DPP-M)**:ITIC in 1:1 chlorobenzene:o-dichlorobenzene was stirred overnight at 85° C. 3% by volume of CN was added to the solution and allowed to stir for ~30 minutes prior to coating. From the 85° C solution, films were blade coated at a speed of 20 mm/s, with a blade height of 200 μm, and an 80° C stage.

P(T4-iI-M):$PC_{71}BM$ (1:1.2): A 30 mg/mL solution of a 1:1.2 blend of **P(T4-iI-M)**:$PC_{71}BM$ in 1:1 chlorobenzene:o-dichlorobenzene was stirred overnight at 85° C. 3% by volume of DIO was added to the solution and allowed to stir for ~30 minutes prior to coating. From the 85° C solution, films were blade coated at a speed of 20 mm/s, with a blade height of 200 μm, and a 70° C stage.

P(T4-iI-M):ITIC (1:1): A 30 mg/mL solution of a 1:1 blend of **P(T4-DPP-M)**:ITIC in 1:1 chlorobenzene:o-dichlorobenzene was stirred overnight at 85° C. 3% by volume of CN was added to the solution and allowed to stir for ~30 minutes prior to coating. From the 85° C solution, films were blade coated at a speed of 20 mm/s, with a blade height of 200 μm, and a 70° C stage.

REFERENCES

1. Tang, C. W.; VanSlyke, S. A., Organic electroluminescent diodes. *Applied Physics Letters* **1987,** *51* (12), 913-915.

2. Kordt, P.; Holst, J. J. M. v. d.; Helwi, M. A.; Kowalsky, W.; May, F.; Badinski, A.; Lennartz, C.; Andrienko, D., Modeling of Organic Light Emitting Diodes: From Molecular to Device Properties. *Advanced Functional Materials* **2015,** *25* (13), 1955-1971.

3. Yang, Z.; Mao, Z.; Xie, Z.; Zhang, Y.; Liu, S.; Zhao, J.; Xu, J.; Chi, Z.; Aldred, M. P., Recent advances in organic thermally activated delayed fluorescence materials. ng m*Chemical Society Reviews* **2017,** *46* (3), 915-1016.

4. Tsumura, A.; Koezuka, H.; Ando, T., Macromolecular electronic device: Field-effect transistor with a polythiophene thin film. *Applied Physics Letters* **1986,** *49* (18), 1210-1212.

5. Sirringhaus, H., 25th Anniversary Article: Organic Field-Effect Transistors: The Path Beyond Amorphous Silicon. *Advanced Materials* **2014,** *26* (9), 1319-1335.

6. Kang, H.; Lee, W.; Oh, J.; Kim, T.; Lee, C.; Kim, B. J., From Fullerene–Polymer to All-Polymer Solar Cells: The Importance of Molecular Packing, Orientation, and Morphology Control. *Accounts of Chemical Research* **2016,** *49* (11), 2424-2434.

7. Zhang, G.; Zhao, J.; Chow, P. C. Y.; Jiang, K.; Zhang, J.; Zhu, Z.; Zhang, J.; Huang, F.; Yan, H., Nonfullerene Acceptor Molecules for Bulk Heterojunction Organic Solar Cells. *Chemical Reviews* **2018**.

8. Liu, C.; Wang, K.; Gong, X.; Heeger, A. J., Low bandgap semiconducting polymers for polymeric photovoltaics. *Chemical Society Reviews* **2016,** *45* (17), 4825-4846.

9. Beaujuge, P. M.; Reynolds, J. R., Color Control in π-Conjugated Organic Polymers for Use in Electrochromic Devices. *Chemical Reviews* **2010,** *110* (1), 268-320.

10. Armin, A.; Jansen-van Vuuren, R. D.; Kopidakis, N.; Burn, P. L.; Meredith, P., Narrowband light detection via internal quantum efficiency manipulation of organic photodiodes. *Nature Communications* **2015,** *6*, 6343.

11. Ostroverkhova, O., Organic Optoelectronic Materials: Mechanisms and Applications. *Chemical Reviews* **2016,** *116* (22), 13279-13412.

12. Yi, H. T.; Payne, M. M.; Anthony, J. E.; Podzorov, V., Ultra-flexible solution-processed organic field-effect transistors. *Nat Commun* **2012,** *3*, 1259.

13. Søndergaard, R. R.; Hösel, M.; Krebs, F. C., Roll-to-Roll fabrication of large area functional organic materials. *Journal of Polymer Science Part B: Polymer Physics* **2013,** *51* (1), 16-34.

14. Liang, Y.; Feng, D.; Wu, Y.; Tsai, S.-T.; Li, G.; Ray, C.; Yu, L., Highly Efficient Solar Cell Polymers Developed via Fine-Tuning of Structural and Electronic Properties. *Journal of the American Chemical Society* **2009,** *131* (22), 7792-7799.

15. Rivnay, J.; Owens, R. M.; Malliaras, G. G., The Rise of Organic Bioelectronics. *Chemistry of Materials* **2013,** *26* (1), 679-685.

16. Su, W. P.; Schrieffer, J. R.; Heeger, A. J., Solitons in Polyacetylene. *Physical Review Letters* **1979,** *42* (25), 1698-1701.

17. Salzner, U.; Lagowski, J. B.; Pickup, P. G.; Poirier, R. A., Comparison of geometries and electronic structures of polyacetylene, polyborole, polycyclopentadiene, polypyrrole, polyfuran, polysilole, polyphosphole, polythiophene, polyselenophene and polytellurophene. *Synthetic Metals* **1998,** *96* (3), 177-189.

18. Lövenich, W., PEDOT-properties and applications. *Polymer Science Series C* **2014,** *56* (1), 135-143.

19. Wang, L.; Nan, G.; Yang, X.; Peng, Q.; Li, Q.; Shuai, Z., Computational methods for design of organic materials with high charge mobility. *Chemical Society Reviews* **2010,** *39* (2), 423-434.

20. Takeya, J.; Yamagishi, M.; Tominari, Y.; Hirahara, R.; Nakazawa, Y.; Nishikawa, T.; Kawase, T.; Shimoda, T.; Ogawa, S., Very high-mobility organic single-crystal transistors with in-crystal conduction channels. *Applied Physics Letters* **2007,** *90* (10), 102120.

21. Tu, G.; Bilge, A.; Adamczyk, S.; Forster, M.; Heiderhoff, R.; Balk, L. J.; Mühlbacher, D.; Morana, M.; Koppe, M.; Scharber, M. C.; Choulis, S. A.; Brabec, C. J.; Scherf, U., The Influence of Interchain Branches on Solid State Packing, Hole Mobility and Photovoltaic Properties of Poly(3-hexylthiophene) (P3HT). *Macromolecular Rapid Communications* **2007,** *28* (17), 1781-1785.

22. Shirota, Y.; Kageyama, H., Charge Carrier Transporting Molecular Materials and Their Applications in Devices. *Chemical Reviews* **2007,** *107* (4), 953-1010.

23. Coropceanu, V.; Cornil, J.; da Silva Filho, D. A.; Olivier, Y.; Silbey, R.; Brédas, J.-L., Charge Transport in Organic Semiconductors. *Chemical Reviews* **2007,** *107* (4), 926-952.

24. Kuo, M.-Y.; Chen, H.-Y.; Chao, I., Cyanation: Providing a Three-in-One Advantage for the Design of n-Type Organic Field-Effect Transistors. *Chemistry – A European Journal* **2007,** *13* (17), 4750-4758.

25. Malagoli, M.; Brédas, J. L., Density functional theory study of the geometric structure and energetics of triphenylamine-based hole-transporting molecules. *Chemical Physics Letters* **2000,** *327* (1–2), 13-17.

26. Klimkāns, A.; Larsson, S., Reorganization energies in benzene, naphthalene, and anthracene. *Chemical Physics* **1994,** *189* (1), 25-31.

27. McNeill, R.; Siudak, R.; Wardlaw, J.; Weiss, D., Electronic Conduction in Polymers. I. The Chemical Structure of Polypyrrole. *Australian Journal of Chemistry* **1963,** *16* (6), 1056-1075.

28. Bolto, B.; Weiss, D., Electronic Conduction in Polymers. II. The Electrochemical Reduction of Polypyrrole at Controlled Potential. *Australian Journal of Chemistry* **1963,** *16* (6), 1076-1089.

29. Bolto, B.; McNeill, R.; Weiss, D., Electronic Conduction in Polymers. III. Electronic Properties of Polypyrrole. *Australian Journal of Chemistry* **1963,** *16* (6), 1090-1103.

30. De Surville, R.; Jozefowicz, M.; Yu, L. T.; Pepichon, J.; Buvet, R., Electrochemical chains using protolytic organic semiconductors. *Electrochimica Acta* **1968,** *13* (6), 1451-1458.

31. Jozefowicz, M.; Yu, L. T.; Perichon, J.; Buvet, R., Propriétés Nouvelles des Polymères Semiconducteurs. *Journal of Polymer Science Part C: Polymer Symposia* **1969,** *22* (2), 1187-1195.

32. Ito, T.; Shirakawa, H.; Ikeda, S., Simultaneous polymerization and formation of polyacetylene film on the surface of concentrated soluble Ziegler-type catalyst solution. *Journal of Polymer Science: Polymer Chemistry Edition* **1974,** *12* (1), 11-20.

33. Chiang, C. K.; Fincher, C. R.; Park, Y. W.; Heeger, A. J.; Shirakawa, H.; Louis, E. J.; Gau, S. C.; MacDiarmid, A. G., Electrical Conductivity in Doped Polyacetylene. *Physical Review Letters* **1977,** *39* (17), 1098-1101.

34. Shirakawa, H.; Louis, E. J.; MacDiarmid, A. G.; Chiang, C. K.; Heeger, A. J., Synthesis of electrically conducting organic polymers: halogen derivatives of polyacetylene, (CH). *Journal of the Chemical Society, Chemical Communications* **1977,** (16), 578-580.

35. Loewe, R. S.; Khersonsky, S. M.; McCullough, R. D., A Simple Method to Prepare Head-to-Tail Coupled, Regioregular Poly(3-alkylthiophenes) Using Grignard Metathesis. *Advanced Materials* **1999,** *11* (3), 250-253.

36. Bredas, J. L.; Silbey, R.; Boudreaux, D. S.; Chance, R. R., Chain-length dependence of electronic and electrochemical properties of conjugated systems: polyacetylene, polyphenylene, polythiophene, and polypyrrole. *Journal of the American Chemical Society* **1983,** *105* (22), 6555-6559.

37. Klaerner, G.; Miller, R. D., Polyfluorene Derivatives: Effective Conjugation Lengths from Well-Defined Oligomers. *Macromolecules* **1998,** *31* (6), 2007-2009.

38. Schaffer, H. E.; Chance, R. R.; Knoll, K.; Schrock, R. R.; Silbey, R., Linear Optical Properties of a Series of Polyacetylene Oligomers. In *Conjugated Polymeric Materials: Opportunities in Electronics, Optoelectronics, and Molecular Electronics*, Brédas, J. L.; Chance, R. R., Eds. Springer Netherlands: Dordrecht, 1990; pp 365-376.

39. Meier, H.; Stalmach, U.; Kolshorn, H., Effective conjugation length and UV/vis spectra of oligomers. *Acta Polymerica* **1997,** *48* (9), 379-384.

40. Lawrence, J.; Goto, E.; Ren, J. M.; McDearmon, B.; Kim, D. S.; Ochiai, Y.; Clark, P. G.; Laitar, D.; Higashihara, T.; Hawker, C. J., A Versatile and Efficient Strategy to Discrete Conjugated Oligomers. *Journal of the American Chemical Society* **2017,** *139* (39), 13735-13739.

41. Brédas, J. L.; Street, G. B.; Thémans, B.; André, J. M., Organic polymers based on aromatic rings (polyparaphenylene, polypyrrole, polythiophene): Evolution of the electronic properties as a function of the torsion angle between adjacent rings. *The Journal of Chemical Physics* **1985,** *83* (3), 1323-1329.

42. McCullough, R. D.; Lowe, R. D.; Jayaraman, M.; Anderson, D. L., Design, synthesis, and control of conducting polymer architectures: structurally homogeneous poly(3-alkylthiophenes). *The Journal of Organic Chemistry* **1993,** *58* (4), 904-912.

43. Kerszulis, J. A.; Amb, C. M.; Dyer, A. L.; Reynolds, J. R., Follow the Yellow Brick Road: Structural Optimization of Vibrant Yellow-to-Transmissive Electrochromic Conjugated Polymers. *Macromolecules* **2014,** *47* (16), 5462-5469.

44. Kerszulis, J. Reading the Rainbow: Tailoring the Properties of Electrochromic Polymers. Dissertation, Georgia Institute of Technology, 2014.

45. Spencer, H. J.; Skabara, P. J.; Giles, M.; McCulloch, I.; Coles, S. J.; Hursthouse, M. B., The first direct experimental comparison between the hugely contrasting properties of PEDOT and the all-sulfur analogue PEDTT by analogy with well-defined EDTT-EDOT copolymers. *Journal of Materials Chemistry* **2005,** *15* (45), 4783-4792.

46. Zhang, Q.; Kelly, M. A.; Bauer, N.; You, W., The Curious Case of Fluorination of Conjugated Polymers for Solar Cells. *Accounts of Chemical Research* **2017,** *50* (9), 2401-2409.

47. Havinga, E. E.; ten Hoeve, W.; Wynberg, H., Alternate donor-acceptor small-band-gap semiconducting polymers; Polysquaraines and polycroconaines. *Synthetic Metals* **1993,** *55* (1), 299-306.

48. Nielsen, C. B.; Giovannitti, A.; Sbircea, D.-T.; Bandiello, E.; Niazi, M. R.; Hanifi, D. A.; Sessolo, M.; Amassian, A.; Malliaras, G. G.; Rivnay, J.; McCulloch, I., Molecular

Design of Semiconducting Polymers for High-Performance Organic Electrochemical Transistors. *Journal of the American Chemical Society* **2016,** *138* (32), 10252-10259.

49. Jiang, H.; Taranekar, P.; Reynolds, J. R.; Schanze, K. S., Conjugated Polyelectrolytes: Synthesis, Photophysics, and Applications. *Angewandte Chemie International Edition* **2009,** *48* (24), 4300-4316.

50. Hsu, W. P.; Levon, K.; Ho, K. S.; Myerson, A. S.; Kwei, T. K., Side-chain order in poly(3-alkylthiophenes). *Macromolecules* **1993,** *26* (6), 1318-1323.

51. Grand, C.; Zajaczkowski, W.; Deb, N.; Lo, C. K.; Hernandez, J. L.; Bucknall, D. G.; Müllen, K.; Pisula, W.; Reynolds, J. R., Morphology Control in Films of Isoindigo Polymers by Side-Chain and Molecular Weight Effects. *ACS Applied Materials & Interfaces* **2017,** *9* (15), 13357-13368.

52. Lei, T.; Dou, J.-H.; Pei, J., Influence of Alkyl Chain Branching Positions on the Hole Mobilities of Polymer Thin-Film Transistors. *Advanced Materials* **2012,** *24* (48), 6457-6461.

53. Graham, K. R.; Cabanetos, C.; Jahnke, J. P.; Idso, M. N.; El Labban, A.; Ngongang Ndjawa, G. O.; Heumueller, T.; Vandewal, K.; Salleo, A.; Chmelka, B. F.; Amassian, A.; Beaujuge, P. M.; McGehee, M. D., Importance of the Donor:Fullerene Intermolecular Arrangement for High-Efficiency Organic Photovoltaics. *Journal of the American Chemical Society* **2014,** *136* (27), 9608-9618.

54. Guo, X.; Watson, M. D., Conjugated Polymers from Naphthalene Bisimide. *Organic Letters* **2008,** *10* (23), 5333-5336.

55. Liu, J.; Feng, G.; Geng, J.; Liu, B., A Facile Strategy toward Conjugated Polyelectrolyte with Oligopeptide as Pendants for Biological Applications. *ACS Applied Materials & Interfaces* **2013,** *5* (11), 4511-4515.

56. Kim, H. J.; Han, A. R.; Cho, C.-H.; Kang, H.; Cho, H.-H.; Lee, M. Y.; Fréchet, J. M. J.; Oh, J. H.; Kim, B. J., Solvent-Resistant Organic Transistors and Thermally Stable Organic Photovoltaics Based on Cross-linkable Conjugated Polymers. *Chemistry of Materials* **2012,** *24* (1), 215-221.

57. Miyanishi, S.; Tajima, K.; Hashimoto, K., Morphological Stabilization of Polymer Photovoltaic Cells by Using Cross-Linkable Poly(3-(5-hexenyl)thiophene). *Macromolecules* **2009,** *42* (5), 1610-1618.

58. Woo, C. H.; Piliego, C.; Holcombe, T. W.; Toney, M. F.; Fréchet, J. M. J., A Quantitative Correlation between the Mobility and Crystallinity of Photo-Cross-Linkable P3HT. *Macromolecules* **2012,** *45* (7), 3057-3062.

59. Charas, A.; Ferreira, Q.; Farinhas, J.; Matos, M.; Alcácer, L.; Morgado, J., Insoluble Patterns of Cross-Linkable Conjugated Polymers from Blend Demixing in Spin Cast Films. *Macromolecules* **2009,** *42* (20), 7903-7912.

60. Scheler, E.; Strohriegl, P., Three Color Random Fluorene-Based Oligomers for Fast Micrometer-Scale Photopatterning. *Chemistry of Materials* **2010,** *22* (4), 1410-1419.

61. Jensen, J.; Dyer, A. L.; Shen, D. E.; Krebs, F. C.; Reynolds, J. R., Direct Photopatterning of Electrochromic Polymers. *Advanced Functional Materials* **2013,** *23* (30), 3728-3737.

62. Patel, D. G.; Graham, K. R.; Reynolds, J. R., A Diels–Alder crosslinkable host polymer for improved PLED performance: the impact on solution processed doped device and multilayer device performance. *Journal of Materials Chemistry* **2012,** *22* (7), 3004.

63. Beaujuge, P. M.; Amb, C. M.; Reynolds, J. R., A Side-Chain Defunctionalization Approach Yields a Polymer Electrochrome Spray-Processable from Water. *Advanced Materials* **2010,** *22* (47), 5383 - 5387.

64. Shi, P.; Amb, C. M.; Dyer, A. L.; Reynolds, J. R., Fast Switching Water Processable Electrochromic Polymers. *ACS Applied Materials & Interfaces* **2012,** *4* (12), 6512-6521.

65. Liu, J.; Kadnikova, E. N.; Liu, Y.; McGehee, M. D.; Fréchet, J. M. J., Polythiophene Containing Thermally Removable Solubilizing Groups Enhances the Interface and the Performance of Polymer−Titania Hybrid Solar Cells. *Journal of the American Chemical Society* **2004,** *126* (31), 9486-9487.

66. Edder, C.; Armstrong, P. B.; Prado, K. B.; Frechet, J. M. J., Benzothiadiazole- and pyrrole-based polymers bearing thermally cleavable solubilizing groups as precursors for low bandgap polymers. *Chemical Communications* **2006,** (18), 1965-1967.

67. Reeves, B. D.; Unur, E.; Ananthakrishnan, N.; Reynolds, J. R., Defunctionalization of Ester-Substituted Electrochromic Dioxythiophene Polymers. *Macromolecules* **2007,** *40* (15), 5344 - 5352.

68. Jakob, S.; Moreno, A.; Zhang, X.; Bertschi, L.; Smith, P.; Schlüter, A. D.; Sakamoto, J., Synthesis of Polyphenylenes from a Soluble Precursor: The "Shaving" Approach. *Macromolecules* **2010,** *43* (19), 7916-7918.

69. Thomas, C. A.; Reynolds, J. R., *ACS Symposium Series: Semiconducting Polymers - Lowering the Band Gap of Ethylenedioxythiophene Polymers: Cyanovinylene-Linked Biheterocycles*. American Chemical Society: Washington, DC, 2009; Vol. 735, p 367 - 373.

70. Smith, Z. C.; Meyer, D. M.; Simon, M. G.; Staii, C.; Shukla, D.; Thomas, S. W., Thiophene-Based Conjugated Polymers with Photolabile Solubilizing Side Chains. *Macromolecules* **2015,** *48* (4), 959-966.

71. Kosugi, M.; Shimizu, Y.; Migita, T., Reaction of allyltin compounds: II. Facile preparation of allyl ketones via allyltins. *J. Organomet. Chem.* **1977,** *129* (2), C36-C38.

72. Stille, J. K., The Palladium-Catalyzed Cross-Coupling Reactions of Organotin Reagents with Organic Electrophiles [New Synthetic Methods (58)]. *Angewandte Chemie International Edition in English* **1986,** *25* (6), 508-524.

73. Carsten, B.; He, F.; Son, H. J.; Xu, T.; Yu, L., Stille Polycondensation for Synthesis of Functional Materials. *Chem. Rev. (Washington, DC, U. S.)* **2011,** *111*, 1493-1528.

74. Bochmann, M.; Kelly, K., Palladium catalysed cross-coupling reactions with difunctional tin reagents: a general route to aromatic polymers. *Journal of the Chemical Society, Chemical Communications* **1989,** (9), 532-534.

75. Giesa, R.; Schulz, R. C., Soluble poly(1,4-phenyleneethynylene)s. *Die Makromolekulare Chemie* **1990,** *191* (4), 857-867.

76. Galarini, R.; Musco, A.; Pontellini, R.; Bolognesi, A.; Destri, S.; Catellani, M.; Mascherpa, M.; Zhuo, G., A new synthetic route to polyheteroarenediylvinylenes. *Journal of the Chemical Society, Chemical Communications* **1991,** (6), 364-365.

77. Bao, Z.; Chan, W.; Yu, L., Synthesis of conjugated polymer by the Stille Coupling Reaction. *Chemistry of Materials* **1993,** *5* (1), 2-3.

78. Bao, Z.; Chan, W. K.; Yu, L., Exploration of the Stille Coupling Reaction for the Synthesis of Functional Polymers. *Journal of the American Chemical Society* **1995,** *117* (50), 12426-12435.

79. Espinet, P.; Echavarren, A. M., The Mechanisms of the Stille Reaction. *Angewandte Chemie International Edition* **2004,** *43* (36), 4704-4734.

80. Gobalasingham, N. S.; Noh, S.; Thompson, B. C., Palladium-catalyzed oxidative direct arylation polymerization (Oxi-DArP) of an ester-functionalized thiophene. *Polymer Chemistry* **2016,** *7* (8), 1623-1631.

81. Estrada, L. A.; Deininger, J. J.; Kamenov, G. D.; Reynolds, J. R., Direct (Hetero)arylation Polymerization: An Effective Route to 3,4-Propylenedioxythiophene-Based Polymers with Low Residual Metal Content. *ACS Macro Letters* **2013,** *2* (10), 869-873.

82. Akira, K.; Taeko, I.; Minoru, Y.; Ryu-ichi, S.; Toru, T.; Toshiaki, S., Arylation and Vinylation Reactions of Benzo[b]furan via Organopalladium Intermediates. *Bulletin of the Chemical Society of Japan* **1973,** *46* (4), 1220-1225.

83. Alberico, D.; Scott, M. E.; Lautens, M., Aryl−Aryl Bond Formation by Transition-Metal-Catalyzed Direct Arylation. *Chemical Reviews* **2007,** *107* (1), 174-238.

84. Mercier, L. G.; Leclerc, M., Direct (Hetero)Arylation: A New Tool for Polymer Chemists. *Accounts of Chemical Research* **2013,** *46* (7), 1597-1605.

85. Wang, Q.; Takita, R.; Kikuzaki, Y.; Ozawa, F., Palladium-Catalyzed Dehydrohalogenative Polycondensation of 2-Bromo-3-hexylthiophene: An Efficient Approach to Head-to-Tail Poly(3-hexylthiophene). *Journal of the American Chemical Society* **2010,** *132* (33), 11420-11421.

86. Pouliot, J.-R.; Grenier, F.; Blaskovits, J. T.; Beaupré, S.; Leclerc, M., Direct (Hetero)arylation Polymerization: Simplicity for Conjugated Polymer Synthesis. *Chemical Reviews* **2016,** *116* (22), 14225-14274.

87. Bura, T.; Blaskovits, J. T.; Leclerc, M., Direct (Hetero)arylation Polymerization: Trends and Perspectives. *Journal of the American Chemical Society* **2016,** *138* (32), 10056-10071.

88. Rudenko, A. E.; Thompson, B. C., Influence of the Carboxylic Acid Additive Structure on the Properties of Poly(3-hexylthiophene) Prepared via Direct Arylation Polymerization (DArP). *Macromolecules* **2015,** *48* (3), 569-575.

89. Kline, R. J.; McGehee, M. D.; Kadnikova, E. N.; Liu, J.; Fréchet, J. M. J., Controlling the Field-Effect Mobility of Regioregular Polythiophene by Changing the Molecular Weight. *Advanced Materials* **2003,** *15* (18), 1519-1522.

90. Brinkmann, M.; Rannou, P., Effect of Molecular Weight on the Structure and Morphology of Oriented Thin Films of Regioregular Poly(3-hexylthiophene) Grown by Directional Epitaxial Solidification. *Advanced Functional Materials* **2007,** *17* (1), 101-108.

91. Noriega, R.; Rivnay, J.; Vandewal, K.; Koch, F. P. V.; Stingelin, N.; Smith, P.; Toney, M. F.; Salleo, A., A general relationship between disorder, aggregation and charge transport in conjugated polymers. *Nat Mater* **2013,** *12* (11), 1038-1044.

92. Himmelberger, S.; Vandewal, K.; Fei, Z.; Heeney, M.; Salleo, A., Role of Molecular Weight Distribution on Charge Transport in Semiconducting Polymers. *Macromolecules* **2014,** *47* (20), 7151-7157.

93. Schilinsky, P.; Asawapirom, U.; Scherf, U.; Biele, M.; Brabec, C. J., Influence of the Molecular Weight of Poly(3-hexylthiophene) on the Performance of Bulk Heterojunction Solar Cells. *Chemistry of Materials* **2005,** *17* (8), 2175-2180.

94. Katsouras, A.; Gasparini, N.; Koulogiannis, C.; Spanos, M.; Ameri, T.; Brabec, C. J.; Chochos, C. L.; Avgeropoulos, A., Systematic Analysis of Polymer Molecular Weight Influence on the Organic Photovoltaic Performance. *Macromolecular Rapid Communications* **2015,** *36* (20), 1778-1797.

95. Liu, C.; Wang, K.; Hu, X.; Yang, Y.; Hsu, C.-H.; Zhang, W.; Xiao, S.; Gong, X.; Cao, Y., Molecular Weight Effect on the Efficiency of Polymer Solar Cells. *ACS Applied Materials & Interfaces* **2013,** *5* (22), 12163-12167.

96. Kang, H.; Uddin, M. A.; Lee, C.; Kim, K.-H.; Nguyen, T. L.; Lee, W.; Li, Y.; Wang, C.; Woo, H. Y.; Kim, B. J., Determining the Role of Polymer Molecular Weight for High-Performance All-Polymer Solar Cells: Its Effect on Polymer Aggregation and Phase Separation. *Journal of the American Chemical Society* **2015,** *137* (6), 2359-2365.

97. Po, R.; Bianchi, G.; Carbonera, C.; Pellegrino, A., "All That Glisters Is Not Gold": An Analysis of the Synthetic Complexity of Efficient Polymer Donors for Polymer Solar Cells. *Macromolecules* **2015,** *48* (3), 453-461.

98. Darling, S. B.; You, F., The case for organic photovoltaics. *RSC Advances* **2013,** *3* (39), 17633-17648.

99. Willmann, J.; Stocker, D.; Dörsam, E., Characteristics and evaluation criteria of substrate-based manufacturing. Is roll-to-roll the best solution for printed electronics? *Organic Electronics* **2014,** *15* (7), 1631-1640.

100. Ro, H. W.; Downing, J. M.; Engmann, S.; Herzing, A. A.; DeLongchamp, D. M.; Richter, L. J.; Mukherjee, S.; Ade, H.; Abdelsamie, M.; Jagadamma, L. K.; Amassian, A.; Liu, Y.; Yan, H., Morphology changes upon scaling a high-efficiency, solution-processed solar cell. *Energy & Environmental Science* **2016,** *9* (9), 2835-2846.

101. Li, J.; Zhao, Y.; Tan, H. S.; Guo, Y.; Di, C.-A.; Yu, G.; Liu, Y.; Lin, M.; Lim, S. H.; Zhou, Y.; Su, H.; Ong, B. S., A stable solution-processed polymer semiconductor with record high-mobility for printed transistors. *Scientific Reports* **2012,** *2*, 754.

102. Padilla, J.; Österholm, A. M.; Dyer, A. L.; Reynolds, J. R., Process controlled performance for soluble electrochromic polymers. *Solar Energy Materials and Solar Cells* **2015,** *140*, 54-60.

103. Søndergaard, R.; Hösel, M.; Angmo, D.; Larsen-Olsen, T. T.; Krebs, F. C., Roll-to-roll fabrication of polymer solar cells. *Materials Today* **2012,** *15* (1), 36-49.

104. Zimmermann, B.; Schleiermacher, H. F.; Niggemann, M.; Würfel, U., ITO-free flexible inverted organic solar cell modules with high fill factor prepared by slot die coating. *Solar Energy Materials and Solar Cells* **2011,** *95* (7), 1587-1589.

105. Krebs, F. C.; Gevorgyan, S. A.; Alstrup, J., A roll-to-roll process to flexible polymer solar cells: model studies, manufacture and operational stability studies. *Journal of Materials Chemistry* **2009,** *19* (30), 5442-5451.

106. Chang, J.; Sonar, P.; Lin, Z.; Zhang, C.; Zhang, J.; Hao, Y.; Wu, J., Controlling aggregation and crystallization of solution processed diketopyrrolopyrrole based polymer for high performance thin film transistors by pre-metered slot die coating process. *Organic Electronics* **2016,** *36*, 113-119.

107. Sandström, A.; Dam, H. F.; Krebs, F. C.; Edman, L., Ambient fabrication of flexible and large-area organic light-emitting devices using slot-die coating. *Nature Communications* **2012,** *3*, 1002.

108. Krebs, F. C.; Jørgensen, M.; Norrman, K.; Hagemann, O.; Alstrup, J.; Nielsen, T. D.; Fyenbo, J.; Larsen, K.; Kristensen, J., A complete process for production of flexible large area polymer solar cells entirely using screen printing—First public demonstration. *Solar Energy Materials and Solar Cells* **2009,** *93* (4), 422-441.

109. Verilhac, J.-M.; Benwadih, M.; Seiler, A.-L.; Jacob, S.; Bory, C.; Bablet, J.; Heitzman, M.; Tallal, J.; Barbut, L.; Frère, P.; Sicard, G.; Gwoziecki, R.; Chartier, I.; Coppard, R.; Serbutoviez, C., Step toward robust and reliable amorphous polymer field-effect transistors and logic functions made by the use of roll to roll compatible printing processes. *Organic Electronics* **2010,** *11* (3), 456-462.

110. Lee, D. H.; Choi, J. S.; Chae, H.; Chung, C. H.; Cho, S. M., Highly efficient phosphorescent polymer OLEDs fabricated by screen printing. *Displays* **2008,** *29* (5), 436-439.

111. Brotherston, I. D.; Mudigonda, D. S. K.; Osborn, J. M.; Belk, J.; Chen, J.; Loveday, D. C.; Boehme, J. L.; Ferraris, J. P.; Meeker, D. L., Tailoring the electrochromic properties of devices via polymer blends, copolymers, laminates and patterns. *Electrochimica Acta* **1999,** *44* (18), 2993-3004.

112. Andersson, P.; Forchheimer, R.; Tehrani, P.; Berggren, M., Printable All-Organic Electrochromic Active-Matrix Displays. *Advanced Functional Materials* **2007,** *17* (16), 3074-3082.

113. de la Fuente Vornbrock, A.; Sung, D.; Kang, H.; Kitsomboonloha, R.; Subramanian, V., Fully gravure and ink-jet printed high speed pBTTT organic thin film transistors. *Organic Electronics* **2010,** *11* (12), 2037-2044.

114. Kopola, P.; Aernouts, T.; Guillerez, S.; Jin, H.; Tuomikoski, M.; Maaninen, A.; Hast, J., High efficient plastic solar cells fabricated with a high-throughput gravure printing method. *Solar Energy Materials and Solar Cells* **2010,** *94* (10), 1673-1680.

115. Kopola, P.; Tuomikoski, M.; Suhonen, R.; Maaninen, A., Gravure printed organic light emitting diodes for lighting applications. *Thin Solid Films* **2009,** *517* (19), 5757-5762.

116. Alem, S.; Graddage, N.; Lu, J.; Kololuoma, T.; Movileanu, R.; Tao, Y., Flexographic printing of polycarbazole-based inverted solar cells. *Organic Electronics* **2018,** *52*, 146-152.

117. Hübler, A.; Trnovec, B.; Zillger, T.; Ali, M.; Wetzold, N.; Mingebach, M.; Wagenpfahl, A.; Deibel, C.; Dyakonov, V., Printed Paper Photovoltaic Cells. *Advanced Energy Materials* **2011,** *1* (6), 1018-1022.

118. Huebler, A. C.; Doetz, F.; Kempa, H.; Katz, H. E.; Bartzsch, M.; Brandt, N.; Hennig, I.; Fuegmann, U.; Vaidyanathan, S.; Granstrom, J.; Liu, S.; Sydorenko, A.; Zillger, T.; Schmidt, G.; Preissler, K.; Reichmanis, E.; Eckerle, P.; Richter, F.; Fischer,

T.; Hahn, U., Ring oscillator fabricated completely by means of mass-printing technologies. *Organic Electronics* **2007,** *8* (5), 480-486.

119. Maisch, P.; Tam, K. C.; Lucera, L.; Egelhaaf, H.-J.; Scheiber, H.; Maier, E.; Brabec, C. J., Inkjet printed silver nanowire percolation networks as electrodes for highly efficient semitransparent organic solar cells. *Organic Electronics* **2016,** *38*, 139-143.

120. Österholm, A. M.; Shen, D. E.; Gottfried, D. S.; Reynolds, J. R., Full Color Control and High-Resolution Patterning from Inkjet Printable Cyan/Magenta/Yellow Colored-to-Colorless Electrochromic Polymer Inks. *Advanced Materials Technologies* **2016,** *1* (4), 1600063.

121. Conti, S.; Lai, S.; Cosseddu, P.; Bonfiglio, A., An Inkjet-Printed, Ultralow Voltage, Flexible Organic Field Effect Transistor. *Advanced Materials Technologies* **2017,** *2* (2), 1600212.

122. Amb, C. M.; Dyer, A. L.; Reynolds, J. R., Navigating the Color Palette of Solution-Processable Electrochromic Polymers. *Chemistry of Materials* **2011,** *23* (3), 397 - 415.

123. Nie, W.; Coffin, R. C.; Liu, J.; Li, Y.; Peterson, E. D.; MacNeill, C. M.; Noftle, R. E.; Carroll, D. L., High efficiency organic solar cells with spray coated active layers comprised of a low band gap conjugated polymer. *Applied Physics Letters* **2012,** *100* (8), 083301.

124. Bartelt, J. A.; Douglas, J. D.; Mateker, W. R.; Labban, A. E.; Tassone, C. J.; Toney, M. F.; Fréchet, J. M. J.; Beaujuge, P. M.; McGehee, M. D., Controlling Solution-Phase Polymer Aggregation with Molecular Weight and Solvent Additives to Optimize Polymer-Fullerene Bulk Heterojunction Solar Cells. *Advanced Energy Materials* **2014,** *4* (9), 1301733.

125. Liu, Y.; Zhao, J.; Li, Z.; Mu, C.; Ma, W.; Hu, H.; Jiang, K.; Lin, H.; Ade, H.; Yan, H., Aggregation and morphology control enables multiple cases of high-efficiency polymer solar cells. *Nature Communications* **2014,** *5*, 5293.

126. Rivnay, J.; Mannsfeld, S. C. B.; Miller, C. E.; Salleo, A.; Toney, M. F., Quantitative Determination of Organic Semiconductor Microstructure from the Molecular to Device Scale. *Chemical Reviews* **2012,** *112* (10), 5488-5519.

127. Mas-Torrent, M.; Rovira, C., Role of Molecular Order and Solid-State Structure in Organic Field-Effect Transistors. *Chemical Reviews* **2011,** *111* (8), 4833-4856.

128. Duhm, S.; Heimel, G.; Salzmann, I.; Glowatzki, H.; Johnson, R. L.; Vollmer, A.; Rabe, J. P.; Koch, N., Orientation-dependent ionization energies and interface dipoles in ordered molecular assemblies. *Nature Materials* **2008,** *7*, 326.

129. Ruderer, M. A.; Guo, S.; Meier, R.; Chiang, H. Y.; Körstgens, V.; Wiedersich, J.; Perlich, J.; Roth, S. V.; Müller-Buschbaum, P., Solvent-Induced Morphology in Polymer-

Based Systems for Organic Photovoltaics. *Advanced Functional Materials* **2011,** *21* (17), 3382-3391.

130. Liao, H.-C.; Tsao, C.-S.; Lin, T.-H.; Chuang, C.-M.; Chen, C.-Y.; Jeng, U. S.; Su, C.-H.; Chen, Y.-F.; Su, W.-F., Quantitative Nanoorganized Structural Evolution for a High Efficiency Bulk Heterojunction Polymer Solar Cell. *Journal of the American Chemical Society* **2011,** *133* (33), 13064-13073.

131. Zen, A.; Pflaum, J.; Hirschmann, S.; Zhuang, W.; Jaiser, F.; Asawapirom, U.; Rabe, J. P.; Scherf, U.; Neher, D., Effect of Molecular Weight and Annealing of Poly(3-hexylthiophene)s on the Performance of Organic Field-Effect Transistors. *Advanced Functional Materials* **2004,** *14* (8), 757-764.

132. Chang, J.-F.; Sun, B.; Breiby, D. W.; Nielsen, M. M.; Sölling, T. I.; Giles, M.; McCulloch, I.; Sirringhaus, H., Enhanced Mobility of Poly(3-hexylthiophene) Transistors by Spin-Coating from High-Boiling-Point Solvents. *Chemistry of Materials* **2004,** *16* (23), 4772-4776.

133. DeLongchamp, D. M.; Vogel, B. M.; Jung, Y.; Gurau, M. C.; Richter, C. A.; Kirillov, O. A.; Obrzut, J.; Fischer, D. A.; Sambasivan, S.; Richter, L. J.; Lin, E. K., Variations in Semiconducting Polymer Microstructure and Hole Mobility with Spin-Coating Speed. *Chemistry of Materials* **2005,** *17* (23), 5610-5612.

134. Graham, K. R.; Wieruszewski, P. M.; Stalder, R.; Hartel, M. J.; Mei, J.; So, F.; Reynolds, J. R., Improved Performance of Molecular Bulk-Heterojunction Photovoltaic Cells through Predictable Selection of Solvent Additives. *Advanced Functional Materials* **2012,** *22* (22), 4801-4813.

135. Chae, G. J.; Jeong, S.-H.; Baek, J. H.; Walker, B.; Song, C. K.; Seo, J. H., Improved performance in TIPS-pentacene field effect transistors using solvent additives. *Journal of Materials Chemistry C* **2013,** *1* (27), 4216-4221.

136. Morin, P.-O.; Bura, T.; Sun, B.; Gorelsky, S. I.; Li, Y.; Leclerc, M., Conjugated Polymers à la Carte from Time-Controlled Direct (Hetero)Arylation Polymerization. *ACS Macro Letters* **2015,** *4* (1), 21-24.

137. Cardona, C. M.; Li, W.; Kaifer, A. E.; Stockdale, D.; Bazan, G. C., Electrochemical Considerations for Determining Absolute Frontier Orbital Energy Levels of Conjugated Polymers for Solar Cell Applications. *Advanced Materials* **2011,** *23* (20), 2367-2371.

138. Vazquez, G.; Alvarez, E.; Navaza, J. M., Surface Tension of Alcohol Water + Water from 20 to 50 .degree.C. *Journal of Chemical & Engineering Data* **1995,** *40* (3), 611-614.

139. Österholm, A. M.; Shen, D. E.; Dyer, A. L.; Reynolds, J. R., Optimization of PEDOT Films in Ionic Liquid Supercapacitors: Demonstration As a Power Source for

Polymer Electrochromic Devices. *ACS Applied Materials & Interfaces* **2013,** *5* (24), 13432-13440.

140. Burrell, A. K.; Sesto, R. E. D.; Baker, S. N.; McCleskey, T. M.; Baker, G. A., The large scale synthesis of pure imidazolium and pyrrolidinium ionic liquids. *Green Chemistry* **2007,** *9* (5), 449-454.

141. Hyung, L. K.; Sung, K. M.; Sipei, Z.; Yuanyan, G.; P., L. T.; Daniel, F. C., "Cut and Stick" Rubbery Ion Gels as High Capacitance Gate Dielectrics. *Advanced Materials* **2012,** *24* (32), 4457-4462.

142. Lampert, M. A., Simplified Theory of Space-Charge-Limited Currents in an Insulator with Traps. *Physical Review* **1956,** *103* (6), 1648-1656.

143. Murgatroyd, P. N., Theory of space-charge-limited current enhanced by Frenkel effect. *Journal of Physics D: Applied Physics* **1970,** *3* (2), 151.

144. Huiqiong, Z.; Yuan, Z.; Jason, S.; D., C. S.; Chan, L.; C., B. G.; Thuc-Quyen, N.; J., H. A., High-Efficiency Polymer Solar Cells Enhanced by Solvent Treatment. *Advanced Materials* **2013,** *25* (11), 1646-1652.

145. Mihailetchi, V. D.; Blom, P. W. M.; Hummelen, J. C.; Rispens, M. T., Cathode dependence of the open-circuit voltage of polymer:fullerene bulk heterojunction solar cells. *Journal of Applied Physics* **2003,** *94* (10), 6849-6854.

146. Puodziukynaite, E.; Oberst, J. L.; Dyer, A. L.; Reynolds, J. R., Establishing Dual Electrogenerated Chemiluminescence and Multicolor Electrochromism in Functional Ionic Transition-Metal Complexes. *Journal of the American Chemical Society* **2012,** *134* (2), 968 - 978.

147. Muccini, M.; Koopman, W.; Toffanin, S., The photonic perspective of organic light-emitting transistors. *Laser & Photonics Reviews* **2012,** *6* (2), 258-275.

148. Deng, Y.; Liu, J.; Wang, J.; Liu, L.; Li, W.; Tian, H.; Zhang, X.; Xie, Z.; Geng, Y.; Wang, F., Dithienocarbazole and Isoindigo based Amorphous Low Bandgap Conjugated Polymers for Efficient Polymer Solar Cells. *Advanced Materials* **2014,** *26* (3), 471-476.

149. Son, S. Y.; Kim, Y.; Lee, J.; Lee, G.-Y.; Park, W.-T.; Noh, Y.-Y.; Park, C. E.; Park, T., High-Field-Effect Mobility of Low-Crystallinity Conjugated Polymers with Localized Aggregates. *Journal of the American Chemical Society* **2016,** *138* (26), 8096-8103.

150. Zhang, W.; Smith, J.; Watkins, S. E.; Gysel, R.; McGehee, M.; Salleo, A.; Kirkpatrick, J.; Ashraf, S.; Anthopoulos, T.; Heeney, M.; McCulloch, I., Indacenodithiophene Semiconducting Polymers for High-Performance, Air-Stable Transistors. *Journal of the American Chemical Society* **2010,** *132* (33), 11437-11439.

151. Pingel, P.; Zen, A.; Abellón, R. D.; Grozema, F. C.; Siebbeles, L. D. A.; Neher, D., Temperature-Resolved Local and Macroscopic Charge Carrier Transport in Thin P3HT Layers. *Advanced Functional Materials* **2010,** *20* (14), 2286-2295.

152. Liu, J.; Zhang, R.; Sauvé, G.; Kowalewski, T.; McCullough, R. D., Highly Disordered Polymer Field Effect Transistors: N-Alkyl Dithieno[3,2-b:2′,3′-d]pyrrole-Based Copolymers with Surprisingly High Charge Carrier Mobilities. *Journal of the American Chemical Society* **2008,** *130* (39), 13167-13176.

153. Lee, J.; Cho, S.; Yang, C., Highly reproducible organic field-effect transistor from pseudo 3-dimensional triphenylamine-based amorphous conjugated copolymer. *Journal of Materials Chemistry* **2011,** *21* (24), 8528-8531.

154. Yasuda, T.; Shinohara, Y.; Ishi-i, T.; Han, L., Use of benzothiadiazole–triphenylamine amorphous polymer for reproducible performance of polymer–fullerene bulk-heterojunction solar cells. *Organic Electronics* **2012,** *13* (10), 1802-1808.

155. Thelakkat, M., Star-Shaped, Dendrimeric and Polymeric Triarylamines as Photoconductors and Hole Transport Materials for Electro-Optical Applications. *Macromolecular Materials and Engineering* **2002,** *287* (7), 442-461.

156. Thelakkat, M.; Hagen, J.; Haarer, D.; Schmidt, H. W., Poly(triarylamine)s-synthesis and application in electroluminescent devices and photovoltaics. *Synthetic Metals* **1999,** *102* (1), 1125-1128.

157. Schmitz, C.; Thelakkat, M.; Schmidt, H. W., A Combinatorial Study of the Dependence of Organic LED Characteristics on Layer Thickness. *Advanced Materials* **1999,** *11* (10), 821-826.

158. Bach, U.; Lupo, D.; Comte, P.; Moser, J. E.; Weissörtel, F.; Salbeck, J.; Spreitzer, H.; Grätzel, M., Solid-state dye-sensitized mesoporous TiO2 solar cells with high photon-to-electron conversion efficiencies. *Nature* **1998,** *395*, 583.

159. Jeon, N. J.; Lee, H. G.; Kim, Y. C.; Seo, J.; Noh, J. H.; Lee, J.; Seok, S. I., o-Methoxy Substituents in Spiro-OMeTAD for Efficient Inorganic–Organic Hybrid Perovskite Solar Cells. *Journal of the American Chemical Society* **2014,** *136* (22), 7837-7840.

160. Ohishi, H.; Tanaka, M.; Kageyama, H.; Shirota, Y., Amorphous Molecular Materials with High Carrier Mobilities: Thiophene- and Selenophene-Containing Tris(oligoarylenyl)amines. *Chemistry Letters* **2004,** *33* (10), 1266-1267.

161. Zhang, W.; Smith, J.; Hamilton, R.; Heeney, M.; Kirkpatrick, J.; Song, K.; Watkins, S. E.; Anthopoulos, T.; McCulloch, I., Systematic Improvement in Charge Carrier Mobility of Air Stable Triarylamine Copolymers. *Journal of the American Chemical Society* **2009,** *131* (31), 10814-10815.

162. Zhang, J.; Chen, W.; Rojas, A. J.; Jucov, E. V.; Timofeeva, T. V.; Parker, T. C.; Barlow, S.; Marder, S. R., Controllable Direct Arylation: Fast Route to Symmetrical and Unsymmetrical 4,7-Diaryl-5,6-difluoro-2,1,3-benzothiadiazole Derivatives for Organic Optoelectronic Materials. *Journal of the American Chemical Society* **2013,** *135* (44), 16376-16379.

163. Okamoto, K.; Zhang, J.; Housekeeper, J. B.; Marder, S. R.; Luscombe, C. K., C–H Arylation Reaction: Atom Efficient and Greener Syntheses of π-Conjugated Small Molecules and Macromolecules for Organic Electronic Materials. *Macromolecules* **2013,** *46* (20), 8059-8078.

164. Pouliot, J.-R.; Sun, B.; Leduc, M.; Najari, A.; Li, Y.; Leclerc, M., A high mobility DPP-based polymer obtained via direct (hetero)arylation polymerization. *Polymer Chemistry* **2015,** *6* (2), 278-282.

165. Beaupré, S.; Dumas, J.; Leclerc, M., Toward the Development of New Textile/Plastic Electrochromic Cells Using Triphenylamine-Based Copolymers. *Chemistry of Materials* **2006,** *18* (17), 4011-4018.

166. Roncali, J., Molecular Engineering of the Band Gap of π-Conjugated Systems: Facing Technological Applications. *Macromolecular Rapid Communications* **2007,** *28* (17), 1761-1775.

167. Cao, K.; Shen, D. E.; Österholm, A. M.; Kerszulis, J. A.; Reynolds, J. R., Tuning Color, Contrast, and Redox Stability in High Gap Cathodically Coloring Electrochromic Polymers. *Macromolecules* **2016,** *49* (22), 8498-8507.

168. Wang, T.; Ravva, M. K.; Brédas, J.-L., Impact of the Nature of the Side-Chains on the Polymer-Fullerene Packing in the Mixed Regions of Bulk Heterojunction Solar Cells. *Advanced Functional Materials* **2016,** *26* (32), 5913-5921.

169. Lee, J.; Han, H.; Lee, J.; Yoon, S. C.; Lee, C., Utilization of "thiol-ene" photo cross-linkable hole-transporting polymers for solution-processed multilayer organic light-emitting diodes. *Journal of Materials Chemistry C* **2014,** *2* (8), 1474-1481.

170. Reeves, B. D.; Grenier, C. R. G.; Argun, A. A.; Cirpan, A.; McCarley, T. D.; Reynolds, J. R., Spray Coatable Electrochromic Dioxythiophene Polymers with High Coloration Efficiencies. *Macromolecules* **2004,** *37* (20), 7559-7569.

171. Zhu, H.; Huang, W.; Huang, Y.; Yang, J.; Wang, W., Narrow band-gap donor–acceptor copolymers based on diketopyrrolopyrrole and diphenylethene: Synthesis, characterization and application in field effect transistor. *Dyes and Pigments* **2016,** *127*, 37-44.

172. Søndergaard, R. R.; Hösel, M.; Krebs, F. C., Roll-to-Roll fabrication of large area functional organic materials. *Journal of Polymer Science Part B: Polymer Physics* **2013,** *51* (1), 16-34.

173. Andersen, T. R.; Larsen-Olsen, T. T.; Andreasen, B.; Böttiger, A. P. L.; Carlé, J. E.; Helgesen, M.; Bundgaard, E.; Norrman, K.; Andreasen, J. W.; Jørgensen, M.; Krebs, F. C., Aqueous Processing of Low-Band-Gap Polymer Solar Cells Using Roll-to-Roll Methods. *ACS Nano* **2011,** *5* (5), 4188-4196.

174. Zhao, J.; Li, Y.; Yang, G.; Jiang, K.; Lin, H.; Ade, H.; Ma, W.; Yan, H., Efficient organic solar cells processed from hydrocarbon solvents. *Nature Energy* **2016,** *1*, 15027.

175. Cai, W.; Liu, P.; Jin, Y.; Xue, Q.; Liu, F.; Russell, T. P.; Huang, F.; Yip, H.-L.; Cao, Y., Morphology Evolution in High-Performance Polymer Solar Cells Processed from Nonhalogenated Solvent. *Advanced Science* **2015,** *2* (8), 1500095.

176. Zhou, Y.; Gu, K. L.; Gu, X.; Kurosawa, T.; Yan, H.; Guo, Y.; Koleilat, G. I.; Zhao, D.; Toney, M. F.; Bao, Z., All-Polymer Solar Cells Employing Non-Halogenated Solvent and Additive. *Chemistry of Materials* **2016,** *28* (14), 5037-5042.

177. Fu, B.; Wang, C.-Y.; Rose, B. D.; Jiang, Y.; Chang, M.; Chu, P.-H.; Yuan, Z.; Fuentes-Hernandez, C.; Kippelen, B.; Brédas, J.-L.; Collard, D. M.; Reichmanis, E., Molecular Engineering of Nonhalogenated Solution-Processable Bithiazole-Based Electron-Transport Polymeric Semiconductors. *Chemistry of Materials* **2015,** *27* (8), 2928-2937.

178. Sonar, P.; Chang, J.; Kim, J. H.; Ong, K.-H.; Gann, E.; Manzhos, S.; Wu, J.; McNeill, C. R., High-Mobility Ambipolar Organic Thin-Film Transistor Processed From a Nonchlorinated Solvent. *ACS Applied Materials & Interfaces* **2016,** *8* (37), 24325-24330.

179. Lee, S. M.; Lee, H. R.; Han, A. R.; Lee, J.; Oh, J. H.; Yang, C., High-Performance Furan-Containing Conjugated Polymer for Environmentally Benign Solution Processing. *ACS Applied Materials & Interfaces* **2017,** *9* (18), 15652-15661.

180. Ho, C. H.; Yeol, B. J.; Eunjoo, S.; Boseok, K.; Kilwon, C.; Soon-Ki, K.; Yun-Hi, K., A Pseudo-Regular Alternating Conjugated Copolymer Using an Asymmetric Monomer: A High-Mobility Organic Transistor in Nonchlorinated Solvents. *Advanced Materials* **2015,** *27* (24), 3626-3631.

181. Lim, B.; Sun, H.; Lee, J.; Noh, Y.-Y., High Performance Solution Processed Organic Field Effect Transistors with Novel Diketopyrrolopyrrole-Containing Small Molecules. *Scientific Reports* **2017,** *7* (1), 164.

182. McDowell, C.; Bazan, G. C., Organic solar cells processed from green solvents. *Current Opinion in Green and Sustainable Chemistry* **2017,** *5*, 49-54.

183. Prat, D.; Wells, A.; Hayler, J.; Sneddon, H.; McElroy, C. R.; Abou-Shehada, S.; Dunn, P. J., CHEM21 selection guide of classical- and less classical-solvents. *Green Chemistry* **2016,** *18* (1), 288-296.

184. Mei, J.; Bao, Z., Side Chain Engineering in Solution-Processable Conjugated Polymers. *Chemistry of Materials* **2014,** *26* (1), 604-615.

185. Lee, W.; Seo, J. H.; Woo, H. Y., Conjugated polyelectrolytes: A new class of semiconducting material for organic electronic devices. *Polymer* **2013,** *54* (19), 5104-5121.

186. Zeglio, E.; Vagin, M.; Musumeci, C.; Ajjan, F. N.; Gabrielsson, R.; Trinh, X. T.; Son, N. T.; Maziz, A.; Solin, N.; Inganäs, O., Conjugated Polyelectrolyte Blends for Electrochromic and Electrochemical Transistor Devices. *Chemistry of Materials* **2015,** *27* (18), 6385-6393.

187. Henson, Z. B.; Zhang, Y.; Nguyen, T.-Q.; Seo, J. H.; Bazan, G. C., Synthesis and Properties of Two Cationic Narrow Band Gap Conjugated Polyelectrolytes. *Journal of the American Chemical Society* **2013,** *135* (11), 4163-4166.

188. Inal, S.; Rivnay, J.; Leleux, P.; Ferro, M.; Ramuz, M.; Brendel, J. C.; Schmidt, M. M.; Thelakkat, M.; Malliaras, G. G., A High Transconductance Accumulation Mode Electrochemical Transistor. *Advanced Materials* **2014,** *26* (44), 7450-7455.

189. K., L.; R., M.; U., S.; R., G.; U., A.; S., P.; D., N.; T., K., Semiconducting Polymer Nanospheres in Aqueous Dispersion Prepared by a Miniemulsion Process. *Advanced Materials* **2002,** *14* (9), 651-655.

190. Millstone, J. E.; Kavulak, D. F. J.; Woo, C. H.; Holcombe, T. W.; Westling, E. J.; Briseno, A. L.; Toney, M. F.; Fréchet, J. M. J., Synthesis, Properties, and Electronic Applications of Size-Controlled Poly(3-hexylthiophene) Nanoparticles. *Langmuir* **2010,** *26* (16), 13056-13061.

191. Cho, J.; Cheon, K. H.; Ahn, H.; Park, K. H.; Kwon, S.-K.; Kim, Y.-H.; Chung, D. S., High Charge-Carrier Mobility of 2.5 cm2 V−1 s−1 from a Water-Borne Colloid of a Polymeric Semiconductor via Smart Surfactant Engineering. *Advanced Materials* **2015,** *27* (37), 5587-5592.

192. Shao, M.; He, Y.; Hong, K.; Rouleau, C. M.; Geohegan, D. B.; Xiao, K., A water-soluble polythiophene for organic field-effect transistors. *Polymer Chemistry* **2013,** *4* (20), 5270-5274.

193. Reeves, B. D.; Unur, E.; Ananthakrishnan, N.; Reynolds, J. R., Defunctionalization of Ester-Substituted Electrochromic Dioxythiophene Polymers. *Macromolecules* **2007,** *40* (15), 5344-5352.

194. Beaujuge, P. M.; Amb, C. M.; Reynolds, J. R., A Side-Chain Defunctionalization Approach Yields a Polymer Electrochrome Spray-Processable from Water. *Advanced Materials* **2010,** *22* (47), 5383-5387.

195. Zhao, H.; Sterner, E. S.; Coughlin, E. B.; Theato, P., o-Nitrobenzyl Alcohol Derivatives: Opportunities in Polymer and Materials Science. *Macromolecules* **2012,** *45* (4), 1723-1736.

196. Hansen, M. J.; Velema, W. A.; Lerch, M. M.; Szymanski, W.; Feringa, B. L., Wavelength-selective cleavage of photoprotecting groups: strategies and applications in dynamic systems. *Chemical Society Reviews* **2015,** *44* (11), 3358-3377.

197. Bredas, J. L.; Street, G. B., Polarons, bipolarons, and solitons in conducting polymers. *Accounts of Chemical Research* **1985,** *18* (10), 309-315.

198. Bach, C. M. G.; Reynolds, J. R., Rapid Ion Exchange during Redox Switching of Poly(3-methylthiophene) Studied by X-ray Photoelectron Spectroscopy. *The Journal of Physical Chemistry* **1994,** *98* (51), 13636-13642.

199. Kanai, K.; Miyazaki, T.; Suzuki, H.; Inaba, M.; Ouchi, Y.; Seki, K., Effect of annealing on the electronic structure of poly(3-hexylthiophene) thin film. *Physical Chemistry Chemical Physics* **2010,** *12* (1), 273-282.

200. Huang, J.-H.; Yang, C.-Y.; Hsu, C.-Y.; Chen, C.-L.; Lin, L.-Y.; Wang, R.-R.; Ho, K.-C.; Chu, C.-W., Solvent-Annealing-Induced Self-Organization of Poly(3-hexylthiophene), a High-Performance Electrochromic Material. *ACS Applied Materials & Interfaces* **2009,** *1* (12), 2821-2828.

201. Yuning, L.; P., S. S.; Prashant, S., A High Mobility P-Type DPP-Thieno[3,2-b]thiophene Copolymer for Organic Thin-Film Transistors. *Advanced Materials* **2010,** *22* (43), 4862-4866.

202. Bulloch, R. H.; Reynolds, J. R., Photostability in dioxyheterocycle electrochromic polymers. *Journal of Materials Chemistry C* **2016,** *4* (3), 603-610.

203. Hong, K.; Kim, S. H.; Mahajan, A.; Frisbie, C. D., Aerosol Jet Printed p- and n-type Electrolyte-Gated Transistors with a Variety of Electrode Materials: Exploring Practical Routes to Printed Electronics. *ACS Applied Materials & Interfaces* **2014,** *6* (21), 18704-18711.

204. O., G. J.; Alberto, S., Structural Effects of Gating Poly(3-hexylthiophene) through an Ionic Liquid. *Advanced Functional Materials* **2017,** *27* (32), 1701791.

205. Atallah, T. L.; Gustafsson, M. V.; Schmidt, E.; Frisbie, C. D.; Zhu, X. Y., Charge Saturation and Intrinsic Doping in Electrolyte-Gated Organic Semiconductors. *The Journal of Physical Chemistry Letters* **2015,** *6* (23), 4840-4844.

206. Khodagholy, D.; Rivnay, J.; Sessolo, M.; Gurfinkel, M.; Leleux, P.; Jimison, L. H.; Stavrinidou, E.; Herve, T.; Sanaur, S.; Owens, R. M.; Malliaras, G. G., High transconductance organic electrochemical transistors. *Nat Commun* **2013,** *4*.

207. Cho, J. H.; Lee, J.; Xia, Y.; Kim, B.; He, Y.; Renn, M. J.; Lodge, T. P.; Daniel Frisbie, C., Printable ion-gel gate dielectrics for low-voltage polymer thin-film transistors on plastic. *Nature Materials* **2008,** *7*, 900.

208. Sahika, I.; Jonathan, R.; Pierre, L.; Marc, F.; Marc, R.; C., B. J.; M., S. M.; Mukundan, T.; G., M. G., A High Transconductance Accumulation Mode Electrochemical Transistor. *Advanced Materials* **2014,** *26* (44), 7450-7455.

209. Choi, J.; Kim, K.-H.; Yu, H.; Lee, C.; Kang, H.; Song, I.; Kim, Y.; Oh, J. H.; Kim, B. J., Importance of Electron Transport Ability in Naphthalene Diimide-Based Polymer Acceptors for High-Performance, Additive-Free, All-Polymer Solar Cells. *Chemistry of Materials* **2015,** *27* (15), 5230-5237.

210. Efrem, A.; Lei, Y.; Wu, B.; Wang, M.; Ng, S. C.; Ong, B. S., Dithienobenzochalcogenodiazole-based electron donor–acceptor polymers for organic electronics. *Dyes and Pigments* **2016,** *129*, 90-99.

211. Beljonne, D.; Cornil, J.; Muccioli, L.; Zannoni, C.; Brédas, J.-L.; Castet, F., Electronic Processes at Organic−Organic Interfaces: Insight from Modeling and Implications for Opto-electronic Devices. *Chemistry of Materials* **2011,** *23* (3), 591-609.

212. Holcombe, T. W.; Norton, J. E.; Rivnay, J.; Woo, C. H.; Goris, L.; Piliego, C.; Griffini, G.; Sellinger, A.; Brédas, J.-L.; Salleo, A.; Fréchet, J. M. J., Steric Control of the Donor/Acceptor Interface: Implications in Organic Photovoltaic Charge Generation. *Journal of the American Chemical Society* **2011,** *133* (31), 12106-12114.

213. Ravva, M. K.; Wang, T.; Brédas, J.-L., Nature of the Binding Interactions between Conjugated Polymer Chains and Fullerenes in Bulk Heterojunction Organic Solar Cells. *Chemistry of Materials* **2016,** *28* (22), 8181-8189.

214. Chao, W.; Kyohei, N.; Fang, L. H.; Yujiao, C.; You-Lee, H.; Yusuke, N.; Keisuke, T., Intermolecular Arrangement of Fullerene Acceptors Proximal to Semiconducting Polymers in Mixed Bulk Heterojunctions. *Angewandte Chemie International Edition* **2018***, 57,* 7034 –7039.

215. Clare, D. S.; A., H. I.; Clément, C.; Abdulrahman, E. L.; M., B. P.; Frédéric, L., Interplay Between Side Chain Pattern, Polymer Aggregation, and Charge Carrier Dynamics in PBDTTPD:PCBM Bulk-Heterojunction Solar Cells. *Advanced Energy Materials* **2015,** *5* (9), 1401778.

216. Tonghui, W.; Kumar, R. M.; Jean-Luc, B., Impact of the Nature of the Side-Chains on the Polymer-Fullerene Packing in the Mixed Regions of Bulk Heterojunction Solar Cells. *Advanced Functional Materials* **2016,** *26* (32), 5913-5921.

217. Constantinou, I.; Lai, T.-H.; Klump, E. D.; Goswami, S.; Schanze, K. S.; So, F., Effect of Polymer Side Chains on Charge Generation and Disorder in PBDTTPD Solar Cells. *ACS Applied Materials & Interfaces* **2015,** *7* (48), 26999-27005.

218. Sun, X.; Zhang, Z.; Hou, R.; Huang, M.; Zhao, B.; Tan, S., The effect of the length of alkyl side-chains on the molecular aggregation and photovoltaic performance of the isoindigo-based polymers. *Dyes and Pigments* **2017,** *139*, 403-411.

219. Berrouard, P.; Dufresne, S.; Pron, A.; Veilleux, J.; Leclerc, M., Low-Cost Synthesis and Physical Characterization of Thieno[3,4-c]pyrrole-4,6-dione-Based Polymers. *The Journal of Organic Chemistry* **2012,** *77* (18), 8167-8173.

220. Zou, Y.; Najari, A.; Berrouard, P.; Beaupré, S.; Réda Aïch, B.; Tao, Y.; Leclerc, M., A Thieno[3,4-c]pyrrole-4,6-dione-Based Copolymer for Efficient Solar Cells. *Journal of the American Chemical Society* **2010,** *132* (15), 5330-5331.

221. Wolfe, R. M. W.; Reynolds, J. R., Direct Imide Formation from Thiophene Dicarboxylic Acids Gives Expanded Side-Chain Selection in Thienopyrrolediones. *Organic Letters* **2017,** *19* (5), 996-999.

222. Jung, J. W.; Russell, T. P.; Jo, W. H., Highly Crystalline Low Band Gap Polymer Based on Thieno[3,4-c]pyrrole-4,6-dione for High-Performance Polymer Solar Cells with a >400 nm Thick Active Layer. *ACS Applied Materials & Interfaces* **2015,** *7* (24), 13666-13674.

223. Cheon, Y. R.; Kim, Y. J.; Ha, J.-j.; Kim, M.-J.; Park, C. E.; Kim, Y.-H., TPD-Based Copolymers with Strong Interchain Aggregation and High Hole Mobility for Efficient Bulk Heterojunction Solar Cells. *Macromolecules* **2014,** *47* (24), 8570-8577.

224. Wang, K.; Xu, Z.; Guo, B.; Guo, X.; Zhang, M.; Li, Y., TPD-based polythiophene derivatives with higher Voc for polymer solar cells. *RSC Advances* **2016,** *6* (68), 63338-63346.

225. Mateker, W. R.; Douglas, J. D.; Cabanetos, C.; Sachs-Quintana, I. T.; Bartelt, J. A.; Hoke, E. T.; El Labban, A.; Beaujuge, P. M.; Frechet, J. M. J.; McGehee, M. D., Improving the long-term stability of PBDTTPD polymer solar cells through material purification aimed at removing organic impurities. *Energy & Environmental Science* **2013,** *6* (8), 2529-2537.

226. Cui, C.; He, Z.; Wu, Y.; Cheng, X.; Wu, H.; Li, Y.; Cao, Y.; Wong, W.-Y., High-performance polymer solar cells based on a 2D-conjugated polymer with an alkylthio side-chain. *Energy & Environmental Science* **2016,** *9* (3), 885-891.

227. Wan, Q.; Guo, X.; Wang, Z.; Li, W.; Guo, B.; Ma, W.; Zhang, M.; Li, Y., 10.8% Efficiency Polymer Solar Cells Based on PTB7-Th and PC71BM via Binary Solvent Additives Treatment. *Advanced Functional Materials* **2016,** *26* (36), 6635-6640.

228. Guo, X.; Facchetti, A.; Marks, T. J., Imide- and Amide-Functionalized Polymer Semiconductors. *Chemical Reviews* **2014,** *114*, 8943-9021.

229. Li, W.; Hendriks, K. H.; Wienk, M. M.; Janssen, R. A. J., Diketopyrrolopyrrole Polymers for Organic Solar Cells. *Accounts of Chemical Research* **2016,** *49* (1), 78-85.

230. Khlyabich, P. P.; Burkhart, B.; Ng, C. F.; Thompson, B. C., Efficient Solar Cells from Semi-random P3HT Analogues Incorporating Diketopyrrolopyrrole. *Macromolecules* **2011,** *44* (13), 5079-5084.

231. Ashraf, R. S.; Meager, I.; Nikolka, M.; Kirkus, M.; Planells, M.; Schroeder, B. C.; Holliday, S.; Hurhangee, M.; Nielsen, C. B.; Sirringhaus, H.; McCulloch, I., Chalcogenophene Comonomer Comparison in Small Band Gap Diketopyrrolopyrrole-Based Conjugated Polymers for High-Performing Field-Effect Transistors and Organic Solar Cells. *Journal of the American Chemical Society* **2015,** *137* (3), 1314-1321.

232. Hendriks, K. H.; Heintges, G. H. L.; Gevaerts, V. S.; Wienk, M. M.; Janssen, R. A. J., High-Molecular-Weight Regular Alternating Diketopyrrolopyrrole-based Terpolymers for Efficient Organic Solar Cells. *Angewandte Chemie International Edition* **2013,** *52* (32), 8341-8344.

233. Hendriks, K. H.; Li, W.; Wienk, M. M.; Janssen, R. A. J., Small-Bandgap Semiconducting Polymers with High Near-Infrared Photoresponse. *Journal of the American Chemical Society* **2014,** *136* (34), 12130-12136.

234. Stalder, R.; Mei, J.; Graham, K. R.; Estrada, L. A.; Reynolds, J. R., Isoindigo, a Versatile Electron-Deficient Unit For High-Performance Organic Electronics. *Chemistry of Materials* **2014,** *26* (1), 664 - 678.

235. Stalder, R.; Mei, J.; Reynolds, J. R., Isoindigo-Based Donor−Acceptor Conjugated Polymers. *Macromolecules* **2010,** *43* (20), 8348 - 8352.

236. Stalder, R.; Mei, J.; Subbiah, J.; Grand, C.; Estrada, L. A.; So, F.; Reynolds, J. R., n-Type Conjugated Polyisoindigos. *Macromolecules* **2011,** *44* (16), 6303 - 6310.

237. Wang, E.; Ma, Z.; Zhang, Z.; Vandewal, K.; Henriksson, P.; Inganäs, O.; Zhang, F.; Andersson, M. R., An Easily Accessible Isoindigo-Based Polymer for High-Performance Polymer Solar Cells. *Journal of the American Chemical Society* **2011,** *133* (36), 14244-14247.

238. Ottone, C.; Berrouard, P.; Louarn, G.; Beaupre, S.; Gendron, D.; Zagorska, M.; Rannou, P.; Najari, A.; Sadki, S.; Leclerc, M.; Pron, A., Donor-acceptor alternating copolymers containing thienopyrroledione electron accepting units: preparation, redox behaviour, and application to photovoltaic cells. *Polymer Chemistry* **2012,** *3* (9), 2355-2365.

239. Yi, Z.; Ma, L.; Li, P.; Xu, L.; Zhan, X.; Qin, J.; Chen, X.; Liu, Y.; Wang, S., Enhancing the organic thin-film transistor performance of diketopyrrolopyrrole-benzodithiophene copolymers via the modification of both conjugated backbone and side chain. *Polymer Chemistry* **2015,** *6* (30), 5369-5375.

240. C., T. B.; J., F. J. M., Polymer–Fullerene Composite Solar Cells. *Angewandte Chemie International Edition* **2008,** *47* (1), 58-77.

241. Yuze, L.; Jiayu, W.; Zhi-Guo, Z.; Huitao, B.; Yongfang, L.; Daoben, Z.; Xiaowei, Z., An Electron Acceptor Challenging Fullerenes for Efficient Polymer Solar Cells. *Advanced Materials* **2015,** *27* (7), 1170-1174.

242. Elumalai, N. K.; Uddin, A., Open circuit voltage of organic solar cells: an in-depth review. *Energy & Environmental Science* **2016,** *9* (2), 391-410.

243. He, Z.; Zhong, C.; Su, S.; Xu, M.; Wu, H.; Cao, Y., Enhanced power-conversion efficiency in polymer solar cells using an inverted device structure. *Nature Photonics* **2012,** *6*, 591.

244. Jao, M.-H.; Liao, H.-C.; Su, W.-F., Achieving a high fill factor for organic solar cells. *Journal of Materials Chemistry A* **2016,** *4* (16), 5784-5801.

245. Feng, G.; Scott, H.; Mattias, A.; David, H.; Yuxin, X.; Shaoqing, Z.; Jianpu, W.; Jianhui, H.; Alberto, S.; Olle, I., The Effect of Processing Additives on Energetic Disorder in Highly Efficient Organic Photovoltaics: A Case Study on PBDTTT-C-T:PC71BM. *Advanced Materials* **2015,** *27* (26), 3868-3873.

246. Piliego, C.; Holcombe, T. W.; Douglas, J. D.; Woo, C. H.; Beaujuge, P. M.; Fréchet, J. M. J., Synthetic Control of Structural Order in N-Alkylthieno[3,4-c]pyrrole-4,6-dione-Based Polymers for Efficient Solar Cells. *Journal of the American Chemical Society* **2010,** *132* (22), 7595-7597.

247. Mei, J.; Graham, K. R.; Stalder, R.; Reynolds, J. R., Synthesis of Isoindigo-Based Oligothiophenes for Molecular Bulk Heterojunction Solar Cells. *Organic Letters* **2010,** *12* (4), 660 - 663.